Universidad de Murcia
Facultad de Química
Departamento de Química Física

Study of the IR spectrum and the vibrational relaxation of peptides in water solution

Estudio del espectro de infrarrojo y la relajación vibracional de péptidos en disolución acuosa

Marwa Hamdi Abdelrahman Farag

2012

Contents

CHAPTER 1

Introduction

Recent advances in computer simulations of the condensed phase have made possible the investigation of dynamics in large systems at a quantum level [Car 85, Laasonen 93, Silvestrelli 97, Silvestrelli 98, Carloni 02, Iftimie 05]. The use of a quantum Hamiltonian and the definition of the wave function of the whole electronic system result in an accurate description of polarization and charge transfer. This is crucial for modeling bond making/breaking, a feature that is lacking in most molecular dynamics (MD) simulations based on molecular mechanics (MM) force fields. The possibility of treating at a quantum level the electronic Hamiltonian of bio-organic systems in their real environment is thus becoming closer, even for molecular dynamics simulations.

In molecular biology studies, infrared spectroscopy often complements the widely employed X-ray diffraction and NMR techniques, in particular to study proteins and peptides. Amide bands are used to probe the secondary structure when exploring the folding dynamics of proteins [Gilmanshin 97, Montalvo 10]. A theoretical model of these systems should therefore be able to describe the effect of the environment on the infrared signature of peptide bonds [Schultheis 08]. In addition, theoretical investigations at the DFT-molecular dynamics level have stressed the importance of conformational sampling for an accurate description of specific infrared features, such as for example the experimental line shape resulting from a mixture between two different conformations of a peptide [Gaigeot 09, Gaigeot 10].

The most popular molecular model for the peptide link is *N*-methylacetamide (NMA), whose IR spectrum has been extensively studied both by experiments and theory [Ataka 84, Rodrigo 86, Chen 95, Kubelka 01, Torii 04, Mirkin 04, Hayashi 05, la Cour Jansen 06]. The most significant bands in the IR spectrum of a peptide group are the Amide I, II and III bands, and the one corresponding to N-H stretch (Amide A). The Amide I mode is mostly related to the C-O stretching motion, which was shown to be coupled with water motions in aqueous solution [Chen 94]. Amide II arises mostly from C-N-H bending motion combined with C-N stretch, whereas a larger contribution of C-N stretch combined with C-N-H bend generates Amide III.

The IR spectrum of NMA obtained through classical MM simulations has been compared to the one obtained through a QM/MM approach [Yang 05]. The authors have concluded that reliable modeling of IR spectra in solution should include the effect of the time-dependent solvent-induced dipole on the solute. The effect of hydrogen bonding with surrounding water molecules on the vibrational frequencies of NMA has been extensively studied by means of quantum chemistry calculations on NMA-water clusters [Mennucci 05], and it has been described in terms of a spatially inhomogeneous electric field generated by the solvent acting on the solute [Hayashi 05]. Quantum chemistry calculations have been performed on NMA-water clusters (8000 structures) extracted from MM simulations [Besley 04]. The results obtained through this approach for the position and for the shape of Amide I-III bands are in good agreement with experiments: solute-solvent hydrogen bonding plays a relevant role in reproducing band profiles.

The importance of hydrogen bonding and nonspecific electrostatic interactions between solute and solvent has been analyzed in depth by modeling the harmonic frequencies and by including anharmonic effects in a joint quantum chemistry and experimental study [Andrushchenko 09]. Another study based on the interplay between quantum chemistry and experiments has focused on the influence of the environment and of the temperature on the Amide I band [Ackels 09]. According to this work, the intensity of this band depends strongly on the solvent and it varies with temperature. Concerning the solvent effect on the band position, the authors have shown that a simple approach based on the Onsager reaction field can reasonably predict both the solvent-induced and the temperature-induced frequency shifts.

Recent work on theoretical modeling of two-dimensional (2D) IR spectroscopy has been carried out by Jeon and Cho and applied to deuterated NMA in a cluster of 16 D_2O molecules, based on a QM/MM scheme [Jeon 10]. The approach has been shown to be successful in reproducing the main features of the experimental 2D IR spectrum. The authors have pointed out that a better description of inhomogeneous broadening might be achieved by including more solvent molecules and by describing them at a quantum level.

Most of the work on IR spectra of small peptides in solution points towards the importance of including polarization and of specific solute-solvent interactions (i.e. hydrogen bonding) in the theoretical description of vibrational properties. In particular, we believe that the mutual polarization between solute and solvent should be included, as well as charge transfer, which might be relevant in the case of NMA, due to the presence of a hydrogen bond donor and of a hydrogen bond acceptor within the peptide bond. All these terms are taken into account if the electronic Hamiltonian of the full system is treated at the quantum level.

The two conformers of NMA immersed in water, as well as more complex examples of peptides, have already been investigated at the DFT molecular dynamics level, in particular by Gaigeot et al. (see Ref. [Gaigeot 10] for a recent review). However, due to their high computational cost, DFT-based MD simulations are in general limited to simple systems and/or small simulation times. As explained below, the method proposed here is intended to address such limitation by relaxing the level of the quantum chemistry approach used

to describe the electronic structure of the solution. This is particularly important when dealing with the calculation of infrared spectra [Yang 05, Kinnaman 06], which requires good statistics [Richardi 05].

The method used here is based on a semiempirical Born-Oppenheimer molecular dynamics (SEBOMD) approach [Monard 05]. At each step of the MD simulation, the electronic wave function of the system is computed with a semiempirical quantum method making use, if necessary, of a linear scaling algorithm, such as the Divide and Conquer method [Yang 95, Dixon 96]. Obviously, semiempirical Hamiltonians strongly reduce the computational cost of the simulations compared to ab initio or density functional theory-based molecular dynamics. The price to be payed is a lower accuracy in the computed molecular properties, though reasonable results are expected for the IR spectra of isolated molecules [Mokrane 97, Garcia-Viloca 04, Li 06].

The amide I band of NMA is very sensitive to the environment. In particular, in aqueous solution the carbonyl bond is a hydrogen bond (H-bond) acceptor, and this bond involves on average two water molecules. The -NH group is a potential H-bond donor, interacting with one water molecule [Guo 92, Torii 98]. In NMA, having to deal with just one peptide unit strongly simplifies the analysis of the solvent effect on the amide I band, which is complicated in di- and poly-peptides by the presence of different local environments and of different conformations.

The presence of hydrogen bonded water molecules on the -CO group influences the stretch vibration. It has been shown that the amide I band of NMA is strongly coupled to the water bending motion: this has been related to the observed splitting of the amide I Raman band [Chen 94].

Hydrogen bonding has thus two effects. On one hand, it modifies the average structure of the peptide bond, and its local dipole, through electrostatic and polarization interaction. Some charge transfer along the hydrogen bond may also be expected. The extent to which such interactions affect the amide I frequency depends indeed on the number of H-bonds and on their geometry. On the other hand, the -CO stretching oscillator couples with the water bending oscillation, giving rise to correlations in the motions of solute and solvent affecting the absorption spectrum in the region of the amide I band.

NMA-water complexes have been widely used as model systems in theoretical work performed by other groups working on the vibrational properties of peptides. Guo and Karplus [Guo 92] focused on the effect of H-bonding on the structure and on the rotations around the N-C^{α} bonds. By means of quantum chemistry calculations at the Hartree-Fock and Moller-Plesset second-order perturbation theory levels, they showed that there is a cooperative effect, given by a water molecule H-bonded on the N-H bond side, strengthening the H-bond on the carbonyl side. Hydrogen bonds with water also rise the barrier for the rotation of the methyl groups of NMA, hinting that polarization effects may be necessary to be included in the development of force fields of proteins.

Mirkin and Krimm [Mirkin 96] explored the effect of two water molecules (a H-bond donor and a H-bond acceptor) on the NMA harmonic frequencies, and they evaluated the solvent effect using a reaction field in a medium having a dielectric constant of 20.

They calculated a splitting of the amide I band, which is enhanced by the presence of the dielectric medium. The dielectric solvent effect was also included in later work by Torii and collaborators [Torii 98] and by Mennucci and Martinez [Mennucci 05]. In former case, the experimental shift in water is well reproduced by considering NMA and three water molecules immersed in a continuum solvent using the Hartree Fock method and a 6-31G++G* basis set. In the latter case, DFT calculations using a B3LYP hybrid functional and a 6-31+G(d,p) basis set were used to calculate the harmonic frequencies of NMA surrounded by one to three water molecules and immersed in a continuum described at the polarizable continuum model level with the integral equation formalism [Cances 98a, Cances 98b], finding a reasonably good agreement for the solvent induced shift on the amide I band, but much worse results for the shift on the amide II and III bands.

Empirical expressions to correct force fields that are based on gas phase calculations were also derived by Bouř and Keiderling [Bouř 03] based on DFT calculations at the BPW91/6-31G** level. These calculations were performed on NMA-water cluster geometries extracted from classical MD simulations. In later work, Bouř and collaborator [Andrushchenko 09] show the deficiency in DFT methods to reproduce correctly the out of plane bend potential of the N atom belonging to the peptide bond. Combination bands of the CO stretch with lower frequency motions in the condensed phase and the anharmonicity of the amide I potential results from non-specific solute-solvent interactions as well as from H-bonding.

IR solvent induced shifts have also been modeled by la Cour Jansen and Knoester [la Cour Jansen 06] using a map of the electrostatic field generated on the solute by the presence of the solvent. DFT-based calculations are used to parametrize the frequency of the normal mode, the anharmonicity and the transition dipole for the first three vibrational states. This method allows to reproduce both the solvent shift and the line width of IR experimental spectra obtained with the Fourier transform technique.

In the present thesis, we use a simple model to study the effect of a H-bond on the amide I frequency of NMA. We developed a methodology allowing to extract the relative effect of interactions of different nature in the H-bonded system: electrostatic, polarization, charge transfer, and the deformation of the potential energy surface corresponding to the amide I oscillator. We thus provide a quantitative interpretation of the effect of a H-bond on the amide I band. The frequency shift in complexes formed by NMA and one water molecule is discussed after analyzing the bulk solvent effect on the peptide bonds of *cis* and *trans* NMA in water.

Understanding the vibrational motions of a polyatomic molecule in solution is critical in describing the intramolecular energy redistribution and intermolecular energy transfer processes that take place during the vibrational relaxation of the solute molecule. Recent advances in ultrafast infrared-Raman techniques have been shown to provide a remarkably detailed description of the vibrational energy flows throughout polyatomic molecules in liquids [Hill 96, Hamm 98, Peterson 99, Dlott 01, Iwaki 01, Fayer 01a, Fayer 01b, Cremeens 06, Shigeto 07, Wang 07, Shigeto 08, Schade 09b, Fang 09]. Transient spectroscopic data give quantitative measures of the instantaneous populations of all the observed vibrations of

the molecule in real time. The information extracted from these experiments is usually discussed in terms of the vibrational spectra assigned using the standard Equilibrium Normal Modes (ENM). However, since the definition of these modes is based on the second-order expansion of the potential energy function of the isolated solute molecule about its equilibrium configuration, their ability to describe the intramolecular vibrational dynamics of the molecule in aqueous solution at room temperature in terms of individual normal modes seems to be questionable [Nguyen 03].

Structural perturbations caused by the interaction of the solute molecule with the solvent and by the effect of the thermal energy stored in the molecule produce, in fact, large conformational changes driven by the vibrational dynamics anharmonicities. This behavior is particularly well-known in bio molecules, where rugged energy landscapes indicate the presence of a very large number of nearly isoenergetic conformations which are accessible in solution at room conditions [Frauenfelder 97, Frauenfelder 01, Frauenfelder 03, Lubchenko 05]. Mode couplings have indeed been revealed as a basic requirement to describe the vibrational energy transfer and vibrational absorption spectra of proteins [Moritsugu 00, Roitberg 97]. The effect of anharmonic motions in the vibrational dynamics of macromolecules has also been extensively studied by Go and co-workers [Hayward 94, Go 83, Hayward 95], who use the ENMs and conclude that while high frequency ENMs preserve significant harmonic aspects, low frequency modes remain essentially anharmonic.

The inherent structures of large systems can be determined through molecular dynamics simulations by quenching the instantaneous structures to local minima of the potential energy surface. The so-called Quenched Normal Modes (QNMs) [Ohmine 90, Ohmine 93, Sagnella 99, Rao 10, Elber 87, Fujisaki 08] can be therefore calculated by diagonalization of the corresponding Hessian matrices. Furthermore, QNMs can be evaluated for super molecules, including the solute molecule and its first solvation shell. However, the QNMs do not provide an expression for the vibrational energy of the molecule as a sum of individual contributions from every single mode at the instantaneous configurations of the solute molecule. We also note that the presence of the solvent can increase the number of conformers, each with a different set of QNMs, significantly. Another approach to deal with the vibrational dynamics which is far from the equilibrium configuration consists of calculating effective quadratic force constants by averaging on the potential of mean force at a given temperature. This method is called the quasi-harmonic approximation [Karplus 81, Levy 82, Levy 84] and although it can deal with the effective force constants as a function of temperature, its application to nonequilibrium molecular dynamics simulations is not straightforward.

The strong couplings emerging between the ENMs of the solute molecule when it executes wide amplitude vibrational motions severely complicate the interpretation of the vibrational dynamics of the molecule in terms of individual contributions of each mode. The same happens with the vibrational energy flows, which cannot therefore be quantified in terms of the energy stored in each individual ENM. Achieving this is, however, essential to describe the evolution with time of the excess of vibrational energy deposited in a given mode, both for the understanding of the process and above all because this energy

can now be experimentally tracked by ultrafast infrared-Raman spectroscopy, thus making direct comparison with the experiment possible. One way to tackle this problem is to use the Instantaneous Normal Modes (INMs), which are those obtained by diagonalizing the Hessian matrix of the potential energy function at every instantaneous configuration of the molecule. The INM theory was originally developed to study short-time dynamics properties of liquids [Buchner 92, Goodyear 97, Keyes 97, David 98, Kramer 98, Moore 98, Ahlborn 99, Ji 00, Stratt 01, Garberoglio 02, Deng 02, Perry 03], where it is shown to provide a conceptually and computationally simple harmonic picture of the system, and it has been extended later to study the vibrational dynamics of polyatomic molecules in solution [Sagnella 99, Bu 03a, Nguyen 03, Fujisaki 08, Fujisaki 09, Schulz 09, Bastida 10a, Bastida 10b], thus widening its range of applications.

The INM formalism is based on the fact that, at any instant, intramolecular vibrations closely resemble a set of well-defined and independent harmonic oscillators. Accordingly, the INMs change as the configuration of the molecule evolves with time, and this INMs evolution can be related to time-resolved spectroscopic observables. In this respect, for instance, time correlation functions obtained using INMs have been calculated and tested for a variety of atomic and molecular liquids [Cho 94, Stratt 94, Stratt 95, Goodyear 96, Ladanyi 96, Kalbfleisch 96, Goodyear 97, Egorov 97]. Clearly, a single set of INMs cannot represent the long-time dynamics of the solute molecule, since its validity is limited to the vicinity of the configuration from which the set has been extracted. It is necessary then to compute successive sets of INMs of the evolving molecule from molecular dynamics simulations and find a meaningful way to connect them, and this requires in turn an efficient method to assign and, therefore, identify the individual INMs.

The simplest way to identify the INMs with time is to sort them by increasing frequencies, provided that the INMs are calculated at time steps short enough to get a smooth variation. Even in this case, however, the identification of the INMs based on their history poses some difficulties that make it impractical [David 98]. These difficulties arise basically from the fact that the time-dependent vibrational frequencies of the INMs may become very close and even cross with either significant or no effects on the INM definitions, thus complicating their identification severely. Accordingly, a more efficient method of identification of the INMs with time must be devised based on the specific assignments of the INMs at every time step of the MD simulation.

In this thesis, we extensively develop a novel method previously proposed by our group [Bastida 10a, Bastida 10b] to track the identity of the INMs over time, which is based on the use of the ENMs as templates to assign the INMs at a given time. The method therefore reconciles the descriptions of the vibrational dynamics based on both sets of modes and provides, in addition, a unique relationship between them.

The vibrational relaxation (VR) of deuterated *N*-methylacetamide (NMAD) in solution has been the subject of a wide number of both experimental [Hamm 98, Zanni 01, Rubtsov 03b, DeCamp 05, DeFlores 06, Fang 09, Piatkowski 10, Piatkowski 12] and theoretical [Gregurick 02, Nguyen 03, Kwac 03, Schmidt 04, Hayashi 05, Fujisaki 06, Dijkstra 07, Fujisaki 08, Fujisaki 09, Bastida 10a, Bastida 10b, Bastida 12] studies, which altogether have

provided a qualitative picture of the main relaxation channels involved in the process. Discrepancies however in the kinetic interpretation of the vibrational energy decay and uncertainties in the values of the relaxation lifetimes of the amide I mode, as extracted from different experimental measurements [Hamm 98, DeCamp 05] show that an ultimate accurate description of the VR of NMAD is still pending.

From a theoretical point of view, the intramolecular vibrational energy flow in biomolecules has also received a great deal of attention [Leitner 05, Leitner 10b] through different approaches including harmonic theories [Moritsugu 00, Segal 03, Yu 03, Yu 05, Fujisaki 05, Leitner 09, Piazza 09], Molecular Dynamics (MD) simulations [Leitner 05, Ota 05, Sharp 06, Nguyen 06b, Nguyen 06a, Kong 07, Kong 09a, Moritsugu 03, Ishikura 06, Schröder 09, Kandratsenka 09, Nguyen 10, Kobus 11], coarse-grained models [Chennubhotla 05, Piazza 09] and quantum methods [Yu 03, Gruebele 04, Fujisaki 07a, Fujisaki 08, Fujisaki 09, Schade 09a, Leitner 10a]. Despite this diversity of theoretical treatments, comparison between experimental and theoretical studies is still unsatisfactory because it faces the major difficulty that whereas experiments provide information on the energy transport spectroscopically from the vibrational modes which are active in the technique employed, most of the theoretical treatments discuss the energy flow in terms of residue-based models which, although shown to be quite useful in describing the spatial evolution of the energy [Ishikura 06, Kong 07, Kong 09a, Nguyen 10], are nor well suited for direct comparison with observed data since the residues are not the experimentally active units. In addition, the total content of vibrational energy of a biomolecule cannot be expressed as a sum of the individual contributions of the residues due to the potential energy couplings existing among them, which preclude a detailed and accurate quantification of the vibrational energy flow. Some methods have been proposed to address this problem based on the use of the ENM [Raff 88, Segal 03, Schröder 09, Jacob 09], which provide a separable description of the vibrational energy of the molecule at the equilibrium geometry. However, during the dynamics of a biomolecule in solution at room temperature, it frequently samples phase space regions dominated by strong intra- and intermolecular couplings that undermine the use of the ENMs. In this thesis we extend the methodology previously proposed by our group to analyze vibrational energy redistribution processes based on the use of the so-called Instantaneous Normal Modes (INM) [Bastida 10a, Bastida 10b, Kalstein 11], which permits to monitor the time-evolution of the energy stored in every INM of the molecule in solution during MD simulations. This method has been employed to analyze the vibrational energy relaxation for two different peptide models: *N*-methylacetamide and alanine dipeptide molecule.

CHAPTER 2

Methodology

In this chapter, we introduce the methods that have been applied in this thesis to analyze the vibrational energy relaxation and the vibrational spectroscopy properties of peptides in water solution. Firstly in Section 2.1, we provide a short note about Molecular Dynamics simulations of liquids. Then in Section 2.2 we present different methodologies that have been considered through this thesis to compute the potential energy function during the simulations. Later in Section 2.3 we discuss the normal mode analysis that has been employed in order to analyze the vibrational energy redistribution during the relaxation process. Finally in Section 2.4, we describe the computation of the Infrared (IR) spectrum and the analysis of the solvent induced shift on the frequency of the amide I band.

2.1 MOLECULAR DYNAMICS SIMULATION OF LIQUIDS

2.1.1 Initialization and periodic boundary condition

Molecular Dynamics MD simulations are in many respects very similar to real experiments. MD method generates a series of time-correlated points in phase space (a trajectory) by propagating a starting set of coordinates and velocities according to Newton's second equation by a series of finite time steps.

To start the simulation, we should assign initial positions and velocities to all particles in the system. Consider a system composed of N particles. The easiest way to establish the initial structure of a liquid whose density ρ, is assigning random positions to the N particles within a volume N/ρ. However, this stochastic procedure present serious practical disadvantages, as some particles can be very close together, so that the interaction energy between them is extremely high, a situation very unlikely in reality and which, moreover, difficult the integrations equations of motion of the system [Allen 87, Haile 97]. Therefore it is appropriate to put the particles initially in the positions of a crystal lattice, thereby

avoiding the incidental overlaps between them. This crystal lattice structure will melt at the start of the propagation of the system, since at typical temperatures and densities of the liquids, the solid state is not thermodynamically stable [Frenkel 96]. In principle any lattice can be chosen. It is found that the simulation results are practically independent of what is the initial lattice. Thus we use the simplest of all, the Face Centered Cubic (FCC) [Allen 87, Haile 97]. In the case of the velocities, the usual procedure [Allen 87, Frenkel 96, Haile 97] is to choose these velocities randomly within certain interval. Once assigned the initial velocities we must displace it through a factor, so that, the total momentum of the system is zero and there is no net translation, since we assume that the system is not subject to any external force. In addition, these velocities must be compatible with the macroscopic temperature of the system T_0, so it is necessary to scale their values.

An important aspect to consider when a MD simulation is performed is the number of particles that make up the system. Typically simulations that involve several hundred or at most a few thousand atoms are performed. MD programs run-time grows rapidly with the number of atoms in the system, mainly due to the evaluation of the forces between the atoms, which is why it is necessary to maintain such a small number as possible. The problem is that a system of such a small size (compared to the number of particles in one mole, on the order of 10^{23}) is not representative of a liquid, since the system is dominated by the effects of surface. For example, in a cube made up of 1000 atoms, approximately half of them are found on the surface of it. As a result, the liquid is surrounded by surfaces in which the molecules do not undergo the same forces as in the interior, which is not a realistic simulation of the liquid.

The problem is solved through the use of the so-called periodic boundary conditions [Allen 87, Haile 97]. This technique assumes that the cubic box that contains the system, the primary cell, is surrounding by replicas of itself in all direction, the cell image, forming an infinite network. These cells images contain the same atoms that the primary and, during a simulation, each cell images moves atoms in the same way as the atoms of the primary cell. Thus, if an atom of the primary cell moves through a boundary, its opposite face image enters the primary cell. In this way there are no limiting surfaces of the system. Figure 2.1 illustrates periodic boundary conditions in a two-dimensional system. While we have generated infinite periodic system, it is only necessary to store the data of the atoms of the primary cell, because the images can be easily deduce from them.

The implementation of periodic boundary conditions requires the assessment of forces exerted on each molecule by all other molecules of the system. If we consider a system whose primary cell contains N molecules and assume that the potential is expressed as the sum of interactions between pairs of molecules, then there are $N - 1$ terms in this sum. But in principle we should also include interactions with molecules of cell images. Therefore, this sum has therefore infinite terms, and in practice its assessment requires the realization of approaches. If the forces that operate are short-range, it can limit the number of terms of this sum considering that the molecule in question is located in the center of a cubic box of the same size as the original box and only interacts with molecules that are inside this box, i.e. with the closest images of the other $N - 1$ molecules. This is called the

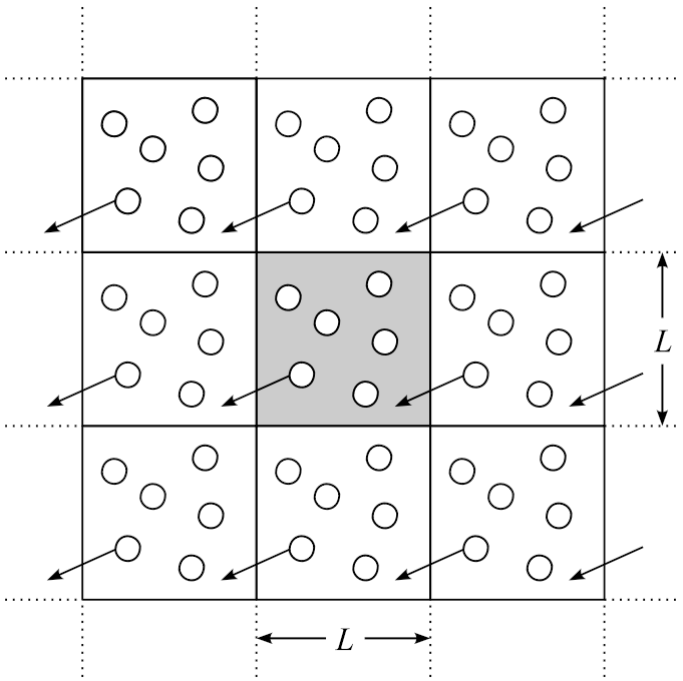

Figure 2.1: A two-dimensional periodic system.

minimum image convention [Allen 87], and is a natural consequence of the use of periodic boundary conditions. In the case of long range interaction potentials this approach cannot be applied, as is, since the forces are still intense around the typical lengths of the boxes used in MD simulations making necessary the use of special treatments as the Ewald sum for the electrostatic interactions [Allen 87].

2.1.2 Numerical integration of the equations of motion

Consider a system composed of N particles of mass m_i interacting by couples through a potential which depends on the distance between them $V(r_{ij})$. The Hamiltonian of the system is the sum of the kinetic and potential energies of all particles, which in Cartesian coordinates can be written as

$$H = T + V = \frac{1}{2} \sum_{i=1}^{N} \frac{\boldsymbol{P}_i^2}{m_i} + \sum_{i=1}^{N} \sum_{j>i}^{N} V(r_{ij}) \tag{2.1}$$

being $\boldsymbol{P}_i$ the linear momentum of the particle i, $\boldsymbol{P}_i = m_i \dot{\boldsymbol{r}}_i$, where the dot indicates the derivative with respect to time. The motion of each particle is typically determined by the second law of Newton

$$m_i \ddot{\boldsymbol{r}}_i = -\nabla_{\boldsymbol{r}_i} \sum_{\substack{j=1 \\ j1=i}}^{N} V(r_{ij}) = \boldsymbol{F}_i \qquad i = 1, \ldots, N \tag{2.2}$$

where $\ddot{\boldsymbol{r}}_i$ is the acceleration of the particle i and $\boldsymbol{F}_i$ is the force to act on it. Alternatively we can solve the Hamilton equations for the system

$$\dot{\boldsymbol{r}}_i = \boldsymbol{P}_i/m_i \tag{2.3a}$$

$$\dot{\boldsymbol{P}}_i = -\nabla_{\boldsymbol{r}_i} \sum_{\substack{j=1 \\ j1= \\ i}}^{N} V(r_{ij}) = \boldsymbol{F}_i \qquad i = 1, \ldots, N \tag{2.3b}$$

formed by a set of $6N$ coupled first order differential equations, $3N$ for positions and $3N$ for a moment.

The system is composed of particles whose potential energy varies continually over time, since each particle simultaneously interacts with many others, so that their paths do not follow straight lines and their velocities are not constant between collisions. Therefore the analytic resolution of the set of differential equations is impossible and consequently the resolution need to be addressed numerically.

The usual way is to use the so-called finite difference methods [Allen 87, Haile 97]. This is a problem of initial conditions, i.e. given positions and velocities at a time t, have to be obtained at a time $t + dt$. The basis of the method is to replace the infinitesimal time interval dt for an interval finite Δt, during which it is supposed that forces acting on the particles are constant. Thus, the equations of motion are solved step by step, integrating them to every interval Δt.

Most of the finite difference methods are based on the Taylor series expansion of the variable to propagate. Thus for example, for the component x position

$$x(t+\Delta t) = x(t) + \frac{dx(t)}{dt}\Delta t + \frac{1}{2}\frac{d^2x(t)}{dt^2}\Delta t^2 + \frac{1}{3!}\frac{d^3x(t)}{dt^3}\Delta t^3 + \cdots + \frac{1}{n!}\frac{d^nx(t)}{dt^n}\Delta t^n + \ldots \tag{2.4}$$

This Taylor series has infinite terms, then it has to be truncated to be applied. Thus, a method of integration where the Taylor series includes up to the term corresponding to the derivative n-th is said is a method of order n.

There is a large number of algorithms of integration [Allen 87, Frenkel 96, Haile 97] and each of them is appropriate or not according to the constituents of the particular study system, the type of existing interactions, the coordinate system used, etc. In the present thesis, we employ TINKER program version 5.0 [Ren 02, Ren 03] and Amber code, version 9 [Case 06] in order to run a MD simulations. In the former case velocity verlet algorithm [Allen 87, Frenkel 96, Haile 97] is used, however in the latter case leap frog algorithm is employed [Allen 87, Frenkel 96, Haile 97].

2.1.3 NVT and NVE ensembles

The initial conditions of a Molecular Dynamics simulations are far from thermodynamic equilibrium. Thus, it is necessary to execute the simulation over a period of time until reach thermodynamic equilibrium, what is commonly referred to equilibration. After this period and once it has reached thermodynamic equilibrium, they can generate the paths

and calculate different variables of interest for the study in particular you want to perform on the system. This is the period of simulation which called production or generation.

During the equilibration, the temperature of the system is maintained constant to ensure that the equilibrium is achieved to the desired temperature. To this end, the velocity rescaling approach is proposed [Haile 97] for the particles of the liquid at each step of simulation or every certain number of steps. In this case, the total energy of the system will not remain constant during the simulation, but the kinetic energy which will oscillate around a constant value. Some more sophisticated methods have been developed to perform constant temperature MD simulations [Allen 87, Frenkel 96] generating less drastic changes in the velocities such as Andersen [Andersen 80] and Berendsen [Berendsen 84] thermostats which have been employed in this thesis.

In simulations where the energy dissipated in the liquid is relatively small, for example, when introducing a little excited solute, artificial warming of the liquid in constant energy simulations is negligible. In this case, both simulations at constant energy and constant temperature yield the same results. In this situation it is preferable to perform the simulation in the period of constant energy generation, as the temperature fluctuates around the initial value to avoid introducing more or less arbitrary changes in the velocities of the atoms. In addition, it helps to follow the temporal evolution of the total energy of the system during the simulation to verify that it fluctuates around a constant value and thus verify the reliability of the simulation.

2.1.4 Calculation of the torsion angles

In geometry, a dihedral or torsion angle is the angle between two planes. Suppose that we have four atoms of a dihedral angle and they are forming two planes $\boldsymbol{m}$ and $\boldsymbol{n}$ (see Figure 2.2). Mathematically, the unsigned dihedral angle can be computed as

$$\varphi = \arccos \frac{\boldsymbol{m} \cdot \boldsymbol{n}}{|\boldsymbol{m}||\boldsymbol{n}|} \tag{2.5}$$

Looking at this equation sounded like if the calculation of the dihedral angle is quite simple. However, to obtain the distribution of the dihedral angles appearing in the Ramachandran plot, it is essential to figure out the right sign (positive or negative) of the torsion angle that cannot be derived just by using Eq. (2.5). We have found the method proposed by Bekker [Bekker 96] and Rainey [Rainey 03] as the most useful in this aspect. Let us consider four atoms $ijkl$ connected consecutively, being $\boldsymbol{r}_i, \boldsymbol{r}_j, \boldsymbol{r}_k$ and $\boldsymbol{r}_l$ their cartesian vectors. Bekker *et al* provides two different dihedral angle definitions, depending on the use of the dot or cross vector products. Based on the cross product definition, the dihedral angle φ (see Figure 2.3) is defined as

$$\varphi = \text{sign}(\varphi)\ \arccos(\hat{\boldsymbol{m}} \cdot \hat{\boldsymbol{n}}) \tag{2.6}$$

where

$$\boldsymbol{m} = \boldsymbol{r}_{ij} \times \boldsymbol{r}_{kj} \tag{2.7}$$

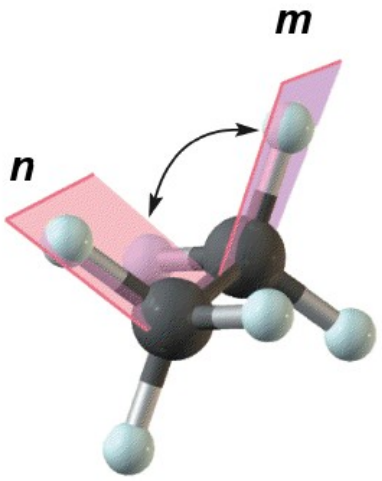

Figure 2.2: The dihedral angle between two planes $\boldsymbol{m}$ and $\boldsymbol{n}$.

$$\boldsymbol{n} = \boldsymbol{r}_{kj} \times \boldsymbol{r}_{kl} \tag{2.8}$$

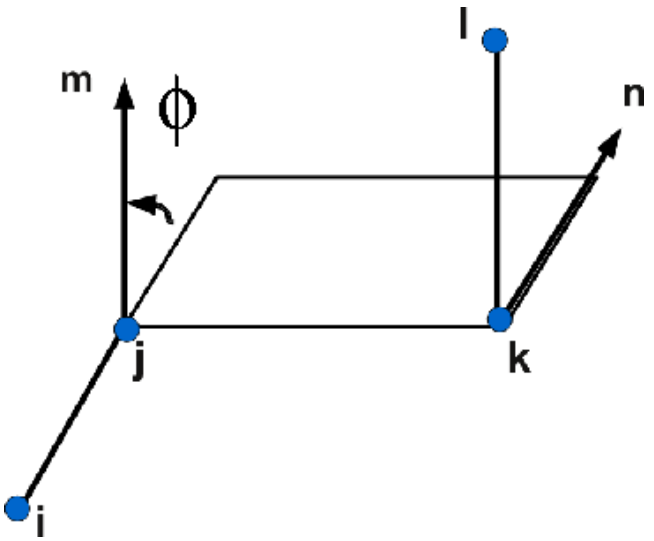

Figure 2.3: The dihedral angle φ defined by Eq. (2.6). $\boldsymbol{m}$ is normal to the i, j, k plane and $\boldsymbol{n}$ is normal to the j, k, l plane

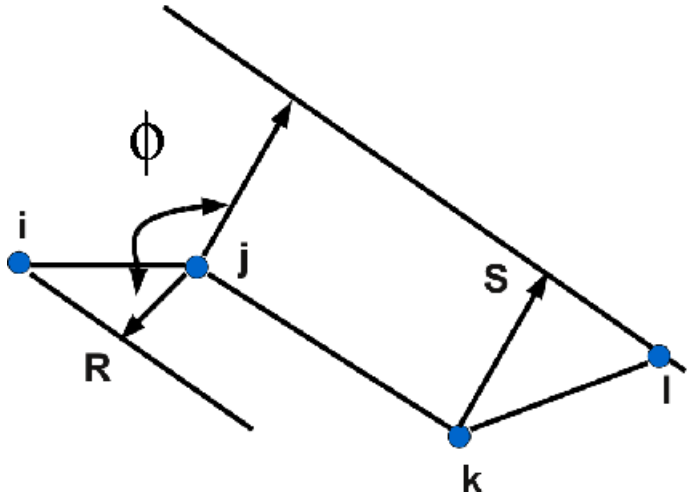

Figure 2.4: The definition of the dihedral angle φ in terms of the dot product Eq. (2.9)

being $\boldsymbol{r}_{ij} = \boldsymbol{r}_i - \boldsymbol{r}_j$, $r_{ij} = |\boldsymbol{r}_{ij}|$ and $\hat{\boldsymbol{m}} = \boldsymbol{m}/|\boldsymbol{m}|$. On the other side the definition of the dihedral angle φ in terms of dot products (see Figure 2.4) is

$$\varphi = \text{sign}(\varphi)\ \arccos(\hat{\boldsymbol{R}} \cdot \hat{\boldsymbol{S}}) \tag{2.9}$$

where

$$\boldsymbol{R} = \boldsymbol{r}_{ij} - (\boldsymbol{r}_{ij} \cdot \hat{\boldsymbol{r}}_{kj})\,\hat{\boldsymbol{r}}_{kj} \tag{2.10}$$

$$\boldsymbol{S} = \boldsymbol{r}_{lk} - (\boldsymbol{r}_{lk} \cdot \hat{\boldsymbol{r}}_{kj})\,\hat{\boldsymbol{r}}_{kj} \tag{2.11}$$

Th sign (φ) is given either by

$$\text{sign}(\varphi) = \text{signum}(\boldsymbol{r}_{kj} \cdot (\boldsymbol{m} \times \boldsymbol{n})) \tag{2.12}$$

or by a simpler definition

$$\text{sign}(\varphi) = \text{signum}(\boldsymbol{r}_{ij} \cdot \boldsymbol{n}) \tag{2.13}$$

where the signum function is an odd mathematical function that extracts the sign of a real number. For a real number signum(x) is varies between -1 for a negative number, 0 for the number zero and +1 for a positive number.

Our test shows that, the dihedral angle as obtained from cross or dot product give the same value and the sign calculated using Eq. (2.12) and Eq. (2.13) is the same. In our analysis we have chosen the dot product method to compute the dihedral angle and Eq. (2.13) to determine the sign of the dihedral angle.

2.2 POTENTIAL ENERGY SURFACE

2.2.1 Molecular mechanics force fields

One of the major problems to analyze the potential energy surface for any molecule, is the calculation of the electronic energy for different nuclear configurations. In Molecular Mechanics (MM) force fields, this step is bypassed by writing the electronic energy as a parametric function of the nuclear coordinates, and by fitting the parameters to experimental or higher level *ab-initio* data. The building blocks in the MM force fields are atoms, i.e. electrons are not considered as individual particles. This means that bonding information must be provided explicitly, rather than being the result of solving the electronic Schrödinger equation. MM force fields are widely used for the investigation of a variety of properties of biological macromolecules. In combinations with growing computational resources, these methods allow for atomic detailed simulations on heterogeneous systems that may contains hundreds or even thousands of atoms.

Most of the MM force fields for simulations of biomolecules are described by an expression of the form [Cornell 95, Duan 03]

$$V = \sum_{\text{bond}} K_r(r - r_{\text{eq}})^2 + \sum_{\text{angles}} K_\theta(\theta - \theta_{\text{eq}})^2 + \sum_{\text{dihedrals}} \frac{V_n}{2}[1 + \cos(n\varphi - \delta_n)] + \sum_{i<j} \left\{ \frac{A_{ij}}{r_{ij}^{12}} - \frac{B_{ij}}{r_{ij}^{6}} + \frac{q_i q_j}{E r_{ij}} \right\} \tag{2.14}$$

The first three terms comprise the intramolecular or bonded interactions, where the bonds and the angles are represented by a simple harmonic expression and the dihedral energies are modeled by a Fourier expansion. K_r and K_θ are the harmonic force constants for the bonds r and bond angles θ respectively, r_{eq} and θ_{eq} are the equilibrium bond lengths and bond angles. φ are the dihedral angles, V_n are the corresponding force constant and the phase angles δ_n take values of either 0° or 180°. The last term accounts for the intermolecular or nonbonded interactions which are calculated for all atom pairs that are either separated by more than three bonds or are not bonded. The nonbonded part of the potential is represented by Van der Waals (VDW) (A_{ij}) and London dispersion terms (B_{ij}) and coulomb interactions between partial atomic charges (q_i and q_j). r_{ij} is the distance between the particles, and E is the dielectric constant that takes into account of the effect of the medium that is not explicitly represented and usually equals to 1.0 in a typical solvated environment where solvent is represented explicitly.

Let us focus our attention on the nonbonded terms, in particularly the Lennard-Jones (LJ) potential. In CHARMM [MacKerell 98] and AMBER [Cornell 95] force fields this term is defined as

$$E_{\text{LJ}} = \sum_{i<j} E_{ij} \left\{ \frac{R_{\min_{ij}}^{12}}{r_{ij}^{12}} - \frac{R_{\min_{ij}}^{6}}{r_{ij}^{6}} \right\} \tag{2.15}$$

where E_{ij} is the LJ well depth and the values are obtained via the geometric mean $E_{ij} = \sqrt{E_{ii}E_{jj}}$ and $R_{\min_{ij}}$ is the minimum interaction radius used to treat the VDW interaction and the values are based on arithmetic mean $R_{\min_{ij}} = (R_{\min_{ii}} + R_{\min_{jj}})/2$ where E_{ii} and $R_{\min_{ii}}$ are obtained for individual atom types. However, in OPLS-AA [Jorgensen 96, Kaminski 01] force field the LJ is defined as

$$E_{\text{LJ}} = \sum_{i<j} 4E_{ij} \left(\frac{\sigma_{ij}^{12}}{r_{ij}^{12}} - \frac{\sigma_{ij}^{6}}{r_{ij}^{6}} \right) \tag{2.16}$$

where σ_{ij} is the finite distance at which the interparticle potential is zero and standard combining rules are used to compute these values $\sigma_{ij} = \sqrt{\sigma_{ii}\sigma_{jj}}$. If we differentiate Eq. (2.16) with respect to r_{ij} and set the derivative equal to zero in order to find the minimum in the LJ potential one obtains

$$R_{\min_{ij}} = 2^{1/6}\sigma_{ij} \tag{2.17}$$

2.2.2 Born-Oppenheimer Molecular Dynamics

In systems where polarizability and charge transfer effects are not negligible, and when the chemical reactivity of some species needs to be taken into account, a description based on non-polarizable classical force fields is not suitable. Although new generation polarizable force fields are more and more employed [Warshel 07, Piquemal 12] (and references therein) their parametrization is often not transferable, and it requires a laborious validation process. In addition, intermolecular charge transfer is still rarely taken into account, and, though a few exceptions exist (see for example Ref. [Pinilla 12]), reactivity cannot generally be treated since the quantum nature of the electrons is not explicitly considered.

Molecular dynamics methods based on a quantum description of the electrons have become increasingly popular after the development of the Car-Parrinello approach [Car 85]. The forces acting on the nuclei are evaluated from electronic structure calculations that are performed on the fly along the trajectory, thus considering the electronic degrees of freedom explicitly. The dynamics of the nuclei follows the classical equations of motion, whereas the electronic degrees of freedom are either propagated (in the so called extended Lagrangian approaches [Car 85]) or optimized (in Born-Oppenheimer molecular dynamics [Marx 00]). In the first case, the electronic wave function or density is not converged at each time step, while in the latter case convergency is assured by a self-consistent field (SCF) iteration procedure. The electronic Hamiltonian can be treated at different levels of quantum theory, such as Density Functional Theory, Hartree-Fock, Generalized Valence Bond, Complete Active Space SCF, Full Configuration Interaction and Semiempirical (see Ref. [Marx 00] for a review). The main advantage in using semiempirical (SE) electronic structure calculations to solve the Schrödinger equation for the electronic wave function resides in the much lower calculation time compared to ab initio based approaches, thus allowing the treatment of systems of large size over much longer time scales.

2.2.2.1 Semiempirical electronic Hamiltonians

In this thesis we have employed a semiempirical Born-Oppenheimer MD scheme developed in Nancy (SEBOMD [Monard 05]). According to this approach, at each time step the Schrödinger equation for the electronic part is solved at a QM level through SCF iterations, obtaining the energy, the gradient and therefore the forces acting on the system. The nuclei dynamics is propagated by classical equations of motions. The system is included in a simulation box, and periodic boundary conditions are used, exactly as in the MM MD case. Long range electrostatics can be treated according to modified Ewald schemes [Nam 05].

In the following, we shall give a few insights on the level of quantum chemistry that was used to describe the electronic Hamiltonian. We used molecular orbitals (MOs) based semiempirical methods relying on the Hartree-Fock approximation and on a variational solution of the Schrödinger equation. The Hartree-Fock equations are solved iteratively through an SCF procedure and the wave function of the system is expanded in terms of molecular orbitals that are given by a linear combination of atomic orbitals.

In MOs based semiempirical methods, some approximations are introduced to neglect or simplify the calculation of the matrix elements of the Fock matrix. First of all, only valence electrons are explicitly considered, while a minimal basis set of Slater MOs is built for the valence electrons. Overlap integrals are neglected, as well as all bi-electron integrals over three or four centers. Those that are on one or two centers are fitted to experimental data in the gas phase collected for a large training set of molecules.

In addition, we used semiempirical methods based on the Neglect of Diatomic Differential Overlap (NDDO) hypothesis, according to which the overlap between the atomic orbitals belonging to different atoms is neglected. In particular, we used the PM3 method [Stewart 89], originally introduced to improve semiempirical techniques such as the MNDO [Dewar 77] and AM1 [Dewar 85] methods with respect to the description of the interactions between different cores (a core is a nucleus plus the core electrons of an atom). However, the PM3 Hamiltonian still maintains a few shortcomings, especially for intermolecular interactions. For instance, the potential energy surface of the water dimer is not well described, and unphysical artifacts are obtained for H-H interactions at short distance [Harb 04]. This method has been recently improved by means of a careful reparametration of the interaction energies based on high level ab initio calculations on a large set of complexes, leading to the development of the PIF and the MAIS methods [Berenal-Uruchurtu 00].

A correct representation of the intermolecular interactions is especially important in the condensed phase. Therefore, our SEBOMD simulations were performed by using the PM3-PIF electronic Hamiltonian. The SEBOMD code developed in Nancy allows for an additional saving in computational costs thanks to the application of a Divide and Conquer strategy [Yang 95, Dixon 96].

In this framework, the whole system is divided in smaller overlapping subsystems, for each of which the Fock matrix is calculated and diagonalized through standard techniques according to the self-consistent field (SCF) scheme. This ensures that the electronic density converges at each step of the simulation, and that the dynamics follows the Born-

Oppenheimer potential energy surface [Herbert 05, Niklasson 06]. The full Fock matrix is built using the minimum image convention for all direct interactions inside the periodic box (direct sum). The Ewald reciprocal sum is incorporated as a correction to the Fock matrix in a way similar to the one proposed by Nam *et al* [Nam 05]: atomic partial charges computed from the semiempirical wave function define an Ewald field in the reciprocal space that can be incorporated in the core Hamiltonian as long as derivatives of these atomic charges with respect to the density matrix elements are defined. In our implementation, Ewald summation can be performed by using either Mulliken or CM1 [Storer 95] atomic charges to represent the long-range electrostatic field that self-consistently polarizes the semiempirical wave function.

A typical SCF procedure proceeds as follows: from an initial guess for the density matrix, (1) the atomic charges are computed (Mulliken or CM1 charges); (2) the minimum image Fock matrix is perturbed by the Ewald field (i.e., both the minimum image Fock matrix and the Ewald field are derived from the same density matrix); (3) the total Fock matrix is diagonalized to obtain the wave function coefficients; (4) a new density matrix is built from the coefficients of the molecular orbitals; (5) check on convergence, and back to 1) if the procedure has not converged yet.

During the MD simulation, the different sets of charges can be derived from the wave function evaluated at each time step. We also evaluated CM2 [Li 98] partial charges. We recall that CM1 and CM2 charges are parametrized to obtain reliable charge-dependent molecular properties, in particular the molecular dipole moment.

During the SEBOMD simulation in the gas phase, the dipole moment of the *N*-methylacetamide (NMA) can be obtained by applying the dipole moment operator to the wave function of the molecule. However, the same procedure cannot be applied to NMA in water, due to the delocalization of the wave function over the entire system. This issue has already been discussed in a previous paper [Monard 05], and we adopt here the same approximation proposed there. We evaluate the dipole moment of NMA based on partial atomic charges (instantaneous Mulliken, CM1 and CM2 charges) and instantaneous atomic positions, exactly as it is done for the classical MM simulations.

2.3 NORMAL MODES ANALYSIS

Recently, our research group [Bastida 10a, Bastida 10b] has carried out the nonequilibrium molecular dynamics (MD) simulation of the deuterated *N*-methylacetamide molecule in liquid deuterated water (NMAD/D_2O), to study the vibrational relaxation of the excited amide I mode and the C-H stretching mode of the NMAD molecule. In these works, the NMAD motions were described using the set of coordinates $\{\boldsymbol{R}_{\mathrm{CM}}, \boldsymbol{q}, \boldsymbol{Q}^{\mathrm{e}}\}$ where, $\boldsymbol{R}_{\mathrm{CM}}$ is the center of mass vector, $\boldsymbol{q} = (q_1, q_2, q_3, q_4)$ are the quaternions that specify the rotation of the molecule, and $\boldsymbol{Q}^{\mathrm{e}} = (Q^{\mathrm{e}}_1, \ldots, Q^{\mathrm{e}}_N)$ are the equilibrium normal modes (ENMs) that describe the vibrational motion. On the other side, the D_2O motions were described using

the atomic cartesian coordinates. In these studies, subroutines of the TINKER modeling package have been used within our codes to evaluate the forces and the potential energy function. The use of the ENMs to describe the vibrational motion of the NMAD molecule makes these codes highly specific and make difficult the application of the INM analysis to the results provided by other modeling packages. Therefore in the present thesis we have generalized the INM analysis so that it can be easily applied by using directly the input and output file formats used by the standard MD package. Since these codes use atomic cartesian coordinates to describe the molecular system the assigment method was also reformatted and by pass generalized to deal with flexible biomolecules.

2.3.1 Cartesian coordinate systems

The total energy of the system can be expressed as

$$E_{\mathrm{tot}} = E_{\mathrm{s}} + E_{\mathrm{v}} + V_{\mathrm{s/v}} \tag{2.18}$$

where E_{s}, E_{v} are the energy of the solute and solvent respectively and $V_{\mathrm{s/v}}$ is the intermolecular potential energy between the solute and the solvent molecules.

The total energy of solute is given by

$$E_{\mathrm{s}} = T_{\mathrm{s}} + V_{\mathrm{s}} \tag{2.19}$$

where T_{s} and V_{s} are the kinetic and the intramolecular potential energy of the solute respectively. The kinetic energy after neglecting the vibrational rotational coupling [Levine 75, Vikhrenko 99, Fujisaki 09] is expressed as the sum of translational, vibrational and rotational contributions

$$T_{\mathrm{s}} = T_{\mathrm{trans}} + T_{\mathrm{vib}} + T_{\mathrm{rot}} \tag{2.20}$$

To analyze the vibrational energy, which is the main target of the present study, the overall translational and rotational energies have to be removed from the total kinetic energy.

The translational kinetic energy corresponds to the motion of the whole system and it is expressed in terms of the conjugate momentum of the center of mass vector

$$\boldsymbol{R}_{\mathrm{CM}} = \frac{1}{M_{\mathrm{s}}} \sum_{i=1}^{N_{\mathrm{s}}} m_i \boldsymbol{r}_i^{\mathrm{lab}} \tag{2.21}$$

$$\boldsymbol{P}_{\mathrm{CM}} = \sum_{i=1}^{N_{\mathrm{s}}} \boldsymbol{p}_i^{\mathrm{lab}} \tag{2.22}$$

as follows

$$T_{\mathrm{trans}} = \frac{|\boldsymbol{P}_{\mathrm{CM}}|^2}{2 M_{\mathrm{s}}} \tag{2.23}$$

where N_{s} is the number of atoms of the solute molecule, M_{s} is the total mass, $\boldsymbol{r}_i^{\mathrm{lab}}$ and $\boldsymbol{p}_i^{\mathrm{lab}}$ are the atomic vectors and their conjugate momenta in a laboratory fixed coordinate system respectively. In order to separate the translational motion of the solute, we use

a space fixed (sf) coordinate system which origin is at the center of mass of the solute molecule

$$\boldsymbol{r}_i^{\mathrm{sf}} = \boldsymbol{r}_i^{\mathrm{lab}} - \boldsymbol{R}_{\mathrm{CM}} \tag{2.24}$$

$$\boldsymbol{p}_i^{\mathrm{sf}} = \boldsymbol{p}_i^{\mathrm{lab}} - \boldsymbol{P}_{\mathrm{CM}} \tag{2.25}$$

To separate the rotational motion we can define a body fixed (bf) coordinate system which rotates with the solute molecule. In order to specify the orientation of the bf system we firstly calculate the instantaneous moment of inertia tensor in the sf frame

$$\mathbf{I}^{\mathrm{sf}} = \begin{bmatrix} I_{xx}^{\mathrm{sf}} & I_{xy}^{\mathrm{sf}} & I_{xz}^{\mathrm{sf}} \\ I_{yx}^{\mathrm{sf}} & I_{yy}^{\mathrm{sf}} & I_{yz}^{\mathrm{sf}} \\ I_{zx}^{\mathrm{sf}} & I_{zy}^{\mathrm{sf}} & I_{zz}^{\mathrm{sf}} \end{bmatrix} \tag{2.26}$$

which elements are defined as

$$I_{xx}^{\mathrm{sf}} = \sum_{i=1}^{N_{\mathrm{s}}} m_i((y_i^{\mathrm{sf}})^2 + (z_i^{\mathrm{sf}})^2) \tag{2.27a}$$

$$I_{yy}^{\mathrm{sf}} = \sum_{i=1}^{N_{\mathrm{s}}} m_i((x_i^{\mathrm{sf}})^2 + (z_i^{\mathrm{sf}})^2) \tag{2.27b}$$

$$I_{zz}^{\mathrm{sf}} = \sum_{i=1}^{N_{\mathrm{s}}} m_i((x_i^{\mathrm{sf}})^2 + (y_i^{\mathrm{sf}})^2) \tag{2.27c}$$

$$I_{xy}^{\mathrm{sf}} = I_{yx}^{\mathrm{sf}} = -\sum_{i=1}^{N_{\mathrm{s}}} m_i x_i^{\mathrm{sf}} y_i^{\mathrm{sf}} \tag{2.27d}$$

$$I_{xz}^{\mathrm{sf}} = I_{zx}^{\mathrm{sf}} = -\sum_{i=1}^{N_{\mathrm{s}}} m_i x_i^{\mathrm{sf}} z_i^{\mathrm{sf}} \tag{2.27e}$$

$$I_{yz}^{\mathrm{sf}} = I_{zy}^{\mathrm{sf}} = -\sum_{i=1}^{N_{\mathrm{s}}} m_i y_i^{\mathrm{sf}} z_i^{\mathrm{sf}} \tag{2.27f}$$

Then, let $\boldsymbol{A}$ be the matrix of eigenvectors of $\boldsymbol{I}^{\mathrm{sf}}$; since $\boldsymbol{I}^{\mathrm{sf}}$ is symmetric, $\boldsymbol{A}$ can be chosen to be orthogonal. Then we have

$$\boldsymbol{A}^{\dagger}\, \boldsymbol{I}^{\mathrm{sf}}\, \boldsymbol{A} = \boldsymbol{I}_{\mathrm{abc}} \tag{2.28}$$

where the diagonal elements of $\boldsymbol{I}_{\mathrm{abc}}$ are the eigenvalues which are known as the principle moments of inertia $I_{\mathrm{a}}, I_{\mathrm{b}}$ and I_{c}. The transpose of the orthogonal matrix of eigenvectors $\boldsymbol{A}$ gives the direction cosines of the (abc) principle axis system with respect to the sf coordinate axes [Levine 75, Goldstein 02]. Finally, these eigenvectors are used as an orthogonal transformation from coordinates fixed in the space (non rotating) to coordinates fixed in the molecule (rotating)

$$\begin{bmatrix} x^{\mathrm{bf}} \\ y^{\mathrm{bf}} \\ z^{\mathrm{bf}} \end{bmatrix} = \begin{bmatrix} a_{11} & a_{21} & a_{31} \\ a_{12} & a_{22} & a_{32} \\ a_{13} & a_{23} & a_{33} \end{bmatrix} \begin{bmatrix} x^{\mathrm{sf}} \\ y^{\mathrm{sf}} \\ z^{\mathrm{sf}} \end{bmatrix} \tag{2.29}$$

which can be written as

$$\boldsymbol{r}^{\mathrm{bf}} = \boldsymbol{A}^{\dagger} \cdot \boldsymbol{r}^{\mathrm{sf}} \tag{2.30}$$

and the corresponding momenta are given by

$$\boldsymbol{p}^{\mathrm{bf}} = \boldsymbol{A}^{\dagger} \cdot \boldsymbol{p}^{\mathrm{sf}} \tag{2.31}$$

At this point, it seems that we would be able to reproduce the coordinates in the body fixed frame. However, we note that the matrix $\boldsymbol{A}$ defined in Eq. (2.28) is not unique. Any of the three eigenvectors can be multiply by -1 without change of the eigenvalues. Therefore we have different bf systems which provide the same principal moments of inertia. Since our INM analysis is based on the ENMs defined at the equilibrium geometry using a given bf system, we need to use during the simulations bf systems attached to the molecule in the same way that the bf system originally used to define the ENMs.

To solve this problem we firstly obtain the $\boldsymbol{A}$ matrix by numerical diagonalization of the inertia tensor. Then we search for an atom in the peptide skeleton which absolute value of one x bf cartesian coordinate at the equilibrium geometry is high. We calculate the same coordinate in the present configuration of the molecule using the $\boldsymbol{A}$ matrix previously calculated. If the two values of the coordinate have opposite signs we consider that the orientation of the bf x-axis is wrong and consequently we multiply the first column of $\boldsymbol{A}$ by -1. We repeat the same procedure for the y coordinates. However, in our case, the values of $\boldsymbol{z}^{\mathrm{bf}}$ at the equilibrium geometry are very small, due to the perpendicularity of the $\boldsymbol{z}$ axis on the peptide bond. To overcome on this problem, firstly we consider the $\boldsymbol{i}^{\mathrm{bf}}, \boldsymbol{j}^{\mathrm{bf}}, \boldsymbol{k}^{\mathrm{bf}}$ unit vectors are given by

$$\boldsymbol{i}^{\mathrm{bf}} = \begin{bmatrix} 1 \\ 0 \\ 0 \end{bmatrix} \qquad \boldsymbol{j}^{\mathrm{bf}} = \begin{bmatrix} 0 \\ 1 \\ 0 \end{bmatrix} \qquad \boldsymbol{k}^{\mathrm{bf}} = \begin{bmatrix} 0 \\ 0 \\ 1 \end{bmatrix} \tag{2.32}$$

Then, we transform these to the space fixed frame

$$\boldsymbol{i}^{\mathrm{sf}} = \boldsymbol{A} \cdot \boldsymbol{i}^{\mathrm{bf}} \tag{2.33}$$

$$\boldsymbol{j}^{\mathrm{sf}} = \boldsymbol{A} \cdot \boldsymbol{j}^{\mathrm{bf}} \tag{2.34}$$

$$\boldsymbol{k}^{\mathrm{sf}} = \boldsymbol{A} \cdot \boldsymbol{k}^{\mathrm{bf}} \tag{2.35}$$

taking in our account that the first two columns in the rotation matrix $\boldsymbol{A}$ have been already modified. For a clockwise coordinate system the cross product for the three unit vectors is

$$\boldsymbol{i}^{\mathrm{sf}} \times \boldsymbol{j}^{\mathrm{sf}} = \boldsymbol{k}^{\mathrm{sf}} \tag{2.36}$$

Then if the $\boldsymbol{k}^{\mathrm{sf}}$ vector obtained using Eq. (2.36) satisfies Eq. (2.35) the orientation of the bf z-axis is right. In the opposite case we multiply the third column of the matrix $\boldsymbol{A}$ by -1. Following the procedure described above, the bf coordinates of the atoms of the peptide can be determined unambiguously at any time during the simulation.

2.3.2 Equilibrium normal modes

Normal mode analysis is a direct way to analyze vibrational motions. The starting point for the normal mode analysis is one particular stable conformation of the system that represents a minimum of the potential energy surface. In order to analyze the solute vibrational energy [Requena 04], we define the mass weighted cartesian displacement coordinates with respect to body fixed coordinate system as follows

$$\begin{aligned} q_1^{\mathrm{bf}} &= \sqrt{m_1}(x_1^{\mathrm{bf}} - x_{1,e}^{\mathrm{bf}}), & q_2^{\mathrm{bf}} &= \sqrt{m_1}(y_1^{\mathrm{bf}} - y_{1,e}^{\mathrm{bf}}), & q_3^{\mathrm{bf}} &= \sqrt{m_1}(z_1^{\mathrm{bf}} - z_{1,e}^{\mathrm{bf}}) \\ q_4^{\mathrm{bf}} &= \sqrt{m_2}(x_2^{\mathrm{bf}} - x_{2,e}^{\mathrm{bf}}), & q_5^{\mathrm{bf}} &= \sqrt{m_2}(y_2^{\mathrm{bf}} - y_{2,e}^{\mathrm{bf}}), & q_6^{\mathrm{bf}} &= \sqrt{m_2}(z_2^{\mathrm{bf}} - z_{2,e}^{\mathrm{bf}}) \end{aligned}$$

$$q_{3N_s-2}^{\mathrm{bf}} = \sqrt{m_{N_s}}(x_{N_s}^{\mathrm{bf}} - x_{N_s,e}^{\mathrm{bf}}), \quad q_{3N_s-1}^{\mathrm{bf}} = \sqrt{m_{N_s}}(y_{N_s}^{\mathrm{bf}} - y_{N_s,e}^{\mathrm{bf}}), \quad q_{3N_s}^{\mathrm{bf}} = \sqrt{m_{N_s}}(z_{N_s}^{\mathrm{bf}} - z_{N_s,e}^{\mathrm{bf}}) \tag{2.37}$$

as well as their conjugate momenta given by

$$\begin{aligned} \dot{q}_1^{\mathrm{bf}} &= \sqrt{m_1}\,\dot{x}_1^{\mathrm{bf}}, & \dot{q}_2^{\mathrm{bf}} &= \sqrt{m_1}\,\dot{y}_1^{\mathrm{bf}}, & \dot{q}_3^{\mathrm{bf}} &= \sqrt{m_1}\,\dot{z}_1^{\mathrm{bf}} \\ \dot{q}_4^{\mathrm{bf}} &= \sqrt{m_2}\,\dot{x}_2^{\mathrm{bf}}, & \dot{q}_5^{\mathrm{bf}} &= \sqrt{m_2}\,\dot{y}_2^{\mathrm{bf}}, & \dot{q}_6^{\mathrm{bf}} &= \sqrt{m_2}\,\dot{z}_2^{\mathrm{bf}} \end{aligned}$$

$$\dot{q}_{3N_s-2}^{\mathrm{bf}} = \sqrt{m_{N_s}}\,\dot{x}_{N_s}^{\mathrm{bf}}, \quad \dot{q}_{3N_s-1}^{\mathrm{bf}} = \sqrt{m_{N_s}}\,\dot{y}_{N_s}^{\mathrm{bf}}, \quad \dot{q}_{3N_s}^{\mathrm{bf}} = \sqrt{m_{N_s}}\,\dot{z}_{N_s}^{\mathrm{bf}} \tag{2.38}$$

where $x_{i,e}^{\mathrm{bf}}$, $y_{i,e}^{\mathrm{bf}}$, $z_{i,e}^{\mathrm{bf}}$ are the corresponding equilibrium values. The ENMs are defined as the following linear combinations of the mass weighted cartesian displacement coordinates and momenta

$$Q_j^e = \sum_{i=1}^{3N_s} l_{ij}^{\mathrm{ENM}}\, q_i^{\mathrm{bf}} \qquad j = 1, \ldots 3N_s \tag{2.39}$$

$$\dot{Q}_j^e = \sum_{i=1}^{3N_s} l_{ij}^{\mathrm{ENM}}\, \dot{q}_i^{\mathrm{bf}} \qquad j = 1, \ldots 3N_s \tag{2.40}$$

where l_{ij}^{ENM} are the elements of the orthogonal eigenvector matrix $\boldsymbol{L}^{\mathrm{ENM}}$ that diagonalizes the mass weighted hessian matrix $\boldsymbol{U}^{\mathrm{bf}}$ calculated at the solute equilibrium configuration,

$$\boldsymbol{L}^{\mathrm{ENM}\,\dagger}\, \boldsymbol{U}^{\mathrm{bf}}\, \boldsymbol{L}^{\mathrm{ENM}} = \boldsymbol{\Lambda}^{\mathrm{ENM}} \tag{2.41}$$

where

$$u_{ij}^{\mathrm{bf}} = u_{ji}^{\mathrm{bf}} = \left(\frac{\partial^2 V_s}{\partial q_i^{\mathrm{bf}}\, \partial q_j^{\mathrm{bf}}} \right)_e \tag{2.42}$$

and $\boldsymbol{\Lambda}^{\mathrm{ENM}}$ is the diagonal eigenvalue matrix. The six lowest eigenvalues, that we consider to be $(\lambda_{3N_s-5}^{\mathrm{ENM}}, \ldots, \lambda_{3N_s}^{\mathrm{ENM}})$, are null and correspond to the rotational and translational motion of the molecule. For the remaining $3N_s - 6$ eigenvalues we can define the vibrational frequency for each individual ENM as

$$\nu_i^{\mathrm{ENM}} = \sqrt{\lambda_i^{\mathrm{ENM}}}/2\pi \qquad i = 1, \ldots, 3N_s - 6 \tag{2.43}$$

If we neglect the third and higher order terms in the expansion of the solute intramolecular potential energy, the solute vibrational energy is then given as the sum of harmonic terms for each ENM

$$E_{\mathrm{s}}^{\mathrm{vib}} = \frac{1}{2}\sum_{i=1}^{3N_{\mathrm{s}}-6}(\dot{Q}_i^e)^2 + \frac{}{2}\sum_{i=1}^{3N_{\mathrm{s}}-6}\lambda_i^e (Q_i^e)^2 \tag{2.44}$$

2.3.3 Instantaneous normal modes

The fundamental restriction of Eq. (2.44) is its limitation to describe the vibrational motion of the molecule at configurations close to the equilibrium geometry i.e. ENMs are not well suited to the study of conformations far away from the equilibrium geometry [Cui 06]. During the relaxation of the initially excited jth normal mode, the molecule of solute may explore regions of the phase space which are far away from the equilibrium geometry due to its proper thermal motion, to the energy fluxes originated in the relaxation and to the intermolecular interaction with the solvent molecules [Frauenfelder 91, Frauenfelder 97]. The coupling between the ENMs are then enhanced, making it eventually difficult to quantify the energy stored in each individual normal mode [Nguyen 03]. A convenient way of tackling this problem is to use the instantaneous normal modes (INMs), to analyze the dynamics of the system [Buchner 92, Keyes 97, Stratt 01].

The INMs are defined as the eigenvectors of the mass weighted cartesian hessian matrix of the total potential energy V including intra and intermolecular interactions computed at snapshot configurations generated during the MD simulations of the system. These modes provide an instantaneous decoupled second order description of the vibration motions of the solute molecule as it evolves over time. In order to relate the INMs with the ENMs, we firstly expand the potential energy in a power series of the ENMs about the configuration of the molecule at a given time t_0, as follows [Stratt 01, Nguyen 03, Bastida 10a, Kalstein 11]

$$\begin{aligned} V &= V(Q_i^{\mathrm{e}}(t_0)) + \sum_{i=1}^{3N_{\mathrm{s}}-6} K_i\,(Q_i^{\mathrm{e}} - Q_i^{\mathrm{e}}(t_0)) \\ &\quad + \frac{1}{2}\sum_{i=1}^{3N_{\mathrm{s}}-6}\sum_{j=1}^{3N_{\mathrm{s}}-6} K_{ij}\,(Q_i^{\mathrm{e}} - Q_i^{\mathrm{e}}(t_0))(Q_j^{\mathrm{e}} - Q_j^{\mathrm{e}}(t_0)) + \ldots \end{aligned} \tag{2.45}$$

where K_i and K_{ij} are defined as

$$K_i = \left.\frac{\partial V}{\partial Q_i^{\mathrm{e}}}\right|_{Q_i^{\mathrm{e}}(t_0)} \tag{2.46}$$

$$K_{ij} = \left.\frac{\partial^2 V}{\partial Q_i^{\mathrm{e}}\partial Q_j^{\mathrm{e}}}\right|_{Q_i^{\mathrm{e}}(t_0),Q_j^{\mathrm{e}}(t_0)} \qquad i,j = 1,\ldots,3N_{\mathrm{s}} - 6 \tag{2.47}$$

Then the ENM hessian matrix Eq. (2.47) is diagonalized

$$\boldsymbol{L}^{\mathrm{INM}\dagger}\,\boldsymbol{K}\,\boldsymbol{L}^{\mathrm{INM}} = \boldsymbol{\Lambda}^{\mathrm{INM}} \tag{2.48}$$

where $\boldsymbol{L}^{\mathrm{INM}}$ and $\boldsymbol{\Lambda}^{\mathrm{INM}}$ are the eigenvector and eigenvalue matrixes respectively. The eigenvalues provide the vibrational frequencies of the INMs as,

$$\nu_i^{\mathrm{INM}} = \sqrt{\lambda_i^{\mathrm{INM}}}/2\pi \qquad i = 1, \ldots, 3N_{\mathrm{s}} - 6 \tag{2.49}$$

In addition the eigenvector matrix defines the relationship between the INMs and the ENMs [Bastida 10a]

$$Q_j^{\mathrm{INM}} = \sum_{i=1}^{3N_{\mathrm{s}}-6} l_{ij}^{\mathrm{INM}} \left(Q_i^{\mathrm{e}} - Q_i^{\mathrm{e}}(t_0)\right) \tag{2.50}$$

and the corresponding momenta

$$\dot{Q}_j^{\mathrm{INM}} = \sum_{i=1}^{3N_{\mathrm{s}}-6} l_{ij}^{\mathrm{INM}} \dot{Q}_i^{\mathrm{e}} \tag{2.51}$$

Since the $\boldsymbol{L}^{\mathrm{INM}}$ matrix is orthonormal, we can conversely express the ENMs in terms of the INMs

$$Q_i^{\mathrm{e}} = \sum_{j=1}^{3N_{\mathrm{s}}-6} l_{ij}^{\mathrm{INM}} Q_j^{\mathrm{INM}} + Q_i^{\mathrm{e}}(t_0) \tag{2.52}$$

By substituting this expression into Eq. (2.45) we obtain

$$V \approx V(Q_i^{\mathrm{e}}(t_0)) + \sum_{i=1}^{3N_{\mathrm{s}}-6} K_i \sum_{j=1}^{3N_{\mathrm{s}}-6} l_{ij}^{\mathrm{INM}} Q_j^{\mathrm{INM}} \tag{2.53}$$

$$+ \frac{1}{2} \sum_{i=1}^{3N_{\mathrm{s}}-6} \sum_{j=1}^{3N_{\mathrm{s}}-6} K_{ij} \left(\sum_{k=1}^{3N_{\mathrm{s}}-6} l_{ik}^{\mathrm{INM}} Q_k^{\mathrm{INM}}\right) \left(\sum_{m=1}^{3N_{\mathrm{s}}-6} l_{jm}^{\mathrm{INM}} Q_m^{\mathrm{INM}}\right)$$

$$= V(Q_i^{\mathrm{e}}(t_0)) + \sum_{j=1}^{3N_{\mathrm{s}}-6} \left(\sum_{i=1}^{3N_{\mathrm{s}}-6} K_i\, l_{ij}^{\mathrm{INM}}\right) Q_j^{\mathrm{INM}} + \frac{1}{2} \sum_{i=1}^{3N_{\mathrm{s}}-6} \lambda_i^{\mathrm{INM}} (Q_i^{\mathrm{INM}})^2$$

$$= V(Q_i^{\mathrm{e}}(t_0)) + \sum_{j=1}^{3N_{\mathrm{s}}-6} \lambda_j^{\mathrm{INM}} \left(\frac{1}{\lambda_j^{\mathrm{INM}}} \sum_{i=1}^{3N_{\mathrm{s}}-6} K_i\, l_{ij}^{\mathrm{INM}}\right) Q_j^{\mathrm{INM}} + \frac{1}{2} \sum_{i=1}^{3N_{\mathrm{s}}-6} \lambda_i^{\mathrm{INM}} (Q_i^{\mathrm{INM}})^2 \tag{2.54}$$

If we define the coordinate shift as

$$a_j = \frac{1}{\lambda_j^{\mathrm{INM}}} \sum_{i=1}^{3N_{\mathrm{s}}-6} K_i\, l_{ij}^{\mathrm{INM}} \qquad j = 1, \ldots, 3N_{\mathrm{s}} - 6 \tag{2.55}$$

and we substitute into Eq. (2.54) we have,

$$V \approx V(Q_i^{\mathrm{e}}(t_0)) + \sum_{i=1}^{3N_{\mathrm{s}}-6} \lambda_i^{\mathrm{INM}} a_i Q_i^{\mathrm{INM}} + \frac{1}{2} \sum_{i=1}^{3N_{\mathrm{s}}-6} \lambda_i^{\mathrm{INM}} (Q_i^{\mathrm{INM}})^2 =$$

$$= V(Q_i^{\mathrm{e}}(t_0)) - \frac{1}{2} \sum_{i=1}^{3N_{\mathrm{s}}-6} \lambda_i^{\mathrm{INM}} a_i^2 + \frac{1}{2} \sum_{i=1}^{3N_{\mathrm{s}}-6} \lambda_i^{\mathrm{INM}} \left((Q_i^{\mathrm{INM}})^2 + 2a_i Q_i^{\mathrm{INM}} + a_i^2\right) \tag{2.56}$$

Then we can write the potential energy function V in terms of the INMs as

$$V = V_0^t + \frac{1}{2}\sum_{i=1}^{3N_s-6} \lambda_i^{\mathrm{INM}}(Q_i^{\mathrm{INM}} + a_i)^2 \tag{2.57}$$

where V_0^t is defined as

$$V_0^t = V(Q_i^e(t_0)) - \frac{1}{2}\sum_{i=1}^{3N_s-6} \lambda_i^{\mathrm{INM}}\, a_i^2 \tag{2.58}$$

and it is the potential shifted from the equilibrium configuration. Also the vibrational kinetic energy can be expressed in terms of the INMs as

$$T^{\mathrm{vib}} = \frac{1}{2}\sum_{i=1}^{3N_s-6} (\dot{Q}_i^{\mathrm{INM}})^2 \tag{2.59}$$

By neglecting the third and higher order terms in the potential energy function, we can write the vibrational energy of each INM as

$$E_i^{\mathrm{INM}} = \frac{1}{2}(\dot{Q}_i^{\mathrm{INM}})^2 + \frac{1}{2}\lambda_i (Q_i^{\mathrm{INM}} + a_i)^2 \qquad i = 1, \ldots 3N_s - 6 \tag{2.60}$$

so the total vibrational energy of the solute is approximated by [Bastida 10b]

$$E_s^{\mathrm{vib}} = V_0^t + \sum_{i=1}^{3N_s-6} E_i^{\mathrm{INM}} \tag{2.61}$$

In order to analyze the vibrational energy relaxation of the solute molecule as well as each individual INM, it is necessary to excite a given INM . The excitation energy which corresponds to one vibrational quantum of energy for a given vibrational mode ith is defined as

$$\Delta E_i^{\mathrm{INM}} = h\nu_i^{\mathrm{INM}} \tag{2.62}$$

This energy excess is deposited in the solute molecule by displacing the ith mode until its energy reaches the proper value (see Eq. (2.60))

$$E_{i,\mathrm{exc}}^{\mathrm{INM}} = E_i^{\mathrm{INM}} + \Delta E_i^{\mathrm{INM}} \tag{2.63}$$

where the subscript exc refers to excitation.

Even though, this excess energy can be introduced either by kinetic or potential excitation, a previous study [Nguyen 03] has pointed out that the kinetic excess energy dissipates nonphysically more rapidly than the potential excess energy. For that reason we have chosen to introduce the excess energy as potential energy so that Eq. (2.63) can be rewritten as

$$V_{i,\mathrm{exc}}^{\mathrm{INM}} = V_i^{\mathrm{INM}} + \Delta E_i^{\mathrm{INM}} \tag{2.64}$$

where V_i^{INM} is the vibrational potential energy of the ith INM before the excitation

$$V_i^{\mathrm{INM}} = \frac{1}{2}\lambda_i^{\mathrm{INM}} a_i^2 \tag{2.65}$$

and $V_{i,\mathrm{exc}}^{\mathrm{INM}}$ is given by

$$V_{i,\mathrm{exc}}^{\mathrm{INM}} = \frac{1}{2}\lambda_i^{\mathrm{INM}} \left(Q_{i,\mathrm{exc}}^{\mathrm{INM}} + a_i \right)^2 \tag{2.66}$$

where $Q_{i,\mathrm{exc}}^{\mathrm{INM}}$ is the value of the ith INM after the excitation. From this expression we obtain that the initial position for the excited ith mode is

$$Q_{i,\mathrm{exc}}^{\mathrm{INM}} = \sqrt{\frac{2(V_{i,\mathrm{exc}}^{\mathrm{INM}})}{\lambda_i^{\mathrm{INM}}}} - a_i \tag{2.67}$$

Then, Eq. (2.52) was used to obtain the initial values of the ENMs for the excited molecule. To find the cartesian coordinates in the laboratory frame, we convert the ENMs to mass weighted bf cartesian displacement coordinates using the following expression

$$q_i^{\mathrm{bf}} = \sum_{j=1}^{3N_\mathrm{s}} l_{ij}^{\mathrm{ENM}} Q_j^{\mathrm{e}} \qquad i = 1, \ldots, 3N_\mathrm{s} \tag{2.68}$$

which can be derived from Eq. (2.39) taking into account that $\boldsymbol{L}^{\mathrm{ENM}}$ matrix is orthonormal. Then, Eq. (2.37) was used to get the mass weighted cartesian coordinates in the bf frame. The sf coordinates can be derived by transforming Eq. (2.30) as follows

$$\boldsymbol{r}^{\mathrm{sf}} = \boldsymbol{A} \cdot \boldsymbol{r}^{\mathrm{bf}} \tag{2.69}$$

and finally the lab coordinates are obtained using Eq. (2.24)

$$\boldsymbol{r}_i^{\mathrm{lab}} = \boldsymbol{r}_i^{\mathrm{sf}} + \boldsymbol{R}_{\mathrm{CM}} \tag{2.70}$$

In order to define the mass weighted hessian matrix for an instantaneous configuration in terms of ENMs, it is essential to define the mass weighted hessian matrix in a bf cartesian frame in agreement with that of the molecular structure that was used to generate the ENMs eigenvectors. This method is suitable to define the INMs for rigid biological system which has only one stable conformation in the gas phase or in the solution [Bastida 10a, Bastida 10b, Kalstein 11]. However, for a flexible biological system with different stable local conformations in the gas phase or in the solution there are as many ENMs as local minima. Consequently, we have different body fixed frames according to each conformation. Clearly, we can not apply the previously described method directly for such biological systems.

Let us now consider the case of a flexible molecule at an instantaneous configuration at $t = t_0$, $\boldsymbol{Q}^{\mathrm{lab}}(t_0) = (q_1^{\mathrm{lab}}(t_0), \ldots, q_{3N_\mathrm{s}}^{\mathrm{lab}}(t_0))$ specified by the atomic mass weighted cartesian coordinates in the laboratory frame

$$\begin{aligned} q_1^{\mathrm{lab}} &= \sqrt{m_1}(x_1^{\mathrm{lab}} - x_1^{\mathrm{lab}}(t_0)), \quad q_2^{\mathrm{lab}} = \sqrt{m_1}(y_1^{\mathrm{lab}} - y_1^{\mathrm{lab}}(t_0)), \quad q_3^{\mathrm{lab}} = \sqrt{m_1}(z_1^{\mathrm{lab}} - z_1^{\mathrm{lab}}(t_0)) \\ q_4^{\mathrm{lab}} &= \sqrt{m_2}(x_2^{\mathrm{lab}} - x_2^{\mathrm{lab}}(t_0)), \quad q_5^{\mathrm{lab}} = \sqrt{m_2}(y_2^{\mathrm{lab}} - y_2^{\mathrm{lab}}(t_0)), \quad q_6^{\mathrm{lab}} = \sqrt{m_2}(z_2^{\mathrm{lab}} - z_2^{\mathrm{lab}}(t_0)) \end{aligned}$$

$$q_{3N_\mathrm{s}-2}^{\mathrm{lab}} = \sqrt{m_{N_\mathrm{s}}}(x_{N_\mathrm{s}}^{\mathrm{lab}} - x_{N_\mathrm{s}}^{\mathrm{lab}}(t_0)), \quad q_{3N_\mathrm{s}-1}^{\mathrm{lab}} = \sqrt{m_{N_\mathrm{s}}}(y_{N_\mathrm{s}}^{\mathrm{lab}} - y_{N_\mathrm{s}}^{\mathrm{lab}}(t_0)), \quad q_{3N_\mathrm{s}}^{\mathrm{lab}} = \sqrt{m_{N_\mathrm{s}}}(z_{N_\mathrm{s}}^{\mathrm{lab}} - z_{N_\mathrm{s}}^{\mathrm{lab}}(t_0)) \tag{2.71}$$

The potential energy function can be expressed as [Stratt 95]

$$V(\boldsymbol{Q}^{\text{lab}}(t)) = V(\boldsymbol{Q}^{\text{lab}}(t_0)) + \sum_i K_i^t(\boldsymbol{Q}^{\text{lab}}(t_0))\,(q_i^{\text{lab}}(t) - q_i^{\text{lab}}(t_0)) + \frac{1}{2}\sum_{ij} K_{ij}^t(\boldsymbol{Q}^{\text{lab}}(t_0))\,(q_i^{\text{lab}}(t) - q_i^{\text{lab}}(t_0))(q_j^{\text{lab}}(t) - q_j^{\text{lab}}(t_0)) + \ldots \tag{2.72}$$

where K_i^t constants

$$K_i^t = \left.\frac{\partial V}{\partial q_i^{\text{lab}}}\right|_{\boldsymbol{Q}_i^{\text{lab}}(t_0)} \tag{2.73}$$

are nonzero if the instantaneous configuration does not represent a minima and the K_{ij}^t constants are the matrix elements of the hessian matrix in the laboratory frame

$$K_{ij}^t = H_{ij}^{\text{lab}} = \left.\frac{\partial^2 V}{\partial q_i^{\text{lab}}\,\partial q_j^{\text{lab}}}\right|_{\boldsymbol{Q}_i^{\text{lab}}(t_0),\boldsymbol{Q}_j^{\text{lab}}(t_0)} \qquad i,j = 1,\ldots,3N_{\text{s}} \tag{2.74}$$

Upon diagonalization of the mass weighted Hessian matrix

$$\boldsymbol{L}^{t\,\text{INM}\dagger}\,\boldsymbol{H}^{\text{lab}}\,\boldsymbol{L}^{t\,\text{INM}} = \boldsymbol{\Lambda}^{t\text{INM}} \tag{2.75}$$

we obtain the corresponding eigenvalue matrix $\boldsymbol{\Lambda}^{t\text{INM}}$ which diagonal elements provide the INM frequencies at t_0 given by

$$\nu_i^{t\text{INM}} = \sqrt{\lambda_i^{t\text{INM}}}/2\pi \qquad i = 1,\ldots,3N_{\text{s}} \tag{2.76}$$

The INMs are given as the following linear combinations of the mass weighted cartesian displacement coordinates

$$Q_j^{t\text{INM}} = \sum_{i=1}^{3N_{\text{s}}} l_{ij}^{t\text{INM}}\,q_i^{\text{lab}} \qquad j = 1,\ldots,3N_{\text{s}} \tag{2.77}$$

where $l_{ij}^{t\text{INM}}$ are the element of the $\boldsymbol{L}^{t\text{INM}}$ matrix, while the corresponding momenta are obtained

$$\dot{Q}_j^{t\text{INM}} = \sum_{i=1}^{3N_{\text{s}}} l_{ij}^{t\text{INM}}\,\dot{q}_i \qquad j = 1,\ldots,3N_{\text{s}} \tag{2.78}$$

By an analogous algebraic way to that described in Eq. (2.54), we can recast Eq. (2.72) in terms of INMs as following,

$$V = V_0^t + \frac{1}{2}\sum_{j=1}^{3N_{\text{s}}} \lambda_j^{t\text{INM}}(Q_j^{t\text{INM}} + a_j^t)^2 \tag{2.79}$$

where a_j^t is the coordinate shift which is defined as

$$a_j^t = \frac{1}{\lambda_j^{t\text{INM}}}\sum_{i=1}^{3N_{\text{s}}} K_i^t\,l_{ij}^{t\text{INM}} \qquad j = 1,\ldots,3N_{\text{s}} \tag{2.80}$$

Similarly, the vibrational kinetic energy also in terms of INMs is given by

$$T^{\text{vib}} = \frac{1}{2}\sum_{i=1}^{3N_s} (\dot{Q}_i^{t\text{INM}})^2 \tag{2.81}$$

We finally can be express the vibrational energy for each INM approximately as

$$E_i^{\text{INM}} = \frac{1}{2}(\dot{Q}_i^{t\text{INM}})^2 + \frac{1}{2}\lambda_i^{t\text{INM}}(Q_i^{t\text{INM}} + a_i)^2 \qquad i = 1, \ldots, 3N_s \tag{2.82}$$

The main modification within our new definition, is that we have expressed the INMs in terms of laboratory mass weighted cartesian displacement coordinates without any reference to a bf frame.

2.3.4 Instantaneous normal modes assignment

The fact that the INMs provide a decoupled harmonic description of the vibrational motions of the solute molecule at any instantaneous configuration is fundamental to evaluate the averaged energies and populations of the vibrational modes of the molecule as a function of time and thus compare them with the observed values extracted from time resolved infrared-Raman experiments. To achieve this, the INMs have to be identified as they evolve over time, and this is not a simple task since the complexity of the potential energy function of the molecule may cause them to vary substantially during the dynamics and, eventually, to mix them strongly, inducing crossings between them when some of their time-dependent frequencies come close [David 98]. This is essentially the reason why previous applications of the INMs have been restricted to study short time dynamical properties of the system [Cho 94, Goodyear 96, Goodyear 97, Ladanyi 98]. In this context also, the identification of the INMs simply by sorting them in increasing order of frequencies has been revealed to be useless [David 98, Bastida 10a, Bastida 10b].

The identification of the INMs as they evolve over time requires their assignment at each instantaneous snapshot in order to connect the successive sets of the INMs. The ENMs become in this respect the natural candidates to track the identity of the INMs over time [Bastida 10a, Bastida 10b, Kalstein 11].

2.3.4.1 Min-Cost algorithm

We assign the INMs at each instantaneous configuration by analyzing the relative values of $(l_{ij}^{\text{INM}})^2$ coefficients which, according to Eq. (2.50), measure the weight of the ith ENM in the jth INM. Depending on the contributions of the ENMs, the resulting INMs can be classified as pure or mixed [Bastida 10a, Bastida 10b, Kalstein 11]. In a pure INM, one of the $(l_{ij}^{\text{INM}})^2$ coefficients is dominant so the INM is quite similar to the corresponding ENM. A mixed INM includes, however, significant contributions from different ENMs. The pure INMs are easy to identify at any time during the simulations and basically mimic the well defined motions of the molecule associated with the dominant ENM. In contrast, the mixed INMs are difficult to identify due to the variations with time of their sparse ENM

contributions. These modes sometimes appear as groups of modes which exchange the contributions of a given number of ENMs, displaying complicated motions of the molecule.

In previous works of our group [Bastida 10a, Bastida 10b, Kalstein 11], we have shown that the assignment of the INMs based on the selection of the highest values of the corresponding $(l_{ij}^{\mathrm{INM}})^2$ coefficient is not practical since it may give assignment of different INMs to the same ENM, which complicates the connection between both sets. To identify the INMs over time in terms of the ENMs, it is therefore necessary to establish a one to one correspondence between both sets of modes. This can be done by selecting those elements of the $\boldsymbol{L}^{\mathrm{INM}}$ matrix, one for each row, and each pertaining to a different column, which maximize the sum of their squared values. This is, in fact, a variant of the well known Min-Cost or Min-sum assignment problem, which in general states the following: given an $N \times N$ cost matrix $\boldsymbol{C} = c_{ij}$, with $c_{ij} \geq 0$ for all i and j, assign each row to one column, and viceversa, so as to minimize the cost given by the sum of the row- column assignments. The Min-Cost assignment problem consists therefore of finding a permutation $\boldsymbol{f}_i$ of the integers $1, 2, \ldots, N$ which minimize the trace z given by

$$z = \sum_{i=1}^{N} c_{i,f_i} \tag{2.83}$$

and can be efficiently solved using the so called Hungarian algorithm [Carpaneto 88]. For a given matrix, this algorithm then provides a set of elements, each one belonging to a different row and column, whose sum is minimal. So, in order to maximize z, as required in our case, we apply the algorithm to the matrix of negative values of the $(l_{ij}^{\mathrm{INM}})^2$ elements, that is we set $c_{ij} = -(l_{ij}^{\mathrm{INM}})^2$.

The direct Min-Cost assignment method of INMs, in some cases, leads to unphysical assignments when two or more INMs have significant contributions of some ENMs with frequencies quite part [Bastida 10a, Bastida 10b]. Reiterated crossed assignments of the INMs give place in this case to critical displacements in their averaged frequencies and to large uncertainties in their vibrational energies. This behavior supposes, then, a serious problem in monitoring the vibrational energy stored in a given mode. In order to avoid such problems, a restriction to the Min-cost algorithm has been applied [Bastida 10b,Kalstein 11] to ranges of frequencies of width $\Delta\omega$ centered at the ENM frequencies ω_i^e. Thus, only those INMs whose frequencies lie in the window $(\omega_i^e - \Delta\omega/2, \omega_i^e + \Delta\omega/2)$ are susceptible to being assigned to the jth ENM. In practice, this restriction is implemented by giving arbitrary high values to the corresponding $c_{ij} = -(l_{ij}^{\mathrm{INM}})^2$ matrix elements, thus eliminating the possibility of them being included in the permutation which minimize the trace given by Eq. (2.83). Including this restriction in the Min-Cost algorithm is expected to take away some of the efficiency of the method at maximizing the overlaps between the two sets of normal modes. The optimal choice of the frequency window width $\Delta\omega$ should compromise then the smallest as possible decrease in the averaged values of the highest $(l_{i,f_i}^{\mathrm{INM}})^2$ coefficients relative to those obtained using the unrestricted Min-Cost algorithm $(\Delta\omega = \infty)$, with the need to avoid any possible unphysical assignment of the INMs that may arise.

2.3.4.2 Effective Atomic Min-Cost algorithm

The study of flexible biomolecules presenting different local minima in their potential energy surface and therefore different sets of ENMs requires the development of a new assignment method.

We define the overlap matrix $\boldsymbol{O}$ between the ENM and the INM via

$$O_{ij} = \sum_{k=1}^{N_s} A_{ki}^{\mathrm{ENM}} A_{kj}^{\mathrm{INM}} \qquad i,j = 1,\ldots,3N_s \tag{2.84}$$

with

$$A_{ki}^{\mathrm{ENM}} = \sqrt{(l_{x_k i}^{t\mathrm{ENM}})^2 + (l_{y_k i}^{t\mathrm{ENM}})^2 + (l_{z_k i}^{t\mathrm{ENM}})^2} \qquad k = 1,\ldots,N_s \text{ and } i = 1,\ldots,3N_s \tag{2.85}$$

and

$$A_{kj}^{\mathrm{INM}} = \sqrt{(l_{x_k j}^{t\mathrm{INM}})^2 + (l_{y_k j}^{t\mathrm{INM}})^2 + (l_{z_k j}^{t\mathrm{INM}})^2} \qquad k = 1,\ldots,N_s \text{ and } j = 1,\ldots,3N_s \tag{2.86}$$

where $l_{x_k i}^{t\mathrm{ENM}}$, $l_{y_k i}^{t\mathrm{ENM}}$, $l_{z_k i}^{t\mathrm{ENM}}$ and $l_{x_k j}^{t\mathrm{INM}}$, $l_{y_k j}^{t\mathrm{INM}}$, $l_{z_k j}^{t\mathrm{INM}}$ are the elements of the matrixes relatively the ENMs and INMs with the mass weighted cartesian coordinates in the laboratory fixed frame corresponding to the kth atom and the ith ENM and jth INM respectively. The values of these elements will change with any global rotation of the whole molecule or with partial rotations due to variation in some torsional angles. On the contrary, the values of the molecule A parameters will remain constant, because they provide the total contribution of every atom to a given normal mode which does not depend on the molecule orientation. Consequently, the overlap elements defined in Eq. (2.84) will measure the coincident between ENMs and INMs even in flexible molecules. If the ith ENM and the jth INM involve the displace of the same atoms with similar contribution the O_{ij} element will be close to 1. On the other side if they involve the displacement of completely different atoms the overlap will be close to 0. We note that the $\boldsymbol{O}$ matrix is not orthonormal.

In our assignment method, we also have to consider the almost free rotations of some functional groups as -CH_3, -NH_2,... at room temperature which can exchange the contributions of the H atoms to the normal modes. That is why we consider the contribution of these atoms collectively. For instance, for the three H atoms of a methyl group we define only one A parameter presents as

$$A_{3\mathrm{H},i} = \sqrt{(l_{x_{H1} i}^{t\mathrm{ENM}})^2 + (l_{x_{H2} i}^{t\mathrm{ENM}})^2 + (l_{x_{H3} i}^{t\mathrm{ENM}})^2 + (l_{y_{H1} i}^{t\mathrm{ENM}})^2 + \ldots} \tag{2.87}$$

Finally, to identify the INMs over time, we select those elements within the $\boldsymbol{O}$ matrix, one for each row and each pertaining to a different column, which maximize the sum of the diagonal elements. To do that, we applied the restricted Min-Cost algorithm $\Delta\omega$ to the matrix $\boldsymbol{O}$, in a similar fashion to our previous described method (Min-Cost algorithm). From the above considerations we call this assignment method the Effective Atomic Min-Cost algorithm (EAMC).

2.3.5 Statistical Minimum Flow method

Despite the efficiency of the MD-INM methodology, there is no simple way of accounting for the flow of energy between the individual INMs, that is, for the relaxation channels, using solely the information extracted from the time evolution of the energy that flows through individual vibrations, a problem that also comes up in experimental studies. In our previous works [Bastida 10a, Bastida 10b], we used perturbation theory and kinetic models, as reported by a number of authors [Fujisaki 07b, Fujisaki 08, Fujisaki 09, Zhang 09], to identify the main relaxation pathways of the energy deposited in the parent modes of the molecule. This approach is, however, not satisfactory since the perturbation treatments can be confidently applied only during the first steps of the energy redistribution, usually governed by a few third-order resonances, and it becomes impractical at longer times, when excitation of lower-frequency vibrational modes begins. As for the use of kinetic models, they also struggle with problems when the size of the molecule and the number of vibrations involved in the relaxation process increase. These methods therefore present serious drawbacks when used to unravel and quantify the pathways through which energy is exchanged between the individual vibrational modes of the molecule.

With the aim of facilitating the task of gaining physical insights into the elucidation of the vibrational dynamics of bio-molecules, we propose here a practical method to quantify the amount and the rate at which energy flows between the vibrational modes during relaxation of the molecule in solution. The method makes use of the snapshot data provided by the standard MD packages employed to simulate the vibrational relaxation process, which are subsequently analyzed using the INM methodology [Bastida 10a, Bastida 10b, Kalstein 11] to provide the time-dependent evolution of the vibrational energy that flows through every INM. Then, an algorithm based on the minimization of the vibrational energy flow between the vibrational modes and the assumption that the global process is essentially statistical is applied to quantify the amount of energy transferred between the different modes during a given time interval and the rate at which the process takes place.

Let us consider a system formed by a solute molecule and a number of solvent molecules, with the bath assumed to be composed by the sum of all the degrees of freedom of the solvent plus the translational and rotational degrees of freedom of the solute. The vibrational energy of the solute can be precisely written as the sum of the harmonic INM contributions [Bastida 10a, Bastida 10b, Kalstein 11], so the total energy of the system is given by,

$$E = E_{\text{bath}}(t_k) + \sum_{i=1}^{N_v} E_i(t_k) \tag{2.88}$$

where N_v is the number of vibrational degrees of the solute and $E_i(t_k)$ is the vibrational energy of the ith INM at time t_k. We assume thereafter that the INMs and the bath energies are obtained by averaging their corresponding values extracted from a representative set of independent MD runs. The INMs and the bath energies change with time because of the intra and intermolecular vibrational energy transfer processes that the system undergoes, while the total energy remains constant. The change of energy of the bath in the time

interval (t_k, t_{k+1}) is given accordingly by

$$\Delta E_{\text{bath}}(t_k) = E_{\text{bath}}(t_{k+1}) - E_{\text{bath}}(t_k) = -\sum_{i=1}^{N_v} \Delta E_i(t_k) \tag{2.89}$$

where

$$\Delta E_i(t_k) = E_i(t_{k+1}) - E_i(t_k) \tag{2.90}$$

is the change of energy in the ith INM.

In order to map the transfer of energy through the system in a detailed way, we introduce the so-called energy flow matrix $\mathbf{F}$, whose off-diagonal elements, $f_{ij}(t_k)$, contain the amounts of energy transferred from the ith to jth INM in the time interval $\Delta t = t_{k+1} - t_k$. The diagonal elements of the flow matrix are set to zero since the INMs are not allowed to interchange energy. To ensure that the total energy is conserved, an additional row and additional column are included in the flow matrix to account for the exchange of energy with the bath, that is, for the intermolecular energy flow. The energy flow matrix $\mathbf{F}$ is therefore a $(N_v + 1) \times (N_v + 1)$ antisymmetric, since $f_{ij} = -f_{ji}$, matrix.

By using the sign criterion that $f_{ij} > 0$ if the energy is transferred from the ith to the jth INM, we calculate the variation of energy of the ith INM in the interval Δt as the sum of the matrix elements in the ith column as follows

$$\Delta E_i(t_k) = E_i(t_{k+1}) - E_i(t_k) = \sum_{j=1}^{N_v+1} f_{ji}(t_k) \qquad i = 1, \ldots, N_v + 1 \tag{2.91}$$

There are then $N_v(N_v + 1)/2$ independent elements of the energy flow matrix to be determined and only $N_v + 1$ restrictions among them given by Eq. (2.91), so we need to consider additional constrains in order to fully specify the $\mathbf{F}$ matrix. Within all the possible energy flow matrices existing, we select accordingly as the most physically meaningful those derived by imposing the condition that amount of energy exchanged by the INMs of the solute molecule during the time interval Δt be minimum. This minimum flow criterion allows us to classify the INMs in the time intervals as energy donors (D modes), if the vibrational energy that accumulates in the specific INM decreases, and energy acceptors (A modes), if the energy accumulated in the mode increases. To achieve the minimum energy exchange we assume that energy flows exclusively from D to A modes. Thus, if the ith INM is a D mode in the Δt interval, it transfers to the A modes its excess of energy equal to $|\Delta E_i(t_k)| = |E_i(t_{k+1}) - E_i(t_k)|$. In turn, if the jth INM is an A mode in the Δt interval, it receives an amount of energy from the D modes equal to $\Delta E_j(t_k) = E_j(t_{k+1}) - E_j(t_k)$. The total energy exchanged among the INMs in the Δt time interval is equal to

$$E_{\text{exc}}(t_k) = \sum_{i \in \text{D}} |\Delta E_i(t_k)| = \sum_{j \in \text{A}} \Delta E_j(t_k) \tag{2.92}$$

The application of only the minimum flow criterion does not allow us to calculate the specific amounts of energy transferred from every D mode to each A mode. We invoke then an additional purely statistical criterion for the distribution of the vibrational energy

exchanged based on writing the amount of energy that flows from the ith to the jth INMs as the flow probability between these two modes, $P_{i\to j}(t_k)$, multiplied by the total energy exchanged, that is,

$$\boldsymbol{f}_{ij}(t_k) = E_{\text{exc}}(t_k) P_{i\to j}(t_k) \qquad i \in \text{D},\ \boldsymbol{j} \in \text{A} \tag{2.93}$$

The flow probability between the ith and jth INMs is, in turn, factorized as the product of the flow probability from the ith INM, $P_{i\to}(t_k)$, and the flow probability towards the jth INM, $P_{\to j}(t_k)$, as follows

$$P_{i\to j}(t_k) = P_{i\to}(t_k) P_{\to j}(t_k) \qquad i \in \text{D},\ \boldsymbol{j} \in \text{A} \tag{2.94}$$

where

$$P_{i\to}(t_k) = \frac{|\Delta E_i(t_k)|}{E_{\text{exc}}(t_k)} \qquad i \in \text{D} \tag{2.95}$$

and

$$P_{\to j}(t_k) = \frac{\Delta E_j(t_k)}{E_{\text{exc}}(t_k)} \qquad \boldsymbol{j} \leftarrow \text{A} \tag{2.96}$$

The donor modes therefore distribute their excess energy proportionally to their contribution to the total energy exchanged, as do the acceptor modes. It can be straightforwardly verified using Eqs. (2.92), (2.95) , and (2.96) that the flow probabilities $P_{i\to}$ and $P_{\to j}$ are normalized. Substitution of Eqs. (2.94), (2.95) and (2.96) in Eq. (2.93) then provides the final expression for the amount of energy that flows between the ith and jth INM in the Δt time interval,

$$\boldsymbol{f}_{ij}(t_k) = -\boldsymbol{f}_{ji}(t_k) = \frac{|\Delta E_i(t_k)| \Delta E_j(t_k)}{E_{\text{exc}}(t_k)} \qquad i \in \text{D},\ \boldsymbol{j} \in \text{A} \tag{2.97}$$

$$\boldsymbol{f}_{ij}(t_k) = 0 \qquad i, \boldsymbol{j} \in \text{A} \ \text{ or } \ i, \boldsymbol{j} \in \text{D} \tag{2.98}$$

as given by the Statistical Minimum Flow (SMF) method. Obviously, the energy flow matrix changes with time during the relaxation process, and the role of the modes as donors or acceptors also switch with time. These changes might be indicative of real changes in the system or just unphysical by-products produced by fast local oscillations of energy which are expected to cancel out along the successive time intervals. It is, then, convenient to use the accumulated amount of energy that flows between the INMs during a number of consecutive time intervals between times t_k and t_k^t given by

$$\boldsymbol{f}_{ij}^{\text{ac}}(t_k, t_{k^t}) = \sum_{m=k}^{k^t-1} \boldsymbol{f}_{ij}(t_m) \tag{2.99}$$

which, to a large extent, filters the unphysical energy variations.

During the intramolecular vibrational relaxation process, energy flows from D modes to A modes. The way in which the accumulated amount of energy flows between INMs $\boldsymbol{f}_{ij}^{\text{ac}}(t_k, t_{k^t})$ is shown in Figure 2.5. This curve can be nicely fitted to first order exponential function of the type

$$\boldsymbol{f}_{ij}^{\text{ac}} = A_{ij}(1 - e^{-t/\tau_{ij}}) \tag{2.100}$$

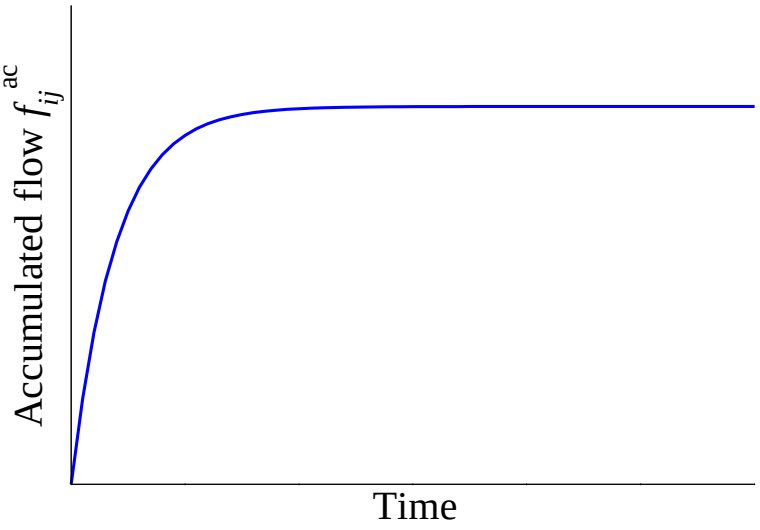

Figure 2.5: Time evolution of the accumulated energy that flows from a D mode to an A mode.

where A_{ij} is the asymptotic value of the energy transferred, i.e., the total energy transferred, and τ_{ij} is the corresponding lifetime. However this expression must be interpreted with caution when applied to evaluate the energy flows for intermediate modes in the relaxation process. Let us consider B to be a mode which is excited from the A mode with a rate equal to $\tau_{\rm exc}^{-1}$ and simultaneously it relaxes to the C mode with a rate equal to $\tau_{\rm rel}^{-1}$. If both processes are modelled through first order reactions, the time evolution of the vibrational energy stored in the B mode is

$$[B](t) = \frac{\tau_{\rm exc}^{-1}}{\tau_{\rm rel}^{-1} - \tau_{\rm exc}^{-1}} \left(e^{-t_{\rm max}/\tau_{\rm exc}} - e^{-t_{\rm max}/\tau_{\rm rel}} \right) \tag{2.101}$$

where we have assumed that the energy initially stored in the A mode is unity. In Figure 2.6 we represent the shape of this function, that reaches its maximum value at

$$t_{\rm max} = \left(\frac{1}{\tau_{\rm exc}} - \frac{1}{\tau_{\rm rel}} \right)^{-1} \ln \frac{\tau_{\rm rel}}{\tau_{\rm exc}} \tag{2.102}$$

According to the SMF method the B mode acts as an acceptor in the time interval $(0, t_{\rm max})$ and as donor when $t > t_{\rm max}$. Then the accumulated flow from A to B will be $1 - e^{-t_{\rm max}/\tau_{ij}}$, that is, smaller than unity.

Moreover, the apparent lifetime τ for the A $\rightarrow$B transfer can be defined as the time when the accumulated flows reach $1 - e^{-1}$ times its maximum value that is

$$e^{-\tau/\tau_{ij}} = e^{-1} + \left(1 - e^{-1}\right) e^{-t_{\rm max}/\tau_{\rm exc}} \tag{2.103}$$

In Table 2.1 we show the values of $\tau/\tau_{\rm exc}$ and $e^{-t_{\rm max}/\tau_{\rm exc}}$ for different $\tau_{\rm rel}/\tau_{\rm exc}$ ratios. As seen both the excitation time and the amount of energy transfer are underestimated for small value of $\tau_{\rm rel}/\tau_{\rm exc}$ while they tend to unity as this ratio increase. Therefore, the lifetime

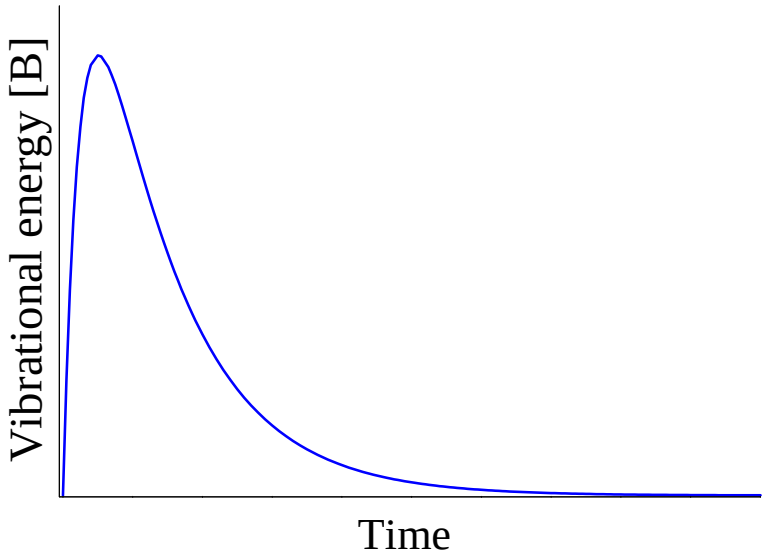

Figure 2.6: Time evolution of the vibrational energy of a B intermediate in the consecutive first order reaction A →B →C.

Table 2.1: Values of t_{max}/τ_{exc}, t_{max}/τ_{rel}, $[B]_{max}$, τ/τ_{exc} and $1-e^{-t_{max}/\tau_{exc}}$ for different τ_{rel}/τ_{exc} ratios.

τ_{rel}/τ_{exc}	t_{max}/τ_{exc}	t_{max}/τ_{rel}	$[B]_{max}$	τ/τ_{exc}	$1-e^{-t_{max}/\tau_{exc}}$
1.5	1.216	0.811	0.443	0.554	0.703
2	1.386	0.693	0.500	0.642	0.750
3	1.648	0.549	0.578	0.714	0.808
4	1.848	0.462	0.629	0.760	0.842
5	2.012	0.402	0.669	0.793	0.866
6	2.150	0.358	0.680	0.817	0.884
8	2.377	0.297	0.743	0.852	0.907
10	2.558	0.256	0.774	0.875	0.923

and flows obtained from the SMF method have to be corrected in those intermediate modes with relaxation times not much bigger than the excitation one.

2.4 COMPUTATIONAL VIBRATIONAL SPECTROSCOPY

Vibrational spectroscopy is a valuable tool for the elucidation of molecular structure. It also provides important information about the intramolecular forces acting between the atoms in a molecule, the intermolecular forces in condensed phase and the nature of the chemical bond. However, its interpretation may become arduous when dealing with

large systems, where different modes are active in the same frequency regions. Computer modeling and simulations are thus extremely important to provide an interpretation of IR spectroscopy at the molecular level.

2.4.1 Infrared spectrum

The most basic method to simulate an IR absorption spectrum is the evaluation of the frequencies of the normal modes of the system under the harmonic approximation (see Section 2.3). The IR intensities are obtained from the gradient of the dipole moment. However, this approximation is too drastic for low frequency bands and for systems in the condensed phase, since the anharmonicity of the IR bands and coupling between different modes can be lead to large effects.

In these cases, the evaluation of the absorption spectra is based on a development originally due to Kubo and Anderson [Kubo 54, Anderson 54], who formulated the theoretical description of the IR absorption line shapes in terms of a fluctuating transition frequency that was regarded as a classical stochastic variable with experimentally correlated Gaussian statistics. In the limit that these fluctuations are sufficiently slow, the IR absorption spectrum corresponds to the ensemble average of the distribution of transition frequencies, and the line shape is Gaussian. Conversely, when the environmental fluctuations are fast, the IR absorption spectrum is "motionally narrowed" (i.e., the spectrum is narrower than the distribution of frequencies) and its line shape is Lorentzian. Under the Born Oppenheimer approximation and by applying first order perturbation theory to model the interaction between matter (isotropic fluid) and an external electric field at a quantum level, it was shown that the line shape of absorption in the infrared region can be expressed as the Fourier transform of the time correlation function (TCF) of the total dipole moment $\hat{\boldsymbol{M}}$ of the absorbing molecules in the absence of the field: [Gordon 68, McQuarrie 00]

$$I(\omega) = \frac{1}{2\pi} \int_{-\infty}^{\infty} dt e^{-i\omega t} \left\langle \hat{\boldsymbol{M}}(0) \cdot \hat{\boldsymbol{M}}(t) \right\rangle = \frac{3\ \varepsilon^*(\omega)}{4\pi^2 (1 - e^{-\beta\ \omega})} \tag{2.104}$$

where $\beta = 1/k_B T$ in which k_B is Boltzmann's constant and T the temperature and,

$$\varepsilon^*(\omega) = \frac{nc\alpha(\omega)}{\omega} \tag{2.105}$$

being n the index of the refraction of the medium, c the speed of light, and $\alpha(\omega)$ the absorption coefficient of Lambert's law, $I = I_0 \exp(-\alpha x)$. Eq. (2.104) provides a link between a variable that can be evaluated based on a simulation and spectroscopic variables that can be experimentally measured. In particular, in order to be able to use the results of classical dynamics, the classical analog of the quantum time correlation function can be used and the quantum dipole moment operator $\hat{\boldsymbol{M}}(t)$ can be approximated by its classical analog $\boldsymbol{M}(t)$, leading to the expression: [Gordon 65, Berens 81, McQuarrie 00, Ramírez 04, Schmidt 08]

$$I(\omega) \sim Q(\omega) \int_{-\infty}^{\infty} dt\, e^{-i\omega t} \left\langle \boldsymbol{M}(0) \cdot \boldsymbol{M}(t) \right\rangle \tag{2.106}$$

where the effect of approximating quantum operators with their classical counterparts is compensated by the use of the quantum correction factor $Q(\omega)$.

Although different forms for $Q(\omega)$ have been proposed in the literature [Egorov 99], this factor is often omitted, and it has been recently proven that its inclusion does not significantly affect $\boldsymbol{I}(\omega)$ [Lawrence 05]. In the present thesis, we calculate IR spectra by omitting the prefactor, and they are thus expressed in arbitrary units. In addition, we do not introduce any scaling factor to rescale our computed frequencies in order to better reproduce the experimental results.

In solution, experiments aimed at recording the IR spectrum of a solute use a subtraction method (the spectrum of a blank is subtracted from the spectrum of the full solution). In simulations, this would translate into considering cross-correlation (solute (s)-solvent (sv)) to calculate the TCF of the dipole moment as well as solute-solute correlations. However, this approach requires taking into account correlation between solute and solvent motions, and much better statistics are necessary compared to the calculation of self-correlation functions [Iuchi 02]:

$$C_{\mu\mu}(t) = C_{\mathrm{s}/\mathrm{s}}(t) + C_{\mathrm{sv}/\mathrm{s}}(t) + C_{\mathrm{sv}/\mathrm{sv}}(t) \tag{2.107}$$

where $C_{\mu\mu}(t)$ represent the total dipole time correlation of the system, and

$$C_{\mathrm{s}/\mathrm{s}}(t) = (\boldsymbol{M}_{\mathrm{s}}(t) \cdot \boldsymbol{M}_{\mathrm{s}}(0)) \tag{2.108}$$

$$C_{\mathrm{sv}/\mathrm{sv}}(t) = (\boldsymbol{M}_{\mathrm{sv}}(t) \cdot \boldsymbol{M}_{\mathrm{sv}}(0)) \tag{2.109}$$

$$C_{\mathrm{sv}/\mathrm{s}}(t) = (\boldsymbol{M}_{\mathrm{sv}}(t) \cdot \boldsymbol{M}_{\mathrm{s}}(0)) + (\boldsymbol{M}_{\mathrm{s}}(t) \cdot \boldsymbol{M}_{\mathrm{sv}}(0)) \tag{2.110}$$

where, $\boldsymbol{M}_{\mathrm{sv}}$ and $\boldsymbol{M}_{\mathrm{s}}$ are the total dipole moment of solvent and solute molecules respectively. In this work, we restrict our calculation to self-correlations of the solute dipole moment.

According to Eq. (2.106), we should calculate the Fourier transform of the TCF of the dipole moment. We analyzed the IR spectra by applying different numerical method to calculate the FT of a TCF [Press 92], Wiener-Khinchin theorem, Maximum Entropy method and direct integration of the dipole correlation function.

Peak assignment on the IR spectra was carried out by using a decomposition of the total vibrational density of states (VDOS) into atomic contributions. This procedure is often used when dealing with peak assignment in calculated IR spectra [Gaigeot 03, Gaigeot 05].

$$C_{\mathrm{s}/\mathrm{s}}(t) = (\boldsymbol{V}(t) \cdot \boldsymbol{V}(0)) \tag{2.111}$$

where $\boldsymbol{V}$ is the total molecular velocity of the solute. The same procedure described above to calculate the FT of a time correlation function was applied. This equation can be used to characterize the nature of the vibration, by decomposing the total VDOS in terms of atomic contributions. This help clarifying what atoms are involved in the mode corresponding to a particular frequency. Some additional calculation can be performed for a further confirmation of mode assignment, such as for example the FT of $(\boldsymbol{R}_{ij}(0) \cdot \boldsymbol{R}_{ij}(t))$ to assign stretching motions ($\boldsymbol{R}_{ij}$ being the distance between the two atoms involved in the elongation) and of $(\theta(0) \cdot \theta(t))$ (θ) being a bend angle.

2.4.2 Analysis of the solvent induced shift

In order to relate the solvent-induced shift on the amide I band of a model peptide to different terms contributing to the solute-solvent hydrogen bond interaction energy, we proposed a method allowing to extract the relative effect of interactions of different nature: electrostatics, polarization, charge transfer, and the contribution due to the deformation of the potential energy surface corresponding to the amide I oscillator. To assess the impact of each interaction energy decomposition term on the solvent-induced shift, we developed an expression based on a perturbative approach. Our method is then applied to calculations run at the PM3 level using the interaction energy decomposition scheme developed by van der Vaart and Merz [der Vaart 99]. However, the methodological development is general and could be applied to any other decomposition scheme and to different levels of quantum chemistry.

Our goal is to relate the solvent-induced shift on the amide I vibration to the different contributions arising from the interaction energy decomposition. In the harmonic approximation, the relative solvent-induced shift in terms of the force constant k and of the reduced mass μ for the normal mode in the gas phase (g) and in the condensed phase (c). Making use of a first order expansion, we can write:

$$\frac{\nu_c - \nu_g}{\nu_g} = \sqrt{\frac{k_c - k_g}{k_g} + 1} - 1 \approx \frac{1}{2}\frac{k_c - k_g}{k_g} \tag{2.112}$$

in which the quantity $(k_c - k_g)/k_g$ is considered to be small compared to one. In the case of the amide I band of NMA in water, the (absolute) solvent induced shift is just about 6% of the gas phase frequency [Ingrosso 11], making this approximation a reasonable one.

In order to simplify the analysis of the solute-solvent interactions, we study a very simple system, comprising one NMA molecule and one water molecule. In this case, the total potential energy of the complex E_c is just given by:

$$E_c = E_{\mathrm{NMA,g}} + E_{\mathrm{w,g}} + E_{\mathrm{int}} \tag{2.113}$$

where $E_{\mathrm{NMA,g}}$ and $E_{\mathrm{w,g}}$ are the equilibrium gas phase energies of isolated NMA and water, respectively, and E_{int} is the interaction energy. The first two terms on the right hand side disappear when calculating the second derivative, since they are constant values corresponding to the minima of the potential energy surfaces of the two isolated molecules, finally obtaining

$$k_c = \frac{\partial^2 E_{\mathrm{int}}}{\partial Q_c^2} \tag{2.114}$$

From now on, the subscript c will be related to the NMA-H_2O complexes.

According to the scheme proposed in Ref. [der Vaart 99], interaction energies can be decomposed into electrostatic, polarization and charge transfer components. This approach takes advantage of some features of the Divide and Conquer approach, according to which

the Fock matrix of the system is partitioned into submatrices during the process of diagonalization, and the overlap between the subsystem together with the Fermi energy are used to control the charge flow between subunits.

The decomposition is achieved by performing three distinct calculations after evaluating the total interaction energy. First, the system is brought to the equilibrium distance in the complex starting from the infinitely separated molecules, and no charge transfer is allowed. Secondly, intramolecular charge redistribution is activated. Finally, intermolecular charge transfer is allowed as well. For more details about the calculation we refer the reader to the original work.

As in any other interaction decomposition scheme, one should pay some caution in the interpretation of each term. As it was noted by Kitaura and Morokuma [Kitaura 76], the electrostatic contribution represents the interaction between occupied molecular orbitals (MOs) without mixing, the polarization term is related to mixing between occupied and virtual MOs on the same molecule, and finally the charge transfer term contains also a contribution arising from exchange interactions.

When applying this method to the study of our system, we need to take into account an additional term, which accounts for the changes in the geometrical structure arising from intermolecular interactions, compared to the gas phase equilibrium geometry of each molecule in the complex (deformation contribution).

To summarize, we assumed that the total interaction energy E_{int} can be partitioned into the following terms:

$$E_{\text{int}} = E_{\text{ele}} + E_{\text{pol}} + E_{\text{CT}} + E_{\text{def}} \tag{2.115}$$

being E_{ele}, E_{pol}, E_{CT} and E_{def} the electrostatic, polarization, charge transfer and deformation contribution, respectively.

Substituting Eq. (2.115) into Eq. (2.114), we obtain:

$$k_c = \frac{\partial^2 E_{\text{ele}}}{\partial Q_c^2} + \frac{\partial^2 E_{\text{pol}}}{\partial Q_c^2} + \frac{\partial^2 E_{\text{CT}}}{\partial Q_c^2} + \frac{\partial^2 E_{\text{def}}}{\partial Q_c^2} = k_{\text{ele}} + k_{\text{pol}} + k_{\text{CT}} + k_{\text{def}}\,, \tag{2.116}$$

where the four constants on the right hand side have been introduced for simplicity, but they do not correspond to force constants.

The second derivatives in Eq. (2.116) are evaluated numerically and compared with the results of a complete exploration of the potential energy surface (see Section 3.1.4 for mode details). By substitution of Eq. (2.116) into Eq. (2.112), we finally have:

$$\frac{\Delta\nu}{\nu_g} = \Delta\nu^r \approx \frac{1}{2}\left(\Delta\nu^r_{\text{ele}} + \Delta\nu^r_{\text{pol}} + \Delta\nu^r_{\text{CT}} + \Delta\nu^r_{\text{def}}\right) \tag{2.117}$$

In the last equality, the first three terms come from the interaction energy decomposition scheme by van der Vaart and Merz [der Vaart 99] ($\Delta\nu^r_x = \frac{k_x}{k_g}$, where x = ele, pol or CT), whereas the last term gives direct information on the deformation of the potential energy surface induced by the NMA-H_2O interactions along the normal mode compared to the gas phase ($\Delta\nu^r_{\text{def}} = \frac{k_{\text{def}}}{k_g} - 1$).

CHAPTER 3

Results and discussion

In this chapter, we present and discuss the results of the vibrational energy relaxation of the amide I mode of the *N*-methylacetamide (NMA, monopeptide model) and alanine dipeptide (AlaD, dipeptide model) molecules in water solution (D_2O), as well the vibrational spectroscopic properties of the NMA molecule.

N-methylacetamide (NMA) is a model molecule for the peptide bond, which is omnipresent in the backbone of proteins. NMA is widely used for investigations into the physical and chemical properties of the amide group, particularly for the purpose of understanding the behavior of one of many peptide linkages in proteins and peptides [Guo 92, Herrebout 01, Rubtsov 03b, Hayashi 05, DeFlores 06, Fang 09]. Figure 3.1 shows a schematic representation of the two conformers of the NMA molecule *trans*-NMA and *cis*-NMA. The *trans* form is the most stable in the gas phase and in solution [Jorgensen 88, Gao 97, Villani 99, Cuevas 02], and an experimental evaluation of the energy difference between the two forms in a rigid matrix gives a value of 2.3 kcal/mol [Ataka 84], while NMR measurements in 1,2-dichloroethane gave a difference ranging from 2.8 to 3.4 kcal/mol [Drankenberg 71]. The free energy barrier between the two forms has been investigated by means of different computational techniques and it varies between 15 and 20 kcal/mol depending on the method [Luque 93, Villani 99, Mantz 04, Mantz 06, Mantz 09]. The presence of a solvent enhances the barrier height by 2-3 kcal/mol [Jorgensen 88, Luque 93, Mantz 04].

Beginning with the efforts to assign IR frequencies of isolated NMA and its N-deuterated form (NMAD) [Miyazawa 58], a number of studies have been devoted to narrow the gap between observed and calculated geometries and IR frequencies of aqueous NMA and NMAD. The solute-solvent interaction and polarization are important aspects in theoretical chemistry. A challenge in the studies of solvation and solvent effects is to incorporate explicity the polarization and charge transfer effects into the potential surface. At this end, we present in this thesis a study of the IR spectrum of the NMA molecule in aqueous solution and the vibrational energy relaxation of the initially excited amide I mode (mainly CO stretch) of the NMAD in heavy water by employing MD simulations with MM and quantum electronic Hamiltonian force fields. Our study aims to shed the light

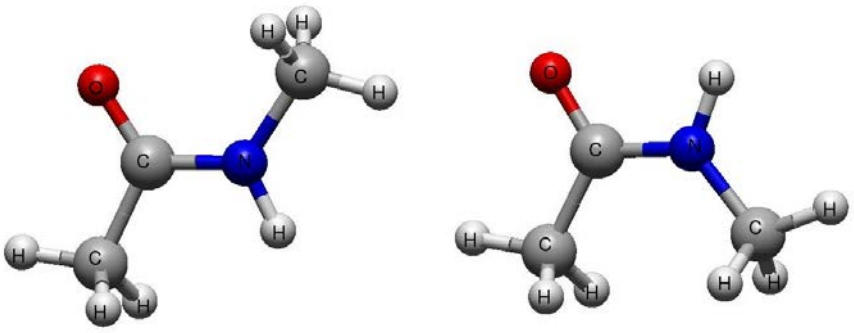

Figure 3.1: *Trans* (left) and *cis* (right) NMA conformation.

on the importance of incorporate the polarization and the charge transfer effects into an accurate modeling of the solute solvent interactions. In Section 3.1 we introduce a study of the infrared spectrum of NMA performed using Molecular Dynamics and quantum electronic Hamiltonian at semiempirical level (SEBOMD). In this study we assess the validity of the SEBOMD approach to predict solvent effects on the vibrational frequencies. This is important for implementing the SEBOMD method and the INM analysis for studying the vibrational relaxation of the NMA molecule in solution. Since the biological function of a protein is considered to be coupled with the anharmonic protein dynamics [Frauenfelder 91], elucidation of the mechanism of this coupling, that is between protein dynamics and protein function is extremely important. In this context, it is known that the study of the vibrational energy relaxation play an essential role for understanding the functions of the biomolecules since their structure and dynamics are determined by the energy transfer [Leitner 08]. In Section 3.2 we analyze the vibrational energy relaxation of the amide I mode of the deuterated NMA (NMAD) by employing both an MM nonpolarizable force field and SEBOMD.

Finally, in Section 3.3 we present a study of the vibrational energy relaxation of the amide I mode of the deuterated alanine dipeptide (AlaD-d_2, $CH_3CONDCHCH_3CONDCH_3$) molecule (see Figure 3.2) in deuterated water through nonequilibrium MD simulations following the experimental work by Hochstrasser *et al* [Kim 05a]. To our knowledge, this is the first time that the vibrational energy relaxation of the amide I mode of the AlaD molecule is presented theoretically. The dynamics of the AlaD molecule is quite different from the NMA molecule because of its flexibility (see Figure 3.3), and the presence of two amide I groups in the acetyl end (acend) and in the amino end (amend). We have also analyzed the vibrational energy relaxation of the two amide I modes, using the isotopic substitution of the acend carbonyl group $^{12}C{=}O$ with $^{13}C{=}O$ in order to separate the otherwise overlapping amide I modes. Special attention has been paid to follow the time

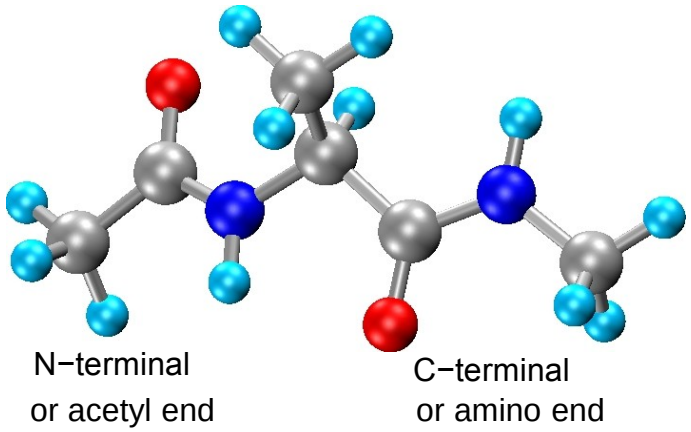

Figure 3.2: Chemical structure of the alanine dipeptide molecule. Color key: C (gray), N (blue), O (red) and H (cyan)

evolution of the conformational distributions during the relaxation process.

3.1 IR SPECTRUM OF THE N-METHYLACETAMIDE MOLECULE

3.1.1 Computational details

Before providing a discussion of our results on the infrared spectrum of NMA, with particular emphasis on the solvent effect on the band position, we briefly summarize the computational procedure that we used for the simulations. The SEBOMD results were compared to molecular mechanics MD using the Amber03 [Duan 03] force field, recently introduced to overcome some of the shortcomings of previous non-polarizable force field in the simulations of proteins in the condensed phase, especially in the prediction of molecular dipole moments and for properties related to the torsional parameters. We used the Amber code, version 9 [Case 06], and a local version of the same code for SEBOMD.

After performing MM MD simulations of isolated *cis* and *trans* NMA, we immersed each of the two molecules in boxes containing 64 SPC/E [Berendsen 87] water molecules at 300 K. Box size effects were analyzed by using larger boxes. Simulations were run both in the microcanonical ensemble and at constant temperature. In the latter case, the Andersen method [Andersen 80] was used for temperature control, and the frequency for velocity randomization was 1 ps^{-1}. The SPC/E model was used since it gives very similar results to the ones obtained with the semiempirical electronic Hamiltonian and PIF corrections with respect to the structure of liquid water [Monard 05]. In addition, SPC/E is one of the best available MM models to describe the dielectric properties (and thus electrostatic solvation properties) of water [Reddy 89]. We do not expect large effects

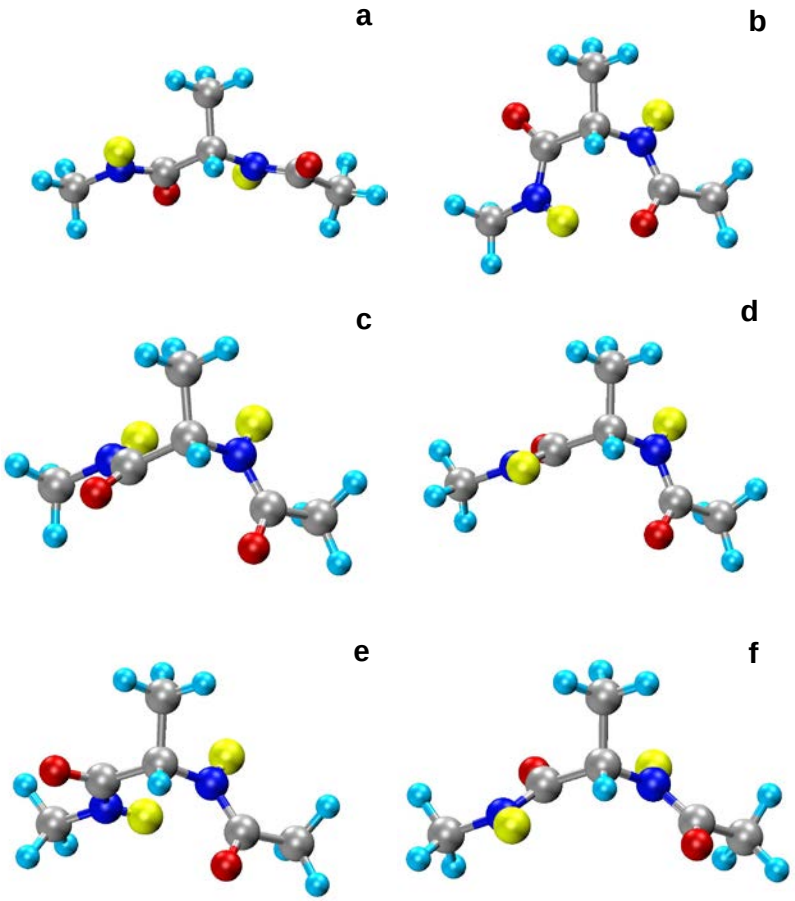

Figure 3.3: The deuterated alanine dipeptide molecule conformations (φ,ψ) (a) C5 (-151.4, 170.6) (b) $C7_{eq}$ (-81.4, 70.6) (c) α_R (-78.8, -50.0) (d) P_{II}(-80.0,140.0) (e) α^d (-100.0, -5.0) (f) β(-120.0, 130.0). The yellow color represents the deuterium atoms.

on the infrared spectrum of NMA due to using a rigid water model, since the solute-solvent correlations are not included in our calculation.

Simulations in the condensed phase were run with periodic boundary conditions. Long-range electrostatics was treated within the Ewald sum scheme [Allen 87]. The size of the boxes was adapted to reproduce the room temperature density of water (0.996 g/ml [Lemmom 11]), by taking into account the volume occupied by the solute. Equilibration at constant temperature (T = 300 K) was performed for 500 ps, followed by data acquisition over 1 ns for each simulation. We used a time step of 1 fs. The SHAKE procedure [Ryckaert 77, Ciccotti 86] was used to keep water molecules rigid, whereas all bonds in the solute molecule were flexible.

Regarding MD simulations with a semiempirical quantum mechanical Hamiltonian, we compared the results obtained in the gas phase with those obtained in the condensed phase by using the standard PM3 Hamiltonian for intramolecular interactions and the PIF cor-

Table 3.1: Geometrical parameters for isolated *cis* and *trans* NMA. Average values from molecular mechanics MD and from SEBOMD with a PM3 Hamiltonian. Distances are in Å[a]

Atom	Amber03 *cis*	Amber03 *trans*	PM3 *cis*	PM3 *trans*
C_{ACE}-H_{ACE}	1.09	1.09	1.10	1.10
C_{NMet}-H_{NMet}	1.09	1.09	1.10	1.10
C-O	1.22	1.22	1.22	1.22
N-H	1.01	1.01	1.00	1.00
C_{ACE}-C	1.52	1.52	1.51	1.51
C-N	1.33	1.34	1.43	1.43
N-C_{NMet}	1.46	1.47	1.47	1.47

[a] The standard deviation on distances is 0.03 Å with the exception of the CO and CN distances, for which it is 0.02 Å.

rection for water-water [Berenal-Uruchurtu 00] and solute-water [Harb 04] intermolecular interactions. In water solution, each of the two NMA conformers were dissolved in a box with 64 water molecules, and we ran dynamics on a 300 ps time scale, at the same temperature and using the same time step as in the MM simulations. No SHAKE constraints were applied. Previous equilibration for each MD run was performed over 100 ps starting from a configuration extracted from the molecular mechanics force field MD simulations. Simulations in the condensed phase were run with periodic boundary conditions, and long range electrostatic interactions were taken into account by using the Ewald method [Nam 05].

In all (isolated, condensed phase) simulations, we monitored the O-C-N-H dihedral, in order to make sure that the NMA molecule would stay in the original *cis* or *trans* conformation during the simulation, in agreement with the observation of a high barrier between the two conformers predicted by other calculations [Luque 93, Mantz 04, Mantz 06, Mantz 09]. An analysis of partial charges was also carried out using Mulliken charges and the CM1 and CM2 models [Storer 95, Li 98], both for the gas phase and the condensed phase simulations.

3.1.2 Gas phase spectrum

We first analyze the average intramolecular properties calculated from our MD simulations. When considering the equilibrium geometry of NMA, no differences in the average bond distances are observed between the *cis* and the *trans* conformer, and the values that we found by using the PM3 Hamiltonian are similar to those found when using the Amber03 force field, with the exception of the C-N distance. Results are collected in Table 3.1. We recall that the PIF parameters only modify the intermolecular (solvent-solvent and solvent-solute) interactions and therefore do not affect the intramolecular properties of NMA in the gas phase. A well-known issue with the PM3 method is an artificial tendency toward pyramidal hybridization of the N atom. A specific correction term (PM3-MM) has

Table 3.2: Comparison of NMA dipole moment (in Debye) as obtained from different methods in the gas phase: Car-Parrinello molecular dynamics (CP-MD), quantum chemistry calculations at the B3LYP/6-31G* and HF/6-31G(d) levels of theory, our results for quantum calculations at the PM3 level (in the case of standard PM3 parameters as well as PM3 with the correction for the peptide bond (PM3-MM)), our results from SEBOMD at the PM3 level (average value of the molecular dipole - from the dipole moment operator- and the corresponding values from partial atomic charges using different schemes), and our results from simulations with the Amber03 force field.

Method	*cis* NMA	*trans* NMA
CP-MD [Gaigeot 05]	4.38	3.99
B3LYP/6-31G* [Garcia-Martinez 02]	4.00	3.81
B3LYP/6-311++G* [Han 96]	4.31	3.97
HF/6-31G(d) [Du 03]	4.37	4.22
MP2/6-31G(d) [Jorgensen 88]	4.21	4.04
PM3	3.39	3.10
PM3-MM	3.68(TS)[(a)]	3.31
PM3-SEBOMD	3.36	3.09
PM3-SEBOMD (Mulliken charges)	3.09	2.64
PM3-SEBOMD (CM1 charges)	3.24	3.79
PM3-SEBOMD (CM2 charges)	3.54	3.54
Amber03 molecular mechanics MD	4.09	4.50
Exp. (in benzene) [Rodrigo 86]	3.85	
Exp. (vapor) [Meighan 64]	3.71-3.73	

[(a)]In this case, geometry optimization of the *cis* conformer led to a transition state (TS).

thus been introduced to keep peptide bonds planar through a harmonic constraint on the H-N-C-O dihedral. In our calculations, we used the Gaussian03 [Frisch 03] implementation of this potential. In order to test the effect of this correction on the vibrational frequencies of NMA, we performed gas phase calculations on both the *cis* and the *trans* conformers by carrying out geometry optimization and normal modes analysis in Gaussian [Frisch 03]. We used both the standard PM3 parameters and the PM3-MM parameters. Other than the different values for the H-N-C-O dihedral and for the molecular dipole moment, no remarkable difference was found in the normal modes frequencies of *cis* and *trans* NMA as well as in the interatomic distances.

In Table 3.2 we report the results obtained for the molecular dipole moment of *cis* and *trans* NMA, and a comparison with other results obtained with different levels of calculations and from experiments in the literature. Atomic charges parameters for the Amber03 simulations and the Mulliken, CM1 and CM2 charges for the quantum Hamiltonian are provided in Table 3.3.

Table 3.3: Atomic charges (atomic units) for *cis* and *trans* NMA as obtained in the gas phase from molecular dynamics with the Amber03 force field and from SEBOMD with a PM3 Hamiltonian. The average standard deviation on the quantum charges is 0.02 *e*.

	Amber03	SEBOMD-Mulliken	
Atom		*cis*	*trans*
C_{ACE}	-0.19	-0.13	-0.14
H_{ACE}	0.08	0.07	0.06
H_{ACE}	0.08	0.07	0.06
H_{ACE}	0.08	0.07	0.06
C	0.51	0.24	0.24
O	-0.55	-0.37	-0.36
N	-0.42	-0.06	-0.05
H	0.29	0.08	0.07
C_{NMet}	-0.05	-0.09	-0.08
H_{NMet}	0.06	0.04	0.05
H_{NMet}	0.06	0.04	0.05
H_{NMet}	0.06	0.04	0.05
		SEBOMD-CM1	
Atom		*cis*	*trans*
C_{ACE}		-0.14	-0.14
H_{ACE}		0.07	0.07
H_{ACE}		0.07	0.07
H_{ACE}		0.07	0.07
C		0.41	0.41
O		-0.45	-0.44
N		-0.51	-0.51
H		0.35	0.33
C_{NMet}		0.00	0.01
H_{NMet}		0.05	0.05
H_{NMet}		0.05	0.05
H_{NMet}		0.05	0.05
		SEBOMD-CM2	
Atom		*cis*	*trans*
C_{ACE}		-0.14	-0.14
H_{ACE}		0.07	0.07
H_{ACE}		0.07	0.07
H_{ACE}		0.07	0.07
C		0.49	0.49
O		-0.47	-0.47
N		-0.59	-0.59
H		0.33	0.32

Table 3.3: (Continued)

C_{NMet}	0.03	0.04
H_{NMet}	0.05	0.05
H_{NMet}	0.05	0.05
H_{NMet}	0.05	0.05

On average, our PM3 results are in reasonable agreement with the data in the literature, in particular the result obtained for *trans* NMA through CM1 charges is in remarkable agreement with experiments [Rodrigo 86, Meighan 64]. The Mulliken charges lead to an underestimation of the molecular dipole moment. Higher levels of quantum chemistry predict a more polar *cis* conformer as well as the PM3 calculations both from the electronic structure calculations on the minimum geometry and from the average value of the SEBOMD simulations. This is in agreement with the trend based on Mulliken charges from SEBOMD simulations. On the other hand, the MM force field Amber03 and CM1 charges at a PM3 level predict the *trans* conformer to be more polar than *cis*. Finally, no difference in polarity is observed when evaluating the molecular dipole moment through CM2 charges.

We now present our results for the IR spectra of *cis* and *trans* NMA. In Figure 3.4 we show the computed spectra for *cis* and *trans* NMA as obtained from MM MD simulations by using the Amber03 force field [Duan 03].

The procedure based on the VDOS decomposition, described in Section 2.4.1 allows us to deduce the following assignment. The bands between 3200 and 3400 cm^{-1} are due to N-H stretch, those between 2800 and 3100 cm^{-1} to C-H stretch (both for the ACE and the NMet residues). The positions of such bands are quite similar for *cis* and *trans* NMA, though the former is slightly red shifted in *trans* NMA compared to *cis*. Based on low temperature nitrogen matrices, the infrared spectra of *cis* and *trans* NMA were measured [Ataka 84]. According to this study, the N-H stretch absorption due to the *cis* form has a peak at 3458 cm^{-1} and the one due to the *trans* form at 3498 cm^{-1}. Experiments in CCl_4 at ambient temperature found a peak at 3476 cm^{-1}, whereas symmetric and anti-symmetric C-H stretches fall between 2900 and 3000 cm^{-1} [Ataka 84, Kubelka 01].

The analysis of the VDOS decomposition shows that in the simulated spectrum of *trans* NMA the H-N-C bending vibration (amide II) occurs at 1780 cm^{-1} and the C-O stretch (amide I) occurs at 1680 cm^{-1}, whereas in *cis* NMA these two bands superimpose in a broader absorption around 1800 cm^{-1}. Experimental measurements of the IR spectrum (see [Kubelka 01] and references therein for the *trans* conformer) assign absorption between 1714 and 1731 cm^{-1} to amide I and between 1497 and 1500 cm^{-1} to amide II. As for the experimental spectrum of the less stable *cis* conformer [Ataka 84], the amide I mode occurs in the same frequency range as for the *trans* conformer, while the amide II mode is found at lower frequencies (by about 40 cm^{-1}) than in *trans*. In any case, the molecular mechanics force field employed does not give the correct trend between amide I and amide

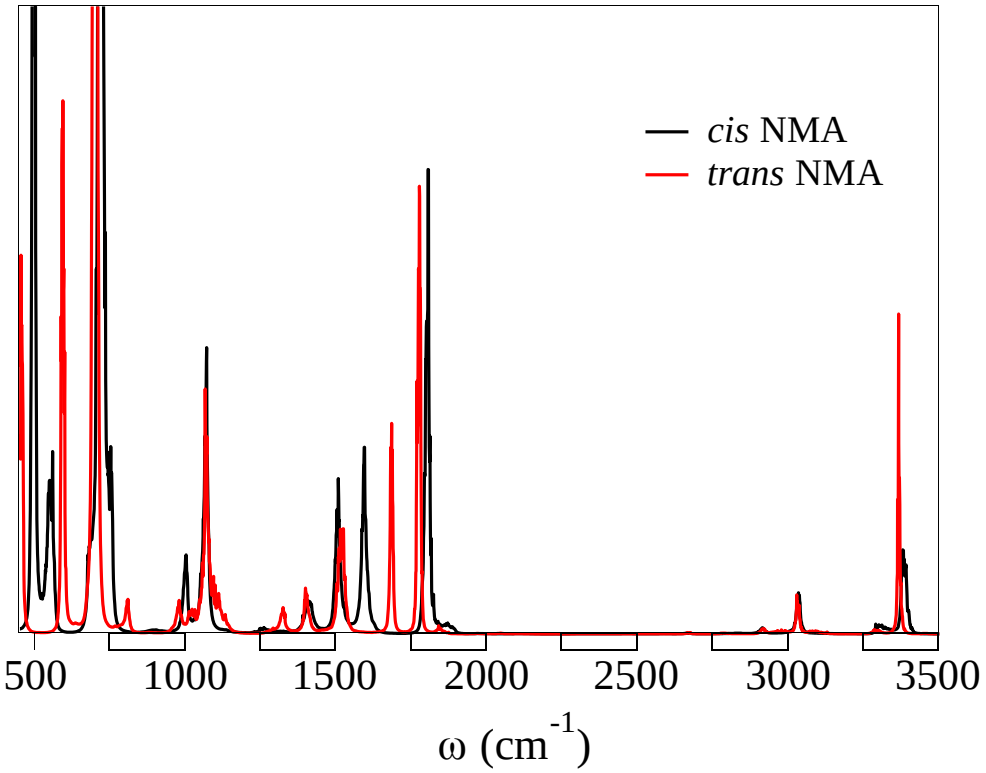

Figure 3.4: Isolated NMA. Calculated infrared spectrum from molecular dynamics simulations with an MM force field. The infrared intensity is arbitrary units.

II absorption. It has been pointed out that pyramidalization at the peptide group N atom needs to be taken into account along an MD simulation [Mannfors 03, Mirkin 04], since the CN torsion and the N-H out-of-plane bending give an important contribution to the NMA IR spectrum. Krimm and collaborators have performed extensive studies showing that including geometry-dependent charges may be more important than developing a polarizable MM force field [Palmo 03, Palmo 07]. An alternative approach has been proposed, generally improving the agreement with experiments compared to the classical MM-based evaluation of the vibrational properties of biological systems [Lagant 04]. This method is based on including additional terms in the potential energy function of the MM force field.

Another band in the IR spectrum from MD simulations, located around 1590 cm^{-1} in *cis* NMA, was assigned to H_{ACE}-C_{ACE}-C bend. This band is red shifted to about 1510 cm^{-1} in *trans* NMA. Between 1320 and 1510 cm^{-1}, in *trans* NMA we find the amide III bend and H-C-C, H-C-N bending motions. As for *cis* NMA, the same bands fall between 1380 and 1590 cm^{-1}. The amide III band position varies between 1255 and 1259 cm^{-1} in experiments, and backbone motions absorb at lower frequencies, where the pattern becomes more and more complicated for both conformers.

In Figure 3.5 we show the results obtained from SEBOMD simulations by using the PM3 Hamiltonian. We recall that we have different results according to the different scheme for partial atomic charges.

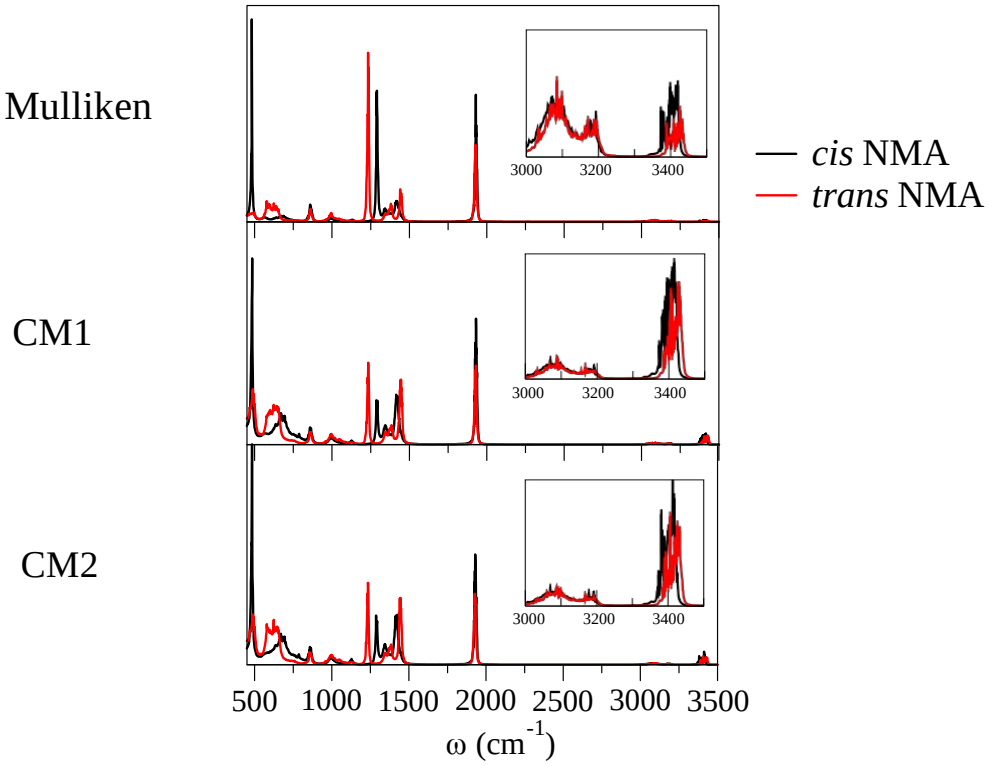

Figure 3.5: Isolated NMA. Calculated infrared spectrum from SEBOMD simulations with a PM3 Hamiltonian. The infrared intensity is arbitrary units.

Table 3.4: Collection of results for the infrared frequencies which are characteristic of the peptide bond of NMA in the gas phase and in water: amide I (AI), amide II (AII), amide III (AIII) and N-H stretch (δ_{NH}). All data in the gas phase (GP), in water (Sol.), and the average shift of the condensed phase results with respect to the gas phase (Δ) are reported in cm^{-1}.

	Amber03			SEBOMD			Experiment[d] Mode		
GP	Sol.	Δ	GP	Sol.		Δ	GP	Sol.	Δ
AI	1680[b],1800[c]	1680[b],1800[c]	0	1920[b,c]	1800[b,c]	-120	1714-1731	1625-1646	-90
AII	1780[b],1800[c]	1780[b],1800[c]	0	1420[b],1440c[c]	1485[b],1522[c]	75	1497,1500	1565-1585	80
AIII	1250[b],1320[c]	1250[b],1330[c]	5	1290[b],1230[c]	1340[b],1370[c]	95	1255-1259	1314-1317	60
δ_{NH}	3380[b],3370[c]	3380[b],3370[c]	0	3405[b],3410[c]	3370[b],3300[c]	-110[c]	3476[a]	3300	-130

[a] In CCl_4 solution.
[b] *cis* NMA.
[c] *trans* NMA.
[d] [Ataka 84, Kubelka 01]

The band positions and their width do not seem to depend on the charge type, which however affects slightly the peak intensities. Results are collected in Table 3.4.

The two regions in the high frequency portion of the spectrum (between 3000 and 3200

cm^{-1} and around 3420 cm^{-1}) are very similar for *cis* and *trans* NMA, the latter being blue shifted by 20 cm^{-1} compared to *cis*. This finding is in agreement with the experiment in Ref. [Ataka 84].

The amide I band is located for both conformers around 1920 cm^{-1}. The result is overestimated compared to the average experimental data. The amide II and amide III bands are spread over the 1230-1480 cm^{-1} region for *trans* NMA, and in a less extended region (between 1290 and 1480 cm^{-1} region) for *cis* NMA. The amide II peak in *cis* NMA is red shifted by 20 cm^{-1} compared to *trans*, again in agreement with the results in ref. [Ataka 84] (red shift of about 40 cm^{-1}). The positions of the amide II and amide III bands in the gas phase seems in quite good agreement with experiments. MD simulations within the Car-Parrinello scheme [Gaigeot 05] have provided the following results: the frequency for amide I is 1609 cm^{-1} in *trans* NMA and 1606 cm^{-1} in *cis* NMA. The frequency calculated for amide II is 1458 cm^{-1} in *trans* and 1369 cm^{-1} in *cis* NMA. Finally, The frequency for amide III is 1189 cm^{-1} in *trans* and 1259 cm^{-1} in *cis* NMA. Our results are in general agreement with the CPMD results. In particular, the amide I frequency is the same in *cis* and *trans* NMA, and the amide II peak in *cis* NMA is red shifted compared to *trans* NMA. However, it seems that the latter approach leads to a better agreement with experiments for the amide I band and to a worse agreement for amide II. In addition, no bands in the N-H stretch region are observed based on CPMD simulations.

In summary, though the amide I experimental band position is not accurately reproduced by our SEBOMD, we obtain a general reasonable agreement with experiments. On the other hand, MD with the Amber03 force field does not reproduce the correct ordering between amide I and II, predicting a lower frequency amide I mode compared to amide II.

3.1.3 Spectrum in water solution

First of all, we examine the solvent effects on the solute geometry. Compared to the results in the gas phase, little or no differences are observed when using the MM force field, whereas quite a few interesting conclusions can be drawn from an analysis of the results obtained with a quantum electronic Hamiltonian. In the latter case we used PM3 parameters with PIF corrections. Results obtained on the intramolecular distances are collected in Table 3.5.

When going from the gas phase to a solution in water, the C-O bond is elongated. The distance between the C and the N atoms is quite shortened. This is in agreement with the results observed in the literature [Gaigeot 05]. To interpret this result, we recall the two possible resonance structure of NMA in Figure 3.6. In a polar solvent, the zwitterionic form is stabilized by electrostatic interactions between the solute and the solvent, and accordingly, the C-O distance elongates and the C-N bond shortens. This effect cannot be reproduced by MM force fields and, not surprisingly, in this case MD simulations of NMA in water do not predict significant changes in NMA geometry with respect to the gas phase.

Table 3.5: Geometrical parameters for *cis* and *trans* NMA in water. Average values from molecular mechanics MD and from SEBOMD with a PM3 Hamiltonian and PIF corrections.[(a)] Distances are in Å. In parenthesis, we report the shifts with respect to the gas phase.

Atom	Amber03 *cis*	Amber03 *trans*	PM3-PIF *cis*	PM3-PIF *trans*
C_{ACE}-H_{ACE}	1.09 (0.00)	1.09 (0.00)	1.11 (+0.01)	1.11 (+0.01)
C_{NMet}-H_{NMet}	1.09 (0.00)	1.09 (0.00)	1.11 (+0.01)	1.11 (+0.01)
C-O	1.23 (0.00)	1.23 (0.00)	1.25 (+0.03)	1.25 (+0.03)
N-H	1.01 (0.00)	1.01 (0.00)	1.00 (0.00)	1.01 (-0.01)
C_{ACE}-C	1.52 (0.00)	1.52 (0.00)	1.50 (-0.01)	1.51 (0.00)
C-N	1.33 (0.00)	1.33 (-0.01)	1.39 (-0.04)	1.39 (-0.04)
N-C_{NMet}	1.46 (0.00)	1.46 (-0.01)	1.48 (+0.01)	1.47 (0.00)

[(a)] The standard deviation on distances is 0.03 Å with the exception of the CO and CN distances, for which it is 0.02 Å.

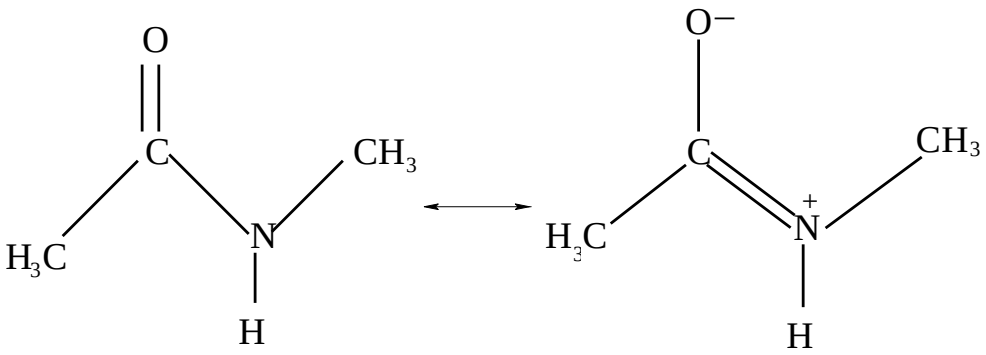

Figure 3.6: Resonance structures for NMA.

As for the out-of-plane position of the N-H bond in the case of simulations with a quantum Hamiltonian, we find distributions corresponding to a pyramidal N atom (see Figure 3.7). The distribution is much broader in solution than in the gas phase, and the out-of-plane angle is smaller ($\pm 16^\circ$ for *cis* and $\pm 25^\circ$ for *trans* NMA). This is consistent with a larger contribution of the zwitterionic resonance structure in a polar solvent.

When analyzing CM1 and CM2 atomic charges (see Table 3.6), we observe a displacement of electrons from the -NH group toward the -CO group, again in agreement with a larger contribution of the zwitterionic form. Charges on the O atom decrease whereas those on the N and the H atoms increase in going from the gas phase to solution. The C atom is less affected. On average, about -0.1*e* is transferred from -NH to -CO. We can therefore expect to observe a strong increase of the molecular dipole moment in solution. We collect our results for the molecular dipole moment together with other values obtained at different levels of theory in Table 3.7.

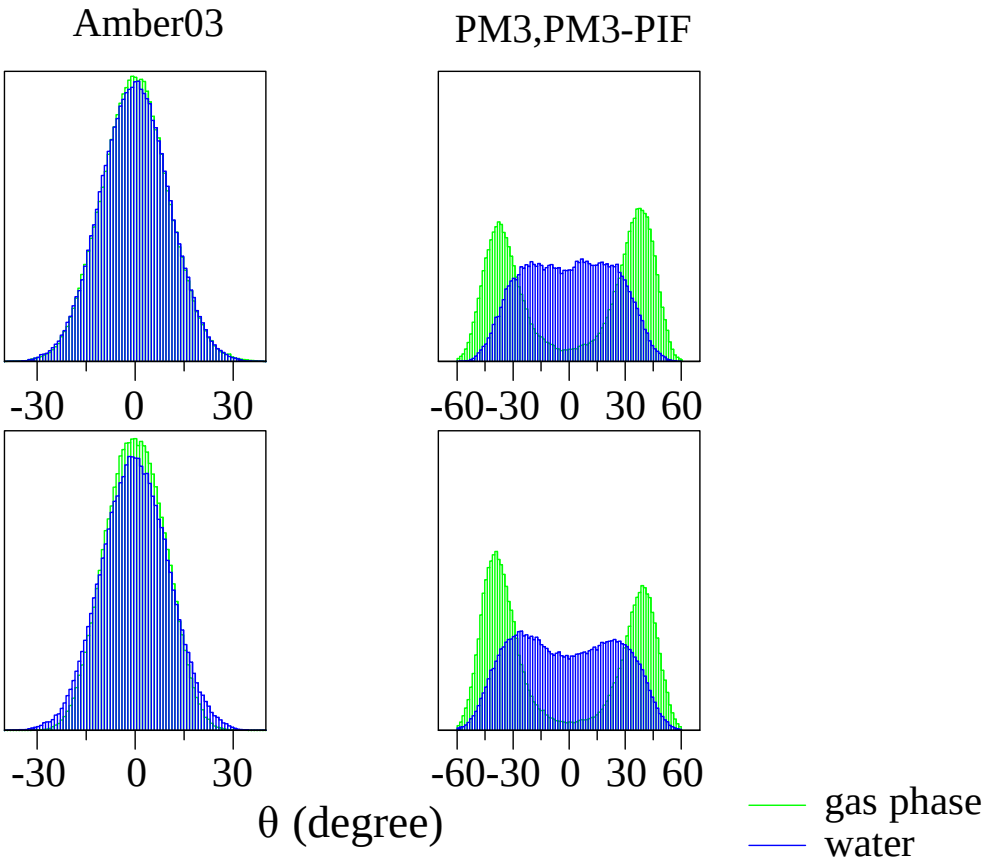

Figure 3.7: Distribution of the angle formed by the N-H bond with the plane instantaneously identified by N and the two C atoms from molecular dynamics with the Amber 03 force field (left side) and from SEBOMD (right side). Top panels: *cis* NMA (gas phase and solution). Bottom panels: *trans* NMA (gas phase and solution).

Table 3.6: Atomic charges (atomic units) for *cis* and *trans* NMA as obtained in water from SEBOMD with a PM3 Hamiltonian and PIF corrections. The average standard deviation on the quantum charges is 0.03 *e*.

	SEBOMD-Mulliken	
Atom	*cis*	*trans*
C_{ACE}	-0.17	-0.17
H_{ACE}	0.09	0.10
H_{ACE}	0.09	0.10
H_{ACE}	0.09	0.10
C	0.24	0.23
O	-0.52	-0.52
N	0.02	0.04
H	0.10	0.12
C_{NMet}	-0.12	-0.13

Table 3.6: (Continued)

H_{NMet}	0.08	0.07
H_{NMet}	0.08	0.06
H_{NMet}	0.09	0.06
	SEBOMD-CM1	
Atom	*cis*	*trans*
C_{ACE}	-0.17	-0.17
H_{ACE}	0.09	0.10
H_{ACE}	0.09	0.10
H_{ACE}	0.10	0.10
C	0.42	0.41
O	-0.61	-0.60
N	-0.44	-0.42
H	0.37	0.38
C_{NMet}	-0.04	-0.04
H_{NMet}	0.09	0.07
H_{NMet}	0.09	0.06
H_{NMet}	0.09	0.07
	SEBOMD-CM2	
Atom	*cis*	*trans*
C_{ACE}	-0.17	-0.17
H_{ACE}	0.10	0.10
H_{ACE}	0.10	0.10
H_{ACE}	0.10	0.10
C	0.49	0.48
O	-0.60	-0.60
N	-0.52	-0.50
H	0.35	0.37
C_{NMet}	0.00	0.00
H_{NMet}	0.09	0.07
H_{NMet}	0.09	0.06
H_{NMet}	0.09	0.07

As in the gas phase, some methods (Car-Parrinello MD, density functional theory with a B3LYP functional and a 6-31G(d) basis set coupled with a continuum solvent, or our PM3 calculation with Mulliken and CM2 charges) predict a more polar *cis* conformer, while others (Hartree-Fock calculations with a 6-31G(d) basis set coupled with a reference interaction site model (RISM) to describe the solvent, molecular mechanics MD with the Amber03 force field or our PM3 calculation with CM1 charges) predict the *trans* conformer to be the most polar in water.

Table 3.7: Comparison of NMA dipole moment (in Debye) as obtained from different methods in aqueous solution. Car-Parrinello molecular dynamics (CP-MD), quantum chemistry calculations (B3LYP/6-31G* in a continuum solvent and HF/6-31G(d) coupled with RISM), our results from SEBOMD at the PM3 and PIF levels (average molecular dipole from partial atomic charges using different schemes), and from simulations with the Amber03 force field. In parenthesis, we report the shifts with respect to the gas phase.

Method	*cis* NMA	*trans* NMA
CP-MD [Gaigeot 05]	7.33(+2.95)	6.96(+2.97)
B3LYP/6-31G*-SCRF [Garcia-Martinez 02]	4.95(+0.95)	4.86(+1.05)
HF/6-31G(d)-RISM [Du 03]	5.79(+1.42)	5.93(+1.71)
PM3,PIF(Mulliken)	5.94(+2.85)	5.41(+2.77)
PM3,PIF(CM1)	6.26(+3.02)	6.63(+2.94)
PM3,PIF(CM2)	6.26(+2.52)	6.22(+2.68)
Amber03 MM MD	4.14(+0.05)	4.54(+0.04)

Not surprisingly, very small induced dipole moments are calculated when running MD simulation with an MM force field. On the contrary, a very large change in the dipole moment of the order of 3 D is calculated from CP-MD and in our simulations when using CM1 charges. The effect is similar when using CM2 charges (about 2.7 D) and Mulliken charges (about 2.7-2.8 D), but much smaller with HF/RISM (1.4-1.7 D) and B3LYP/continuum (about 1 D). Since the two latter methods take into account the solvent as a bulk, specific interactions between solute and solvent are not described explicitly, in particular the formation of hydrogen bonds with water molecules.

The final part of this subsection will be devoted to the analysis of the IR spectra in water, and to a comparison with the gas phase results.

The results obtained for the IR spectrum of *cis* and *trans* NMA in water when running MD simulations with an MM force field (see Figure 3.8) show no remarkable differences both in band positions and shapes compared to the gas phase (compare with Figure 3.4 - peak positions are collected in Table 3.4).

The only perceivable difference in band position involves those modes which are located at lower frequencies (under 1000 cm^{-1}), where one can observe some line broadening both for *trans* and *cis* NMA.

In addition to the wrong frequency ordering of amide I and amide II bands, the Amber03 force field is thus not able to describe the differences in the IR spectrum of peptides going from the gas phase to aqueous solution.

On the other hand, the results obtained with the SEBOMD approach display significant differences in the condensed phase compared to the gas phase. This finding is in agreement with the CPMD results from Ref. [Gaigeot 05]. The effect of the dipole induced by water molecules on the solute has been shown to significantly affect the spectral profile of amide I-III bands [Yang 05]. In this work, the authors have compared the relative intensity and

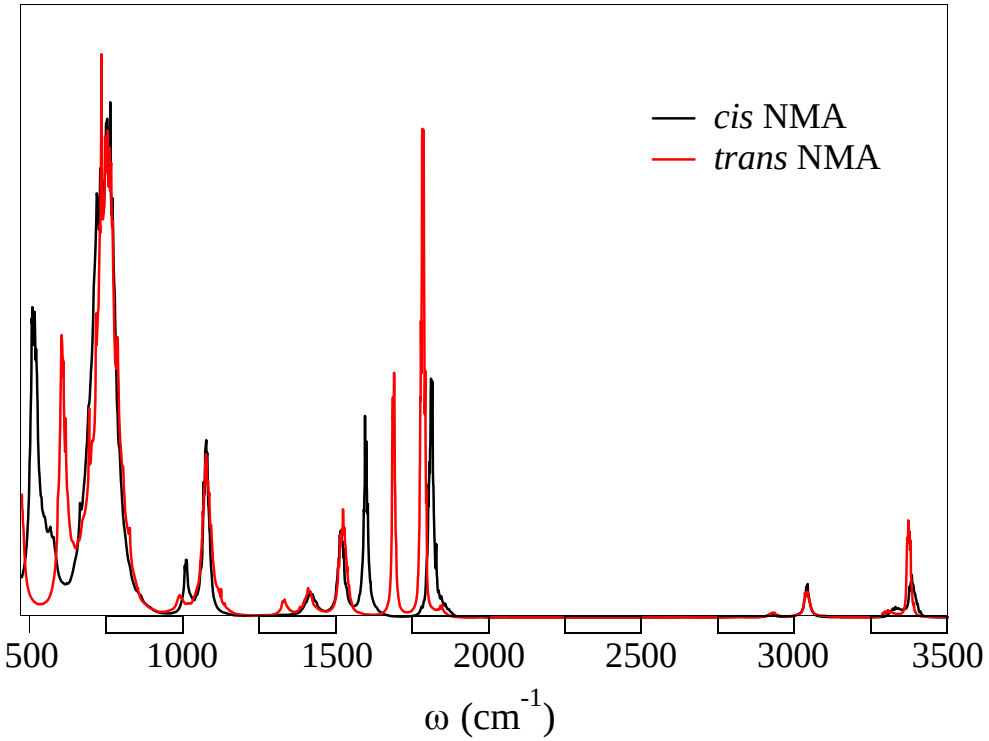

Figure 3.8: NMA in water. Calculated infrared spectrum from MD simulations with an MM force field.The infrared intensity is arbitrary units.

the band shape of amide I-III with experiments. An agreement with experimental features of these bands is achieved only if the solute is treated at a quantum level by means of a semiempirical electronic Hamiltonian.

In Figure 3.9 we collect the IR obtained from the three different charge schemes used in this work. When comparing Figure 3.9 with Figure 3.5, the IR bands in solution are broadened with respect to gas phase spectra. In addition, differences between spectra for the *cis* and *trans* conformers are enhanced in the condensed phase. A more detailed analysis of solvent effects for each vibrational mode is presented below and summarized in Table 3.4.

SEBOMD simulations predict the N-H stretch to be red shifted in both conformers. The *trans* conformer of NMA (band around 3300 cm^{-1}) undergoes a larger effect (red shift of about 110 cm^{-1}) compared to the *cis* one (band around 3370 cm^{-1} , shift of about 35 cm^{-1}). Experimentally, the frequency of N-H stretch was measured in CCl_4 to be 3476 cm^{-1} and 3300 cm^{-1} in water [Herrebout 01]. One should point out that this band is very sensitive to temperature and concentration. A large red shift is observed in experiments, the magnitude of which is compatible with our calculated result based on the most stable conformer *trans* NMA.

The band related to C-H stretch (between 2900 and 3200 cm^{-1}) is similar for *cis* and *trans* NMA. Compared to the gas phase, this band is quite broadened but not shifted. To our knowledge, no experimental data are available for the frequencies of the C-H stretching

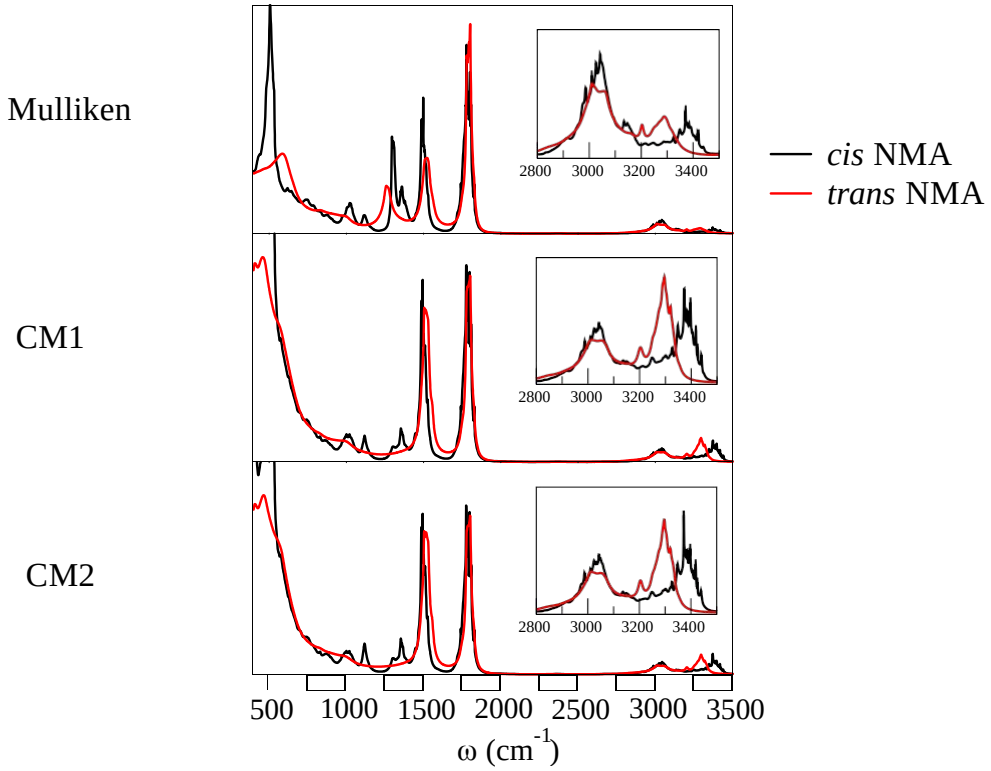

Figure 3.9: NMA in water. Calculated infrared spectrum from SEBOMD simulations with a PM3 Hamiltonian with PIF corrections. The infrared intensity is in arbitrary units.

motions in aqueous solution.

The amide I band is located around 1800 cm^{-1} and the *cis* and *trans* NMA conformers are predicted to absorb at the same frequency. In this case, solvent effects lead to a red shift of about 120 cm^{-1}. Results in the literature for amide I absorption band position vary from 1625 to 1646 cm^{-1} in aqueous solution [Kubelka 01]. An average red shift of about 90 cm^{-1} is thus observed, in good agreement with our results.

In the *cis* NMA spectra, the peak centered at 1485 cm^{-1} is assigned to amide II mode. A similar assignment is made in the case of *trans* NMA for the peak at 1522 cm^{-1}. Compared to gas phase data, we predict a blue shift of 80 cm^{-1} in *cis* NMA and 75 cm^{-1} in *trans* NMA. Experimental results for this band in water vary between 1565 and 1585 cm^{-1} [Kubelka 01]. The average blue shift is thus about 80 cm^{-1} again in quite good agreement with our calculated shift.

Bands between 1260 and 1370 cm^{-1} are quite broadened in solution. In this region, we observe the amide III motion, but some other modes are active too, and it is not easy to quantitatively extract their position. The *cis* absorption appears at slightly lower frequencies compared to the *trans* form. On average, we can estimate a solvent blue shift effect of about 95 cm^{-1}. The experimental results for amide III absorption vary between 1314 and 1317 cm^{-1}, with an average blue shift of 60 cm^{-1} compared to the gas phase [Kubelka 01].

The results obtained with Car-Parrinello MD in Ref. [Gaigeot 05] predict an average blue shift of 110 cm^{-1} for amide I, an average red shift 20 of cm^{-1} for amide II and of 40 cm^{-1} for amide III. The solvent effect obtained at this level of theory is again in fairly good agreement with our description. A comparison with the AM1/MM method used by Cho and collaborators [Yang 05] can only be carried out on the absolute values of the IR frequencies, since the corresponding results in the gas phase are not available. In addition, only the most stable (*trans*) conformer was considered. Amide I, II, III and the N-H stretch are reported to occur at 1896, 1721, 1444 and 3332 cm^{-1} , respectively. With the exception of the last band, it seems as if the AM1/MM combined strategy tends to overestimate the frequencies which are characteristic of the peptide bond.

The IR spectrum of *trans* deuterated NMA in a 16 D_2O molecules cluster has been calculated based on a PM3/MM approach [Jeon 10]. If we compare the results obtained in this work with the experimental measurements [Chen 95, Kubelka 01] on the amide I' band (the band corresponding to amide I in the deuterated system), one obtains an underestimated blue shift (30 cm^{-1} in the simulations vs. 90 cm^{-1} in the experiment). Although not conclusive, this comparison suggests that the solvent effect on the position of the solute IR bands is better described when the full system is treated at the quantum level, thus including mutual polarization and charge transfer.

Finally, broad absorption around 1000 cm^{-1} is related to backbone motion, but it becomes more and more complicated to analyze in depth the lower frequency regions of the spectrum, since many different modes are active there.

Overall, solvent effects are well reproduced by our SEBOMD simulations although the absolute values of the frequencies are not predicted with high accuracy. Specifically, when considering the frequency of the amide I, II and III modes, the calculated frequencies are overestimated, the error being relatively large for amide I, but smaller and similar for amide II and III. As a consequence, the gap between the amide I and II frequencies is too high while the amide II-amide III gap is in reasonable agreement with experiments, both in the gas phase and in solution.

In conclusion, we have discussed the importance of explicitly including the effect of the mutual solute-solvent polarization, as well as of charge transfer, to reasonably describe the effect of water on the infrared spectrum of NMA. In the following, we focus more in depth on showing to what extent each different term of the solute-solvent interaction affects the solvent-induced shift of the amide I band.

3.1.4 Solvent induced shift of the amide I band in water

In this section, we use a simple model to study the effect of a H-bond on the amide I frequency of NMA. We develop a methodology (see Section 2.4.2) allowing to extract the relative effect of interactions of different nature in the H-bond system: electrostatics, polarization, charge transfer, and the deformation of the potential energy surface corresponding to the amide I oscillator and induced by the presence of an intermolecular hydrogen bond.

We aim to provide a quantitative interpretation of the effect of a H-bond on the amide I

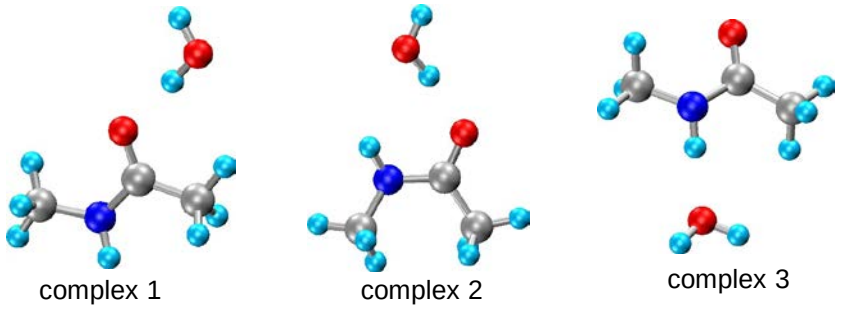

Figure 3.10: Structure of the three NMA-water complex on which we performed an interaction energy decomposition.

band. The main property that we shall discuss is the frequency shift in complex formed by NMA and one water molecule. This analysis will be complemented by a discussion of the geometrical properties and by a study of the charge distribution in the complex compared to the gas phase distribution of the two molecules (NMA and water).

The Divide and Conquer approach implemented in the Amber code, version 9 [Case 06] was used to find the minima for isolated *trans* - and *cis*-NMA (see Figure 3.1) and for NMA water complex the geometry of which is shown in Figure 3.10. Calculations were run at the PM3 [Stewart 89] level of quantum chemistry. An analysis of partial charges was also carried out using Mulliken charges and the CM1 and CM2 models [Storer 95, Li 98], both for the gas phase and for the complex molecule.

For the NMA water complex in the equilibrium geometry, an interaction energy decomposition was performed using the method by Van der Vaart and Merz [der Vaart 99]. Then, to calculate the second derivative of the electrostatic, polarization, charge transfer and deformation terms, we performed more calculations by moving the atoms along the normal mode describing the amide I vibrational motion, generating enough points on the potential energy surface (PES) to evaluate numerically the second derivative.

In Table 3.8 we introduce the geometrical parameters related to the distance between the atoms in the peptide bond unit for the optimized structure of the isolated NMA together with that of the NMA water complex at PM3 level. When the water molecule hydrogen bonded to the carbonyl group (complexes 1 and 2), the C-O bond is slightly elongated whereas the C-N bond is slightly shortened. However, no change has been observed in the N-H bond. On the other hand, in the complex 3, where the water molecule is hydrogen bonded to the -NH group, we find the C-O and C-N bonds do not change, whereas the N-H bond is slightly elongated. When analyzing the atomic charge on the relevant atoms (see Table 3.9), the first remark that we make is that the charge transfer between the two molecules changes its direction when the H_2O molecule switches its behavior, from H-bond donor to acceptor. In complexes 1 and 2 the water-H atom that is closer to the carbonyl group of NMA (H1) becomes more positively charged compared to the isolated molecule, and the water-O atom becomes more negative. In complex 3, the water-O becomes more negative (but to a lesser amount compared to complex 1 and 2), and the two H atoms

Table 3.8: Optimized geometrical parameters (in Å) for the isolated NMA and the NMA water complexes.

	trans-NMA	*cis*-NMA	complex 1	complex 2	complex 3
r(C-O)	1.22	1.22	1.23	1.23	1.22
r(C-N)	1.43	1.43	1.42	1.42	1.43
r(N-H)	1.00	1.00	1.00	1.00	1.01

Table 3.9: The partial atomic charges shift (in e) due to the complex formation with respect to the isolated molecule.

		NMA				water		
		O	C	N	H	O	H1	H2
complex 1	Mulliken	−0.038	0.015	0.016	0.004	−0.065	0.040	−0.003
	CM1	−0.032	0.015	0.014	0.004	−0.053	0.034	−0.003
	CM2	−0.024	0.013	0.013	0.004	−0.046	0.022	−0.003
complex 2	Mulliken	−0.031	0.015	0.011	0.015	−0.066	0.041	−0.001
	CM1	−0.034	0.016	0.009	0.013	−0.054	0.034	−0.002
	CM2	−0.012	0.014	0.010	0.013	−0.047	0.023	−0.001
complex 3	Mulliken	−0.023	0.005	−0.037	0.045	−0.010	0.014	0.011
	CM1	−0.013	0.005	−0.028	0.040	−0.010	0.012	0.009
	CM2	−0.013	0.005	−0.021	0.028	−0.002	0.011	0.008

become more positive. As for the NMA molecule, it can be observed in all cases that the charge transfer is not localized to the atoms that are closer to the water molecule. Due to the resonance between the neutral and zwitterionic forms of the peptide bond, the atoms change their charges in a way that increases the value of the local dipoles in the -NH and -CO groups.

Now, let us focus our attention on the analysis of the amide I vibrational frequency. According to the classical mechanical treatment, the potential energy V does not exceed the total energy E. Accordingly, we find the classical allowed region for the harmonic oscillator of the amide I normal mode coordinate Q should be in the range $-0.06 \leq Q \leq +0.06$ Å $g^{1/2}$ $mol^{-1/2}$ with energy equal to $K_B T$. In Figure 3.11 we show the potential surface of the isolated *cis*- and *trans*-NMA when moving along the amide I normal mode in the gas phase Q_g. Although *trans*-NMA is known to be more stable than the *cis* conformer, our analysis using the PM3 method shows that the *cis*-NMA is 0.2 kcal/mol lower than the *trans*-NMA. The PM3 method seems to over stabilize the *cis*-NMA conformer. This may be related to a well-known artifact of the PM3 core repulsion function describing the core-core interaction between two H atoms [Csonka 93, Cramer 94, Csonka 97].

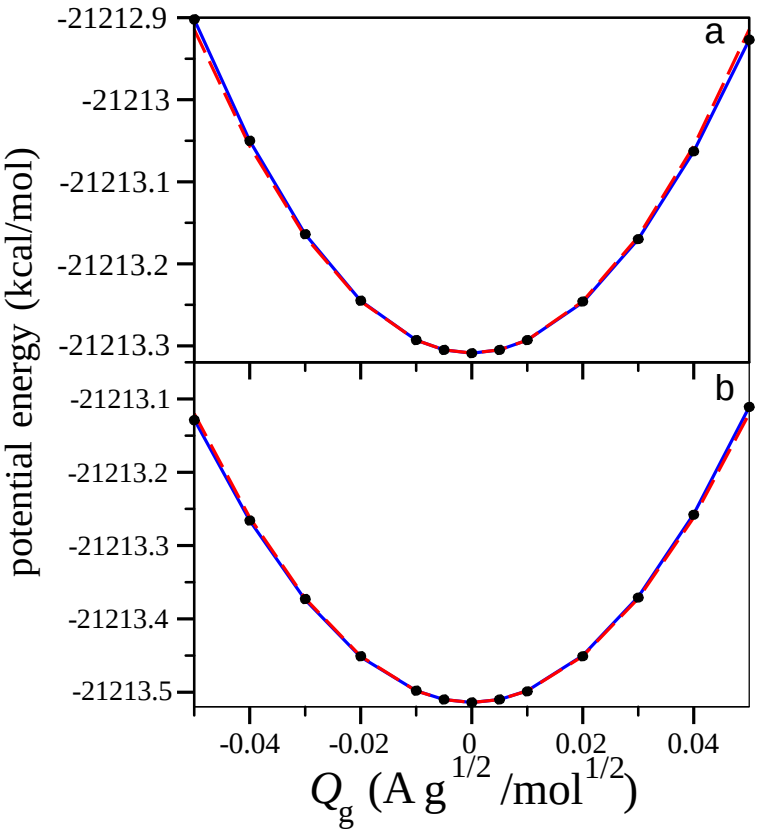

Figure 3.11: Potential energy curve for vibration of the amide I mode of the isolated *trans* (a) and *cis* (b) NMA (black circles) and the corresponding fit curves to Eq. (3.1) (blue lines) and to Eq. (3.2) (dashed red line).

The potential energy curve is well reproduced by a Taylor expansion of order three as

$$V(Q) = a + bQ + \frac{1}{2!}cQ^2 + \frac{1}{3!}dQ^3 \tag{3.1}$$

being a the potential energy at equilibrium geometry ($Q = 0$), and b, c, d the first, second, and third derivative of $V(Q)$, respectively. In Table 3.10 we present the results of the fit for the potential energy of the isolated molecules. The fitted parameters are shown in Figure 3.11. The potential energy surface of the NMA water complexes when moving along the amide I normal mode in the complex Q_c is shown in Figure 3.12. Interestingly, we find the potential energy surfaces for all complexes is well fitted as well to Eq. (3.1). The results of the fit are included in Table 3.10 and the data are superimposed in Figure 3.12.

From Table 3.10 we see in all cases the first derivative of the potential energy is practically zero, since we move around a minimum position. In Figures 3.11-3.12 we, also, show the fitted potential energy curve when considering the potential energy is purely harmonic

$$V(Q) = a + \frac{1}{2!}cQ^2 \tag{3.2}$$

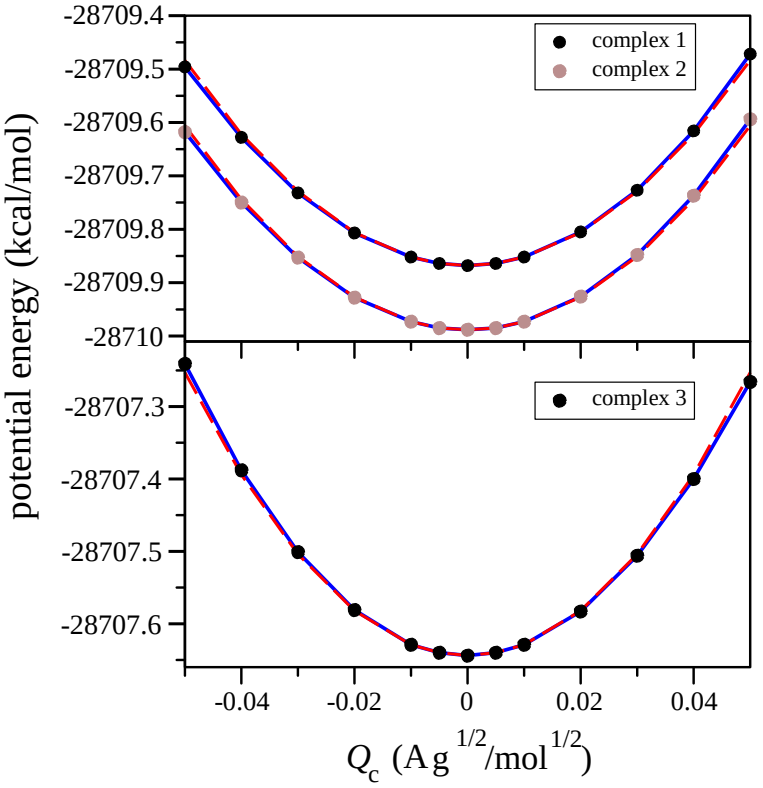

Figure 3.12: Potential energy curve for vibration of the amide I mode of the complex 1, 2 and 3 (black circles) and the corresponding fit curves to Eq. (3.1) (blue lines) and to Eq. (3.2) (dashed red lines).

As seen the fitted curve coincides with the real potential energy curve when we move just slightly from the equilibrium position ($Q = 0$). However, we find a small deviation

Table 3.10: Fit parameters for the potential energy surface for the vibration of the amide I mode for both the isolated NMA and NMA water complexes.

	isolated NMA		NMA complexes		
	trans	*cis*	complex 1	complex 2	complex 3
a^a	-21213.3	-21213.5	-28709.9	-28710.0	-28707.6
b^b	1.0×10^{-6}	1.0×10^{-5}	1.3×10^{-5}	1.0×10^{-5}	1.0×10^{-6}
c^c	315.548	315.400	307.089	306.303	312.813
d^d	-599.695	414.754	585.613	575.415	-597.591

a.- kcal/mol
b.- kcal $Å^{-1}$ $g^{-1/2}$ $mol^{-1/2}$
c.- kcal $Å^{-2}$ g^{-1}
d.- kcal $mol^{1/2}$ $Å^{-3}$ $g^{-3/2}$

Table 3.11: The harmonic force constant k (in kcal Å^{-2} g^{-1}) obtained by computing the second derivative numerically from the potential energy when moving along the amide I normal mode Q (in Å g$^{1/2}$ mol$^{-1/2}$) together with the harmonic frequency v (in cm^{-1}).

	Q	k	v
trans-NMA	±0.005	314.981	1927.240
cis-NMA	±0.005	315.248	1928.666
complex 1	±0.005	306.947	1902.510
complex 2	±0.005	306.154	1900.051
complex 3	±0.005	312.694	1920.237

from the real potential energy curve when we move a little far away from the equilibrium position. In Table 3.11 we introduce the force constant k obtained by evaluating the second derivatives numerically from the potential energy considering $Q = \pm 0.005$ Å g$^{1/2}$/mol$^{1/2}$. The thus obtained force constants are therefore considered to be harmonic. Comparing the results in Table 3.11 with those obtained from the fit in Table 3.10, when the cubic anharmonic term was considered, we note that the force constants are very close, which points to a very small contribution of the cubic anharmonic coefficients.

In Table 3.12 we include the frequencies of the amide I mode of the complexes along with the corresponding frequencies for NMA in the gas phase, as they were evaluated from the fitted force constant in Table 3.10. When comparing these frequency values with those obtained from the harmonic force constants presented in Table 3.11, we see that they are very close. By analyzing the frequency shift in the complexes we observe that, when the water molecule is hydrogen bonded to the carbonyl group of *trans*-NMA, the frequency is red shifted by −26 cm^{-1}. On the other hand, when the water molecule is hydrogen bonded to the -NH group, the frequency is only red shifted by −8 cm^{-1}. In addition, we observe that the frequency is red shifted by −28 cm^{-1} when the water molecule hydrogen bonded to the carbonyl group of *cis*-NMA, which is slightly higher than that observed in the *trans*-NMA. It is worth noting that in the case of our previous analysis using SEBOMD simulations, the total shift of the amide I band was estimated to be −120 cm^{-1}. To provide a deeper analysis of cooperative effects, in the complexes shown in Figure 3.13 we qualitatively investigated the effect of a second (complex a) and of a third (complex b) water molecule interacting with the carbonyl group of NMA, and of two H-bond donating and one H-bond accepting water molecules (complex c). The structures that we considered were obtained by geometry optimization. We find the amide I frequency shift of the complexes a, b and c is −62.0, −67.1, and −57.1 respectively.

On average, about 50% of the total shift in the condensed phase is recovered by adding one additional water molecule interacting with the carbonyl group. When dealing with three water molecules, one obtains a larger absolute shift by having the three of them on the carbonyl side compared to having two of them on the carbonyl side and another one on the -NH side. However, the interaction energy decomposition analysis for these complexes

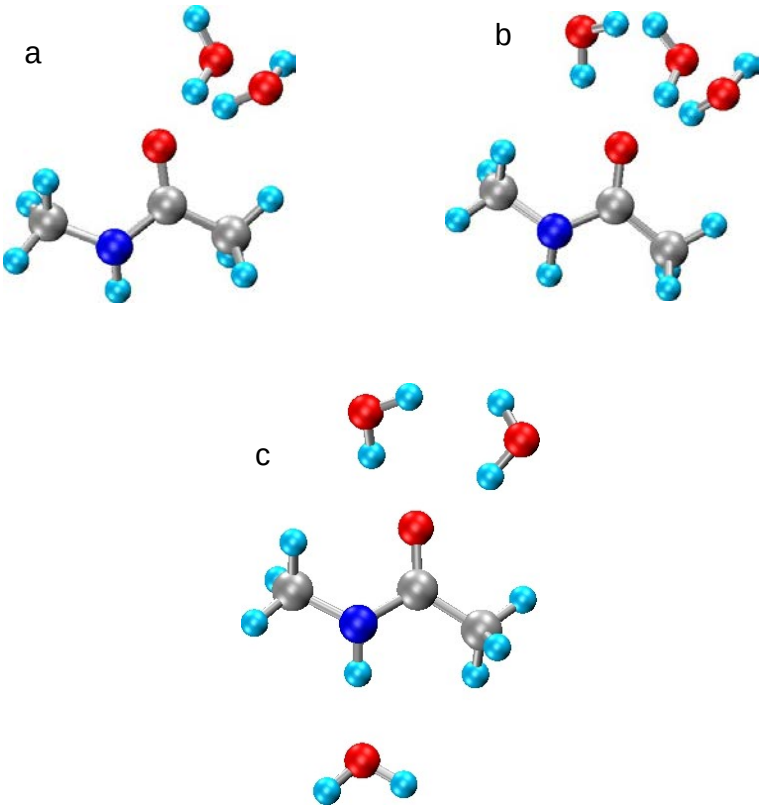

Figure 3.13: *trans* -NMA complexed with two and three H-bonded water molecules.

Table 3.12: Amide I frequency (in cm^{-1}) for the NMA in the gas phase and in the complexes as they were computed from the force constant obtained from the fit in Table 3.10.

	Frequency
trans -NMA	1928.981
cis-NMA	1928.529
complex 1	1902.950
complex 2	1900.514
complex 3	1920.604

was not performed, in order to avoid the contribution of water-water interactions. The importance of including the effect of water molecules in higher solvation shells of NMA to reproduce the solvent effect on the amide I band has already been pointed out in previous studies [Bouř 03, Mennucci 05]. Cho *et al* [Ham 02] have analyzed this issue by studying cluster of NMA and D_2O. They found a linear relationship between the frequency shift of amide I and the hydration induced elongation of the C-O bond, generated by the electric field of the surrounding water molecules. Torii [Torii 04] has investigated cooperative effects on the hydration induced shift, also finding a correlation between the geometry distortion

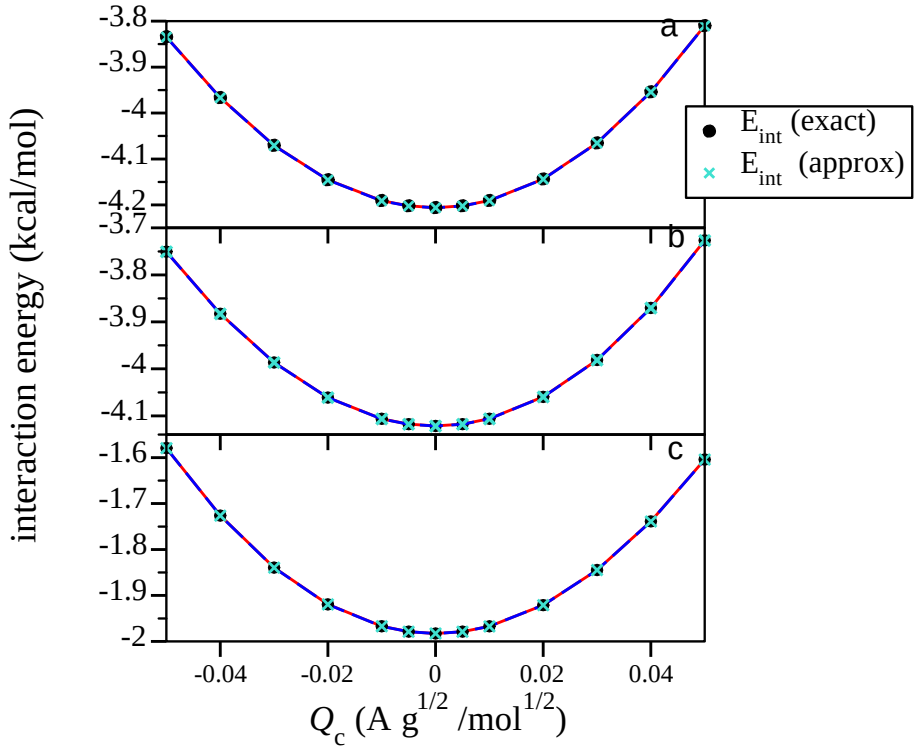

Figure 3.14: Intermolecular potential energy curve for the amide I mode of complex 1 (a), complex 2 (b) and complex 3 (c) when moving along the normal coordinate in the complex Q_c and the corresponding fit curves to Eq. (3.1) for the E_{int} (exact) (red lines) and E_{int}(approx) (dashed blue lines).

of NMA and electric field projected along a specific direction, related to the -CO stretch motion.

We turn now to the analysis of the amide I mode based on the potential energy surface of the different complexes. In Figure 3.14 we show the interaction energy (E_{int}(approx)) as computed from the sum of the electrostatic, polarization, charge transfer and deformation energies (see Eq. (2.115)) and that obtained from the difference between the potential energy of the complex and the minima of the potential energies of the isolated NMA and water molecules (E_{int} (exact)) (see Eq. (2.113)), when moving along the normal mode in the complex, Q_c. The two surfaces are extremely close to one another. We find that the intermolecular potential energy surface is well fitted to Eq. (3.1). The results of the fit are reported in Table 3.13 and the data are superimposed in Figure 3.14. From the table we may notice that the fitted parameter of both E_{int} (exact) and E_{int}(approx) are very similar. Moreover, the fitted parameters corresponding to the second derivatives of the intermolecular potential energy are as same as those obtained from the fitting of the total potential energy surface (see Table 3.10), as expected. To interpret this point we recall Eq. (2.113).

We now discuss the different energetic contributions of the water induced shift in the

Table 3.13: Fit parameters for the electrostatic, polarization, charge transfer and deformation energy along with the total interaction energy when moving along the amide I normal coordinate in the complex Q_c.

		E_{ele}	E_{pol}	E_{CT}	E_{def}	E_{int}(approx)	E_{int}(exact)
complex 1	a^a	7.48196	-0.31302	-11.5306	0.155265	-4.20634	-4.20601
	b^b	0.6373	0.38168	3.8969	-4.91548	0.00041	1.3×10^{-5}
	c^c	2.45141	-0.260859	-0.9848	305.944	307.090	307.094
	d^d	1.550	-0.178217	0.23216	583.941	585.471	585.403
complex 2	a^a	7.5139	-0.331495	-11.3667	0.062477	-4.12183	-4.121
	b^b	0.47844	0.3909450	3.880310	-4.75061	-0.00092	-4.3×10^{-5}
	c^c	2.74541	-0.220979	-1.34137	305.1370	306.320	306.303
	d^d	1.19046	-0.189745	3.201920	574.3090	578.508	575.567
complex 3	a^a	8.20058	-0.215707	-10.0957	0.128033	-1.98284	-1.98271
	b^b	-1.0620	-0.04137	0.242119	0.861214	-6.8×10^{-5}	3.2×10^{-5}
	c^c	0.33403	-0.030087	0.0149001	312.495	312.814	312.813
	d^d	-0.4379	0.0338219	-0.00783019	-597.157	-597.571	-597.682

[a].- Kcal/mol
[b].- Kcal $Å^{-1}$ $g^{-1/2}$ $mol^{-1/2}$
[c].- Kcal $Å^{-2}$ g^{-1}
[d].- Kcal $mol^{1/2}$ $Å^{-3}$ $g^{-3/2}$

NMA-water complexes. In Figure 3.15 we show the energy curve for each term arising from the interaction energy decomposition when moving along the normal coordinate Q_c. The electrostatic, polarization, charge transfer and deformation terms in complex 1 have the same behavior as in complex 2. On the other hand, for complex 3 we observe a different trend in the charge transfer and the deformation terms, whereas the electrostatic and polarization terms have a similar behavior. In addition, the deformation energy in complex 3 seems to be closer to the pure harmonic behavior compared to the other complexes. Interestingly, we find that also in this case the energy curve for each term can be well fitted to a Taylor expansion of order three (see Eq. (3.1)). The results of the fit are reported in Table 3.13 and the corresponding plots are shown in Figure 3.15. From the table we observe that the sign of the fitted parameter c for the charge transfer energy, corresponding to k_{CT}, changes when going from the complexes where the water molecule is on the carbonyl side to the complex where it is on the -NH side. This is most likely related to the observed change in the charge flux from NMA to water.

Finally, in Table 3.14 we present the results of the model that we developed to obtain the decomposition of the solvent-induced shift of amide I (see Eq. (2.117)). When comparing complex 1 and 2, we notice very small differences, whereas they are quite different compared to complex 3. In all cases, the largest contribution to the total shift is given by the deformation term, whereas polarization is one order of magnitude smaller compared to

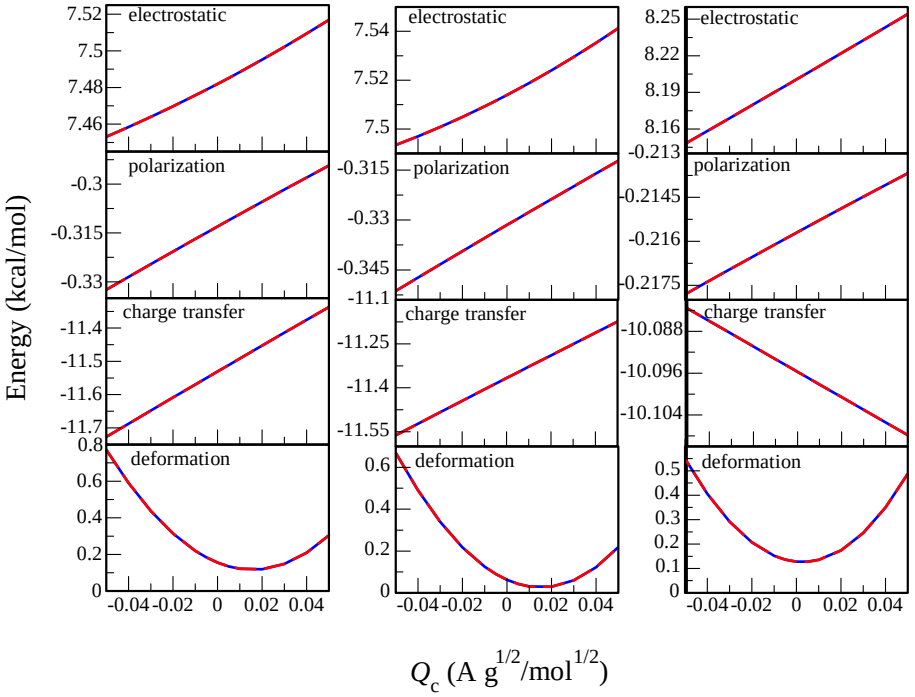

Figure 3.15: The electrostatic, polarization, charge transfer and deformation energies (blue lines) and the corresponding fitting curves (dashed red lines) for complex 1 (left panel), complex 2 (middle panel) and complex 3 (right panel). Note the energy scale difference.

Table 3.14: Amide I solvent induced shift: relative contribution for each term in the interaction energy decomposition.

	$\Delta\nu^r_{\text{ele}}$	$\Delta\nu^r_{\text{pol}}$	$\Delta\nu^r_{\text{CT}}$	$\Delta\nu^r_{\text{def}}$	$\Delta\nu/\nu_{\text{g}}$
complex 1	0.00777	−0.00083	−0.00312	−0.03043	−0.0133
complex 2	0.00870	−0.00070	−0.00425	−0.03254	−0.0144
complex 3	0.00106	−0.00009	0.00005	−0.00967	−0.0043

electrostatics and charge transfer. In these complexes, it would seem that the amide I shift induced by the formation of a H-bond is mainly due to the geometrical distortion of the NMA molecule in the field generated by the H_2O molecule.

3.2 VIBRATIONAL RELAXATION OF THE AMIDE I MODE OF THE NMAD MOLECULE IN $D_2O_{(L)}$

3.2.1 Computational details

We describe here in detail the computational methods that have been adopted to run MD simulations in order to analyze the INMs and the vibrational energy relaxation of the initially excited amide I mode.

Concerning the MD simulations with MM potential we used the AMBER94 [Cornell 95] force field to model the solute NMAD and the flexible TIP3P water model with doubled hydrogen masses included in the CHARMM force field [MacKerell 98] to model the D_2O solvent (see Ref. [Soler 10]). The NMAD molecule was placed in a cubic box of 1.975 nm containing 251 D_2O molecules to reproduce the experimental D_2O density [Nakamura 95] ($\rho = 1.10436$ g/cm^3) with periodic boundary conditions. The simulation was performed using the TINKER modeling package version 5.0 [Ren 02, Ren 03]. A cutoff of 10 Å was applied for the non-bonded interaction calculation, and the particle-mesh Ewald method has been used to treat the long range electrostatic interaction.

The ENMs were obtained from the optimized geometry of the isolated *trans*-NMA conformer, providing normal mode frequencies which are in good agreement with previously reported values [Rey-Lafon 73, Ataka 84, Gregurick 02, Soler 10]. The initial coordinates and momenta for the vibrational relaxation dynamics were taken from 32 previous MD simulations of 1250 ps at 300 K, which were started using random velocities. An initial period of time of 750 ps was used to equilibrate the system, collecting data at 20 ps intervals in the last 500 ps. The time step Δt was 0.5 fs. During the simulations the temperature was maintained at mean value 300 K by coupling to a thermal bath [Berendsen 84]. Thus, 800 sets of initial position and momenta were stored for subsequent nonequilibrium vibrational relaxation simulations.

At $t = 0$, an excess of energy of one vibrational quantum was instantaneously deposited in the NMAD molecule by displacing the amide I mode until its energy reached the proper value. During the relaxation dynamics, the values of the atomic positions, forces, momenta and Hessian matrix of the solute were exported every 50 fs . The Hessian matrix has been computed using the subroutine *hessian* of the TINKER package, taking into account the interactions between the atoms of the solute and solvent.

Regarding the SEBOMD simulations of the NMAD molecule in D_2O solution we used the Amber code, version 9 [Case 06], and the semiempirical quantum mechanical (PM3) Hamiltonian to describe the electronic wave function for the solute and the solvent, whereas the PIF correction for water-water and solute-water intermolecular interactions has been employed.

The simulations were performed by placing a NMAD molecule in a cubic box of length

1.26885 nm contain 64 D_2O water molecules. To sample the initial configurations for the nonequilibrium simulations, a 564 ps NVT ensemble simulation with $\Delta t = 1$ fs was performed starting from a configuration extracted from the MM force field MD simulations. An initial period of 204 ps was used for equilibrating the system during a series of consecutive NVT simulations. First, we run a simulations for 10 ps and velocity was scaled each 500 fs by employing the Andersen thermostat [Andersen 80]. Then, it follows by a simulations for 100 ps with velocity scaling every 1 ps using the Andersen thermostat as well. Finally, we run a simulations for 94 ps by employing Berendsen thermostat [Berendsen 84]. The last 360 ps under Berendsen control temperature were used to collect the equilibrated configurations at 3 ps intervals. Thus we have 120 trajectories for the subsequent nonequilibrium vibrational relaxation simulations.

At $t = 0$ an excess of energy of one vibrational quantum was instantaneously deposited in the NMAD molecule by displacing the amide I mode until its energy reached the proper value. The subsequent nonequilibrium MD simulations were performed in the NVE ensemble for 40 ps with $\Delta t = 0.5$ fs. During the relaxation dynamics, the values of the atomic positions, forces, momenta and the Hessian matrix of the solute (taking into account the solute-solvent intermolecular interactions) were exported every 25 fs.

The simulations were performed with periodic boundary conditions, and long range electrostatic interactions were taken into account by using the Ewald-method [Nam 05]. The cutoff used was 4.1 Å. The full Fock matrix is built using the minimum image convention for all direct interactions inside the periodic box (direct sum). The Fock matrix of the system was built at each time step and diagonalized through standard techniques according to the Self-Consistent Field (SCF) scheme. This ensures that the electronic density converges at each step of the simulation, and that the dynamics follows the Born-Oppenheimer potential energy surface [Herbert 05, Niklasson 06].

Most quantum chemical calculations using Molecular Orbital (MO) methods as in SEBOMD determine the orbitals by some iterative method. When iterations of the SCF process converge, the energy is stationary with respect to infinitesimal variations in the orbitals. Whether this stationary point is stable (local minima) or unstable (maxima in one or more directions) depends on the second derivatives of the energy with respect to the orbital variation [Szabo 96, Cramer 04, Jensen 07]. Because of the iterative nature of the SCF procedure, convergence problems are sometimes encountered. Furthermore when convergence is achieved, there is often no guarantee that the solution to the SCF problem is stable with respect to all permitted changes in the wave function [Szabo 96, Cramer 04, Jensen 07]. At some point, the energy differences between newly determine orbitals fall below some threshold criterion, and we refer to the final set of the wave function as the converged SCF orbitals. In our case we employ 10^{-10} eV as the threshold criterion for the total electronic energy and the energy eigenvalue for MO. Such criteria is of course entirely arbitrary and it is validated by checking different properties derived from the wave functions in order to reach an optimum balance between convergence and accuracy.

Table 3.15: Mean kinetic and harmonic potential energies (in cm^{-1}) for the ENMs and INMs of the NMAD molecule in D_2O solution obtained using the Min-Cost algorithm in equilibrium MD simulations.

Mode	(T_i^{ENM})	$(V_{i,\mathrm{har}}^{\mathrm{ENM}})$	(T_i^{INM})	$(V_{i,\mathrm{har}}^{\mathrm{INM}})$
1	103.5	58.3	104.8	-14.0
2	103.5	113.0	104.8	-93.1
3	105.1	98.7	105.3	151.3
4	104.0	101.5	104.3	98.3
5	104.5	107.3	104.5	106.8
6	103.4	104.1	103.5	110.3
7	103.6	108.1	103.5	104.5
8	103.6	97.6	103.8	94.2
9	104.1	114.5	104.1	110.4
10	103.3	164.1	103.6	110.8
11	102.2	223.0	103.1	107.8
12	103.7	302.5	104.7	109.2
13	104.0	232.0	104.0	107.7
14	103.0	171.2	103.2	109.3
15	104.2	306.4	104.0	102.0
16	102.5	9087.0	102.2	104.3
17	104.0	256.6	103.0	92.8
18	103.0	2723.7	102.8	98.0
19	103.3	7066.8	102.7	103.5
20	102.4	165.4	102.4	98.5
21	103.4	10231.6	103.3	103.5
22	103.4	21177.4	103.4	109.4
23	102.8	675.6	102.8	104.7
24	102.5	272.0	102.6	104.0
25	103.3	421904.0	101.5	103.7
26	103.2	544918.0	101.6	103.7
27	104.0	709.1	103.8	105.0
28	103.4	813.0	103.5	104.6
29	102.6	594.6	102.3	104.7
30	102.4	674.2	102.5	104.3

3.2.2 INMs analysis

We start by analyzing the performance of our method to analyze the vibrational energy for each normal mode during the MD simulations as obtained by employing Eq. (2.44) and Eq. (2.60) when the Min-Cost (MC) algorithm is applied during the assignment of the INMs. Accordingly, in Table 3.15 we include the averaged kinetic and harmonic potential energies for the ENMs and INMs calculated from the equilibrium MD simulations for the NMAD molecule in D_2O solution.

We consider the vibrational energy of the solute molecule in terms of the normal mode individual contributions as given from Eq. (2.44) and Eq. (2.60). As observed the ENM kinetic energies reproduce well the equilibrium thermodynamic value at 300 K ($k_BT/2 =$

104.3 cm^{-1}), while the averages values of the ENM harmonic potential energies deviate from it. This behavior is due to the strong anharmonicities and couplings that emerge between the ENMs when the solute molecule explores regions of the phase space which are far away from the equilibrium configuration, which by way cause a limitation to interpret the vibrational energy content of the individual ENMs based on their averaged kinetic energies as has been proposed [Raff 88, Kabadi 04]. Consequently, it is not possible to express the vibrational energy of the solute molecule accurately, as the sum of harmonic contributions of the ENMs (see Eq. (2.44)). Alternatively, this can be achieved by using the INMs through Eq. (2.60), as will be demonstrated below.

Let us evaluate the use of the INMs to analyze the vibrational dynamics of the solute. As has been demonstrated by previous work of our research group [Bastida 10a, Bastida 10b, Kalstein 11] the identification of the INMs using just the frequency order criterion is meaningless, due to the facility with which the INMs mix and cross. The Min-Cost algorithm provides the best global one-to-one assignments of the INMs to the ENMs [Bastida 10a, Bastida 10b]. This is clearly shown in Figure 3.16 where we depict the averaged $|\boldsymbol{L}|$ matrix elements calculated directly using Eq. (2.48) (upper panel) and the transformed $|\boldsymbol{L}|$ matrix obtained after applying the Min-Cost algorithm (lower panel). The sizes of the bubbles in this figure are proportional to the values of the averaged $|l_{ij}|$ matrix elements. As observed, the Min-Cost $|\boldsymbol{L}|$ matrix is much more diagonal, which indicates that the corresponding assignments are better.

As has been demonstrated [Bastida 10b, Kalstein 11], the Min-Cost method is however not free of unphysical assignments, which occurs when two or more INMs turn out to share appreciable contributions from ENMs with quite different frequencies. In the NMAD/D_2O system, this is the case for the 1st, 2nd, 25th and 26th INMs, which share significant contributions of the 1st, 2nd, 25th and 26th ENMs as clearly shown in Figure 3.16. To see the effect of these erroneous assignments, in Figure 3.17 we show the averaged values of the INM frequencies obtained from the simulations using both the frequency ordering criterion and the Min-Cost algorithm. As observed, the 1st, 2nd, 25th, and 26th INM averaged frequencies become nearly degenerated ($\approx$ 1400 cm^{-1}) when the Min-Cost algorithm is applied without restrictions due to multiple crossed assignments. A similar problem is detected in the 15th-20th and 27th-30th INMs. These anomalies all disappear when we use the restricted Min-Cost algorithm, in which only assignments to normal modes with frequencies lying in the window of width $\Delta\omega$ are considered. This is also clearly seen in Figure 3.17, where we include as well the averaged values of the INM frequencies obtained from MD simulations carried out using a window of width $\Delta\omega$ =200, 400, 600, 800 and 1000 cm^{-1}, noting that they are closer to the meaningful values provided by frequency ordering criterion. In Figure 3.17 we also show the average l^2_{i,f_i} elements obtained using different sizes of $\Delta\omega$. As it was expected, the efficiency increase with the size of the window, being maximal at the unrestricted Min-Cost algorithm. As seen only a small improvement in the efficiency of the method is achieved for windows bigger than 400 cm^{-1}. Accordingly, for the NMAD/D_2O system when the AMBER94 force field is employed, a $\Delta\omega = 400\,cm^{-1}$ frequency window was found to be optimal to prevent undesirable assignments without

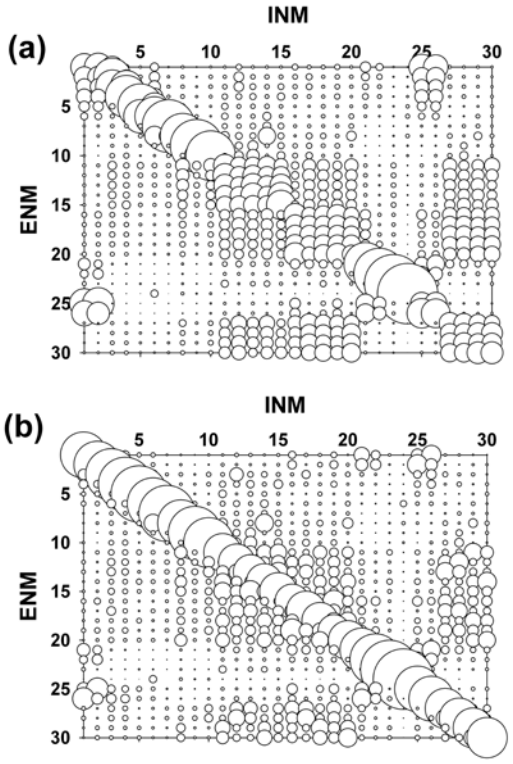

Figure 3.16: Representation of the averaged $|\boldsymbol{L}|$ matrix connecting the INMs to the ENMs of the NMAD molecule in D_2O solution with the INMs assigned (a) by frequency ordering, and (b) by using the Min-Cost algorithm with $\Delta\omega$=400 cm^{-1}. The sizes of the bubbles are proportional to the values of the averaged $|l_{ij}|$ elements.

excessively sacrificing the efficiency of the Min-Cost method [Kalstein 11].

In Table 3.16 we give the time averaged frequencies of the INMs of NMAD assigned using the restricted Min-Cost method, along with the corresponding time averaged highest $(l_{ij}^{\mathrm{INM}})^2$ contributions of the ENMs to the INMs. As may occur [Miller 80], for the first three INMs we found trajectories with negative force constant λ_i which give imaginary frequencies. When averaged, only the vibrational frequency of the first mode remains imaginary and its value is taken to be negative, as is usually done [Buchner 92, Keyes 97, Stratt 01]. The mean value of the time averaged overlaps $(l_{ij}^{\mathrm{INM}})^2$ included in Table 3.16 is 0.469.

Let us consider now the usefulness of the properly identified INMs to evaluate and analyze the content of vibrational energy stored in the solute molecule. In Table 3.15, we have included the kinetic (T_i^{INM}) and harmonic potential $(V_{i,\mathrm{har}}^{\mathrm{INM}})$ energies of the NMAD INMs, in solution, calculated using Eq. (2.60). As observed, in this case both energies

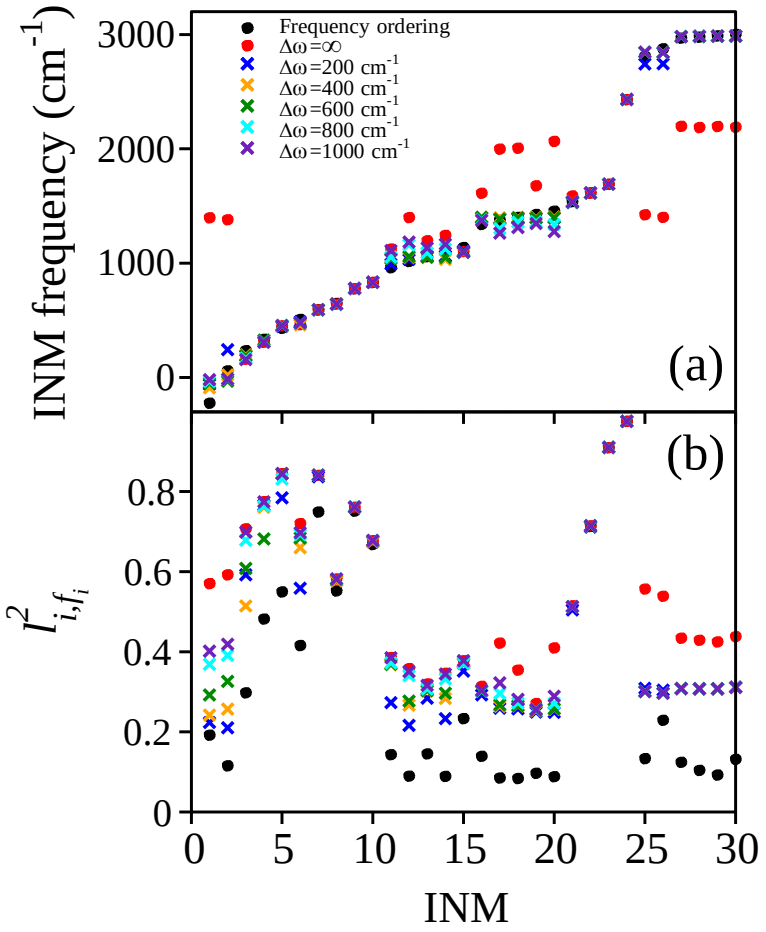

Figure 3.17: Average values of the (a) INM frequencies and (b) the I^2_{i,f_i} elements as defined in Eq. (2.83) obtained using the frequency ordering criteria and using the Min-Cost algorithm for different values of the frequency window. $\Delta\omega = \infty$ means that the Min-Cost assignment was applied without frequency restrictions.

for each INM agree well, in general, with the equilibrium thermodynamic value $k_BT/2 = 104.3\ \text{cm}^{-1}$, in contrast to what occurs with the ENMs. The INMs therefore satisfy the virial theorem. The only exceptions here correspond to the first three INMs, for which trajectories with negative force constants λ_i which therefore give imaginary frequencies as discussed above, are found in the MD simulations.

Comparing our results with those obtained from our group previous study [Bastida 10b, Kalstein 11] we find that they are in good agreement, despite the different MD coordinates performed during the simulations. We recall here that in our group previous study the NMAD motions were described using the set of coordinates $\{\boldsymbol{R}_{\text{CM}}, \boldsymbol{q}, \boldsymbol{Q}^{\text{e}}\}$ where, $\boldsymbol{R}_{\text{CM}}$ is the center of mass vector, $\boldsymbol{q} = (q_1, q_2, q_3, q_4)$ are the quaternions that specify the rotation of the molecule, and $\boldsymbol{Q}^{\text{e}} = (Q^{\text{e}}_1, \ldots, Q^{\text{e}}_N)$ are the equilibrium normal modes (ENMs) that describe the vibrational motion and the D_2O motions were described using the atomic

Table 3.16: Time averaged vibrational frequencies (cm^{-1}) of the INMs of the NMAD molecule in D_2O and averaged values of the highest contributions of the ENMs to the INMs obtained using the MC assignment method with a frequency window of width $\Delta\omega = 400 cm^{-1}$.

	INM	Frequency[c]	Max. overlap[c]	Frequency[d]	Max. overlap[d]	label[a]
	1[b]	-93.11 ± 15.5	0.24	-94.4 ± 286.9	0.24	$\tau(CH_3)$
	2[b]	19.65 ± 16.0	0.26	19.7 ± 308.1	0.25	$\tau(CH_3)$
	3[b]	196.80 ± 6.7	0.52	196.2 ± 126.8	0.51	τ(CN)
	4	311.97 ± 1.5	0.76	311.9 ± 31.4	0.76	δ(CNC)
	5	453.81 ± 0.7	0.85	453.9 ± 14.7	0.85	δ(CCN)
	6	455.55 ± 9.7	0.66	457.4 ± 178.2	0.65	amida V
	7	593.06 ± 0.5	0.84	592.6 ± 10.6	0.84	amida IV
	8	647.34 ± 2.2	0.59	646.3 ± 42.3	0.57	amida VI
	9	780.89 ± 1.2	0.75	778.6 ± 21.8	0.76	ν(CC)
	10	829.33 ± 1.8	0.66	831.2 ± 33.1	0.67	amida III
	11	1038.52 ± 3.7	0.37	1040.2 ± 71.0	0.37	r (CH_3)C
	12	1048.51 ± 4.0	0.27	1050.2 ± 78.3	0.27	$r \perp (CH_3)$N
group a_1	13	1051.28 ± 3.3	0.31	1050.8 ± 66.3	0.30	r (CH_3)N
	14	1035.10 ± 4.0	0.29	1033.4 ± 78.7	0.29	$r \perp (CH_3)$C
	15	1095.06 ± 2.2	0.38	1093.2 ± 43.4	0.37	ν(CN)
	16	1401.17 ± 2.4	0.30	1401.9 ± 48.4	0.30	$\delta_s(CH_3)$C
	17	1397.79 ± 2.3	0.27	1397.0 ± 47.3	0.26	$\delta_a(CH_3)$N
group a_2	18	1401.41 ± 2.6	0.27	1401.1 ± 51.8	0.27	$\delta_s(CH_3)$C
	19	1400.36 ± 2.4	0.25	1400.5 ± 49.4	0.25	$\delta_s(CH_3)$N
	20	1404.81 ± 2.7	0.26	1404.9 ± 52.5	0.26	$\delta_a(CH_3)$C
	21	1538.33 ± 2.4	0.51	1537.7 ± 44.4	0.51	$\delta_s(CH_3)$N
	22	1615.63 ± 1.4	0.71	1614.9 ± 22.4	0.71	amida II
	23	1691.91 ± 0.4	0.91	1691.8 ± 8.0	0.91	amida I
	24	2433.12 ± 0.4	0.98	2432.5 ± 7.1	0.97	amida A
	25	2845.97 ± 2.0	0.31	2845.2 ± 40.3	0.30	$\nu_s(CH_3)$C
group b_1	26	2842.15 ± 2.0	0.30	2842.1 ± 42.9	0.30	$\nu_s(CH_3)$N
	27	2982.37 ± 0.9	0.31	2982.2 ± 20.1	0.31	$\nu_a(CH_3)$N
	28	2984.15 ± 0.8	0.31	2984.2 ± 15.8	0.31	$\nu_s(CH_3)$N
group b_2	29	2986.06 ± 0.9	0.31	2985.7 ± 19.4	0.31	$\nu_a(CH_3)$C
	30	2987.26 ± 1.0	0.32	2987.2 ± 18.5	0.31	$\nu_s(CH_3)$C

a.- Ref. [Rey-Lafon 73]. τ=torsion, δ=bending, ν=stretching, r=rocking a=asymmetric and s=symmetric.

b.- Imaginary frequencies are given as negative frequencies

c.- Present work

d.- Ref. [Bastida 10b]

cartesian coordinates. In the present study the solute and the solvent motions during the simulations were described using the atomic cartesian coordinates.

At the end, we tested as well the ability of the Effective Atomic Min-Cost algorithm (EAMC) to evaluate the vibrational energy of the solute molecule in terms of INMs and the average frequencies of the INMs. In Table 3.17 and Table 3.18 we present the average energies and INM frequencies obtained using the EAMC and MC methods. Comparing these results, we find a good agreement between both INM assignment methods. Conse-

Table 3.17: Mean kinetic and harmonic potential energies (in cm^{-1}) for the INMs of the NMAD molecule in D_2O solution as obtained applying the EAMC and MC methods.

	MC[a]		MC[b]		EAMC	
Mode	$\langle T_i^{\rm INM}\rangle$	$\langle V_{i,\rm har}^{\rm INM}\rangle$	$\langle T_i^{\rm INM}\rangle$	$\langle V_{i,\rm har}^{\rm INM}\rangle$	$\langle T_i^{\rm INM}\rangle$	$\langle V_{i,\rm har}^{\rm INM}\rangle$
1	104.8	-14.0	101.6	18.2	104.5	19.9
2	104.8	-93.1	101.5	-16.3	104.7	4.6
3	105.3	151.3	101.0	-23.2	104.8	82.4
4	104.3	98.3	101.0	96.4	104.6	93.7
5	104.5	106.8	103.3	105.8	104.6	99.3
6	103.5	110.3	104.0	109.5	103.5	113.8
7	103.5	104.5	104.2	105.1	103.5	105.3
8	103.8	94.2	103.4	94.5	103.7	94.6
9	104.1	110.4	101.3	108.0	104.1	108.5
10	103.6	110.8	105.4	112.5	103.5	111.2
11	103.1	107.8	104.6	109.5	103.1	107.3
12	104.7	109.2	106.5	110.8	104.9	108.3
13	104.0	107.7	107.2	111.3	104.4	109.6
14	103.2	109.3	104.5	110.5	103.2	110.2
15	104.0	102.0	107.2	105.1	103.5	100.3
16	102.2	104.3	105.0	106.8	102.5	104.6
17	103.0	92.8	104.6	94.2	102.9	87.6
18	102.8	98.0	104.1	98.9	102.3	109.2
19	102.7	103.5	104.1	104.8	102.7	110.6
20	102.4	98.5	103.2	99.0	102.5	86.3
21	103.3	103.5	103.8	104.0	103.2	99.5
22	103.4	109.4	105.8	112.0	103.5	111.9
23	102.8	104.7	109.0	110.7	102.8	104.8
24	102.6	104.0	106.8	108.2	102.5	103.9
25	101.5	103.7	102.8	104.9	101.6	103.7
26	101.6	103.7	103.5	105.9	101.4	103.6
27	103.8	105.0	102.3	104.5	104.0	104.6
28	103.5	104.6	102.3	104.5	103.8	105.1
29	102.3	104.7	102.7	104.7	101.7	104.5
30	102.5	104.3	103.1	105.0	102.5	104.4

a.- present study
b.- Ref. [Kalstein 11]

quently, the EAMC method generalizes the methodology to identify the INMs in flexible biological systems.

We now present the results for the NMAD/D_2O system when SEBOMD has been used for running the MD simulations. In this part of our study we only use the EAMC algorithm in order to identify the INMs. We start by analyzing how the size for the frequency window $\Delta\omega$ influences on the efficiency of the EAMC method. We have evaluated the maximum atomic overlaps between the ENMs and the INMs (see Eq. (2.84)) and the INMs frequencies Eq. (2.76) obtained using different sizes of $\Delta\omega$ (600, 800 and 1000 cm^{-1}). In Table 3.19 we present the time averaged overlaps between ENMs and INMs. As seen the averaged overlaps

Table 3.18: Time averaged vibrational frequencies (cm^{-1}) of the INMs of the NMAD molecule in D_2O obtained using the EAMC ($\Delta\omega = 400 cm^{-1}$) and the MC methods

	INM	MC[c]	MC[d]	EAMC	label[a]
	1[b]	-93.11 ± 15.5	-94.4 ± 286.9	-20.99 ± 13.3	$\tau(CH_3)$
	2[b]	19.65 ± 16.0	19.7 ± 308.1	-68.54 ± 15.4	$\tau(CH_3)$
	3[b]	196.80 ± 6.7	196.2 ± 126.8	240.86 ± 5.2	τ(CN)
	4	311.97 ± 1.5	311.9 ± 31.4	338.69 ± 3.4	δ(CNC)
	5	453.81 ± 0.7	453.9 ± 14.7	453.96 ± 1.5	δ(CCN)
	6	455.55 ± 9.7	457.4 ± 178.2	468.03 ± 8.7	amida V
	7	593.06 ± 0.5	592.6 ± 10.6	596.81 ± 1.3	amida IV
	8	647.34 ± 2.2	646.3 ± 42.3	646.25 ± 2.3	amida VI
	9	780.89 ± 1.2	778.6 ± 21.8	785.01 ± 1.4	ν(CC)
	10	829.33 ± 1.8	831.2 ± 33.1	825.19 ± 2.4	amida III
	11	1038.52 ± 3.7	1040.2 ± 71.0	1048.05 ± 3.7	r (CH_3)C
	12	1048.51 ± 4.0	1050.2 ± 78.3	1051.80 ± 4.3	$r\perp(CH_3)$N
group a_1	13	1051.28 ± 3.3	1050.8 ± 66.3	1067.00 ± 3.1	r (CH_3)N
	14	1035.10 ± 4.0	1033.4 ± 78.7	1048.20 ± 4.0	$r\perp(CH_3)$C
	15	1095.06 ± 2.2	1093.2 ± 43.4	1085.41 ± 1.6	ν(CN)
	16	1401.17 ± 2.4	1401.9 ± 48.4	1401.51 ± 2.5	$\delta_s(CH_3)$C
	17	1397.79 ± 2.3	1397.0 ± 47.3	1401.00 ± 2.2	$\delta_a(CH_3)$N
group a_2	18	1401.41 ± 2.6	1401.1 ± 51.8	1400.96 ± 2.4	$\delta_s(CH_3)$C
	19	1400.36 ± 2.4	1400.5 ± 49.4	1423.91 ± 2.5	$\delta_s(CH_3)$N
	20	1404.81 ± 2.7	1404.9 ± 52.5	1405.84 ± 2.4	$\delta_a(CH_3)$C
	21	1538.33 ± 2.4	1537.7 ± 44.4	1541.06 ± 3.1	$\delta_s(CH_3)$N
	22	1615.63 ± 1.4	1614.9 ± 22.4	1607.88 ± 1.6	amida II
	23	1691.91 ± 0.4	1691.8 ± 8.0	1692.71 ± 0.3	amida I
	24	2433.12 ± 0.4	2432.5 ± 7.1	2433.84 ± 0.3	amida A
	25	2845.97 ± 2.0	2845.2 ± 40.3	2875.88 ± 0.6	$\nu_s(CH_3)$C
group b_1	26	2842.15 ± 2.0	2842.1 ± 42.9	2876.04 ± 0.6	$\nu_s(CH_3)$N
	27	2982.37 ± 0.9	2982.2 ± 20.1	2985.61 ± 0.9	$\nu_a(CH_3)$N
	28	2984.15 ± 0.8	2984.2 ± 15.8	2988.63 ± 0.9	$\nu_s(CH_3)$N
group b_2	29	2986.06 ± 0.9	2985.7 ± 19.4	2987.10 ± 0.9	$\nu_a(CH_3)$C
	30	2987.26 ± 1.0	2987.2 ± 18.5	2993.35 ± 0.9	$\nu_s(CH_3)$C

[a] τ=torsion, δ=bending, ν=stretching, r=rocking, a=asymmetric and s=symmetric.
[b] Imaginary frequencies are given as negative frequencies
[c] Recent study
[d] Ref. [Bastida 10b]

increase with the frequency window width for most of the INMs. We find that some INMs such as 2nd and 30th INM increase substantially. However, others as the 13rd and 18th INMs are not affected. In Figure 3.18 we show the time average frequencies of the NMAD assigned using the EAMC method for different values of $\Delta\omega$. We note the appearance of some unphysical assignment for frequency windows of 600 and 800 cm^{-1} between the lower frequency normal modes (1st-5th INMs) and the higher frequency normal modes (25th-30th INMs). We have found that the higher INM frequencies oscillate in a much larger scale compared to the gas phase conditions due to the solute-solvent interactions. These frequencies fall often out of the frequency window leading to wrong assignments between

Table 3.19: Overlaps between ENMs and INMs obtained using the EAMC method for different frequency windows.

INM	$\Delta\omega = 1000$ cm^{-1}	$\Delta\omega = 800$ cm^{-1}	$\Delta\omega = 600$ cm^{-1}
1	0.878	0.887	0.903
2	0.868	0.811	0.715
3	0.924	0.894	0.837
4	0.959	0.953	0.923
5	0.960	0.959	0.908
6	0.920	0.912	0.901
7	0.972	0.971	0.959
8	0.940	0.940	0.938
9	0.951	0.946	0.943
10	0.937	0.936	0.936
11	0.922	0.914	0.906
12	0.928	0.926	0.929
13	0.968	0.967	0.968
14	0.957	0.956	0.957
15	0.956	0.956	0.963
16	0.904	0.902	0.885
17	0.988	0.988	0.988
18	0.937	0.938	0.940
19	0.971	0.971	0.968
20	0.932	0.931	0.930
21	0.989	0.989	0.989
22	0.904	0.901	0.890
23	0.985	0.981	0.958
24	0.956	0.940	0.873
25	0.981	0.964	0.940
26	0.968	0.945	0.880
27	0.997	0.993	0.980
28	0.974	0.959	0.914
29	0.978	0.941	0.856
30	0.956	0.898	0.777
Mean	0.949	0.939	0.915

some lower and higher frequency INMs. However, these deviations disappear by applying a larger frequency window $\Delta\omega = 1000$ cm^{-1} .

In Table 3.20 we present the ENM vibrational frequencies as obtained from diagonalization of the mass weighted Hessian matrix at the optimized geometry of the NMAD molecule and the time averaged frequencies of the INMs of the NMAD/D_2O system assigned using $\Delta\omega = 1000$ cm^{-1} along with the experimental values. As seen the frequency of the amide I mode is overestimated compared to the experiments [Ingrosso 11]. However, in

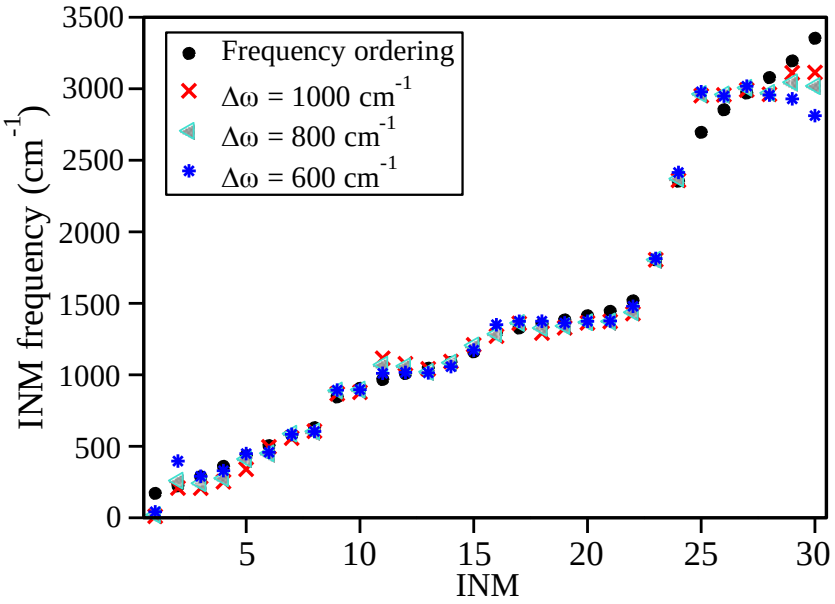

Figure 3.18: Average values of the INM frequencies of the NMAD molecule in D_2O solution obtained from the SEBOMD simulations using the frequency ordering criterion, and the EAMC method with $\Delta\omega = 400, 600$ and $1000\ \mathrm{cm}^{-1}$ frequency windows.

general we find a good agreement between our model and the experimental measurements for the solvent shift. Based on our analysis, we observe that there are some normal modes which are nearly degenerated. This is due to the recurrent crossed assignment during the simulations. We have found the group L of modes composed of the 1st-4th INMs with the lower frequencies, the group a_1 of modes composed of the 11st-14th INMs which are formed mainly by combinations of the rocking methyl ENMs, the group a_2 composed of the 16th-20th INMs which are basically combinations of the bending methyl ENMs, the group b_1 containing the 25th-28th INMs which are composed essentially of the C-H stretches, and finally the group b_2 formed by the 29th-30th INMs, which are made up basically of the more energetic stretching methyl ENMs. As seen these groups are slightly different from those obtained employing MM force fields (see Table 3.18).

Another issue that we have analyzed is the correlation coefficient between the amide I and amide II INMs frequencies for the NMAD/D_2O system. The correlation coefficient is defined as

$$f_{xy} = \frac{\overline{XY} - \overline{X}\,\overline{Y}}{\sqrt{\overline{X^2} - \overline{X}^2}\ \sqrt{\overline{Y^2} - \overline{Y}^2}}$$

Table 3.20: Normal mode vibrational frequencies (in cm^{-1}) of the NMAD molecule obtained using SEBOMD and those measured under different experimental conditions.

	i	ENMs	INMs	Exp.[a,d]	Expt.[a,e]	Expt.[b,f]	Expt.[b,g]	Expt.[c,i]	label[h]
group L	1	120.4	11.5 ± 178	(134)					$\tau(CH_3)$
	2	158.3	208.8 ± 280	(143)					$\tau(CH_3)$
	3	187.8	207.8 ± 267	189					τ(CN)
	4	278.7	252.3 ± 101	292	284				δ(CNC)
	5	423.1	340.1 ± 159	439	437		448		δ(CCN)
	6	451.8	496.2 ± 217	510					amide V
	7	567.8	557.5 ± 112	628	627	627	632	617	amide IV
	8	612.6	605.6 ± 56	(653)					amide VI
	9	863.9	867.6 ± 127	872	872	868	873	850	ν(CC)
group a_1	10	892.2	878.3 ± 114	965	965	975	967	921	amide III
	11	995.2	1115.9 ± 183	1000	999				r (CH_3)C
	12	1008.4	1077.3 ± 171	1098					r ⊥(CH_3)N
	13	1016.3	1041.5 ± 122	1185	1180	1192	1185		r (CH_3)N
	14	1060.0	1093.0 ± 143	1045					r ⊥(CH_3)C
	15	1148.7	1209.5 ± 144	1123	1123	1117	1125		ν(CN)
	16	1332.4	1270.7 ± 152	1372	1370		1371		$\delta_s(CH_3)$C
	17	1369.8	1360.1 ± 102	(1449)	1442		1451		$\delta_a(CH_3)$N
group a_2	18	1376.3	1292.8 ± 150	1446					$\delta_s(CH_3)$C
	19	1385.8	1329.0 ± 117	1406	1406		1412		$\delta_s(CH_3)$N
	20	1394.7	1363.4 ± 84	1440	1442	1435	1436		$\delta_a(CH_3)$C
	21	1401.7	1372.6 ± 75	1471	1479	1476			$\delta_s(CH_3)$N
	22	1422.5	1428.2 ± 187	1485		1490	1493	1399,1440	amide II
	23	1927.2	1804.5 ± 104	1647	1635	1620	1626	1717	amide I
	24	2472.3	2360.0 ± 193	(2439)				2605	amide A
group b_1	25	3043.4	2952.0 ± 225	2938		2945			$\nu_s(CH_3)$C
	26	3062.6	2957.7 ± 200	2938		2945			$\nu_s(CH_3)$N
	27	3082.1	2991.8 ± 226	2984					$\nu_a(CH_3)$N
	28	3085.1	2961.9 ± 194	2994					$\nu_s(CH_3)$N
group b_2	29	3134.7	3112.0 ± 310	2984					$\nu_a(CH_3)$C
	30	3178.7	3114.3 ± 303	2994					$\nu_s(CH_3)$C

a.- Liquid NMAD.
b.- NMAD in liquid D_2O.
c.- NMAD in gas phase.
d.- [Schneider 65, Pivcova 65] Values in brackets are calculated from a fitted potential.
e.- [Sugawara 84]
f.- [Fang 09]
g.- [Chen 95]
h.- [Rey-Lafon 73]
i.- [Mayne 91]

$$= \frac{X_n Y_n - \frac{1}{n} X_n Y_n}{\sqrt{\left(X_n^2 - \frac{1}{n} X_n^2\right)\left(Y_n^2 - \frac{1}{n} Y_n^2\right)}} \tag{3.3}$$

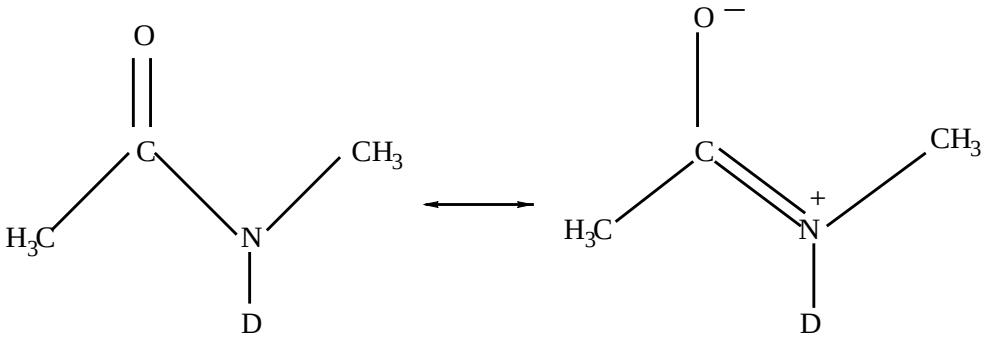

Figure 3.19: Resonance structures of NMAD: neutral (left) and zwitterionic (right).

where n labels the values of the variables at the same time. In our case X_n and Y_n correspond to the frequencies of the amide I and amide II INMs respectively. Possible values of f_{xy} are 1 (full correlation), 0 (no correlation), or -1 (full anticorrelation).

The amide I/amide II INM frequency correlation coefficient is estimated to be -0.01, that is, both frequencies are no correlated. Experimentally the correlation coefficient was measured by femtoscale two color IR spectroscopy for NMA in dimethyl sulfoxide DMSO to be -0.28 [Rubtsov 03a]. The small negative correlation between the amide I and amide II frequencies is due to the contribution of the zwitterionic resonance form induced by a polar solvent on the NMA (see Figure 3.19). As a consequence, the lengthening of the carbonyl bond reduces the vibrational frequency of the amide I mode while shortening the CN bond and inducing a blue shift of the amide II mode [Hayashi 05]. The relative contribution of the zwitterionic structure depends on the stabilization provided by the solute-solvent interactions what could explain the difference between our results obtained in D_2O solution and those measured in DMSO. The amide I/amide II correlation coefficient was also calculated [Bloem 08] to be -0.54 for NMA in gas phase using a simplified model where only the amide I and amide II modes were considered explicity. This high coefficient is some how surprising since the absent of any solvent should favor the neutral resonance structure decreasing the correlation between both modes. Interestingly Mukamel *et al* [Hayashi 05] obtained a small correlation coefficient -0.16 for the NMA molecule in water using a electrostatic DFT map to account for the solvent-solute interactions.

3.2.3 AMBER force field results

In this Section we describe the analysis of the intra- and intermolecular vibrational energy flows occurring in the NMAD/D_2O system during the relaxation processes based on the Statistical Minimum Flow (SMF) method. We recall here that the MC algorithm (see Section 2.3 for details) has been employed through this analysis to compute and identify the INMs.

3.2.3.1 Amide I relaxation lifetime

Before going into the calculation of the amounts and rates at which energy flows between the INMs of the molecule, we have to ensure that the results obtained really correspond to net changes in the energies of the INMs modes, and not to statistical fluctuations. To assess this point, in Figure 3.20 we show, for example, the evolution of the average vibrational energy of the 23rd (amide I) and the 1st (τ (CH_3)) INMs of the NMAD molecule, and the accumulated energy that flows between these modes during the first 0.5 ps after the initial excitation of the amide I mode. As observed, the energy of the amide I mode (Figure 3.20 (a)) decreases monotonously with no oscillations, meaning that this mode transfers its excess energy to other degrees of freedom of the system gradually. During this 0.5 ps time interval, the amide I mode behaves, therefore, as a donor. In contrast, the 1st INM shows large oscillations in the vibrational energy with time (Figure 3.20(b)). The 1st INM is a low- frequency mode and, as reported in reference [Kalstein 11], the potential energy for these INM modes may diverge if their frequencies approach zero. For this reason, their vibrational energies are calculated as twice the kinetic energy (see refs. [Bastida 10a] and [Kalstein 11] for details), and present fluctuations that are significantly higher than those of other modes, whose vibrational energies are obtained as the sum of the kinetic and potential energies. This behavior is also observed in the 2nd, 3rd and 6th low-frequency INMs. Although these modes barely accumulate energy during the relaxation process, their oscillations makes them behave as donors and acceptors alternately. As a result, the flow of energy accumulated from the amide I mode to the 1st INM increases rapidly in the stages in which the 1st INM acts as an acceptor, as observed in Figure 3.20(c). Since the energy flows only from the donor to the acceptor modes, the transfer of energy when both the amide I and the 1st INMs behave as donors is nor permitted and there is no possibility for a negative flow of energy to occur to compensate the positive flow. It becomes quite clear, then, that it is necessary to remove these spurious oscillations of energy because of the undesirable noise that they introduce in the calculation of net flow of energy between the INM modes. Raising the number of trajectories in the simulations does indeed promote statistical convergence and, therefore, the smoothing of the fluctuations. However, the higher computational cost demanded in this case by the simulations makes it more advisable to tackle this problem by performing a linear convolution of time evolving energies.

We have tested different time intervals to carry out the linear convolutions, and opted for a 400 fs interval after verifying that oscillations of the vibrational energy are smoothed enough so as to not alter the results significantly. The convoluted vibrational energies obtained for the amide I and the 1st INMs are plotted in Figure 3.20 and, as observed, the convoluted energies of the amide I mode are very similar to the unconvoluted ones, as expected. In marked contrast however, the convolution of the vibrational energy of the 1st INM removes practically all the statistical fluctuations, leaving only, as shown in Figure 3.20(b), a small net accumulation of energy during the 0.5 ps time interval. As a consequence, the accumulated energy that flows from the amide I mode to the 1st INM,

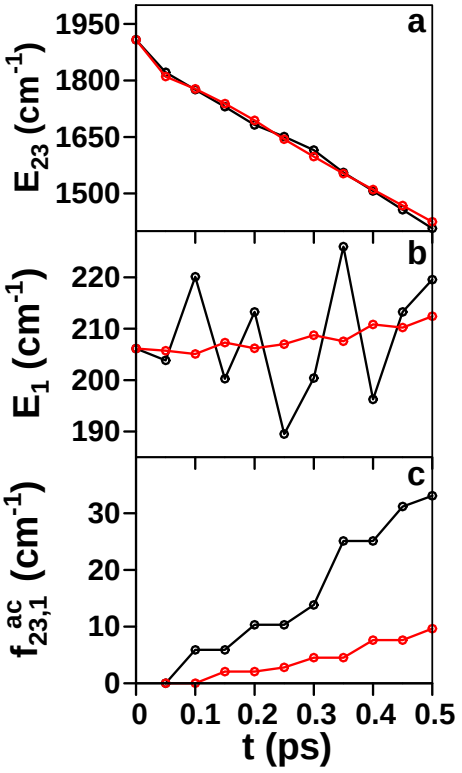

Figure 3.20: Average values of the vibrational energy (a) of the amide I mode (23rd INM), (b) the 1st INM of the NMAD molecule, and (c) accumulated energy flowing from the amide I mode to the 1st INM, during the first 0.5 ps of the relaxation process. Values are shown with no convolution (black) and with a 400 fs linear convolution (red).

calculated using the smoothed vibrational energies, shows only a slight increase, as observed in Figure 3.20(c), compatible with the energy accumulated in the 1st INM.

We therefore present and discuss the results drawn from the convoluted vibrational energy curves as follow. First in Section 3.2.3.2 we analyze the intra- and intermolecular energies released by the amide I mode in order to find out how much of this energy remains in the molecule through intramolecular vibrational energy redistribution (IVR) and what proportion is transferred directly from this mode to the bath. Next in Section 3.2.3.3 we study the IVR channels responsible for the vibrational relaxation of the amide I mode in the individual INMs of the solute molecule. We continue in Section 3.2.3.4 by considering the transfer of energy from the molecule to the bath in order to identify the specific modes which are responsible for the cooling of the molecule. Finally in Section 3.2.3.5 we summarize the global vibrational relaxation process using a flow chart that allows us to clearly visualize the most important channels.

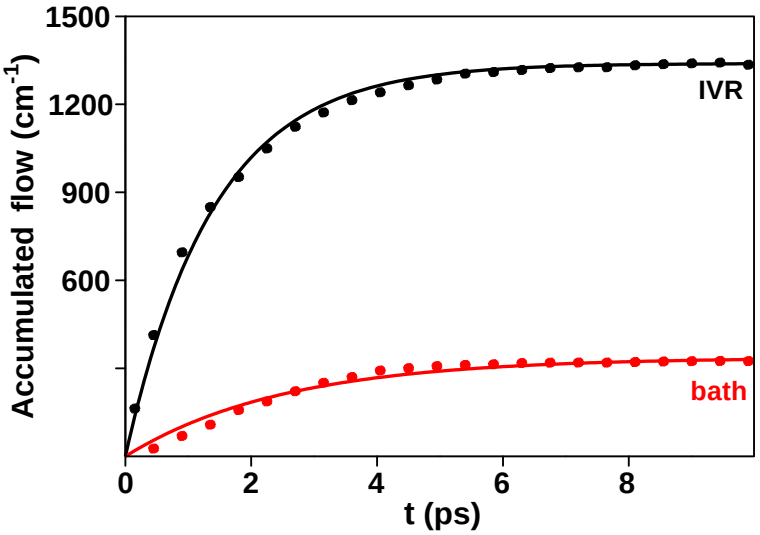

Figure 3.21: Time evolution of the accumulated energy that flows (dots) from the amide I mode to the bath (red) and to the remaining INMs of the NMAD molecule (black), and their fits to first order exponential functions (lines).

3.2.3.2 Intra- and intermolecular pathways

Let us consider, then, the evolution of the accumulated energy that flows from the amide I mode to the rest of the molecule and to the bath. The total intramolecular energy channeled to the molecule through IVR is given by

$$f_{\mathrm{IVR}}^{\mathrm{ac}}(t_n) = \sum_{j=1}^{30} f_{23,j}^{\mathrm{ac}}(t_n) \tag{3.4}$$

and plotted versus time in Figure 3.21, along with the total energy that flows from the amide I mode to the bath. As observed in this figure, in the asymptotic time limit only 20% of the energy released by the amide I mode goes directly to the solvent, and the remaining 80% of this energy is dissipated by IVR. Moreover, the IVR rate is higher than the bath rate. Interestingly, the accumulated energy flow curves can be nicely fitted to first order exponential functions (see Eq. (2.100)). The IVR and bath lifetimes extracted from these fits are 1.40 ps and 2.48, respectively, so the intramolecular dissipation of the energy is nearly twice as fast as the dissipation to the bath. We note also that both, the relative contributions of the IVR and bath channels and their respective lifetimes are in good agreement with the results obtained in our earlier work from the biexponential decay of the amide I mode [Bastida 10a].

3.2.3.3 IVR pathways

Consider now the application of the SMF method to study the individual IVR pathways through which the energy flows from the amide I mode to the other INMs of the molecule.

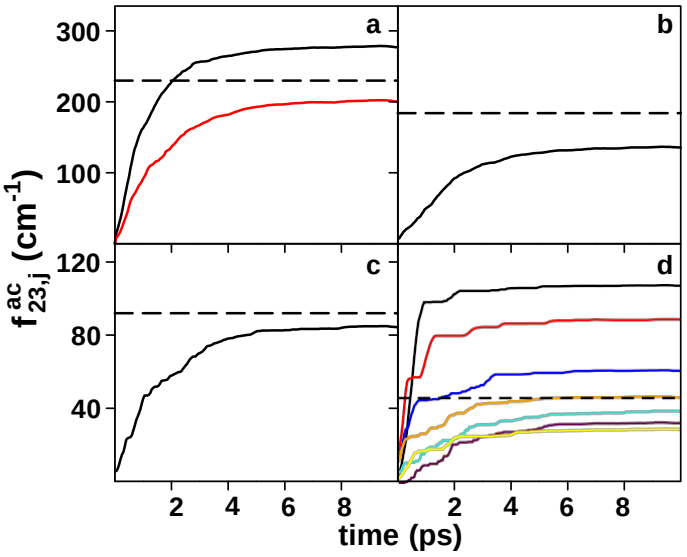

Figure 3.22: Time evolution of the accumulated energy that flows from the amide I mode of the NMAD molecule to (a) groups a_1 (11th-15th INMs, black) and a_2 (16th-20th INMs, red), (b) group b_2 (27th-30th INMs), (c) group b_1 (25th-26th INMs), and (d) 3rd (maroon), 6th (cyan), 7th (yellow), 10th (black), 21st (orange), 22nd (blue) and 24th (red) INMs. Dashed lines indicate the values of the accumulated energy distributed equally among all the INMs.

In Figure 3.22 we show the time evolution of the accumulated energy that flows from the amide I mode to several representative INMs. As noted, we consider here in some cases the flow of energy to well-defined groups of INMs composed by modes that are so strongly coupled they have to be considered collectively (see references [Bastida 10b] and [Kalstein 11] for details). We also depict in Figure 3.22 the accumulated energy obtained when all modes receive the same amount of energy via IVR from the amide I mode (46 cm^{-1} for each INM).

As observed in Figure 3.22, the relaxation channels in which the amide III (10th INM), amide II (22nd INM) and amide A (24th INM) modes participate along with the group a_1 of modes, which consists of rocking modes of the methyl hydrogens and a torsion backbone mode, all exhibit energy transfers above the average energy. Despite the statistical noise shown by some of the curves, it is again possible to fit all of them to first order exponential functions. This means that the energy flow description provided by the SMF method can be modeled by independent first-order state-to-state processes, as done in the Master Equation framework [Van-Kampen 07]. In Table 3.21 we give the values of the A_{23j} and τ_{23j} parameters obtained for all the INMs of the NMAD molecule. The total energy values calculated confirm that the relaxation of the amide I mode into amide III, amide II, amide A and the group a_1 of modes is most favored when compared to the rest of INMs, with the energy channeled through to these modes, accounting for 40% of the IVR energy initially released by the excited amide I mode. The SMF method thus confirms, and quantifies, the participation of these modes as preferential relaxation channels of the amide I mode,

Table 3.21: Total energies (in cm^{-1}), and lifetimes (in ps), transferred from the amide I mode towards the rest of the system (A_{23j}, τ_{23j}) and from all the INMs towards the bath ($A_{j\text{bath}}$, $\tau_{j\text{bath}}$).

jth INM	Label[a]	A_{23j}	τ_{23j}	$A_{j\text{bath}}$	$\tau_{j\text{bath}}$
1	$\tau(CH_3)$	41	2.08	70	12.53
2	$\tau(CH_3)$	35	2.41	69	13.52
3	τ(CN)	39	1.97	50	9.47
4	δ(CNC)	43	2.18	77	12.55
5	δ(CCN)	37	2.17	74	13.69
6	amide V	34	2.50	85	14.73
7	amide IV	29	1.24	29	10.30
8	amide VI	39	1.16	36	11.02
9	ν(CC)	42	1.43	38	12.97
10	amide III	107	0.60	55	8.08
group a_1^b	$r(CH_3)+\nu$(CN)	278	1.17	214	12.25
group a_2^b	$\delta(CH_3)$	203	1.72	218	14.21
21	$\delta_s(CH_3)$N	46	1.11	40	14.45
22	amide II	60	0.80	38	9.68
23	amide I			335	2.48
24	amide A	88	0.58	40	6.25
group b_1^b	$\nu_s(CH_3)$	85	1.68	82	15.63
group b_2^b	$\nu(CH_3)$	138	1.94	150	13.95
Bath		335	2.48		

a.- Ref. [Rey-Lafon 73]. τ=torsion, δ=bending, ν=stretching, r=rocking, a=asymmetric and s=symmetric.
b. - Groups a_1, a_2, b_1 and b_2 are formed by 5, 5, 2 and 4 modes, respectively (see text).

as already asserted in our previous work [Bastida 10a].

Table 3.21 also shows that the transfer of energy to the 1st to 6th low-frequency INMs stays below the average value. Previous studies [Shigeto 07,Shigeto 08,Fang 09,Bastida 10a] have demonstrated, however, that these modes act like doorways of the intermolecular flow of energy to the librations of the solvent, so this is a case in which the limits of the SMF method show up. Those intermediate modes whose relaxation rates are much higher than their excitation rates are not expected to accumulate substantial amounts of energy and therefore become to a certain extent insensitive to the SMF analysis. The convolution method used to smooth the energy flow curves also prevents the detection of the energy transfers occurring in a much shorter time scale than the convolution time interval. In the present case, the role of the low-frequency modes is clearly underestimated by the SMF method due to their fast relaxation into the solvent. In this sense, the low-frequency modes and the bath modes should be considered jointly, an argument supported also by their similar excitation rates of ~ 0.5 ps^{-1}, which are lower than the excitation rates of the other INMs. We should note that this problem could be recognized evaluating

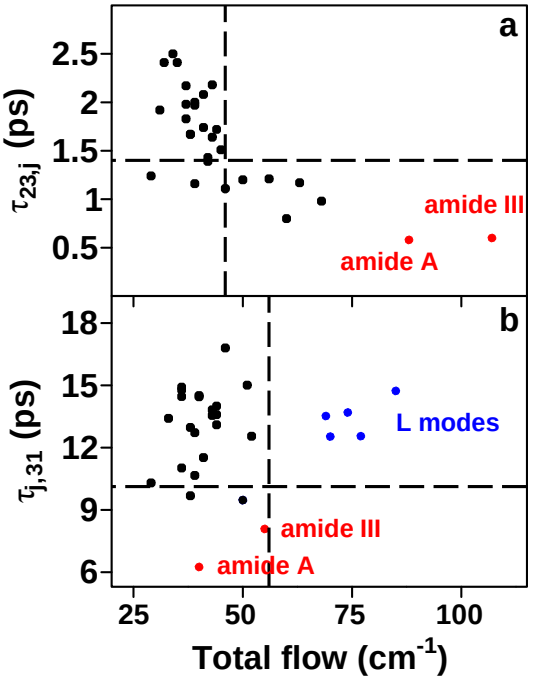

Figure 3.23: Energy transfer lifetimes versus energies transferred (a) from the amide I mode of the NMAD molecule to the remaining INMs, and (b) from all the INMs to the bath. Dashed lines indicate the average energy transfer lifetimes (horizontal lines) and the average total energies (vertical lines).

qualitatively the contribution of the energy flow for the low-frequency modes by applying the SMF analysis to simulations in which the solute molecule is isolated, as proposed in Ref. [Bastida 10a].

The combined use of the total energy that flows between the INMs and the lifetimes thereof allows us to check the efficiency of the different pathways involved in the transport of vibrational energy through the solute molecule. This can be done by plotting the lifetimes versus the total amounts of energy transferred from the amide I mode to the rest of INMs, as shown in Figure 3.23(a), where we include as a reference the average values of both parameters. In the upper-left quadrant of this Figure are the least effective channels (low flow and long lifetimes) whereas in the lower-right quadrant are the most effective channels (high flow and short lifetimes). It is observed then that the most active modes in the amide I relaxation are some of the modes included in the a_1 group, the amide II mode and especially and by far, the amide III and amide A modes. This is in agreement with the fact that the amide I mode is coupled by a 2:1 Fermi resonance to the amide III mode, and that the sum of the amide I and amide III mode frequencies lies quite close to the frequency of the amide A mode thus favoring the energy transfer between these modes, as reported in our earlier work [Bastida 10a].

3.2.3.4 Energy transfer into the solvent

Let us consider next the results provided by the SMF method for the intermolecular relaxation of the NMAD INMs into the solvent. We have verified first that the energy flow in this case is also well-reproduced by Eq. (2.100), and calculated the corresponding total energies and lifetimes. These values are also included in Table 3.21 and plotted in Figure 3.23(b), depicting again as a reference the lines corresponding to the values of an equal distribution of the energy (56 cm^{-1}) and the average lifetime (10.1 ps). This lifetime is very close to the NMAD relaxation time in D_2O solution previously calculated in ref. [Bastida 10a] from the time evolution of the vibrational energy stored in the molecule.

The 1st ($\tau(CH_3)$), 2nd ($\tau(CH_3)$), 4th (δ(CNC)), 5th (δ(CCN)) and 6th (amide V) INM low-frequency modes, along with the initially excited amide I mode (not shown in Figure 3.23(b)), are the only ones for which total energy lies above the average value. Our calculations indicate that 25% of the energy transferred from the molecule to the solvent is channeled through these low-frequency modes. Taking into account that 20% of the energy comes directly from the amide I mode, we conclude that half the total energy is transferred to the solvent through six modes of the NMAD molecule. As for the relaxation lifetimes, it is observed that the shortest ones, excluding that of the amide I mode, correspond as expected to the amide III and amide A modes, which provide the fastest relaxation channels of the amide I mode. The remaining INMs present lifetimes of ~ 14 ps, similar to those of the low-frequency modes, although their contribution to the total flow is much smaller. Accordingly, the results shown in Figure 3.23 demonstrate that the SMF method not only identifies the most effective channels but also reveals the presence of the different kinetics that occur in the relaxation of the solute molecule. This is the case for the amide III and the amide A modes, which provide fast channels for the cooling of the molecule during a short time interval, whereas the transfer of energy through the low-frequency modes is slower and therefore extends longer.

Application of the SMF method allows us to construct a flow chart of the whole relaxation process, like that shown in Figure 3.24, which directly visualizes the main relaxation channels. We have grouped in this flow chart all the stretching and bending modes of the methyl hydrogens of the NMAD molecule into two groups, $\nu(CH_3)$ and $\delta(CH_3)$, formed respectively by groups b_1 and b_2, and by group a_2 and the 21st INM. Also as noted, we place the bath in the frequency part of the flow chart corresponding to typical D_2O librations [Zelsmann 95], since they are the main recipients of the vibrational energy due to the limited participation of intramolecular vibrations of water in the process [Bastida 10a, Bastida 10b]. In order to achieve a better visualization of the relaxation mechanism, in Figure 3.24 we depict only the arrows labeling the pathways in which the accumulation of energy is equal to or higher than 1% of the initial excitation energy. The amount of energy transferred from the $\nu(CH_3)$ and $\delta(CH_3)$ modes is then greater than the energy that these modes receive, because the energies transferred from the amide A, amide II, amide III and group a_1 of modes do not exceed the 1% threshold separately, but become significant when they are taken all together. The flow chart shows a general trend

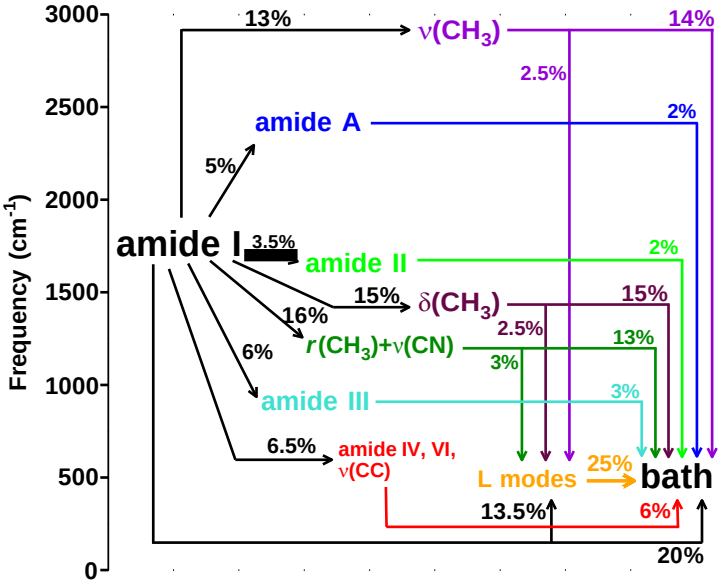

Figure 3.24: Flow chart of the vibrational relaxation of the amide I mode of the NMAD molecule in D_2O solution. Every INM is placed vertically according to its average frequency [Bastida 10b] and horizontally according to its excitation lifetime. In every arrow, the percentage of energy transferred thought the corresponding channel with respect to the initial excitation is given. The groups that appear in the diagram are groups b_1 and b_2 of the $\nu(CH_3)$ modes, group a_2 and the 21st INM of the $\delta(CH_3)$ modes, and the 1st-6th INMs for the low-frequency modes.

for the medium- and high-frequency vibrational modes to transfer their energies to the low-frequency modes and to the bath. However, the percentages of the energy transferred form the individual INMs of the NMAD molecule to the bath differ noticeably. The amide III and amide A modes, which are the first to be excited, transfer about half of the energy that they receive to the bath, while the other half is distributed selectively via IVR into other modes of the solute, mainly in the $\nu(CH_3)$, $\delta(CH_3)$ and low-frequency modes. As we move toward the slower channels in Figure 3.24, from left to right, the ratio of energy transferred to the bath increases until reaching the low-frequency modes, which transfer almost all their energy to the bath. The general picture emerging from the Figure 3.24 flow chart agrees well with the cascade mechanism proposed by Dlott *et al* [Fang 09], in which the solute molecule dissipates its excess energy through low-frequency modes which are excited after successive excitation of high and medium frequency modes. The SMF method provides, therefore, a general description of the vibrational relaxation of the molecule which allows us to quantify the amount of energy transferred in the successive elementary steps involved in the relaxation process and their corresponding lifetimes.

3.2.3.5 Comparison of the assignment methods

We now compare the results provided by the EAMC and the MC [Soler 11] methods. In Figure 3.25 we show the time evolution of the vibrational energy of the amide I mode

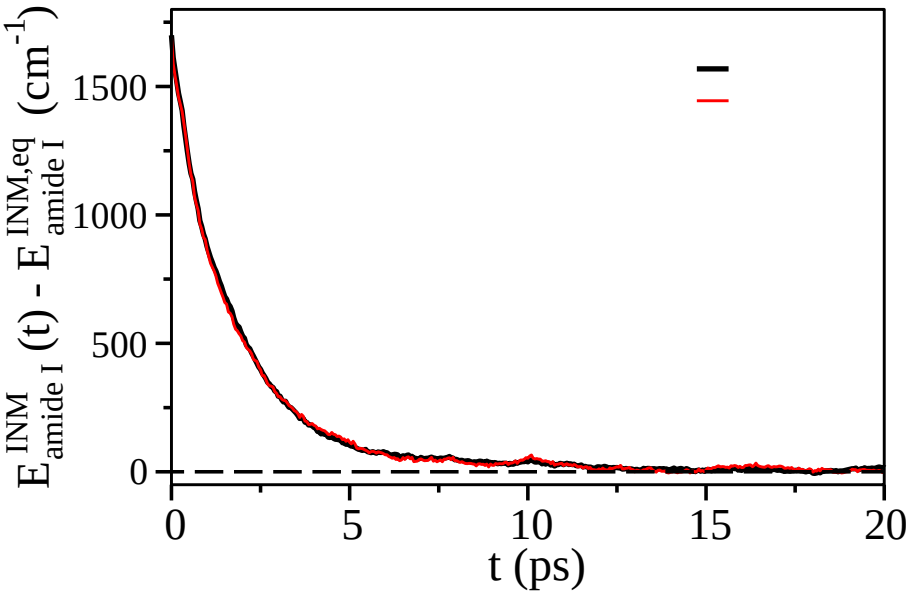

Figure 3.25: Time evolution of the vibrational energy of the amide I (in cm^{-1}) of the NMAD relative to its thermodynamic equilibrium value obtained using the MC [Soler 11] and the EAMC methods.

obtained using both assignment methods. As seen the agreement is excellent.

In Figure 3.26 we show the time evolution of the vibrational energies relative to their equilibrium values for all the INMs assigned by employing the MC [Soler 11] and the EAMC methods. As seen the two methods provide similar results. We also note that the results presented in Figure 3.25 and Figure 3.26 are similar to those presented by our group in Ref. [Bastida 10a] where an alternative method was used to fix the bf frame to the NMAD molecule.

Based on our analysis, we conclude that the EAMC method provide similar results to those obtained by applying the MC method [Bastida 10a, Soler 11] when applied to the NMAD molecule.

3.2.4 SEBOMD results

3.2.4.1 Temperature correction

The application of SEBOMD to nonequilibrium simulations of the excitation process generated some issues related to energy conservation. In Figure 3.27 we show the time evolution of the temperature of the NMAD molecule and the D_2O solvent obtained in equilibrium NVE SEBOMD simulations. As seen the average temperature of the solvent $\sim$ 305 K is hotter than the 300 K equilibration temperature while the temperature of the solute molecule oscillate around this value.

Following this short time solvent temperature jump we observe an additional much

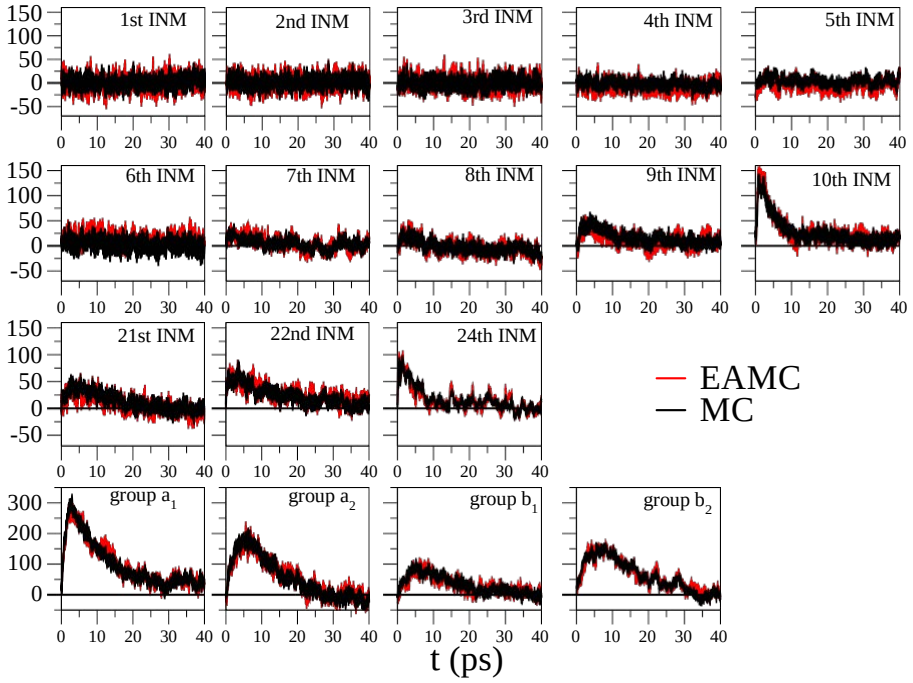

Figure 3.26: Time evolution of the vibrational energies (in cm^{-1}) of the INMs assigned by using the MC [Soler 11] and the EAMC methods for the NMAD molecule relative to their equilibrium values.

slower temperature increase as shown in Figure 3.28(b). In this case the temperature increases almost linearly with time and reaches ~335 K after 40 ps. We recall that the raise of temperature of the solvent exclusively due to the energy released by the initially excited amide I mode accounts for only 4.2 K. The remaining one is due then to energy conservation problems. The heat of the solvent affects the energy flows during the relaxation process as we can see in Figure 3.28(a) where we show the time evolution of the total vibrational energy of the NMAD molecule evaluated as the sum of the energies of every INM using Eq. (2.82) relative to its equilibrium thermodynamic value at 300 K. The NMAD molecule relaxes during the first 20 ps as expected. Then the vibrational energy increases for large times and never reaches its equilibrium value. This behavior is a direct consequence of the heat of the solvent as we can see in Figure 3.29 where we plot the temperature of the solute and solvent during the nonequilibrium NVE SEBOMD simulations. Around 20 ps both temperatures become identical and then the solute heats at the same rate that the solvent. At present we do not have a conclusive answer to the origin of this effect. It can be due to the small box size used in the simulations what could effect the accuracy of the Ewald sum method.

Therefore if we want to evaluate the time evolution of the vibrational energy of the solvent molecule or any INM we cannot use a constant equilibrium value based on $T = 300$ K temperature as done in Figure 3.28(a). Instead we consider a time dependent equilibrium

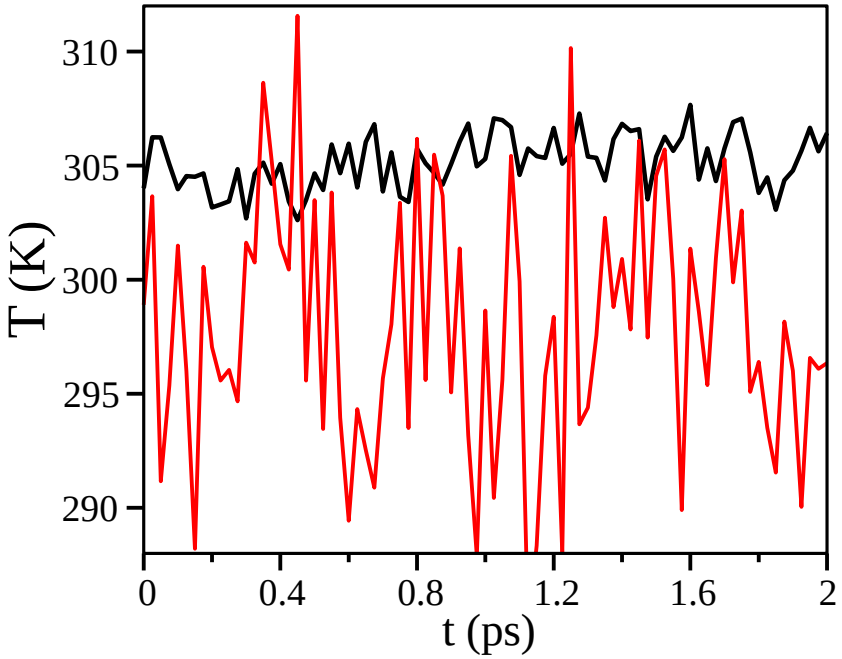

Figure 3.27: Time evolution of the temperature of the NMAD solute molecule (red line) and the D_2O solvent (black line) obtained in equilibrium NVE SEBOMD simulations.

vibrational energy obtained from the instantaneous temperature of the solvent $T_{\text{solv}}(t)$ as follows

$$E^{\text{vib,eq}}_{\text{NMAD}}(t) = (3N_s - 6)K_B(T_{\text{solv}}(t) + \Delta T_{\text{solv}}(t)) \tag{3.5}$$

where we have added a linear term $\Delta T_{\text{solv}}(t) = at - b$ to account for the solvent temperature increase. The a and b parameters are calculated to reproduce the ΔT_{solv} at $t = 0$ ps and the ΔT_{solv} at $t = 40$ ps (see Figure 3.30).

In Figure 3.31 we show the total vibrational energy of the NMAD molecule with respect to the time dependent equilibrium energy evaluated using Eq. (3.5). As seen the vibrational energy shows the right asymptotic value at large times.

As a final remark we consider the influence of the temperature rise on the relaxation process. As we will show later the relaxation of the amide I mode is completed in few picoseconds so that is mostly unaffected by the solvent heating. However, the latter steps of the relaxation process that involve the intramolecular energy transfer from the NMAD molecule to the solvent occurs in the tens of picoseconds scale and can be slightly accelerated by the increase of the temperature of the system.

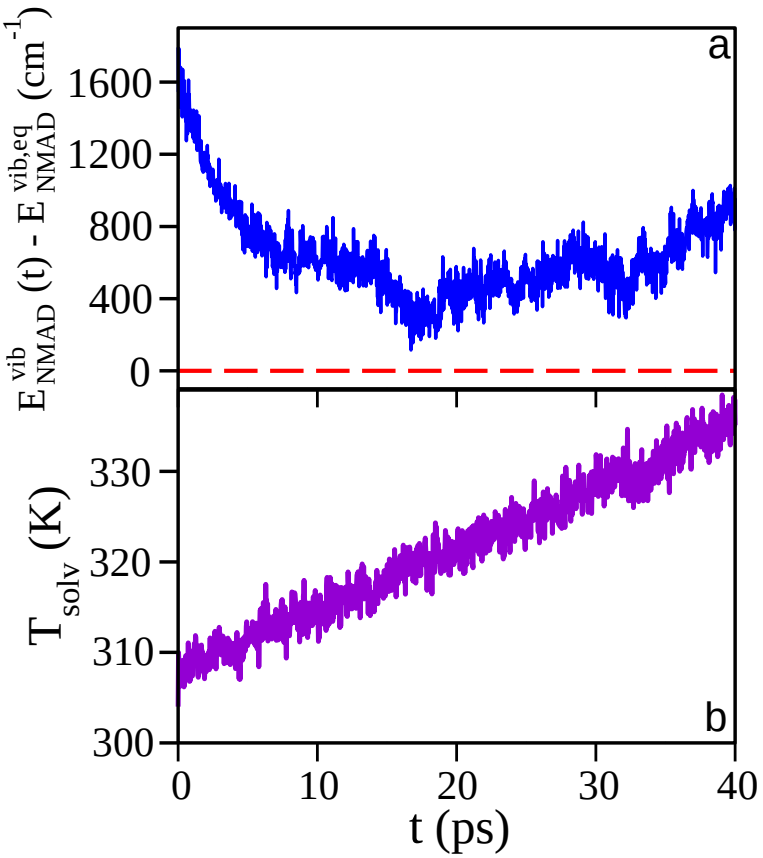

Figure 3.28: (a) Time evolution of the vibrational energy of the NMAD molecule relative to its equilibrium value at 300 K, and (b) the temperature of the solvent obtained in nonequilibrium NVE SEBOMD simulations.

3.2.4.2 Amide I relaxation lifetime

The time evolution of the amide I energy is shown in Figure 3.32. As seen this curve is well reproduced by a triexponential function

$$\frac{E_{\mathrm{amI}}^{\mathrm{vib}}(t) - E_{\mathrm{amI}}^{\mathrm{vib,eq}}(t)}{E_{\mathrm{amI}}^{\mathrm{vib}}(0) - E_{\mathrm{amI}}^{\mathrm{vib,eq}}(0)} = \sum_{i=1}^{3} c_i e^{-t/\tau_i} \tag{3.6}$$

where c_i are the weights which satisfy $c_1 + c_2 + c_3 = 1$. The fit parameters are given in Table 3.22 as well as those obtained from experiments and other theoretical treatments. While a triexponential decay function was also used to describe the QM/MM results [Jeon 11], a biexponential function was enough to reproduce the experimental data [Hamm 98, DeCamp 05] and the MM/MD simulations [Nguyen 03, Bastida 10a], and recently the hybrid quantum-classical Molecular Dynamics with Quantum Transition (MDQT) results [Bastida 12] were fitted to a monoexponential function. We note that each exponential term indicates the presence of a specific relaxation pathway of

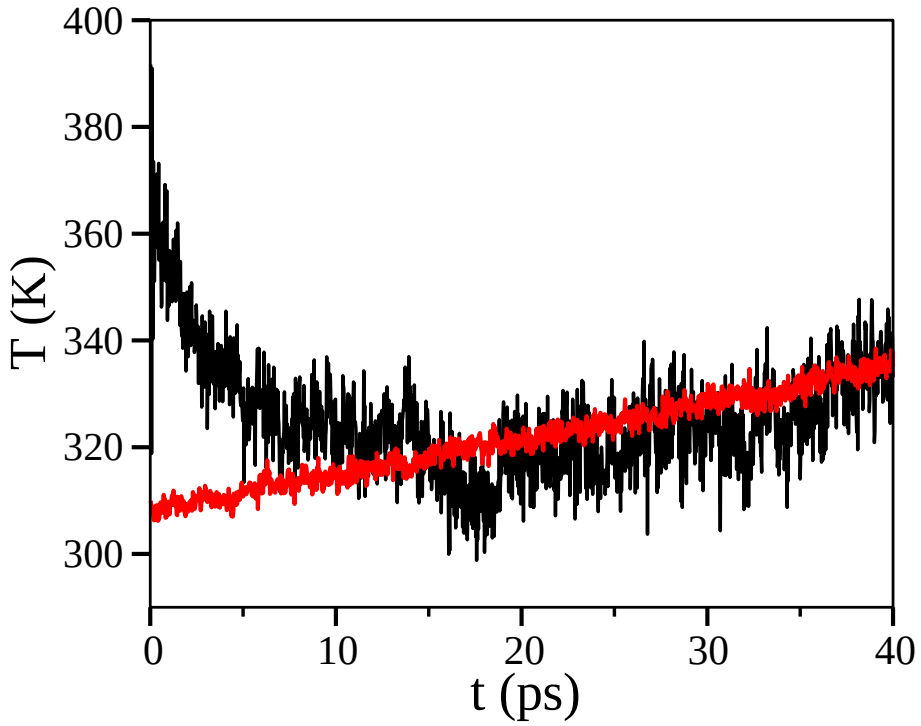

Figure 3.29: Time evolution of the the temperature of the solute NMAD molecule (black line) and the water (red line) obtained in nonequilibrium NVE SEBOMD simulations.

the amide I mode. Since the IVR relaxation pathways depends strongly on the resonance condition between three or more mode frequencies [Fujisaki 07b, Fujisaki 08, Fujisaki 09, Zhang 09, Bastida 10a, Bastida 10b, Bastida 12], the choice of the force field employed to describe the system can modify the details of the relaxation pathways and consequently the slope of the relaxation decay curve.

In Figure 3.33 we show the evolution in time of the fitted normalized vibrational energy of the amide I mode obtained using SEBOMD along with the fits to the measured data obtained from experiments [Hamm 98, DeCamp 05] and the theoretical results obtained using QM/MM at semiempirical PM3 level [Jeon 11], nonequilibrium MM/MD simulations [Nguyen 03, Bastida 10a] and the MDQT method [Bastida 12]. As seen the MM/MD and QM/MM results provide relaxation times longer than the experimental data. There are two main reason for these discrepancies. First the classical description of the vibrational motions which is not justified for high frequency modes as the amide I mode which frequency is much higher than thermal energy at room temperature ($K_BT = 210\,\mathrm{cm}^{-1}$). In this line the use of a quantum description of the amide I vibration [Bastida 12] accelerated the relaxation process providing results closer to the experimental measurements. And second the use of model MM potential energy functions where the polarization and charge transfer effects are neglected. The use of a QM description of the solute while retaining the MM description of the solvent [Jeon 11] did not improve significantly the results. On

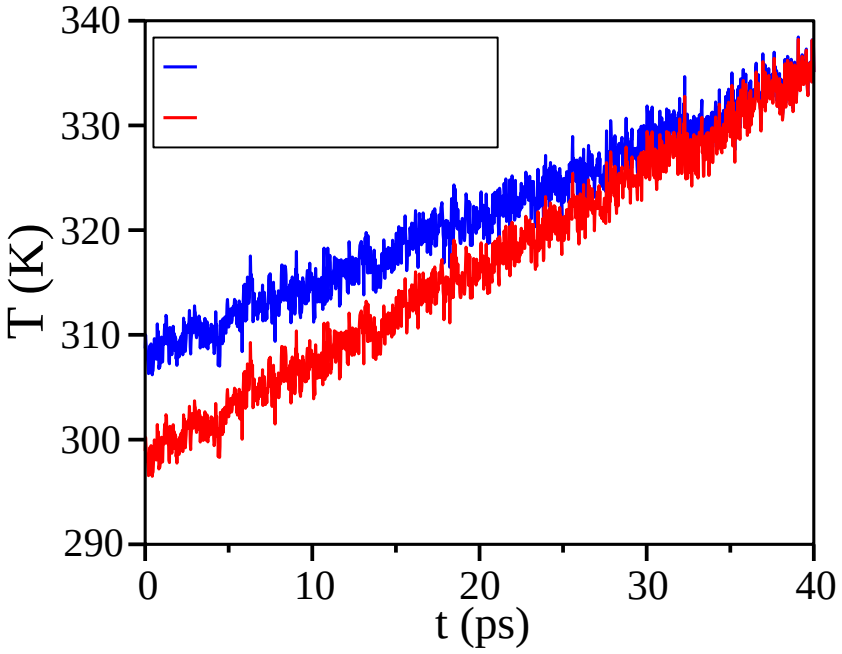

Figure 3.30: Time evolution of the temperature of the solvent without (blue line) and with (red line) linear correction.

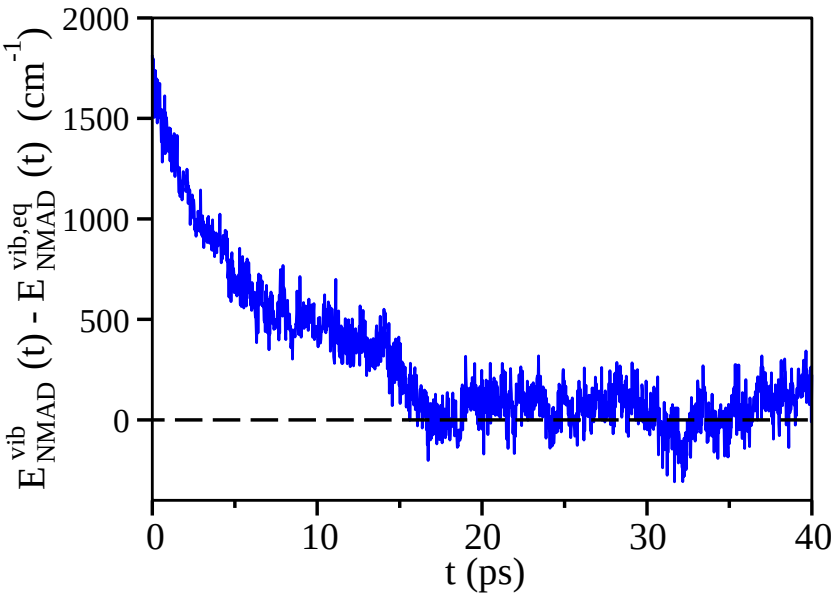

Figure 3.31: Time dependent vibrational energy of the NMAD molecule relative to its time dependent equilibrium value $E^{vib,eq}_{NMAD}(t)$.

the contrary the SEBOMD results agree much better with the experiments what proves the importance of taking into account the electronic interactions between the NMAD and

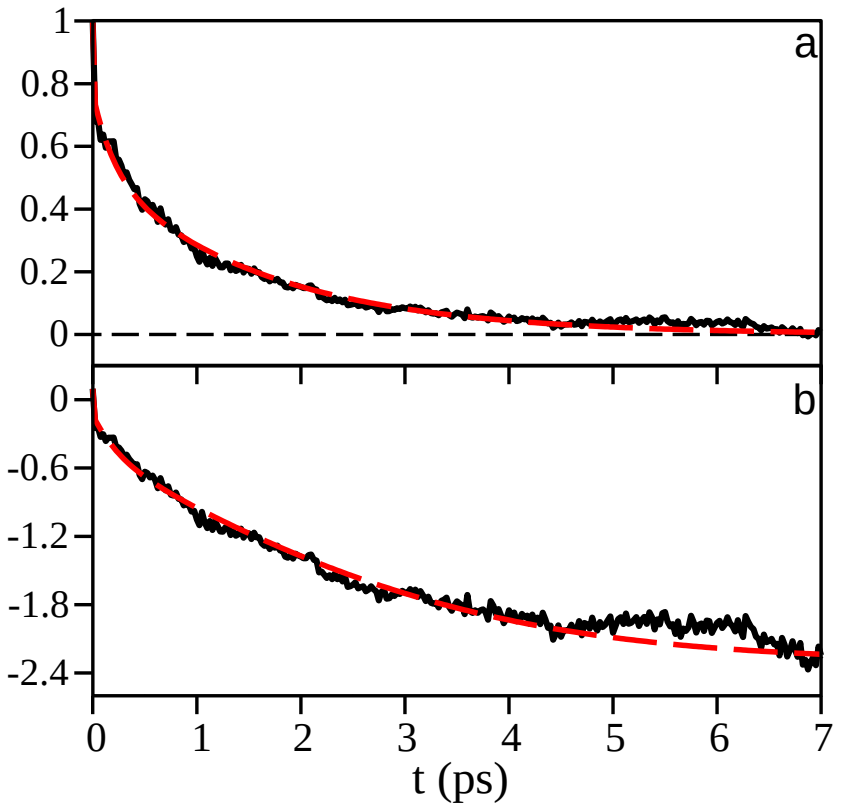

Figure 3.32: (a) Time evolution of the normalized vibrational energy of the amide I mode with respect to its equilibrium value (black line) and the fit to a three exponential function (red dashed line) and (b) its logarithm.

the water molecules.

While the justification of the triexponential decay observed in the SEBOMD results will be detailed in the next section we have found useful to compute the overall relaxation time T_1 when the initial vibrational energy decrease in a factor $1/e$ to compare the different experimental and theoretical results. The values of T_1 are included in Table 3.22 and confirm the tendencies previously described. We emphasize that the best overall agreement with the experimental data is provided by the SEBOMD results what confirms that the inclusion of the electronic interactions is necessary to provide an accurate description of the VER process of the NMAD molecule in water solution.

3.2.4.3 IVR pathways

The next issue that we address is the amide I relaxation pathways. According to our kinetic analysis the relaxation takes place through three different stages. The fast stage is ultrafast and is characterized by a relaxation time of 0.4 fs which is of the same order that the time step used in the same simulation. We have found that the only INMs which are excited in such time scale are the amide II mode and the group a_2 modes (CH bending motions)

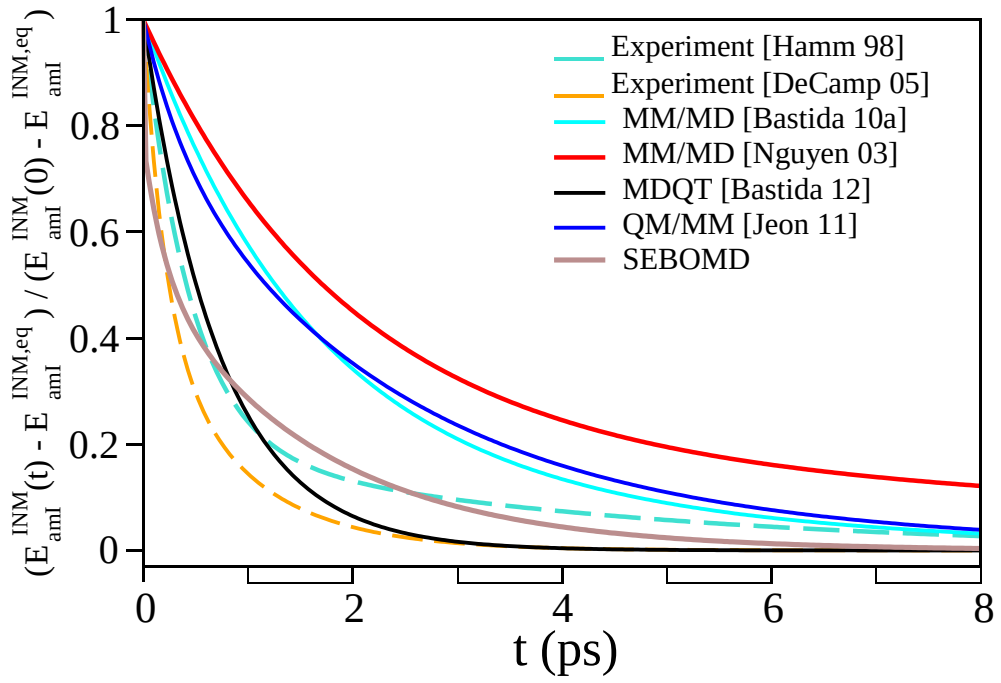

Figure 3.33: Experimental and theoretical time evolutions of the normalized vibrational energy of the NMAD amide I mode with respect to its equilibrium value.

Table 3.22: Vibrational relaxation times of the amide I mode (in ps) obtained by fitting to mono-, bi- and tri-exponential decay functions. Weights are given in brackets

		τ_1 (c_1)	τ_2 (c_2)	τ_3 (c_3)	T_1
Experiment	Hochstrasser *et al*[a]	0.45(0.80)	4.00(0.20)		0.63
	Tokmakoff *et al*[b]	0.20(0.55)	0.86(0.45)		0.39
SEBOMD		0.0004(0.23)	0.20(0.24)	1.61(0.53)	0.63
MM/MD	Bastida *et al*[c]	1.55(0.80)	4.01(0.20)		1.76
	Nguyen and Stock[d]	1.90(0.80)	13.30(0.20)		2.60
MDQT	Bastida *et al*[e]	0.73(1.00)			0.73
QM/MM	Cho *et al*[f]	0.37(0.20)	2.30(0.75)	6.90(0.05)	1.90

a.- Ref. [Hamm 98]
b.- Ref. [DeCamp 05]
c.- Ref. [Bastida 10a]
d.- Ref. [Nguyen 03]
e.- Ref. [Bastida 12] *f*
.- Ref. [Jeon 11]

which energy curves are shown in Figure 3.34. As seen each of them receives ~ 125 cm^{-1} of the energy released by the amide I mode. However, according to the data shown in Table

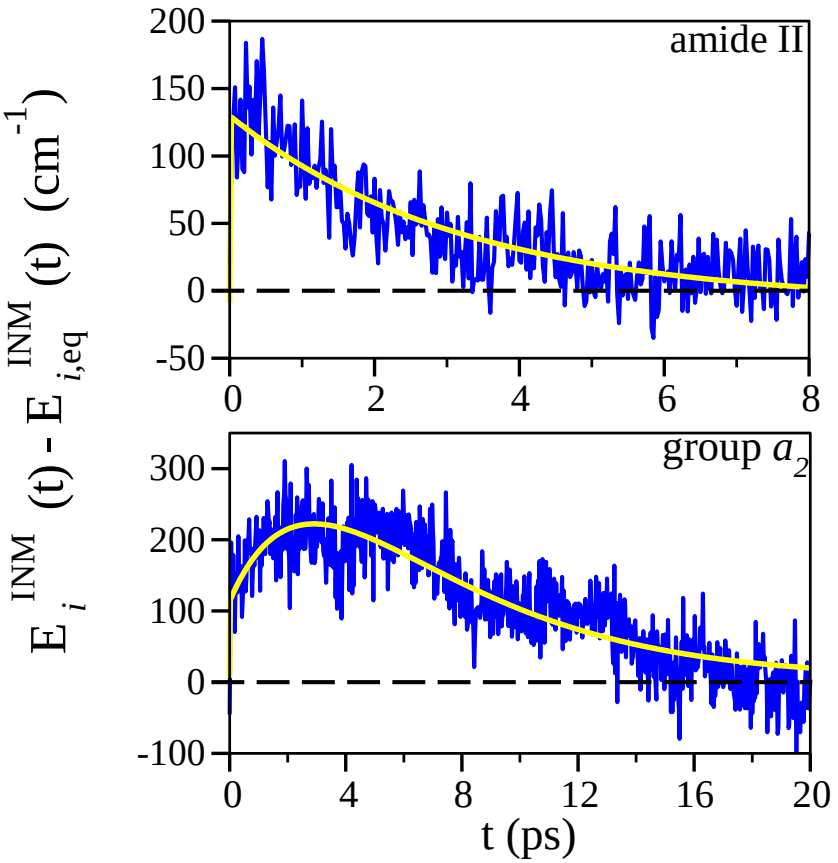

Figure 3.34: Time evolution of the vibrational energy of the amide II and group a_2 modes (blue line) and the corresponding fit curves (yellow line).

3.22 this channel accounts for 23% of the energy released, that is, 415 cm^{-1}. The energy difference must be transferred into low frequency modes which fill the gap between the frequency of the amide I mode (1804 cm^{-1}) and the amide II (1428 cm^{-1}) and the group a_2 modes (1270.4-1363.4 cm^{-1}). These low frequency modes show no significant excitation during the relaxation process because they also relax quickly into the librational motions of the solvent which have similar frequencies. This behavior has been previously noted in MM/MD studies of the same system [Bastida 10a, Bastida 10b]

The time evolution of the vibrational energy of the amide II mode can be well reproduced by considering it as an intermediate in a sequential mechanism (amide I $\xrightarrow{\tau_{exc}}$ amide II $\xrightarrow{\tau_{rel}} \cdots$) so that the evolution over time of the energy is given by

$$E_i^{\mathrm{INM}} - E_{i,\mathrm{eq}}^{\mathrm{INM}} = A(e^{-t/\tau_{\mathrm{rel}}} - e^{-t/\tau_{\mathrm{exc}}}) + B \tag{3.7}$$

where τ_{exc} and τ_{rel} are the corresponding excitation and relaxation lifetimes, A is a parameter related to the maximum of the energy curve and B is a parameter which accounts for small deviations of the curve from the equilibrium value at long times. As we can see in Figure 3.34 the vibrational energy curve of the group a_2 modes show two different

Table 3.23: Fit parameters for the vibrational relaxation of different INMs of the NMAD molecule, including relaxation and excitation times (in ps), exponential amplitudes and parameters A and B (in cm^{-1}).

$A(e^{-t/\tau_{rel}} - a_{exc}e^{-t/\tau_{exc}} - a^t_{exc}e^{-t/\tau_{exc}}) + B$	$\tau_{exc}(a_{exc})$	$\tau^t_{exc}(a^t_{exc})$	τ_{rel}	A	B
group a_2	0.0004(0.075)	3.21(0.925)	4.50	1442.60	5.6
$A(e^{-t/\tau_{rel}} - e^{-t/\tau_{exc}}) + B$	τ_{exc}		τ_{rel}	A	B
amide II	0.0004		3.21	138.84	−9.0
7th INM	0.20		6.80	44.06	11.4
9th INM	0.20		6.80	94.24	15.7
10th INM	0.20		6.80	77.94	0.0
15th INM	0.20		6.80	78.55	5.7
21st INM	1.61		5.39	77.78	0.0
group a_1	1.61		5.44	506.27	0.0

excitation times so that we have used the following function to fit it

$$E_i^{INM} - E_{i,eq}^{INM} = A(e^{-t/\tau_{rel}} - a_{exc}e^{-t/\tau_{exc}} - a^t_{exc}e^{-t/\tau^t_{exc}}) + B \tag{3.8}$$

which contains two excitation times τ_{exc} and τ^t_{exc} and weights a_{exc} and a^t_{exc} which satisfy $a_{exc} + a^t_{exc} = 1$. The fit parameters for both modes are included in Table 3.23 and the curves obtained from these fits are superimposed in Figure 3.34.

Interestingly the longer excitation time of the group a_2 modes (3.21 ps) agree with the relaxation lifetime of the amide II mode. This fact suggests that the energy received by the group a_2 modes in both excitation steps comes mainly from the amide II mode with little contribution from the initially excited amide I mode. This transfer is favored by the small frequency gap between these modes. As seen in Table 3.20 the standard deviation of the frequencies of these modes are higher than the difference between the average values of these frequencies so that their instantaneous values can become practically degenerated during their time evolution.

An additional fact that favors the role of the amide II mode as main relaxation channel of the amide I modes in this first stage is the magnitude of the coupling among these modes. Kidera *et al.* [Moritsugu 00, Moritsugu 03] have shown that this coupling is highly correlated with the geometrical overlap among the corresponding modes. In Figure 3.35 we show the average effective atomic contributions for the amide I, amide II and group a_2 modes. As seen the highest contribution for both the amide I and amide II modes comes from the carbon atom of the carbonyl group what translate into a strong coupling between them. We also note that the atomic contributions for the group a_2 modes overlap better with those for the amide II mode than with those for the amide I mode. Altogether these results points out the participation of the amide II mode as main channel during the first stage of the relaxation of the amide I mode and as intermediate in the excitation of the group a_2 modes.

The second stage of the amide I relaxation shows a relaxation time of 0.20 ps. We found that the 7th (amide IV), 9th (ν(CC)), 10th (amide III) and 15th (ν(CN)) INMs

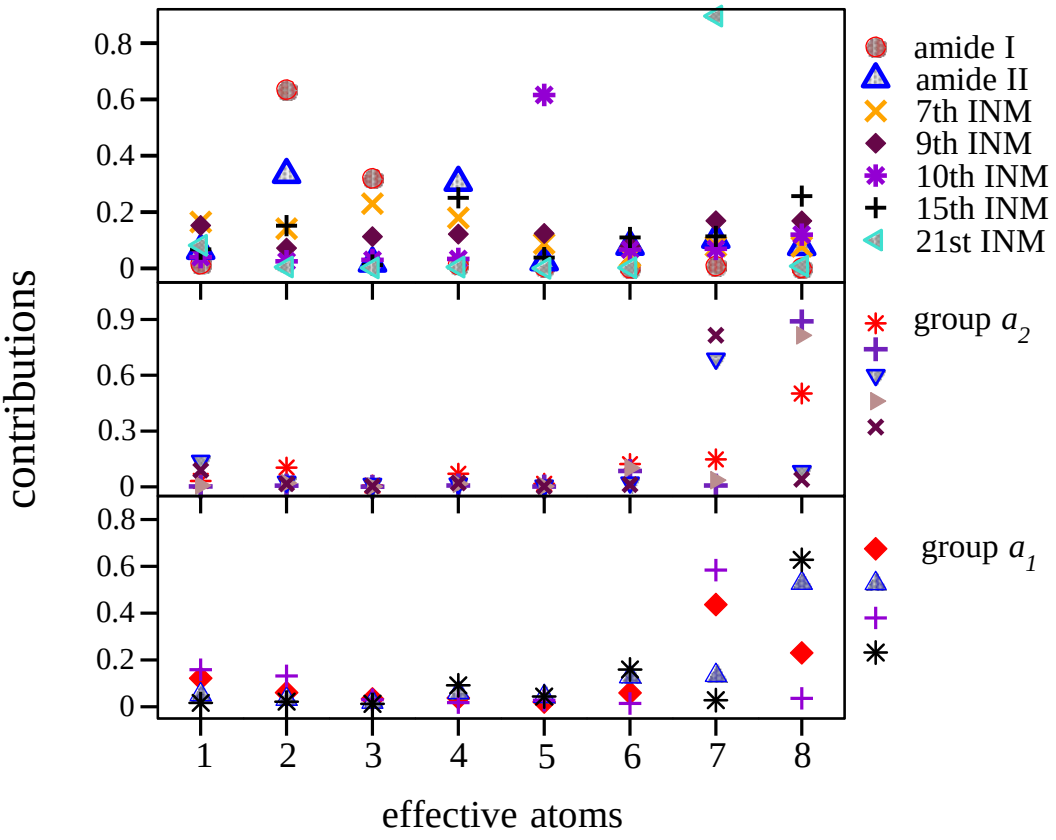

Figure 3.35: Average effective atomic displacement contributions for the amide I, amide II, 7th, 9th, 10th, 15th and 21st INMs (upper panel), group a_2 modes (16th-20th INMs)(middle panel) and group a_1 modes (11st-14th INMs) (lower panel) (see Figure 3.36 for the effective atoms definition).

are excited in that time scale. Their energy curves are shown in Figure 3.37 as well as the fits obtained using Eq. (3.7) where the same relaxation time 6.80 ps was employed (see Table 3.23). We note that the sum of the two average frequencies for the (7th,15th) and (9th,10th) INMs are close to the frequency of the amide I mode (see Table 3.20) so that the resonance condition is fulfilled. Moreover we see in Figure 3.35 that the four INMs considered have non-neglectable effective atomic contributions in one or both atoms of the carbonyl group. However, the energy accumulated in these four INMs only accounts for 16% of the energy released by the amide I mode while the second stage contributes with 24% (see Table 3.22). As we discuss below the additional 8% is probably transferred into the solvent.

The third relaxation stage of the amide I mode proceeds with a 1.61 ps lifetime. In Figure 3.38 we show the energy curve for the group a_1 modes (CH rocking modes) and the 21st INM (CH bending modes) which are excited in that time scale. Both curves are also well reproduced using Eq. (3.7) and have a common relaxation time of 5.4 ps (see Table 3.23). The most important contribution corresponds to the group a_1 modes which frequencies are in the 1041.5-1115.9 cm^{-1} range. Considering that the standard deviations

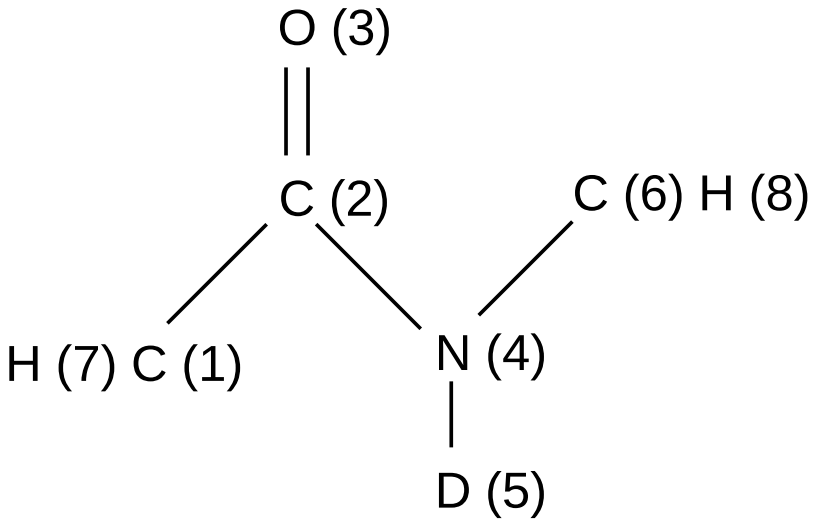

Figure 3.36: The effective atoms definition of the NMAD molecule used in the INM analysis.

of the group a_1 and amide I frequencies are in the order of 100-200 cm^{-1} (see Table 3.20) the energy transfer can be mediated through a 2:1 Fermi resonance. In the case of the 21st

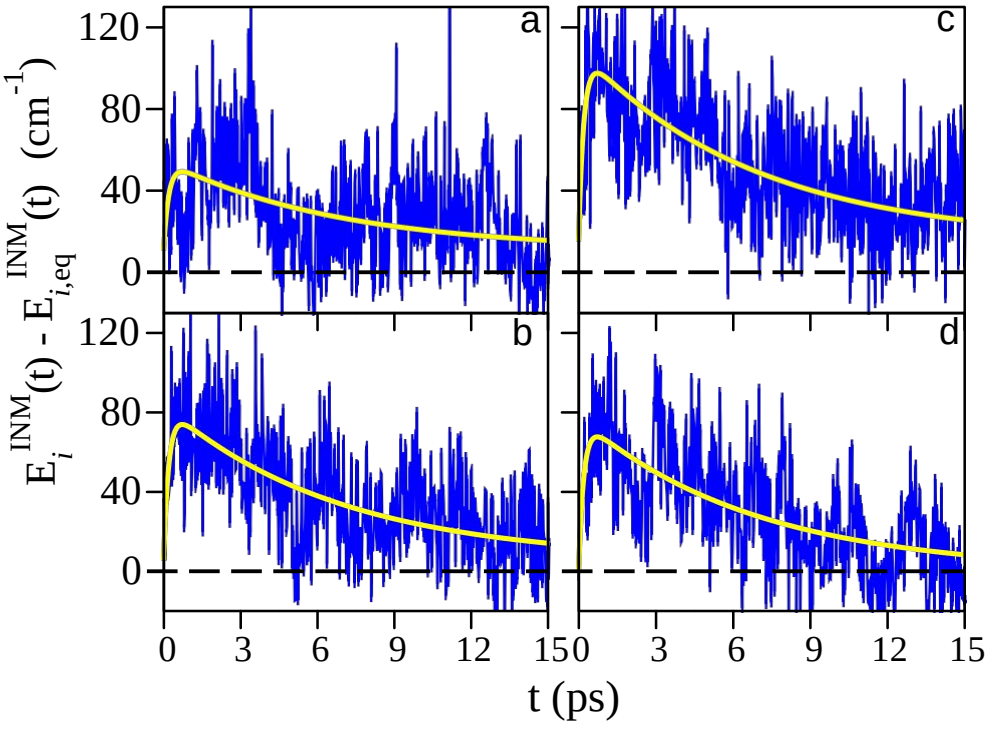

Figure 3.37: Time evolution of the vibrational energy of the (a) 7th INM (b) 15th INM, (c) 9th INM and (d) 10th INM.

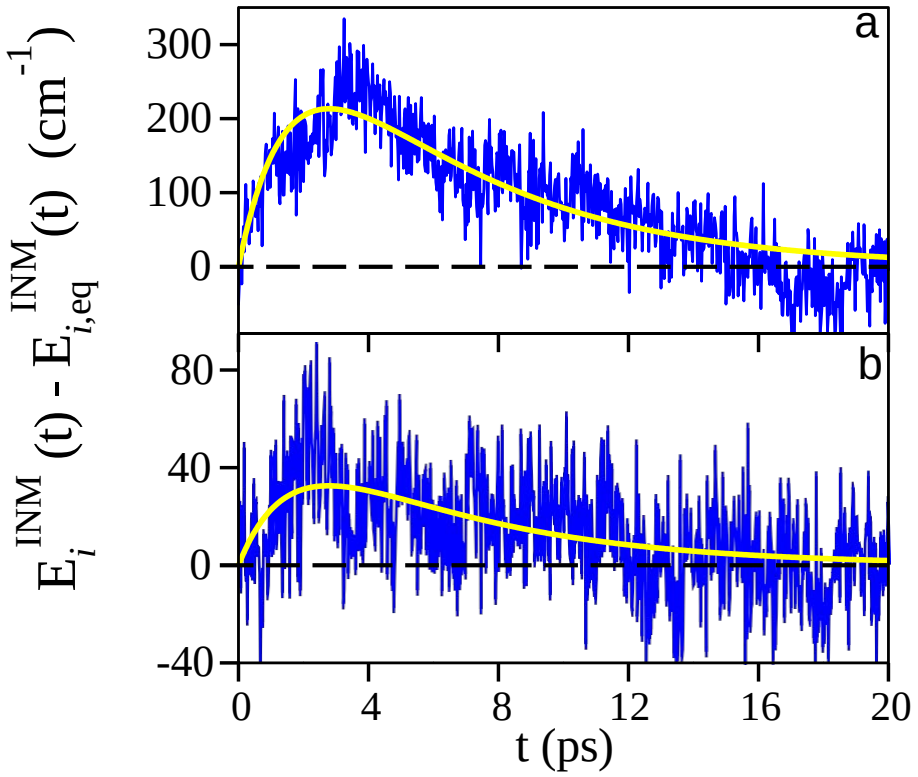

Figure 3.38: Time evolution of the vibrational energy of the (a) group a_1 and (b) 21st INMs

INM the excess energy must be transferred into low frequency modes. We note that the energy stored in these normal modes only accounts for ~16.6% of the energy released by the amide I mode while the third stage contributes with 53% (see Table 3.22). We consider that the additional 36.4% is transferred into low frequency modes and the solvent, as we discuss below.

After the relaxation of the amide I mode, most of the energy is distributed among mid-range frequency modes which subsequently relax into low frequency modes and the solvent. These secondary IVR process are difficult to identify individually because the energy flows are small as the energy is distributed among a higher number of INMs and the intramolecular energy transfer into the solvent becomes important in the picoseconds time scale. Therefore we focus our attention on the time evolution of the total vibrational energy of the NMAD molecule showed in Figure 3.39. This curve can be fitted to a biexponential function as follows

$$\frac{E_{\mathrm{NMAD}}^{\mathrm{vib}}(t) - E_{\mathrm{NMAD}}^{\mathrm{vib,eq}}(t)}{E_{\mathrm{NMAD}}^{\mathrm{vib}}(0) - E_{\mathrm{NMAD}}^{\mathrm{vib,eq}}(0)} = c_1\, e^{-t/\tau_1} + c_2\, e^{-t/\tau_2} \tag{3.9}$$

where the weights satisfy $c_1 + c_2 = 1$ and τ_1 and τ_2 are the NMAD relaxation times. We find that the SEBOMD results are well reproduced using $\tau_1 = 0.20$ ps and $\tau_2 = 7.0$ ps being 0.13 and 0.87 the respective weights. The fastest relaxation lifetime agrees with that

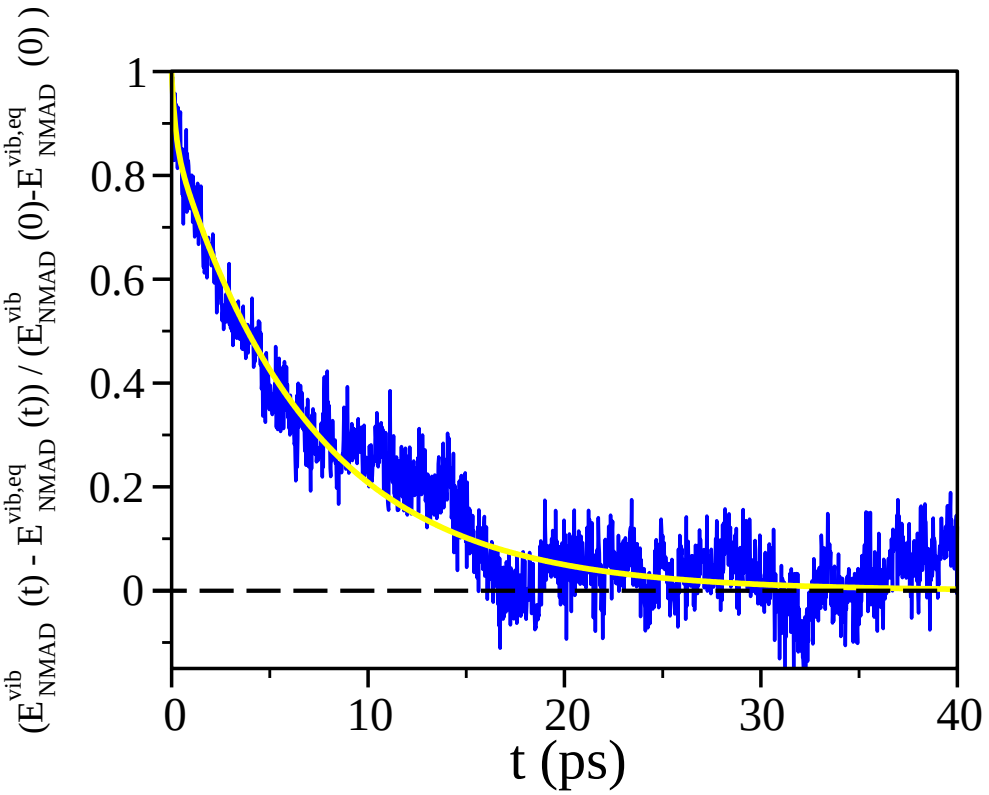

Figure 3.39: Time evolution of the total vibrational energy of the solute NMAD molecule relative to its equilibrium value as obtained from SEBOMD simulations (blue line) and the fit to Eq. (3.9) (yellow line).

second stage amide I relaxation lifetime so that it corresponds to a direct energy flow from the amide I mode to the solvent. However this channel only account for 8% of the energy as we previously detailed. We consider that the remaining 5% is probably released through some lower frequency modes excited during the first amide I relaxation channel.

The longer NMAD relaxation time is similar to those ones found for the INMs excited during the relaxation of the amide I modes (see Table 3.23). Therefore the secondary IVR processes if present must occur in a short time scale. This is not surprising since they involve low frequency modes which relaxation into the solvent is faster than most of the IVR processes. In addition, we observe in Figure 3.39 that after 3 ps ~ 45% of the total vibrational energy is already transferred from the NMAD molecule to the solvent. This fact may indicates that part of the energy released from the amide I during the third stage flows directly to the solvent. However, due to the smoothly energy transfer from the other INMs into the solvent, this stage is counted within the second relaxation time of the NMAD molecule.

The relaxation lifetime of the NMAD molecule in D_2O has been measured by Dlott *et al* [Fang 09] to be 5.1 ps. While this value was obtained after initially exciting the CH stretching mode, our MM/MD simulations [Bastida 10a, Bastida 10b] have shown

that the NMAD relaxation lifetime was similar when exciting the amide I or the CH stretching modes. To make a proper comparison with the experiments we evaluated an average NMAD relaxation lifetime following the procedure previously described for the amide I mode obtaining $T_{1,\mathrm{NMAD}} = 6.0$ ps. This value is closer to the experimental results than those previously obtained using the MM/MD (9.6 ps) [Bastida 10a], QM/MM (8.1 ps) [Jeon 11] or MDQT (6.6 ps) [Bastida 12] methods.

In order to complete our discussion it is interestingly to compare the relaxation pathways derived from SEBOMD simulations with those previously obtained by the MM/MD [Soler 11], QM/MM [Jeon 11] and MDQT [Bastida 12] methods. Such a comparison is limited by the use of different force fields which provide vibrational frequencies which can vary up to 200 cm^{-1} from one to other study. These shifts modify the resonance conditions so that the specific pathways are far from being identical. In spite of this drawback we identify some general trends. The relaxation of the amide I mode is basically an IVR process with a smaller contribution of intermolecular energy flow into the solvent although the specific percentage of energy transferred into the solvent varies significantly for the different theoretical approximation: 24% in MDQT [Bastida 12], 5% in QM/MM [Jeon 11], 20% in MM/MD [Soler 11] and ~20% in SEBOMD simulations.

The main relaxation channel involves the rocking and bending methyl normal modes which receive approximately one third of the amide I vibrational quantum. The second bigger energy acceptors are modes with frequencies in the 500-900 cm^{-1} range as the amide III, amide IV, amide VI and ν(CC) modes.

One interesting point concerns the participation of the amide II mode in the relaxation of the amide I mode which has been considered in different experimental [Rubtsov 03a, DeFlores 06, Piatkowski 10, Piatkowski 12] and theoretical [Fujisaki 06, Dijkstra 07, Fujisaki 07b, Bloem 08, Fujisaki 09, Bastida 10a, Soler 11, Dijkstra 11, Jeon 11, Bastida 12] works. Hochstrasser *et al* [Rubtsov 03a] found a significant coupling between the two modes when studying the NMA molecule in DMSO solution by femtosecond two color IR spectroscopy. This result was confirmed by Tokmakoff *et al* [DeFlores 06] and extended to the fully deuterated NMA molecule in D_2O through 2D-IR experiments. However, Bakker *et al* [Piatkowski 10] found no energy transfer between the amide I and amide II modes using similar spectroscopic techniques, when applied to the study of the NMA molecule solved in CCl_4. We note that in this study the presence of the NMA dimers could modify the relaxation pathways. More recently these authors considered the relaxation of the NMA monomers dissolved in bromoform [Piatkowski 12]. They concluded that only a minor part of the excitation of the amide I mode is transferred to the amide II mode and the dominant relaxation channel for the amide I mode involves transfer of energy to combination tones of other lower frequency (amide) vibrations. The authors also estimate that less than 20% of the energy flows from the amide I to the amide II mode.

From the theoretical point of view the results are even more contradictory. Fujisaki *et al* [Fujisaki 06, Fujisaki 07b, Fujisaki 09] applied different time-dependent perturbation schemes to analyze the relaxation of the amide I mode in NMAD/D_2O_l showing that the main pathways involve the contribution of low and midrange frequency modes of the

solute or a 2:1 Fermi resonance, without any significant contribution of the amide II mode. Later, the same group concluded that the amide II mode was not found to participate in the relaxation of the amide I mode of the isolated NMAD mode [Zhang 09] when studied using the time dependent perturbation theory at the B3LYP/aug-cc-pvdz level. However, the amide II mode was found to be involved in the energy relaxation of the NMAD/$(D_2O)_n$ (n=1-3) clusters. Knoester *et al* [Dijkstra 07, Bloem 08, Dijkstra 11] have analyzed the relaxation of the amide I mode of NMAD and fully deuterated NMA molecules in D_2O solution using a model of reduced dimensionality where only the amide I and amide II modes are considered explicitly. In both systems the authors found a strong coupling between amide I and amide II modes so that the amide II mode was considered to be the predominant relaxation pathway for the amide I mode. Our research group found that the amide II mode receives 3.5% of the amide I vibrational quantum in MM/MD simulations [Soler 11] and this percentage is almost neglectable in MDQT simulations [Bastida 12]. The use of semiempirical Hamiltonians increases mostly this contribution up to 9.2% in QM/MM simulations [Jeon 11]. In line with this studies the SEBOMD results provide a 7.0% percentage. Therefore we conclude that the amide II mode contributes to the relaxation of the amide I mode but it plays just a minor role in line with the most recent experiments [Piatkowski 12].

As a final remark we note that the MM/MD, MDQT, QM/MM and SEBOMD methods describe classically the vibrational modes that receive the energy during the relaxation process. As a consequence we find that unrealistic excitation of modes with vibrational frequencies higher than that of the amide I mode occur over time. In Figure 3.40 we show the time evolution of the total energy stored in those modes obtained in the SEBOMD simulations. As seen the excitation of these modes is slow compared to the IVR process previously discussed in agreement with previous QM/MM results [Jeon 11]. The maximum amount of energy stored in these high frequency modes is 5.5% which is smaller than the percentage obtained in MDQT (10.0%), MM/MD (18%) and QM/MM (23.0%) simulations. Therefore the description provided by the SEBOMD method is more realistic in this particular point.

3.3 VIBRATIONAL RELAXATION OF THE AMIDE I MODES OF THE ALAD MOLECULE IN $D_2O_{(L)}$

3.3.1 AlaD conformations

Molecular Dynamics simulations of proteins are typically limited by the high computational cost of performing calculations on large system. Fortunately, it appears that, with the exception of glycine and proline each amino acid displays a very similar backbone conformational characteristics [Edsall 85]. This finding has been supported as well by a recent

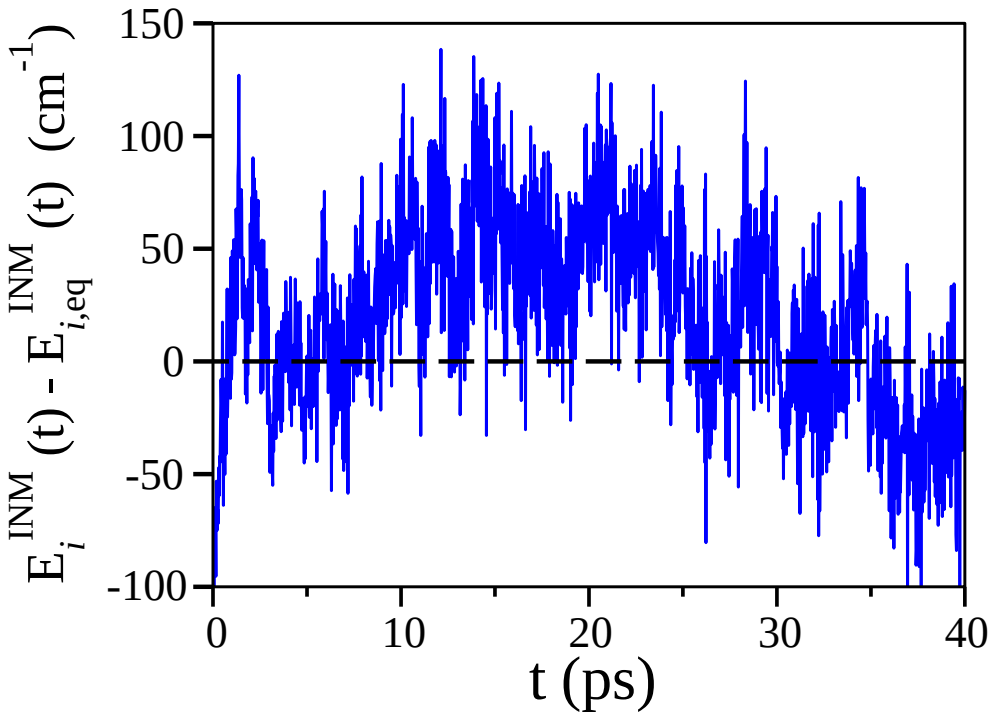

Figure 3.40: Time evolution of the total vibrational energy of the modes with frequencies higher than that of the amide I mode.

study performed by Feig [Feig 08]. The conformations of peptides are defined by flexible torsion angles [Edsall 66] φ (C-N-C$_\alpha$-C) and ψ (N-C$_\alpha$-C-N), as seen in Figure 3.41. Based on the Ramachandran plot [Ramachandran 63, Ramachandran 68] of φ vs ψ (see Figure 3.42) we can analyze the conformational details of any biological molecule.

The rotations around the flexible dihedral angles produce different conformations as C5, C$_{7eq}$, α_R, α^t, P$_{II}$, α_L and β as shown in Figure 3.3. Since all these conformers are not necessarily present for all the force fields available and the limits of every region are not precise, sometimes we will refer to the C5, C$_{7eq}$, P$_{II}$ and β conformers altogether as beta region and to α_R and α^t conformers as alpha R region in order to simplify our discussion.

The isolated alanine dipeptide has been widely studied by high level *ab initio* methods [Head-Gordon 91, Gould 92] and the general conclusion which was supported by gas-electron diffraction analysis study [Schafer 95] is that the internally hydrogen bonded conformation C7$_{eq}$ and extended C5 are of lowest energy.

Although the structure and thermodynamics of the AlaD molecule in water solution have been characterized by different theoretical methods [Han 98, Smith 99, Gnanakaran 01, Hu 03, Alexander 04, Dmitriy 04, Wang 04, Kim 05b, Feig 07, Seabra 07, Kwac 08, Yang 09, Gaigeot 10] and to a lesser extent experimentally [Poon 00, Weise 03, Takekiyo 04, Mehta 04, Kim 05a, Lee 07, Grdadolnik 08] so far the conformational distribution of this molecule is not fully resolved. The NMR experiments [Poon 00, Weise 03, Mehta 04] favor the P$_{II}$

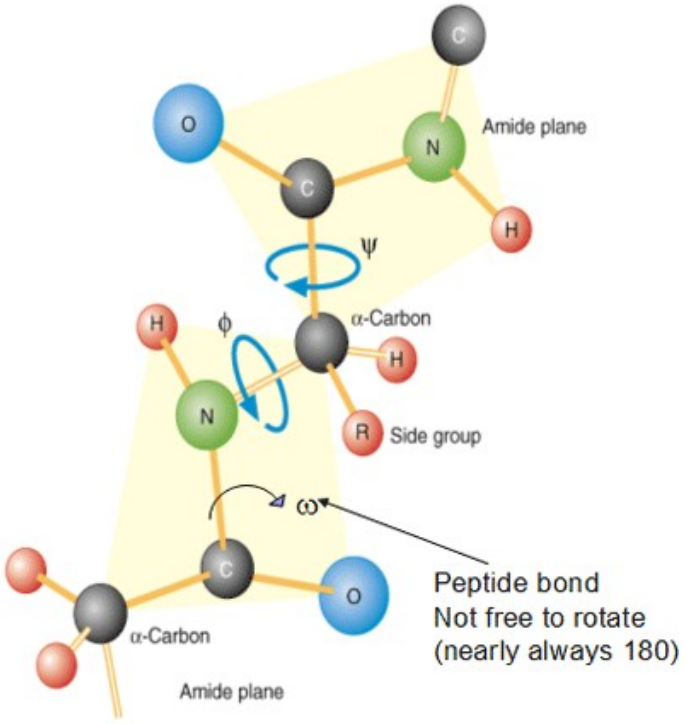

Figure 3.41: The backbone torsion angles φ and ψ.

conformation as the most stable one as well as some Raman and IR spectroscopic studies [Grdadolnik 08]. The two-dimensional IR spectroscopy [Kim 05b] and the Vibrational Circular Dichroism (VCD) measurement provide results with P_{II} -like or β conformations. However, some results obtained using Raman spectroscopy support the presence of the α_R and C_{7eq} conformations [Takekiyo 04].

All of the theoretical results confirm the presence of P_{II} -like or β conformations but some of them also provide a significant contributions of alpha R conformations [Smith 99, Gnanakaran 01, Hu 03, Wang 04, Seabra 07, Feig 08, Kwac 08, Yang 09]. Moreover, the relative percentage of alpha R and beta conformers depends strongly on the force field used to simulate the system [Kwac 08, Yang 09]

3.3.2 Comparison of MM force fields

The choice of the MM force field used to describe the AlaD molecule solved in water is crucial because the accuracy of the different models depends strongly on the composition of the simulated system as well as on the physical properties of interest. In the present study we have tested three different force fields AMBER94 [Cornell 95], OPLS-AA/L [Jorgensen 96, Kaminski 01] and CHARMM22 [MacKerell 98]. AMBER94 force field was designed to simulate the structure, conformational energies and interactions of proteins, nucleic acids and many selected organic molecules in condensed phase. Moreover, in this

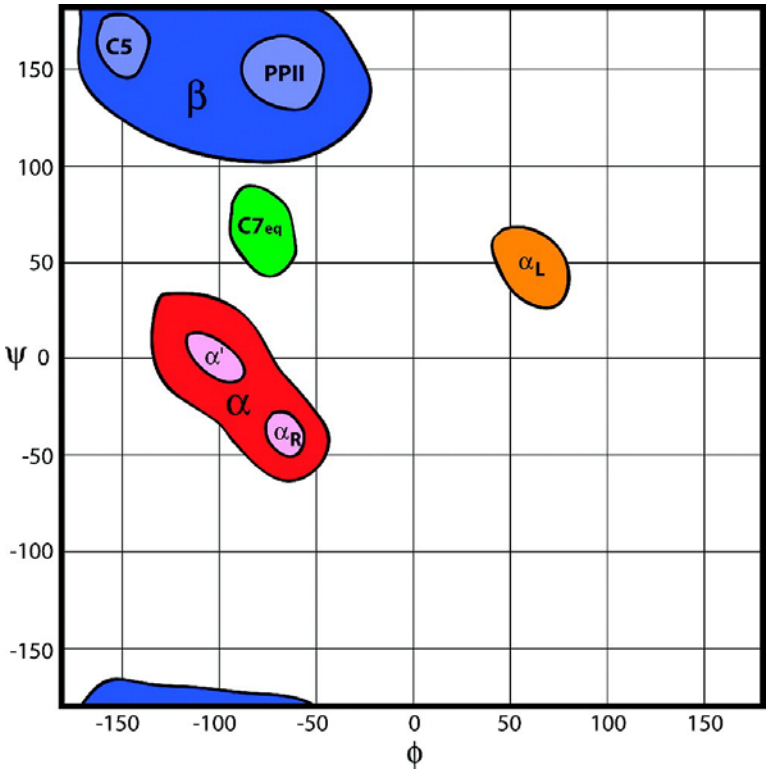

Figure 3.42: Schematic overview of major conformational basins sampled by φ/ψ backbone torsion angles in nonglycine, nonproline peptide residues using Ramachandran plot taken from Ref. [Feig 08].

force field a set of φ and ψ parameters have been developed for the peptide backbone, in order to reproduce the energies of the low energy conformations of glycyl and alanyl dipeptides. The OPLS-AA/L force field was presented to improve the OPLS-AA force field for peptides by means of refitting the key Fourier torsional coefficient. In this force field the fitting technique combines using accurate *ab initio* data, choosing an efficient fitting subspace of the whole potential energy surface, and determining weights for each of the fitting points based on magnitudes of the potential energy gradient. The CHARMM22 force field was introduced for the simulations of peptides and proteins in condensed phase. In this force field the parameters were determined by fitting an extended set of experimental and *ab initio* results. Furthermore, a self consistent approach was employed to obtain a proper balance between the intramolecular and intermolecular terms of the potential energy function, which is essential for accurate condensed phase simulations. In addition, the internal parametrization were chosen to reproduce geometries from crystal structures, infrared and Raman spectroscopic data and *ab initio* calculations.

As a starting point, the optimization of the isolated deuterated AlaD (Ala-d_2) molecule was performed by using the aforementioned force fields and the *optimize* program within TINKER modeling package version 5.0 [Ren 02, Ren 03]. Three force fields agree that the

Table 3.24: Dihedral angles φ/ψ of the AlaD-d_2 molecule at different conformations in D_2O solution (β, P_{II}, α_R, α^d) and in gas phase (C5 and $C7_{eq}$) obtained using different force fields.

Force field	C5	β	P_{II}	$C7_{eq}$	α_R	α^t
AMBER94	(-146.7,170.8)	(-130.0,130.0)	(-73.3,139.9)	(-73.3,65.7)	(-59.9,-49.9)	(-100.0,-5.0)
OPLSAAL	(-152.0,158.3)	(-130.0,130.0)	(-80.0,140.0)	(-79.3,61.6)	(-69.1,-49.9)	(-100.0,-5.0)
CHARMM22	(-151.4,170.6)	(-120.0,130.0)	(-80.0,140.0)	(-81.4,70.6)	(-78.8,-50.0)	(-100.0,-5.0)

C_{7eq} and C_5 conformations (see Figure 3.3) are the only minima for the isolated AlaD-d_2 molecule. Further test were done starting in the AlaD-d_2 geometry of the P_{II}, α^t, α_R and β conformations and finding that the optimization process always provides the C_{7eq} or C_5 conformations depending on which local minima was closer to the starting point. We also found during the optimization that the computed energy for the C_{7eq} conformer is lower than that calculated for the C_5 conformer, in agreement with previous results obtained from the application for the same force fields [Cornell 95, MacKerell 98, Kaminski 01]. Moreover these results are in line with those obtained employing different *ab initio* calculation levels [Balázs 90, Boehm 91, Gould 94, Philipp 99, Vargas 02]. A possible reason that has been pointed out to justify the stability of the C_{7eq} conformer [Han 98, Chipot 98, Gnanakaran 01, Vargas 02, Takekiyo 04, Kim 05b, Lee 09] is the intramolecular H-bonding between the carbonyl group within the acetyl end with the NH/ND group within the amino end (see Figure 3.3) leading to a seven membered ring.

While the P_{II}, α^t α_R and β conformations (see Figure 3.3) are not minima for the isolated AlaD-d_2 molecule they become much more stable in polar solvents due to the intermolecular H-bonds. In Table 3.24 we present dihedral angles of the AlaD-d_2 molecule which are representative of the different conformations in D_2O solution for the MM force fields considered. We have optimized the geometry of the isolated AlaD-d_2 molecule keeping fixed the dihedral angles at the values given in Table 3.24. In that way we obtain partially optimized geometries for every conformer present in solution that we use then to define the corresponding set of ENMs.

We focus now on the equilibrium normal mode analysis for the optimized geometries, in particular the amide I normal modes. Our study is highly motivated by the experimental results obtained by Hochstrasser *et al* [Kim 05a] about the dynamics of the acetyl and amino end amide I groups of the AlaD-d_2 molecule solved in D_2O obtained using 2D-IR spectroscopy. Consequently, we are interested in the ability of the different MM force fields to reproduce the experimental evidences. The authors concluded that the two amide I modes are approximately localized modes in the carbonyl groups. In order to test the MM force fields we include in Table 3.25 the atomic displacement contributions of the C and O atoms of the amino and acetyl end carbonyl groups to the amide I modes which correspond to the 47th and 48th ENMs using the frequency ordering. As seen the sum of the contribution of both carbonyl groups to the amide I ENMs is always over 60% up to 91% what agrees with the accepted association between amide I bands and the motions of the C=O groups [Torii 98, Ham 02, Ham 03]. We note that the AMBER94 and

Table 3.25: Atomic displacement contributions (in %) of the C and O atoms of the amino and acetyl end carbonyl groups to the amide I ENMs for the AlaD-d_2 molecule as obtained by using the AMBER94, OPLS-AA/L and CHARMM22 force fields for different conformations.

Force field	ENM	carbonyl group	C5	β	P_{II}	$C7_{eq}$	α_R	α^t
AMBER94	47th	amino end	41.7	37.6	26.0	31.9	26.6	31.4
	47th	acetyl end	38.2	39.8	50.0	42.0	50.0	47.7
	48th	amino end	30.0	30.6	41.6	37.7	46.1	39.6
	48th	acetyl end	30.0	28.0	23.8	29.6	23.5	23.7
OPLS-AA/L	47th	amino end	42.1	42.6	28.6	23.3	39.9	25.4
	47th	acetyl end	37.7	36.5	49.9	54.2	38.6	52.0
	48th	amino end	34.8	33.8	46.0	52.4	38.1	50.9
	48th	acetyl end	31.5	34.2	24.8	20.0	35.8	20.8
CHARMM22	47th	amino end	80.7	84.5	87.0	73.0	0.1	0.4
	47th	acetyl end	0.7	0.2	0.2	18.2	91.0	88.0
	48th	amino end	0.7	0.2	0.2	16.1	80.2	73.0
	48th	acetyl end	85.0	90.0	89.8	74.5	0.1	0.4

OPLS-AA/L force fields provide ENMs which have important contributions simultaneously from both carbonyl groups. On the contrary the ENMs obtained using the CHARMM22 force field involve the motion of practically only one CO group with the exception of the $C7_{eq}$ conformer. However, this conformer has a negligible contribution in water solution as previously mentioned. Interestingly, the frequency order of the two amide I groups depends on the conformation. The ENM frequency of the amino end amide I mode is lower than that of the acetyl end one for the C5, β, P_{II} and $C7_{eq}$ conformers but higher for the α_R and α^t conformers.

The fact that two or more modes involve or not displacement of the same group of atoms has important consequence in the IVR process. As Kidera *et al* [Moritsugu 00, Moritsugu 03] showed the overlap between ENMs is correlated with their coupling and therefore with the rate of energy transfer among them. We conclude then that the CHARMM22 force field provides amide I modes localized over one carbonyl group of the AlaD-d_2 molecule in line with the experiments [Kim 05a]. On the contrary the AMBER94 and OPLS-AA/L force fields lead to delocalized amide I modes.

We are also interested about the amide I frequencies provided by the different MM force fields which are presented in Table 3.26 for the different AlaD-d_2 conformers. As seen the frequency gap between the two amide I modes is in the 10-20 cm^{-1} range in all cases. We note that the frequency of a given amide I mode does not change substantially with the conformer considered for the AMBER94 and OPLS-AA/L force fields. This is particularly due to the impossibility to identify the two amide I groups previously discussed so that the frequencies are just labeled using their values. On the contrary we observe for the CHARMM22 results that the frequencies obtained for the amino and acetyl end amide I

Table 3.26: Frequencies (in cm^{-1}) for the amide I modes of the AlaD-d_2 molecule in gas phase.

Force field	ENM	C5	β	P_{II}	$C7_{eq}$	α_R	α^t
AMBER94	47th	1684.5	1685.7	1682.4	1682.0	1685.3	1680.2
	48th	1705.8	1704.9	1699.8	1702.7	1703.0	1712.9
OPLS-AA/L	47th	1678.0	1678.8	1673.8	1672.3	1674.4	1674.4
	48th	1688.9	1685.2	1686.2	1693.8	1687.0	1695.4
CHARMM22	amino end	1673.5	1672.7	1670.4	1673.6	1689.6	1693.8
	acetyl end	1678.9	1679.0	1678.4	1680.0	1678.6	1677.9
Experiments				Frequency			
Ar matrix [a]				1674, 1685, 1698-1701			
Ar matrix [b]				1680, 1688, 1704			
Kr matrix [c]				1678, 1680, 1702			

a.- Ref. [Grenie 75] for AlaD-d_2 molecule
b.- Ref. [Pohl 07] for the AlaD molecule
c.- Ref. [Pohl 07] for the AlaD molecule

modes for the C5, β, P_{II} and $C7_{eq}$ conformers are in opposite order with respect to the α_R and α^t ones. This inversion only can be evidenced for the CHARMM22 force field where the two amide I modes are localized in the CO groups. It is interesting to compare the calculated frequencies with those obtained experimentally. To our knowledge there is not direct measurements of the AlaD-d_2 molecule in vacuum. Only the results in Argon matrix [Grenie 75] are available and included in Table 3.26. We also present the results for the AlaD molecule also obtained in Ar and Kr matrix [Pohl 07]. The value of the amide I frequency is only slightly modified by the deuterium since the contribution of the H/D atoms of the NH/ND groups to the definition of the amide I ENMs is small. The IR bands corresponding to the amide I mode show different peaks so that it is impossible to make a one to one assignment. But it is accepted that the high frequency corresponds to the amino end amide I mode [Pohl 07] as the results obtained for the α_R and α^t conformers using the CHARMM22 force field. Overall, we consider the agreement between the ENM frequencies derived for the MM force fields and the experimental measurements satisfactory. From the above considerations we conclude that the CHARMM22 MM force field is the most appropriate to perform our study about the vibrational energy relaxation of the AlaD-d_2 molecule.

In Table 3.27 we present the ENM frequencies for the isolated AlaD-d_2 molecule obtained using the CHARMM22 force field at different conformations. We find some significant differences for the frequencies obtained for the six conformers which, in general, become less important as the frequency increase. That is, the higher frequency vibrational modes are less affected by the molecule conformation. This is expected because these modes are mostly associated with bending and stretching vibrations which are highly localized within the molecule and tend to be largely unaffected by the large atomic displacement

involved in the conformational changes. On the other side the low frequency modes are delocalized [Moritsugu 00, Moritsugu 03] involving the simultaneous motion of many atoms with large oscillations so that the interatomic interactions can be subsequently modified from one conformer to another.

Table 3.27: ENMs frequencies (in cm^{-1}) for the deuterated alanine dipeptide molecule as obtained from the CHARMM22 force field for different conformers in gas phase.

ENM	C5	β	P_{II}	$C7_{eq}$	α_R	α^t
1	32.8	4.9	11.8	50.1	10.6	7.7
2	56.6	37.7	56.1	61.4	55.5	37.9
3	68.4	63.6	68.8	83.1	66.2	60.1
4	90.5	85.5	87.1	88.5	86.5	89.1
5	95.4	94.2	70.0	107.3	98.3	91.2
6	147.8	157.2	157.1	174.4	156.7	155.2
7	160.6	176.7	182.8	185.4	182.3	195.0
8	225.3	233.8	230.5	227.3	215.3	212.6
9	250.1	251.1	260.9	279.5	260.7	263.9
10	262.8	274.4	276.9	281.1	272.8	283.3
11	301.2	282.6	281.9	296.4	305.3	310.7
12	345.7	341.1	338.5	331.7	333.4	356.4
13	380.9	373.5	364.7	422.4	389.5	368.2
14	504.1	498.6	494.9	454.5	511.4	501.7
15	549.7	553.9	540.3	545.6	527.4	535.1
16	563.0	563.7	552.5	568.4	550.5	544.1
17	581.6	573.5	583.2	596.3	587.1	585.2
18	642.2	647.0	637.2	635.9	610.6	619.6
19	746.9	754.0	746.7	747.7	729.5	732.5
20	760.6	768.5	776.7	774.0	768.5	766.4
21	780.9	788.9	782.9	777.9	776.9	775.9
22	843.5	841.8	841.4	840.4	827.9	850.4
23	856.7	856.6	857.6	861.4	853.3	852.1
24	886.6	888.8	893.9	905.5	908.2	902.6
25	962.0	958.3	952.8	944.2	947.9	937.0
26	990.9	985.7	986.2	976.3	972.2	967.3
27	1003.5	1011.6	1009.8	1021.0	1007.5	1014.1
28	1052.6	1039.8	1083.6	1050.0	1064.6	1060.2
29	1065.0	1068.6	1068.2	1070.0	1067.2	1065.3
30	1070.5	1070.3	1076.7	1075.0	1077.4	1076.6
31	1080.4	1081.4	1081.3	1081.7	1081.2	1081.6
32	1084.5	1082.2	1084.3	1087.3	1108.8	1104.6
33	1183.2	1199.9	1180.5	1162.4	1161.3	1178.2
34	1320.5	1296.8	1308.9	1306.1	1306.6	1303.0

Table 3.27: (Continued)

ENM	C5	β	P_{II}	$C7_{eq}$	α_R	α^t
35	1369.3	1379.3	1371.1	1374.9	1376.1	1380.5
36	1384.7	1391.4	1385.3	1389.7	1390.4	1396.3
37	1406.1	1406.4	1403.3	1403.9	1403.7	1403.8
38	1412.5	1413.6	1413.9	1414.8	1412.1	1413.8
39	1416.6	1417.8	1416.9	1416.5	1415.7	1417.6
40	1417.8	1419.9	1418.2	1417.6	1418.3	1418.4
41	1425.6	1425.8	1426.1	1425.4	1426.0	1425.6
42	1426.1	1428.2	1428.9	1432.1	1426.3	1428.3
43	1441.3	1437.2	1436.8	1438.3	1438.3	1438.7
44	1447.2	1454.5	1459.7	1464.2	1439.8	1445.1
45	1548.6	1555.3	1547.4	1541.8	1532.3	1539.8
46	1575.9	1594.0	1576.8	1569.1	1562.4	1563.5
47	1673.5	1672.7	1670.4	1673.6	1678.6	1677.9
48	1678.9	1679.0	1678.4	1680.0	1689.6	1693.8
49	2446.2	2445.9	2446.1	2442.4	2444.9	2445.8
50	2447.5	2447.7	2447.8	2447.6	2448.3	2448.8
51	2852.6	2852.6	2852.5	2852.3	2852.5	2852.5
52	2901.8	2902.0	2901.9	2902.2	2902.1	2902.2
53	2905.4	2905.1	2905.2	2905.0	2907.4	2905.8
54	2913.8	2913.9	2913.9	2914.0	2914.0	2913.9
55	2914.5	2914.5	2914.6	2914.5	2914.4	2914.4
56	2917.0	2917.1	2916.9	2917.2	2917.1	2917.2
57	2957.9	2958.7	2958.7	2959.2	2958.3	2958.8
58	2960.9	2960.7	2960.3	2960.2	2960.4	2960.5
59	2974.9	2974.9	2975.0	2975.0	2975.1	2975.1
60	2975.6	2975.5	2975.5	2975.4	2975.2	2975.2

3.3.3 Computational details

In order to analyze the behavior of the alanine dipeptide molecule in water solution we have performed MD simulations using the TINKER program package v5.0 [Ren 02, Ren 03].

In all our simulations the solvent was composed of the D_2O molecules while two set of independent simulations were carried out using the AlaD-d_2 and ^{13}C isotopic substituted AlaD-d_2 molecule (^{13}C-AlaD-d_2) where the ^{12}C=O carbonyl group is replaced by ^{13}C=O in the acetyl end. The ^{13}C-AlaD-d_2 molecule was studied by Hochstrasser *et al* [Kim 05a] because the isotopic substitution shifts the acetyl end amide I band ~40 cm^{-1} to the red so that the two amide I modes can be selectively excited. In all of the simulations the solvent was described using the flexible TIP3P model with doubled hydrogen masses included in

the CHARMM22 [MacKerell 98] force field and the solute molecule and 248 D_2O molecules were placed in a cubic box with a length of 1.975 nm chosen to reproduce the experimental density of the system [Nakamura 95] ($\rho = 1.10436$ g/cm^3). The simulation time step was $\Delta t = 1$ fs, periodic boundary conditions were apply, a cutoff of 10 Å was used for nonbonded interactions and the Ewald sum method was applied for the long range interactions.

For the AMBER94 [Cornell 95] and OPLS-AA/L [Jorgensen 96,Kaminski 01] force fields simulations the system was equilibrated in the NVT ensemble at T=300 K by coupling to a thermal bath [Berendsen 84] for 750 ps. Afterward, equilibrium propagation were performed in the NVE ensemble for 100 ps and configurations were stored every 5 fs in AMBER94 while the OPLS-AA/L simulations extended up to 2 ns and the data were stored every 50 fs.

For the CHARMM22 force field we carried out 16 independent set of NVT equilibration runs of 1300 ps at 300 K by coupling to a thermal bath [Berendsen 84]. An initial period of 800 ps was used to equilibrate the system while the remaining 500 ps were used to export equilibrated configurations at 20 ps intervals. Thus we stored 400 sets of positions and momenta for our subsequent analysis.

In order to evaluate the dihedral angle distribution for the AlaD-d_2/D_2O system and to perform the INM analysis we ran equilibrium NVE simulations for 100 ps using 200 equilibrated configuration as starting points. During these runs the data were exported each 100 fs so that we collected 200000 snapshots configuration to perform our statistical analysis.

For the AlaD molecule in H_2O water, the equilibrium NVE simulations were carried out for one trajectory for 5 ns and data were stored each 50 fs for the subsequent dihedral angle analysis.

The relaxation process was analyzed in 400 nonequilibrium MD simulations where an excess of energy of one vibrational quantum was suddenly deposited at $t = 0$ in the deuterated alanine dipeptide molecule by displacing either the amino end or the acetyl end amide I INM modes till its energy reached the proper value. The trajectories were propagated in the NVE ensemble in order to avoid any influence of the velocity scaling using a time interval $\Delta t = 0.5$ fs for 40 ps, exporting the configurations (atomic positions, momenta, forces and Hessian matrix of the solute) every 50 fs. Independent sets of simulations were performed for the AlaD-d_2 and ^{13}C-AlaD-d_2 molecules.

In order to obtain a reasonable statistics of the dihedral angles distribution of the AlaD-d_2 molecule, we performed extended simulations up to ~60 ps for 2660 trajectories where only the configuration of the molecules (atomic positions and momenta) was exported at 50 fs intervals but not the forces nor the Hessian matrix to keep the data stored within a reasonable size.

3.3.4 Dihedral angles distribution

In Figures 3.43-3.45 we show the Ramachandran plots of the dihedral angles distributions of the AlaD-d_2 molecule in heavy water as extracted from our equilibrium MD simulations for

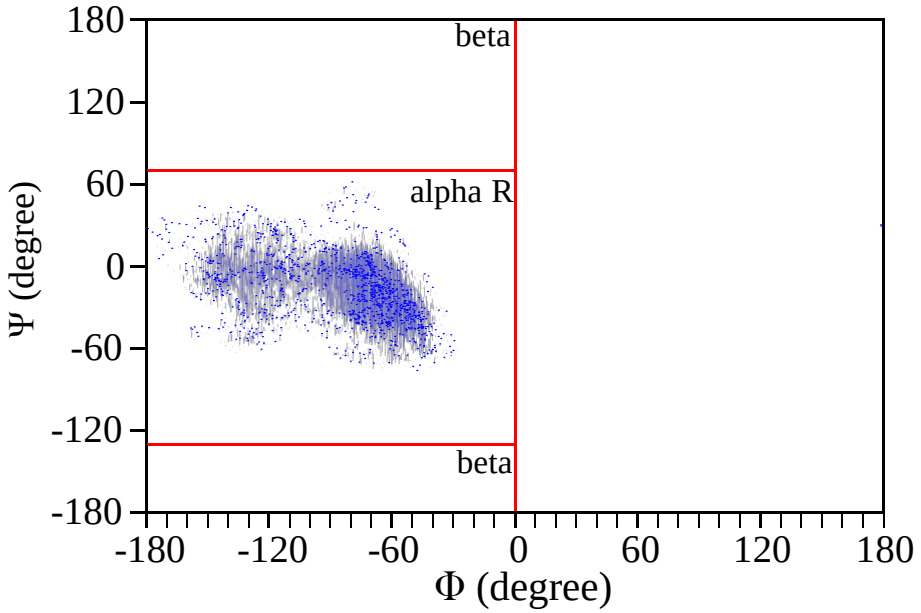

Figure 3.43: Sampled conformational distribution of the two dihedral angles φ and ψ of the AlaD-d_2 molecule in D_2O solvent as obtained using the AMBER94 force field.

the three different MM force fields. As seen in these figures the conformational distributions vary according to the force field employed. Following previous works [Hu 03] we have found useful to consider two main regions named alpha R which includes the α_R and α^t conformers and beta which include P_{II}, β, C5 and C_{7eq} conformers. The definition of these regions is given in Table 3.28.

Table 3.28: Definition of the alpha R and beta regions for the three MM force fields. Angles are given in degrees.

	alpha R				beta			
Force field	φ_{min}	φ_{max}	ψ_{min}	ψ_{max}	φ_{min}	φ_{max}	ψ_{min}	ψ_{max}
AMBER94	-180	0	-130	70	-180	0	-180	-130
					-180	0	70	180
OPLS-AA/L	-180	0	-120	0	-180	0	-180	-120
					-180	0	0	180
					150	180	-180	-120
					150	180	0	180
CHARMM22	-180	0	-150	30	-180	0	-180	-150
					-180	0	30	180
					150	180	-180	-150
					150	180	30	180

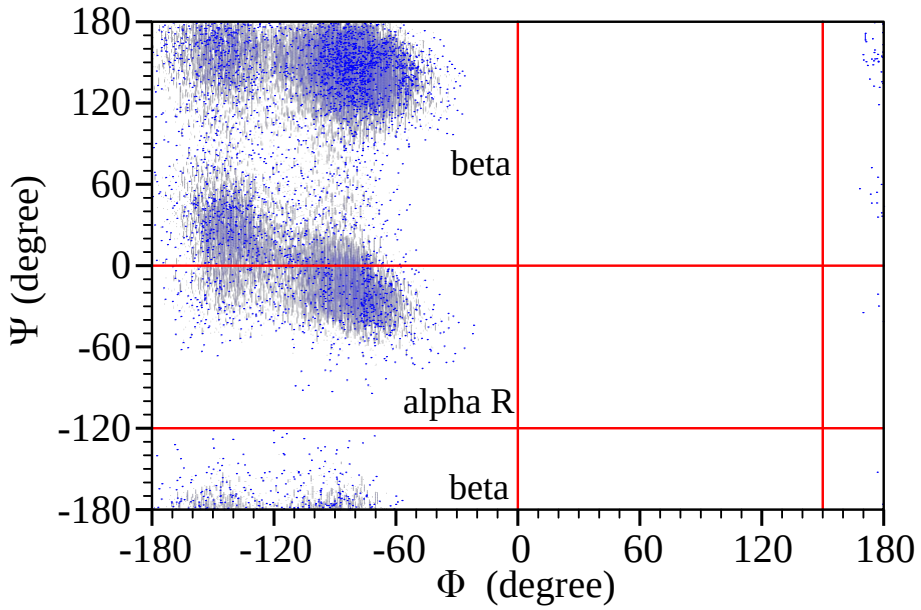

Figure 3.44: Sampled conformational distribution of the two dihedral angles φ and ψ of the AlaD-d_2 molecule in D_2O solvent obtained by using the OPLS-AA/L force field.

In Table 3.29 we include the percentage of the different conformations for the AlaD molecule in water and the AlaD-d_2 molecule in heavy water obtained using the three MM

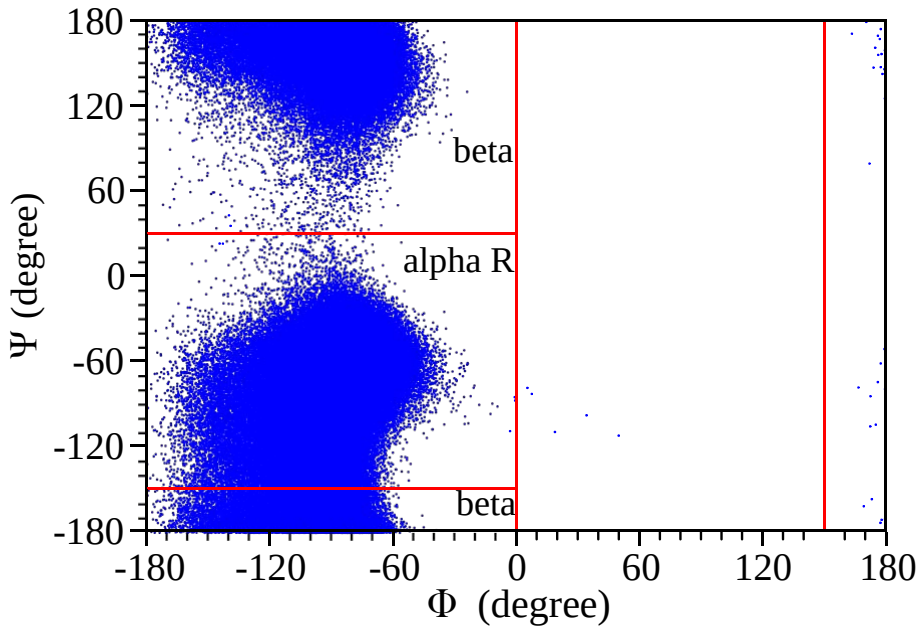

Figure 3.45: Sampled conformational distribution of the two dihedral angles φ and ψ of the AlaD-d_2 molecule in D_2O solvent obtained by using the CHARMM22 force field.

Table 3.29: Percentages of the alpha R and beta conformations of the AlaD molecule in water and the Alad-d_2 molecule in heavy water.

Force field	Solute	Ensemble	alpha R	beta
AMBER94[a]	AlaD-d_2	NVE	100.0	0.0
OPLS-AA/L[a]	AlaD-d_2	NVE	19.7	80.3
CHARMM22[a]	AlaD-d_2	NVE	58.5	41.5
CHARMM22[a]	AlaD	NVE	57.4	42.6
OPLS[b]	AlaD	NPT	13.5	86.0
AMBER98[b]	AlaD	NPT	84.0	16.0
CHARMM22[b]	AlaD	NPT	50.0	50.0
CHARMM22[c]	AlaD	NVT	48.0	48.0

[a].- Present work
[b].- Ref. [Hu 03]
[c].- Ref. [Feig 08]

force fields. We also show some previous results [Hu 03, Feig 08]. We observe that the results are not too affected neither by the hydrogen deuterium isotopic substitution in the AlaD molecule and the solvent (see also Figure 3.46) nor the use of the NVT, NPT or NVE ensembles. So the AMBER94 force field strongly favor the alpha R conformations although a significant percentage of beta conformations (16%) is found for the AMBER98 force field. On the contrary the OPLS force field provide a higher percentage of beta conformers (>80%). Interestingly, the CHARMM22 force field results show a significant contribution of both conformations in a ratio 58/42 for the alpha R and beta conformations. We consider these results to be in a reasonable agreement with previous simulations where an equal percentage of both conformations was stated [Hu 03, Feig 08] if we take into account the different methodological approaches applied.

3.3.5 INMs analysis

The next issue that we address concerns the analysis of the equilibrium vibrational properties of the AlaD-d_2/D_2O system using the CHARMM22 force field. This analysis is important to assess the ability of the EAMC algorithm to assign the INMs of the AlaD-d_2 molecule during the simulation.

In Table 3.30 we give the time averaged INM frequencies obtained using the EAMC method with a frequency window of width 400 cm^{-1}. The ENMs used as templates correspond to the different conformations included in Table 3.24. We note that the frequencies are ordered according to the assignment in terms of the ENMs. That means that when we talk about the 17th INM for the PII conformations we mean all the INMs at different snapshots of the system that have been assigned to the 17th ENM using the ENMs of the PII conformer as template. One direct consequence of this assignment is that the frequen-

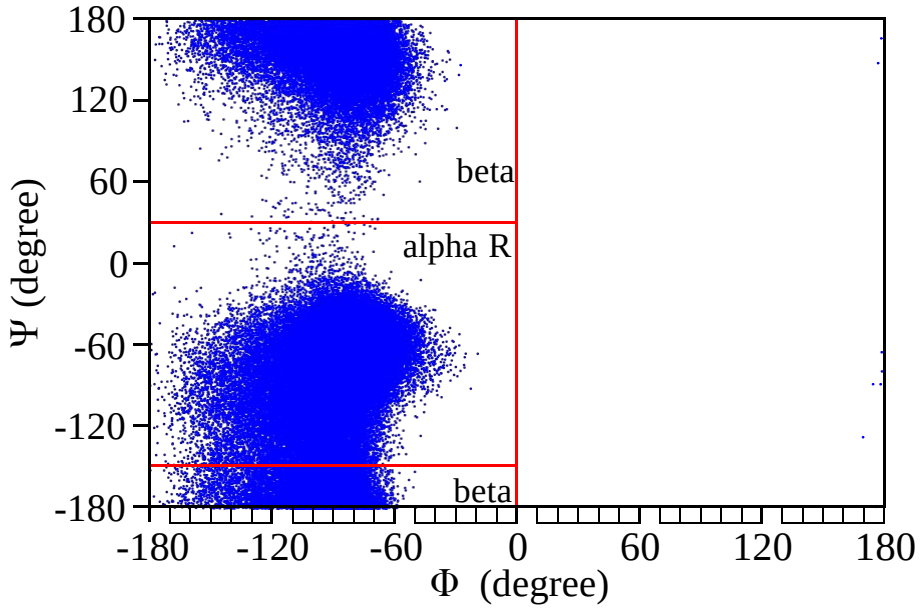

Figure 3.46: Sampled conformational distribution of the two dihedral angles φ and ψ of the AlaD molecule in H_2O water solvent obtained by using the CHARMM22 force field.

cies of the INMs shown in Table 3.30 are not in increasing order, although the original ENMs were ordered following that criterion. Thus the comparison of frequencies within the same row of the table is not always appropriate since the ith INMs of different sets of the ENMs can be quite different.

Table 3.30: Time averaged vibrational frequencies (in cm^{-1}) of the INMs for the AlaD-d_2 molecule in D_2O obtained using the EAMC method with a frequency window of width $\Delta\omega = 400\ cm^{-1}$ using the ENMs of every conformer as templates. Negative values correspond to imaginary frequencies.

INM	C5	β	P_{II}	$C7_{eq}$	α_R	α^t
1	41.2	60.4	94.7	47.5	23.0	63.9
2	−142.1	58.2	67.2	−171.8	83.5	49.5
3	68.3	−164.3	−107.4	−26.1	−14.6	−163.7
4	−16.4	97.4	85.2	67.4	98.4	95.5
5	158.3	11.3	−50.8	136.3	−51.6	−2.4
6	219.7	189.8	196.9	179.4	192.9	180.0
7	183.9	210.4	206.6	220.5	228.2	239.1
8	225.6	256.7	268.3	266.2	262.5	246.5
9	294.1	283.3	266.2	256.5	277.7	231.1
10	173.0	255.6	259.1	264.6	72.1	286.5
11	307.0	302.4	294.1	297.6	319.2	322.4
12	355.6	360.3	365.2	360.2	363.5	372.4
13	419.8	419.8	419.3	422.3	416.8	401.1

Table 3.30: (Continued)

INM	C5	β	P_{II}	$C7_{eq}$	α_R	α^t
14	519.7	501.2	405.7	518.9	501.9	516.4
15	574.4	582.2	553.4	561.3	553.4	540.9
16	555.9	565.1	578.9	556.5	571.7	569.8
17	568.6	573.9	576.3	572.8	579.5	585.1
18	619.1	670.5	659.8	619.5	625.6	624.6
19	745.3	738.7	734.9	745.2	746.6	747.2
20	771.1	783.1	786.0	776.6	776.3	774.2
21	785.5	737.4	746.1	784.8	787.2	786.8
22	843.8	839.2	841.4	844.2	842.9	856.4
23	854.1	855.6	855.7	854.1	855.0	844.8
24	922.6	913.3	918.6	925.2	922.6	922.1
25	973.9	970.9	976.8	996.3	982.1	993.2
26	998.1	999.1	1002.4	986.4	1000.8	983.1
27	1004.3	1013.7	1011.2	1018.3	1010.3	1001.1
28	1066.8	1068.5	1049.6	1020.2	1031.6	1038.5
29	1039.6	1092.6	1094.3	1097.3	1101.8	1103.4
30	1080.0	1034.3	1050.1	1055.1	1052.5	1050.6
31	1074.7	1075.6	1068.6	1066.2	1063.8	1066.6
32	1075.9	1061.9	1062.4	1079.2	1080.0	1078.4
33	1178.1	1182.7	1180.9	1175.7	1170.1	1180.2
34	1304.6	1301.9	1302.9	1299.8	1306.8	1303.7
35	1395.6	1406.6	1399.9	1400.3	1402.5	1401.4
36	1407.3	1411.8	1410.0	1412.6	1407.7	1409.8
37	1422.5	1413.8	1416.7	1415.1	1419.3	1412.7
38	1422.2	1418.6	1420.9	1422.1	1417.6	1418.3
39	1419.1	1414.2	1419.5	1419.3	1422.8	1418.7
40	1410.6	1413.9	1409.6	1409.7	1411.9	1418.6
41	1427.1	1425.7	1431.6	1430.5	1425.8	1427.1
42	1431.2	1441.5	1437.3	1441.1	1438.2	1440.2
43	1448.5	1448.5	1447.9	1446.1	1446.0	1449.9
44	1463.8	1427.9	1484.9	1448.0	1434.3	1431.7
45	1583.5	1587.6	1576.8	1547.5	1563.6	1560.2
46	1547.9	1566.8	1522.6	1584.5	1589.6	1588.5
47	1685.3	1685.2	1685.3	1685.3	1683.8	1683.7
48	1683.8	1683.7	1683.8	1683.9	1685.6	1685.6
49	2444.8	2444.7	2444.8	2444.8	2442.9	2442.9
50	2442.9	2442.9	2442.9	2442.9	2444.8	2444.8
51	2858.3	2858.3	2858.3	2858.3	2858.3	2858.3
52	2909.3	2909.5	2909.3	2909.4	2909.0	2909.2

Table 3.30: (Continued)

INM	C5	β	P_{II}	$C7_{eq}$	α_R	α^t
53	2910.9	2910.9	2910.6	2910.9	2910.9	2910.9
54	2924.9	2921.7	2921.9	2925.1	2925.1	2925.7
55	2915.3	2918.4	2918.4	2915.2	2915.2	2914.6
56	2923.2	2923.2	2923.2	2923.2	2923.2	2923.2
57	2965.5	2966.7	2967.6	2968.2	2967.7	2967.7
58	2965.9	2964.7	2963.9	2963.1	2964.1	2963.8
59	2976.5	2976.6	2976.6	2976.7	2986.3	2979.3
60	2986.9	2986.8	2989.9	2986.8	2977.2	2984.2

An excellent example of this situation are the 47th and 48th ENMs. It was already discussed (see Table 3.26) that the 47th and 48th ENMs corresponds to the amino and acetyl end amide I modes respectively for the beta region conformers while the reverse assignment holds for the alpha R conformations. That means that in Table 3.30 we must compare the frequencies of the 47th INM for beta conformations with the values of the 48th INM for the alpha R conformers. We see that the frequencies then have similar values around 1685.4 cm^{-1}. According to the results presented in Table 3.25 and Table 3.26 that mode corresponds to the amino end amide I mode. Similarly the 48th INM of the beta conformations should be compared with the 47th INM of one alpha R conformers. Again the frequencies are very similar with values around 1683.8 cm^{-1}. This mode corresponds to the acetyl end amide I mode. An additional proof of the above assignments can be found in Figure 3.47 where we present the effective atomic contributions for the 47th and 48th INMs. Using the atom definitions shown in Figure 3.48. As seen the atoms 2-3 and 6-7 correspond to the carbonyl groups in the acetyl and amino end respectively. The results included in Figure 3.47 probe that the 47th and 48th INMs obtained using the alpha R ENMs as templates correspond to the acetyl and amino end amide I modes respectively, while the opposite assignment is found when using the beta ENMs. These results probes the ability of the EAMC method to track the identity of the INMs during the simulations independently of the frequency ordering.

It is interesting to compare these frequencies with those observed experimentally by Hochstrasser [Kim 05a] 1629 and 1642 cm^{-1} for the acetyl and amino end amide I groups respectively. We note that the corresponding INM frequencies are 1683.8 and 1685.4 cm^{-1}, so that they are higher and closer than the experimental data. These values reflect the averaged assignment of the amide I INMs during the simulations. When the AlaD-d_2 molecule lies in the beta region the acetyl end amide I frequency is higher than that of the amino end amide I, but when the conformers occupy the alpha R region the acetyl end amide I frequency is lower than that of the amino end amide I (see Table 3.26). According

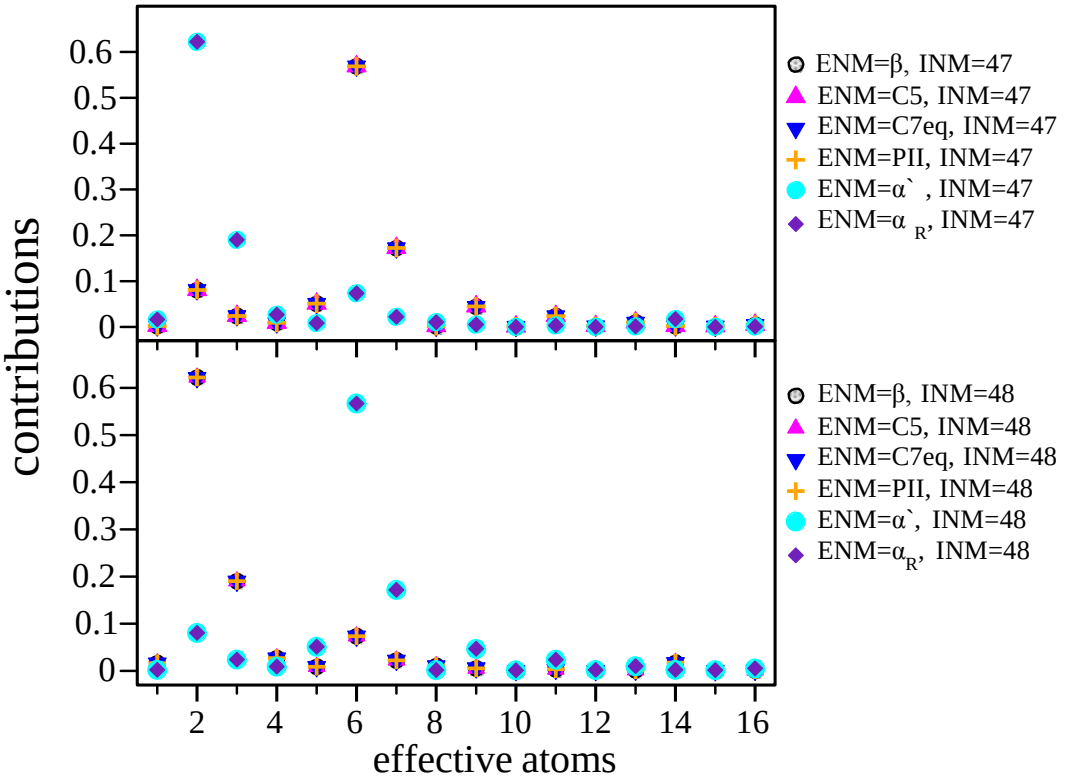

Figure 3.47: Average effective atomic contributions to the amide I modes of the AlaD-d_2 molecule obtained using the ENMs of different conformers as templates.

to the dihedral angle analysis of the AlaD-d_2/D_2O system we have that the ratio between the alpha R and beta regions is 58/42. This explain why the average frequencies of the two amide I modes are so closer in solution that in gas phase.

From the above considerations we conclude that the values of the INM frequencies do not provide a clear criterion to choose one or other ENMs as templates. We have explored an alternative criterion based on the overlaps between the INMs and ENMs given

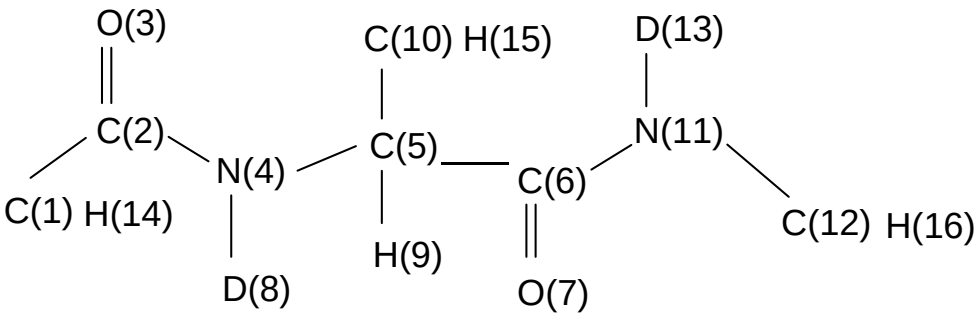

Figure 3.48: The effective atoms definition of the AlaD-d_2 molecule.

by Eq. (2.84), which are included in Table 3.31. In principle the optimal template would corresponds to the ENMs shown to be more similar to the INMs during the dynamics. While we observe noticeable differences for the values of the overlaps in given INMs, specially as the frequencies are lower, the average overlaps are very similar for the six sets of the ENM considered.

Table 3.31: Time averaged diagonal elements (O_{ii}) for the overlap matrix (see Eq. (2.84)) between ENMs and INMs obtained using the EAMC method with a frequency window of width $\Delta\omega = 400$ cm^{-1} and using the ENMs of every conformer as templates

i	C5	β	P_{II}	$C7_{eq}$	α_R	α^t
1	0.866	0.863	0.877	0.894	0.861	0.896
2	0.633	0.838	0.828	0.579	0.807	0.872
3	0.832	0.585	0.654	0.670	0.746	0.591
4	0.705	0.806	0.793	0.797	0.831	0.825
5	0.861	0.686	0.661	0.911	0.670	0.698
6	0.918	0.891	0.905	0.894	0.906	0.890
7	0.887	0.928	0.928	0.913	0.920	0.913
8	0.922	0.927	0.898	0.893	0.911	0.932
9	0.863	0.783	0.889	0.834	0.906	0.832
10	0.778	0.821	0.784	0.875	0.680	0.849
11	0.906	0.926	0.894	0.888	0.860	0.865
12	0.847	0.924	0.917	0.894	0.905	0.893
13	0.887	0.873	0.881	0.876	0.875	0.916
14	0.926	0.927	0.923	0.932	0.942	0.923
15	0.930	0.909	0.882	0.922	0.848	0.887
16	0.900	0.907	0.912	0.878	0.908	0.862
17	0.906	0.949	0.945	0.890	0.951	0.911
18	0.928	0.904	0.894	0.915	0.917	0.931
19	0.939	0.880	0.873	0.915	0.952	0.953
20	0.922	0.939	0.966	0.934	0.930	0.926
21	0.963	0.878	0.877	0.961	0.963	0.968
22	0.925	0.922	0.929	0.929	0.922	0.940
23	0.950	0.957	0.957	0.974	0.944	0.904
24	0.922	0.924	0.927	0.938	0.936	0.905
25	0.921	0.932	0.925	0.897	0.911	0.932
26	0.903	0.922	0.904	0.886	0.872	0.915
27	0.934	0.915	0.923	0.924	0.916	0.919
28	0.915	0.918	0.922	0.931	0.913	0.921
29	0.914	0.957	0.963	0.966	0.967	0.965
30	0.958	0.931	0.916	0.898	0.922	0.943
31	0.944	0.955	0.934	0.895	0.921	0.945
32	0.948	0.929	0.931	0.879	0.914	0.903

Table 3.31: (Continued)

i	C5	β	P_{II}	$C7_{eq}$	α_R	α^t
33	0.959	0.956	0.959	0.936	0.951	0.938
34	0.944	0.927	0.923	0.903	0.944	0.938
35	0.893	0.950	0.891	0.881	0.903	0.949
36	0.920	0.869	0.897	0.858	0.853	0.852
37	0.909	0.831	0.895	0.879	0.901	0.812
38	0.844	0.819	0.863	0.825	0.900	0.902
39	0.853	0.981	0.864	0.852	0.939	0.957
40	0.981	0.848	0.982	0.980	0.981	0.932
41	0.928	0.955	0.951	0.952	0.953	0.951
42	0.934	0.961	0.951	0.952	0.943	0.963
43	0.980	0.974	0.979	0.982	0.956	0.983
44	0.895	0.888	0.892	0.886	0.877	0.903
45	0.876	0.951	0.866	0.893	0.933	0.933
46	0.887	0.930	0.882	0.892	0.957	0.953
47	0.967	0.954	0.957	0.948	0.963	0.973
48	0.974	0.966	0.969	0.962	0.952	0.956
49	0.988	0.988	0.990	0.990	0.888	0.988
50	0.988	0.988	0.990	0.991	0.888	0.988
51	0.999	0.999	0.999	0.999	0.999	0.999
52	0.979	0.978	0.981	0.978	0.980	0.981
53	0.978	0.977	0.979	0.977	0.978	0.980
54	0.999	0.997	0.997	0.999	0.999	0.999
55	0.997	0.999	0.999	0.997	0.997	0.997
56	0.997	0.997	0.997	0.997	0.997	0.997
57	0.999	0.999	0.999	0.999	0.999	0.999
58	0.999	0.999	0.999	0.999	0.999	0.999
59	0.999	0.999	0.999	0.999	0.999	0.999
60	0.999	0.999	0.999	0.999	0.999	0.999
Mean value	0.921	0.918	0.918	0.915	0.918	0.923

Therefore our conclusion is that the INM analysis does not depend on the choice of the ENMs used as template. This conclusion is important for the further extension of the INM analysis to polypeptides or proteins. In our present study we have chosen as template the ENMs corresponding to the C5 conformer.

As a final test we have calculated the time averaged kinetic and potential energies of the INMs which are included in Table 3.32 and Table 3.33. As seen the simulations reproduce

quite well the thermodynamic limit $k_BT/2$ which is 104.3 cm^{-1} at room temperature. The only exceptions correspond to the potential energy of the lower frequency modes due to the singularity in the potential energy expression when the force constants are close to zero [Kalstein 11].

Table 3.32: Time averaged kinetic energy (in cm^{-1}) of the INMs for the AlaD-d_2 molecule in D_2O solution.

INM	C5	β	P_{II}	$C7_{eq}$	α_R	α^t
1	104.7	104.9	104.9	105.1	105.3	104.7
2	105.2	105.3	105.1	105.0	104.8	105.2
3	104.8	105.1	105.3	105.3	104.9	104.9
4	105.2	104.8	104.9	104.8	104.9	104.7
5	104.8	105.3	105.1	105.1	105.3	105.3
6	105.1	105.4	105.5	105.4	105.4	105.1
7	105.5	104.5	104.9	105.1	104.6	104.7
8	110.1	105.2	110.6	104.7	105.2	104.9
9	104.8	105.4	105.0	105.2	105.2	104.8
10	104.4	104.5	104.4	104.4	104.6	104.9
11	105.2	104.7	104.8	105.4	105.3	105.2
12	105.3	104.9	105.0	104.8	105.1	105.4
13	105.3	104.9	104.9	105.3	104.7	104.9
14	103.7	104.8	104.8	104.1	104.8	104.5
15	104.5	104.4	104.3	104.4	104.6	105.2
16	105.3	104.6	104.3	104.9	104.4	104.6
17	104.5	104.5	104.6	104.4	104.3	104.2
18	103.9	103.2	103.6	104.1	104.1	103.7
19	102.8	103.7	103.9	103.0	102.8	102.9
20	103.4	103.5	103.6	103.3	103.3	103.3
21	103.6	103.5	103.1	103.6	103.6	103.6
22	104.7	104.8	104.7	104.8	104.8	105.6
23	105.6	105.7	105.7	105.6	105.7	104.8
24	103.1	103.0	103.0	103.2	103.0	103.3
25	105.1	104.9	104.9	104.8	104.8	104.8
26	105.2	104.8	105.4	105.2	105.1	105.1
27	104.3	104.6	104.4	104.6	104.0	104.2
28	105.5	105.1	104.7	104.5	105.0	104.8
29	104.3	105.1	104.7	104.7	104.6	104.6
30	104.8	104.9	105.4	105.5	105.5	105.4
31	105.5	105.4	105.3	105.2	105.1	105.3
32	104.8	104.7	104.9	104.6	105.2	105.1
33	104.7	104.4	104.4	104.8	104.8	104.5

Table 3.32: (Continued)

INM	C5	β	P_{II}	$C7_{eq}$	α_R	α^t
34	104.1	104.3	104.2	104.1	104.1	104.2
35	103.1	103.8	102.7	103.1	103.7	103.7
36	103.8	103.2	103.7	103.7	103.0	103.4
37	102.6	103.1	103.1	102.9	102.9	103.1
38	103.7	103.4	103.7	103.7	103.3	103.2
39	103.2	103.2	103.2	102.9	104.0	103.7
40	103.2	103.1	103.3	103.3	103.0	103.2
41	102.7	102.9	102.8	103.0	102.9	102.9
42	102.8	102.1	102.5	102.5	102.5	102.2
43	102.3	102.5	102.3	102.4	102.4	102.4
44	103.4	103.5	103.7	103.0	103.2	103.2
45	103.5	103.6	103.4	103.3	102.9	102.9
46	103.1	102.9	103.1	103.5	103.6	103.7
47	103.8	103.7	103.8	103.7	104.6	104.6
48	104.6	104.6	104.6	104.6	103.7	103.7
49	100.9	100.9	100.9	100.9	101.4	101.4
50	101.4	101.4	101.4	101.4	100.9	100.9
51	99.1	99.1	99.1	99.1	99.1	99.1
52	96.4	96.4	96.4	96.4	96.5	96.4
53	99.7	99.7	99.7	99.7	99.7	99.7
54	99.2	99.3	99.3	99.1	99.2	99.1
55	99.7	99.5	99.5	99.8	99.7	99.8
56	98.3	98.3	98.3	98.3	98.3	98.3
57	96.4	96.3	96.2	96.3	96.3	96.2
58	95.6	95.7	95.8	95.7	99.7	95.8
59	101.2	101.2	101.2	101.1	100.6	101.1
60	100.5	100.5	100.5	100.6	101.2	100.6

Table 3.33: Time averaged potential energy (in cm^{-1}) for the INMs of the AlaD-d_2 molecule in D_2O solution.

INM	C5	β	P_{II}	$C7_{eq}$	α_R	α^t
1	8.1	48.1	55.7	220.4	152.7	48.9
2	−61.2	−53.8	141.9	−67.6	−106.2	414.2
3	71.7	−32.8	−137.2	45.4	102.8	−36.5
4	73.2	129.4	136.9	44.0	208.7	93.4

Table 3.33: (Continued)

INM	C5	β	P_{II}	$C7_{eq}$	α_R	α^t
5	111.3	63.1	11.3	141.5	14.3	91.6
6	88.6	334.5	48.2	192.9	139.2	108.2
7	305.7	143.8	187.1	142.9	153.9	157.5
8	126.5	114.4	109.9	109.3	117.5	118.4
9	106.9	104.1	109.7	93.3	109.2	91.9
10	73.0	93.9	87.7	106.7	41.2	105.8
11	101.3	108.7	110.8	107.1	97.8	97.5
12	95.6	101.9	101.2	100.6	103.0	104.2
13	105.1	101.9	103.5	103.2	98.5	104.3
14	103.0	105.1	104.2	102.5	107.9	110.3
15	107.5	108.1	109.5	112.4	110.0	107.8
16	108.1	113.1	107.0	106.3	106.3	106.5
17	112.6	105.1	104.8	104.0	105.1	106.0
18	104.3	104.2	103.9	104.2	104.2	103.9
19	105.9	106.5	106.8	106.6	106.8	106.8
20	107.2	107.8	107.6	107.6	107.6	107.3
21	107.3	104.9	105.2	107.3	107.9	107.7
22	110.7	110.3	110.4	110.6	110.6	112.4
23	111.3	111.9	111.9	111.4	111.6	110.5
24	109.8	110.2	110.2	110.0	110.3	109.8
25	112.8	112.9	111.6	106.8	110.7	107.3
26	106.9	107.2	106.5	111.2	106.7	111.1
27	107.5	105.8	105.6	105.5	105.7	106.1
28	103.6	103.3	104.5	105.7	106.3	105.6
29	104.5	102.0	103.1	102.6	102.1	101.9
30	104.2	104.7	105.2	108.7	109.6	109.9
31	101.8	102.0	103.4	103.4	104.2	103.7
32	107.6	109.8	108.5	104.6	103.3	102.9
33	106.3	106.9	106.9	106.8	106.5	107.2
34	106.6	105.8	106.0	105.9	106.3	105.9
35	102.9	107.0	102.9	105.1	109.4	107.2
36	107.3	104.9	107.8	105.9	101.7	105.1
37	105.5	102.7	104.5	104.6	104.4	101.3
38	100.8	100.5	100.5	100.3	101.8	101.2
39	100.7	104.3	101.1	101.1	102.4	102.8
40	106.3	100.6	106.2	105.8	104.4	105.2
41	94.2	93.7	94.3	94.1	93.0	93.8
42	101.4	103.7	102.8	103.6	102.1	103.2
43	106.9	106.0	106.6	105.7	107.5	106.2

Table 3.33: (Continued)

INM	C5	β	P_{II}	$C7_{eq}$	α_R	α^t
44	103.2	103.5	104.6	101.7	100.7	101.6
45	108.9	109.4	108.1	107.3	107.4	107.3
46	105.6	107.4	104.7	108.5	109.4	108.8
47	107.7	107.6	107.7	107.6	107.5	107.4
48	107.4	107.4	107.4	107.7	107.9	108.1
49	106.6	106.6	106.6	106.6	107.0	107.0
50	107.0	107.0	107.0	107.0	106.6	106.6
51	106.8	106.8	106.8	106.8	106.8	106.8
52	104.3	104.3	104.3	104.3	104.3	104.4
53	107.9	107.9	107.9	107.9	107.9	107.9
54	107.5	107.4	107.3	107.5	107.5	107.6
55	107.7	107.9	107.9	107.8	107.7	107.7
56	106.8	106.8	106.8	106.8	106.8	106.8
57	105.1	104.9	104.8	104.6	104.9	104.9
58	103.7	103.8	103.9	104.2	103.8	103.8
59	110.8	110.8	110.7	110.8	108.2	110.2
60	108.2	108.2	108.4	108.2	110.8	108.8

3.3.6 The AlaD-d_2 molecule

3.3.6.1 INMs assignment

We start our study by considering the choice of the ENMs to be used as templates in the assignment of the INMs through the EAMC method. As discussed in Section 3.3.4 the AlaD-d_2 molecule in D_2O solution explores both the alpha R and beta regions. In order to simplify our analysis we have applied the EAMC method using the ENMs of the α_R and C5 conformations as templates, which are representative of those regions respectively.

In Figure 3.49 we show the time evolution of the vibrational energy of the acend and amend amide I modes after being excited at $t = 0$ obtained using the C5 and α_R ENMs as templates to identify the INMs. As seen both sets of ENMs provide similar results. This similarity is also found for other INMs excited during the relaxation process as we can see in Figure 3.50 and Figure 3.51 where we present the vibrational energies of some representative INMs. In all of these cases the curves are identical within the statistical noise. We note that similar results were obtained using other sets of ENMs as templates (results not shown).

The ability of the EAMC method to provide similar INM vibrational curves when

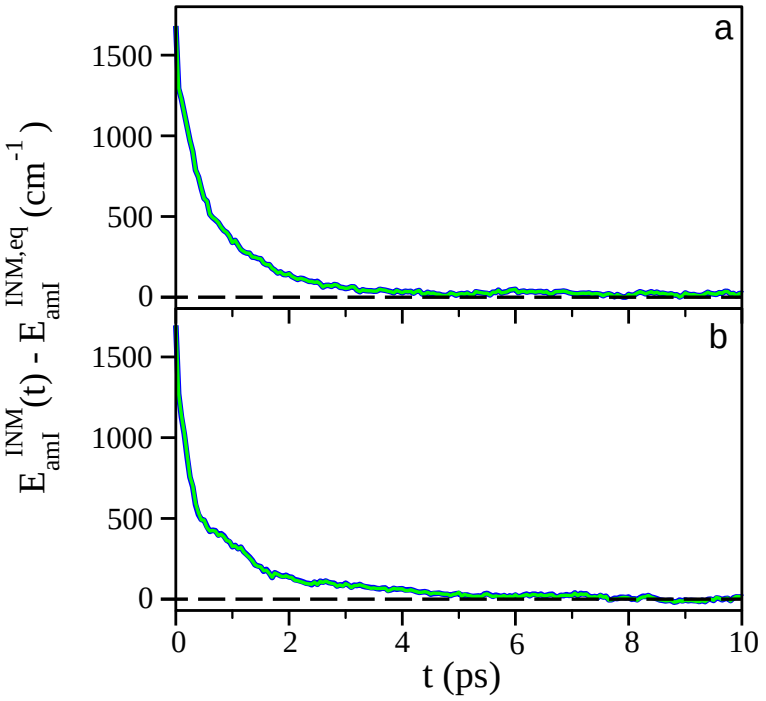

Figure 3.49: Time evolution of the vibrational energy (in cm^{-1}) relative to its equilibrium value of the acend (a) and amend (b) amide I INMs of the AlaD-d_2 molecule assigned using the C5 (green line) and α_R (blue line) ENMs as templates.

different ENMs are used as templates is an important property when studying flexible molecule as polypeptides in solution which present many different conformations. The robustness of the EAMC method comes from the use of the atomic contributions to identify the INMs. The mid-range and high frequency ENMs for different conformations have similar atomic contributions so that the identification of the INMs is largely unaffected by the choice of one or other set of ENMs. On the contrary the identification of some of the low frequency modes can vary significantly with the torsion angles. However, these modes do not store great amounts of vibrational energy during the relaxation process so that their individual identification is not a crucial point to establish the IVR mechanism.

According to the values in Table 3.31 where we gave the average overlaps obtained using different ENMs as templates to assign the INMs and by following the above consideration we mention that all the results presented for the vibrational relaxation of the AlaD-d_2 molecule in the following sections were obtained using the C5 ENMs as template to identify the INMs.

3.3.6.2 Amide I modes relaxation lifetimes

The AlaD-d_2 molecule is characterized by the presence of two amide I modes, the acend amide I mode in the acetyl end and the amend amide I mode in the amino end (see Figure

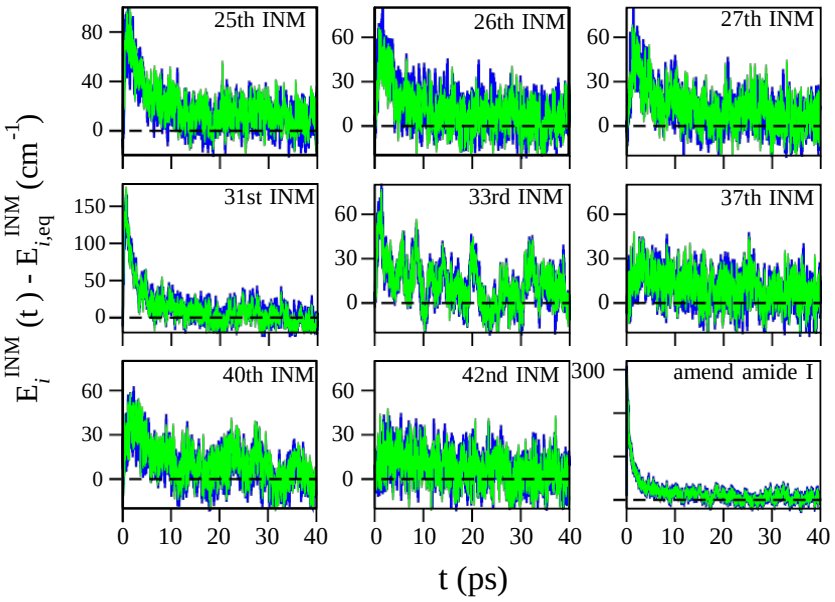

Figure 3.50: Time evolution of the vibrational energy (in cm^{-1}) of the INMs of the AlaD-d_2 molecule assigned using the α_R (blue line) and C5 (green line) ENMs as template following the excitation of the acend amide I mode.

3.2). We present here the analysis of the relaxation lifetimes following the individual excitation of each amide I mode. In Figure 3.52 and Figure 3.53 (upper panels) we show the time evolution of the vibrational energy of the acend and amend amide I modes after being excited at $t = 0$ respectively obtained in our MD simulations. As seen both curves show a sharply fall during the first 50 fs then the decays become gradually slower. We find that the energy curves are well reproduced by a tetraexponential function as follows

$$\frac{E_{\mathrm{amI}}^{\mathrm{vib}}(t) - E_{\mathrm{amI}}^{\mathrm{vib,eq}}}{E_{\mathrm{amI}}^{\mathrm{vib}}(0) - E_{\mathrm{amI}}^{\mathrm{vib,eq}}} = \sum_{i=1}^{N} c_{\mathrm{rel},i} e^{-t/\tau_{\mathrm{rel},i}} \tag{3.10}$$

where $c_{\mathrm{rel},i}$'s are the amplitudes with $\sum_{i=1} c_{\mathrm{rel},i} = 1$, $\tau_{\mathrm{rel},i}$ are the relaxation lifetimes and $N = 4$. In Table 3.34 we include the parameters obtained from the fit. As seen both curves show ultrashort decays in the fs time scale which account for 18.2% of the energy initially stored in the amide I modes. The three longer lifetimes are in the ps time scale and we note significant differences in the values of the amplitudes and the rates between the results obtained for the acend and amend amide I modes. In order to make a proper comparison between the relaxation times for both amide I modes it is useful to calculate the overall relaxation time T_1 when the initial vibrational energy decrease in a factor $1/e$. The values of T_1 are included in Table 3.34 and we notice that the acend amide I mode relax in a larger time scale than the amend mode. These differences probe that both amide I modes follow different relaxation pathways that we now analyze comparatively. In order to distinguish the amide I modes energy flows via intramolecular vibrational redistribution (IVR) and

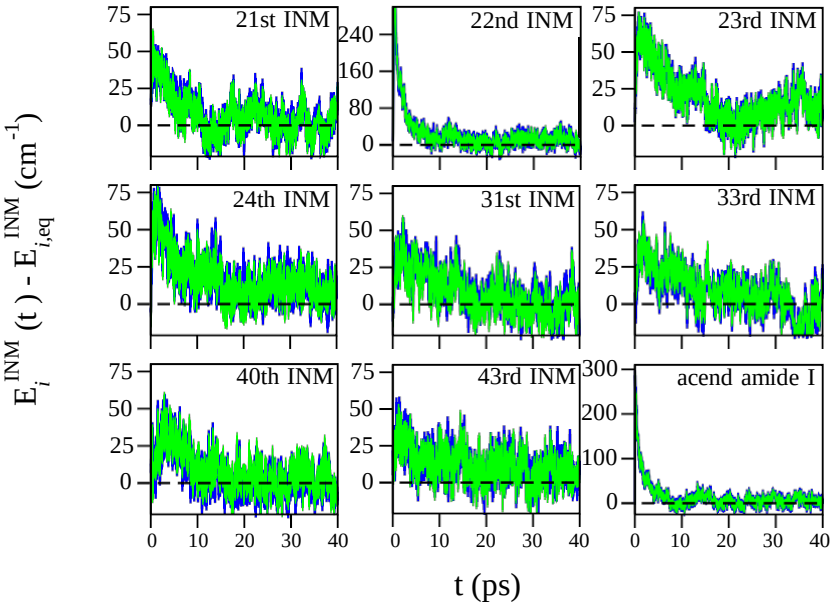

Figure 3.51: Time evolution of the vibrational energy (in cm^{-1}) of the INMs of the AlaD-d_2 molecule assigned using the α_R (blue line) and C5 (green line) ENMs as template following the excitation of the amend amide I mode.

intermolecular energy flow into the bath, an additional analysis has been performed by employing the SMF method [Soler 11]. In Figure 3.52 and Figure 3.53 (lower panels) we show the time evolution of the normalized accumulated energy that flows from the acend and amend amide I modes to the bath and to the rest of the molecule through an IVR process. These energy flow curves are well reproduced by the following functions

$$\frac{f_{IVR}^{ac}(t)}{E_{amideI}^{vib}(0)} = \sum_{i=1}^{N} c_i^{IVR}(1 - e^{-t/\tau_i^{IVR}}) \tag{3.11}$$

$$\frac{f_{bath}^{ac}(t)}{E_{amideI}^{vib}(0)} = c^{bath}(1 - e^{-t/\tau^{bath}}) \tag{3.12}$$

being c_i's the amplitudes with $\sum_i^N c_i^{IVR} + c^{bath} = 1$ and τ_i's the corresponding lifetimes. We should mention here that the linear convolution applied to smooth the energy curves was carried out using 400 fs as the convolution time interval. However, the first 0.15 ps intervals of the curves were unconvoluted in order to detect the energy transfer occurring in the shorter time scale (see Section 3.2.3 for more details).

In Table 3.34 we include the parameters obtained from the fits. Interestingly, we find that the accumulated energy curves are well reproduced by using the same relaxation lifetimes obtained from the kinetic analysis of the amide I modes relaxations. In this way we can identify that only the third terms with relaxation lifetimes 0.919 ps and 0.744 ps for the acend and the amend amide I modes respectively correspond to intermolecular energy transfers into the bath while the remaining terms correspond to the IVR processes.

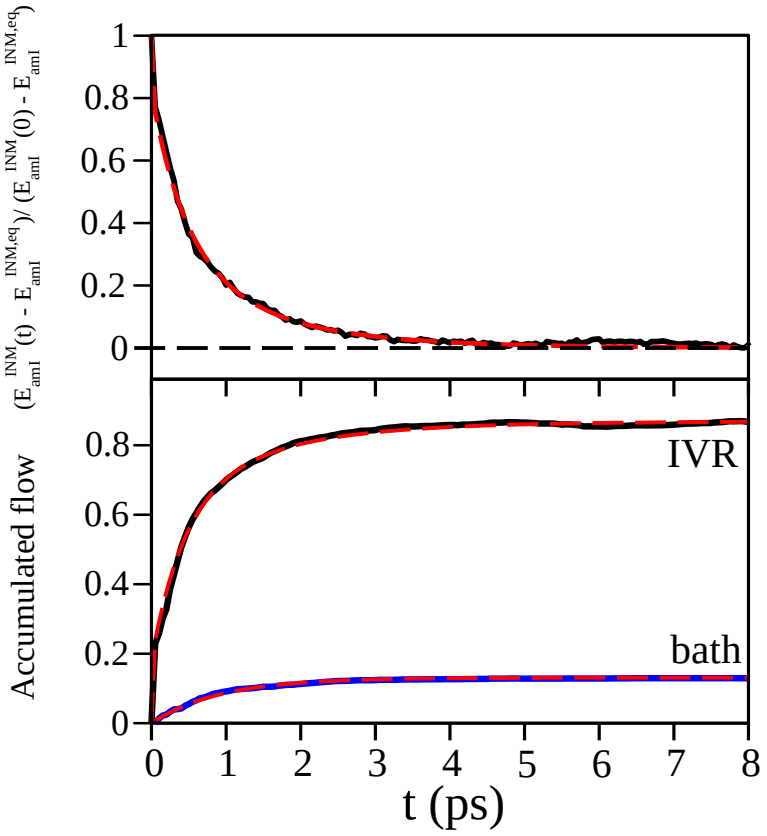

Figure 3.52: (upper panel) Time evolution of the normalized vibrational energy of the acend amide I mode with respect to its equilibrium value at 300 K (black line) and the fit to Eq. (3.10) (red dashed line) and (lower panel) time evolution of the normalized accumulated energy that flows from the acend amide I mode into the remaining INMs of the AlaD-d_2 molecule through IVR processes (black line) and into the bath (blue line) and their fits (red dashed lines) to Eq. (3.11) and Eq. (3.12) respectively.

Moreover, the SMF analysis establishes that only 13% of the energy released by the amide I modes goes directly into the solvent so that most of the energy flows (87%) corresponds to IVR processes within the AlaD-d_2 molecule. In the following section we analyze those IVR pathways.

3.3.6.3 IVR pathways

The next issue that we address is the relaxation pathways of the amide I modes. As discussed above the relaxation of the amide I modes take place through four stages.

The first stage is characterized by an ultrafast relaxation time (1.8 fs) for both amide I modes and accounts for 18% of the energy released. Concerning the relaxation of the acend amide I mode we find that, this stage is characterized by the energy flow into the amend amide I mode with a little contribution from the 46th INM. In Figure 3.54 we show

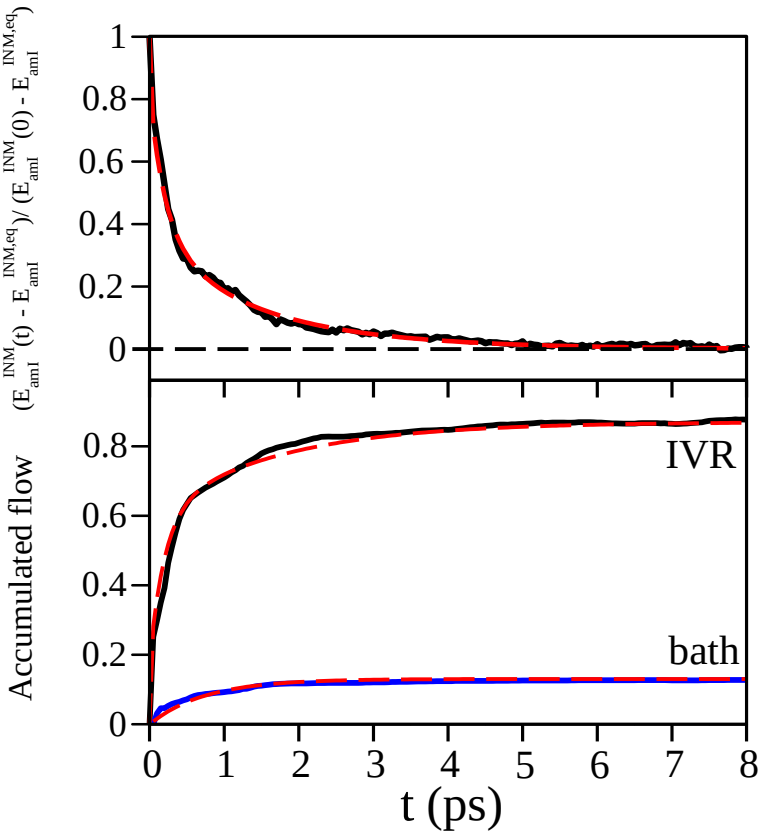

Figure 3.53: (upper panel) Time evolution of the normalized vibrational energy of the amend amide I mode with respect to its equilibrium value at 300 K (blue line) and the fit to Eq. (3.10) (red dashed line) and (lower panel) time evolution of the normalized accumulated energy that flows from the amend amide I mode to the remaining INMs of the AlaD-d_2 molecule through IVR processes (black line) and into the bath (blue line) and their fits (red dashed lines)to Eq. (3.11) and Eq. (3.12) respectively.

the time evolution of the vibrational energy of these two modes. We observe that 280 cm^{-1} of the energy released from the acend amide I mode is transferred into the amend amide I mode, whereas the 46th INM receives just 30 cm^{-1}. Therefore the first stage of the acend amide I relaxation is dominated by a rapid exchange of vibrational excitation between the acend and amend amide I modes.

The time evolution of the energy of the amend amide I mode is well reproduced by the following equation

$$E_i^{\mathrm{INM}}(t) - E_{i,\mathrm{eq}}^{\mathrm{INM}} = A\,(c_{\mathrm{rel},1}\,e^{-t/\tau_{\mathrm{rel},1}} + c_{\mathrm{rel},2}\,e^{-t/\tau_{\mathrm{rel},2}} + c_{\mathrm{rel},3}\,e^{-t/\tau_{\mathrm{rel},3}} - e^{-t/\tau_{\mathrm{exc}}}) + B \quad (3.13)$$

where $\tau_{\mathrm{rel},i}$'s are the relaxation times, $c_{\mathrm{rel},i}$'s are the corresponding weights which satisfy $\sum_i c_{\mathrm{rel},i} = 1$, τ_{exc} is the excitation lifetime, A is a parameter related to the maximum of the energy curve and B is a parameter which accounts for small deviations of the curve from the equilibrium value at long times. The time evolution of the vibrational energy of

Table 3.34: Vibrational relaxation times of the amide I mode (in ps) and amplitudes for the AlaD-d_2 molecule as obtained from the fitting.

	amide I	$\tau_{\mathrm{rel},1}$ ($c_{\mathrm{rel},1}$)	$\tau_{\mathrm{rel},2}$ ($c_{\mathrm{rel},2}$)	$\tau_{\mathrm{rel},3}$ ($c_{\mathrm{rel},3}$)	$\tau_{\mathrm{rel},4}$ ($c_{\mathrm{rel},4}$)	T_1
Kinetic[a]	acend	0.0018(0.182)	0.415(0.401)	0.919(0.269)	1.737(0.148)	0.54
	amend	0.0018(0.182)	0.201(0.420)	0.744(0.130)	1.687(0.268)	0.35
	amide I	τ_1^{IVR} (c_1^{IVR})	τ_2^{IVR} (c_2^{IVR})	τ_3^{IVR} (c_3^{IVR})	τ_4^{IVR} (c_4^{IVR})	τ^{bath} (c^{bath})
SMF[b]	acend	0.0018(0.182)	0.415(0.401)	0.919(0.138)	1.737(0.148)	0.919(0.131)
	amend	0.0018(0.182)	0.201(0.420)		1.687(0.268)	0.744(0.130)

a.- See Eq. (3.10)
b.- See Eq. (3.11) and Eq. (3.12)

the 46th INM is given by

$$E_i^{\mathrm{INM}}(t) - E_{i,\mathrm{eq}}^{\mathrm{INM}} = A\,(e^{-t/\tau_{\mathrm{rel}}} - e^{-t/\tau_{\mathrm{exc}}}) + B \tag{3.14}$$

where τ_{rel} and τ_{exc} are the relaxation and the excitation lifetimes respectively. The curves obtained from the fits are superimposed in Figure 3.54 and the values of the parameters are

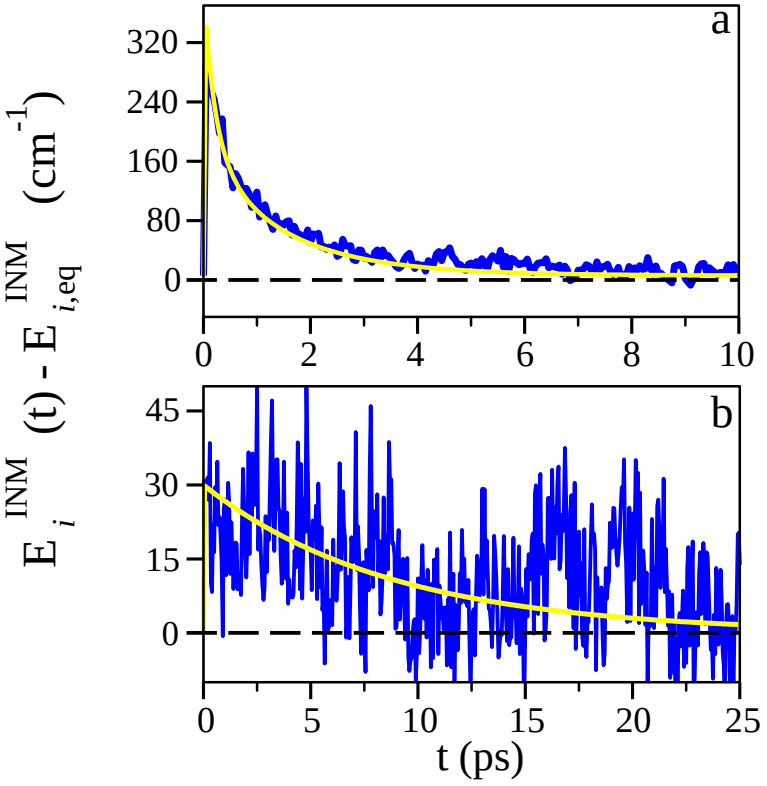

Figure 3.54: Time evolution of the vibrational energy of (a) the amend amide I mode and (b) 46th INM (blue lines) and the corresponding fits (yellow lines) following the initial excitation of the acend amide I mode.

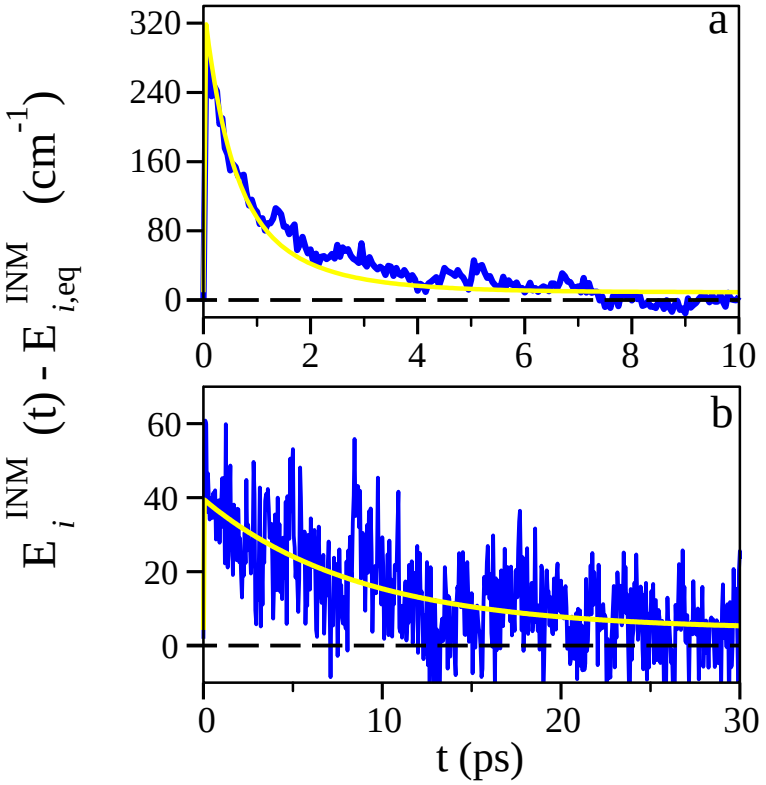

Figure 3.55: Time evolution of the vibrational energy of (a) the acend amide I mode and (b) the 46th INM (blue lines) and the corresponding fits (yellow lines) following the initial excitation of the amend amide I mode.

included in Table 3.35. We note that the relaxation of the amend amide I mode following the initial excitation of the acend amide I mode is well reproduced using the same relaxation lifetimes and similar weights than those used to fit the relaxation of this mode when it was initially excited (see Table 3.34). This fact points out to a common relaxation mechanism of the amend amide I mode independently of the way this mode was excited.

Regarding the results when the amend amide I mode is initially excited we found deep similarities with the results already presented for the relaxation of the acend amide I mode. The first stage is governed by the energy transfer into the acend amide I mode which accounts for 280 cm^{-1} of the energy released (see Figure 3.55) with a less important contribution (40 cm^{-1}) of the 46th INM. The energy curves of the acend amide I mode and the 46th INM are also well fitted using Eq. (3.13) and Eq. (3.14) respectively and the results of the fits are included in Table 3.36. We also see that the relaxation of the acend amide I mode shows a similar pattern to that found when this mode was directly excited. The time evolution of the 46th INM is also similar in both curves.

The ultrafast energy exchange between the two amide I modes is favored by their similar frequencies as we can see in Table 3.37 where the the 47th and 48th INMs correspond to the amend and acend amide I modes respectively. The average frequency of the 46th mode

Table 3.35: Fit parameters for the vibrational energy curves of different INMs of the AlaD-d_2 molecule after the initial excitation of the acend amide I mode. The relaxation and excitation lifetime are in ps and the parameters A and B in cm^{-1}. The amend amide I mode curve was fitted using Eq. (3.13) and the remaining INMs were adjusted using Eq. (3.14). Number in brackets are the corresponding weights (see Eq. (3.13)).

INM	τ_{exc}	τ_{rel}	A	B
amend amide I	0.0018	0.201(0.513) 0.744(0.159) 1.687(0.328)	387.2	5.7
46th	0.0018	8.66	30.0	0.0
14th	0.415	1.38	51.5	4.5
15th	0.415	1.38	86.5	0.0
16th	0.415	1.38	85.1	0.0
17th	0.415	1.38	91.4	0.0
18th	0.415	1.38	89.4	5.0
25th	0.415	3.16	107.6	0.0
31st	0.415	1.20	360.4	4.6
33rd	0.415	4.20	47.8	5.4
44th	0.415	8.66	27.9	3.4
45th	0.415	8.66	16.4	4.4
24th	0.919	4.37	47.8	4.6
26th	0.919	2.94	87.4	2.5
28th	0.919	7.08	34.4	0.3
29th	0.919	3.89	87.4	3.7
30th	0.919	8.66	28.6	2.0
34th	0.919	8.66	26.0	3.4
35th	0.919	8.66	24.6	4.8
acend CH bending[a]	0.919	8.66	96.6	10.2
amend CH bending[b]	1.737	8.66	58.9	4.4
C_βH bending[c]	1.737	8.66	69.6	6.7
19th	0.201	5.20	23.9	8.8
20th	0.201	8.11	42.0	2.7
21st	0.201	8.62	31.0	4.0
22nd	0.201	5.90	46.9	3.0
27th	1.613	2.60	185.9	4.4
32nd	1.613	6.63	46.5	0.0
49th-60th	4.416	8.66	609.1	41.8

a.- 36th, 38th and 40th INMs
b.- 39th and 41st INMs
c.- 37th, 42nd and 43rd INMs

Table 3.36: Fit parameters for the vibrational energy curves of different INMs of the AlaD-d_2 molecule after the initial excitation of the amend amide I mode. The relaxation and excitation lifetime are in ps and the parameters A and B in cm^{-1}. The acend amide I mode curve was fitted using Eq. (3.13) and the remaining INMs were adjusted using Eq. (3.14). Numbers in bracket are the corresponding weights (see Eq. (3.13))

INM	τ_{exc}	τ_{rel}	A	B
acend amide I	0.0018	0.415(0.490) 0.919(0.329) 1.737(0.181)	336.0	8.9
46th	0.0018	8.66	35.3	4.2
19th	0.201	4.89	23.9	5.5
20th	0.201	4.89	43.0	0.0
21st	0.201	3.85	53.5	0.0
22nd	0.201	1.20	405.9	19.7
23rd	0.201	6.76	61.4	0.0
44th	0.201	8.79	28.3	3.8
45th	0.201	8.79	32.3	2.8
34th	1.687	8.79	51.8	0.0
35th	1.687	8.79	32.9	2.7
acend CH bending[a]	1.687	18.79	49.0	7.8
amend CH bending[b]	1.687	48.79	9.9	0.0
C_βH bending[c]	1.687	23.02	45.7	22.1
24th	0.415	65.15	1.3	5.0
25th	1.662	56.83	2.0	0.0
26th	0.919	46.21	6.7	0.0
27th	1.241	65.81	1.7	0.0
28th	1.089	38.79	9.5	0.0
29th	1.007	38.79	8.3	0.0
30th	0.663	38.79	9.4	0.0
31st	0.594	48.79	0.5	0.0
32nd	0.471	38.79	6.2	0.0
33rd	0.526	48.79	0.2	0.0
49th-60th	6.137	18.79	223.6	10.7

a.- 36th, 38th and 40th INMs
b.- 39th and 41st INMs
c.- 37th, 42nd and 43rd INMs

is significantly lower so that the energy flow must be due to fortuitous frequency crossing at given times. Moreover, the overlaps between the two amide I modes and the 46th INM are significant as we can see in Figure 3.56 what favors the coupling facilitating the energy flows.

The second stage of the acend amide I relaxation shows a relaxation time of 0.415 ps

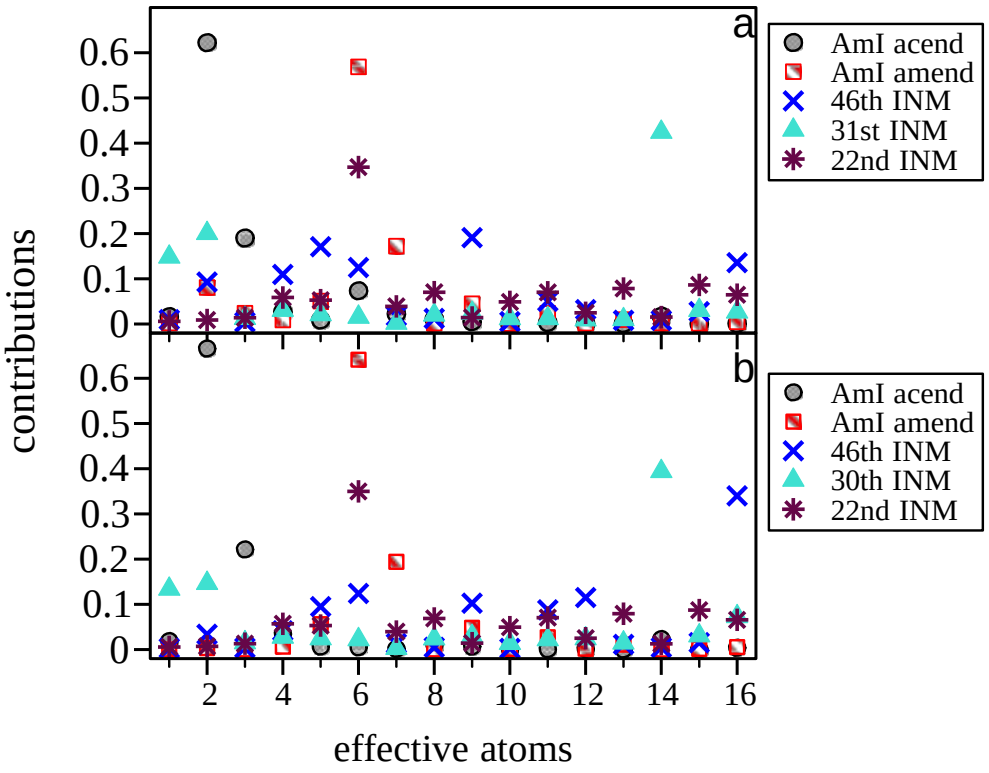

Figure 3.56: Average effective atomic displacement contributions for the INMs of the (a) AlaD-d_2 and (b) ^{13}C-AlaD-d_2 molecules (see Figure 3.48 for effective atom definitions).

and accounts for 40.1% of energy transferred from the amide I mode, that is 675 cm^{-1}. We find that the 14th, 15th, 16th, 17th, 18th, 25th, 31st, 33rd, 44th and 45th INMs are excited during the second stage. In Figure 3.57 we show the time evolution of the vibrational energy of these INMs, together with the fitted curves obtained using Eq. (3.14). The fitting parameters are included in Table 3.35. According to the data included in Table 3.37 we find that the combination of one of the mid frequency modes 25th, 31st, or 33rd INM with one of the lower frequency modes 14th, 15th, 16th, 17th or 18th INMs fulfills the required resonance condition. The comparatively higher amount of energy transferred into the 31st INM can be justified by the significant atomic displacement contribution of the carbon atom of the acend carbonyl group to this INM as shown in Figure 3.56. On the other hand, the transfer of energy from the acend amide I mode to the 44th and 45th INMs is likely to occur due to the small frequency gap between them and the acend amide I mode (see Table 3.37) which may enhance the possibility for the energy flow into these INMs.

In the case of the relaxation of the amend amide I mode the relaxation time is 0.201 ps and accounts for 42% of the energy released that is 708 cm^{-1}. While the percentage of energy transferred in the second stage is similar for both amide I modes, the process is significantly faster for the acend mode. This is a consequence of the different INMs involved

Table 3.37: Time averaged frequencies (in cm^{-1}) of the INMs of the AlaD-d_2 molecule together with their standard deviations as obtained from our MD simulations applying the EAMC assignment method with frequency window of width $\Delta\omega = 400$ cm^{-1}.

INM	Frequency	INM	Frequency
1	40.56 ± 108.1	31	1074.60 ± 46.6
2	-143.46 ± 236.5	32	1075.11 ± 68.9
3	67.66 ± 132.0	33	1177.38 ± 35.9
4	-19.25 ± 249.8	34	1304.54 ± 43.7
5	157.22 ± 111.3	35	1395.48 ± 42.8
6	219.27 ± 95.3	36	1407.24 ± 78.3
7	184.07 ± 109.4	37	1422.30 ± 86.3
8	226.06 ± 82.3	38	1421.81 ± 78.3
9	293.91 ± 101.4	39	1418.84 ± 47.2
10	170.27 ± 277.9	40	1410.61 ± 60.5
11	307.19 ± 85.3	41	1426.90 ± 51.1
12	356.13 ± 71.0	42	1431.06 ± 53.3
13	420.68 ± 74.4	43	1448.29 ± 64.0
14	520.06 ± 60.7	44	1464.81 ± 51.6
15	574.13 ± 129.5	45	1583.90 ± 58.6
16	555.54 ± 555.4	46	1546.56 ± 68.3
17	568.54 ± 91.9	47	1685.55 ± 11.5
18	618.98 ± 46.9	48	1683.82 ± 4.4
19	744.74 ± 57.9	49	2444.78 ± 3.9
20	770.91 ± 59.9	50	2442.96 ± 3.9
21	785.62 ± 50.4	51	2858.34 ± 6.6
22	843.61 ± 34.6	52	2909.46 ± 10.6
23	853.92 ± 58.3	53	2910.89 ± 10.9
24	922.84 ± 68.5	54	2925.19 ± 11.1
25	973.80 ± 65.4	55	2915.12 ± 15.3
26	998.18 ± 66.4	56	2923.24 ± 8.4
27	1004.17 ± 78.3	57	2965.48 ± 18.1
28	1067.08 ± 60.2	58	2966.00 ± 12.1
29	1038.84 ± 59.9	59	2976.45 ± 28.9
30	1080.25 ± 70.2	60	2987.01 ± 9.8

in this stage of the relaxation. We observe that the modes excited are the 19th, 20th, 21st, 22nd, 23rd, 44th and 45th INMs. In Figure 3.58 we show the vibrational energy curves of these INMs obtained from our simulations along with the fits obtained using Eq. (3.14). The values of the fit parameters are included in Table 3.36. As we can see in Table 3.37 there are multiple combinations of the frequencies of the 19th-23rd INMs which satisfy the required resonance condition including the possibility of 2:1 Fermi resonance. We observe that the 22nd INM is the one that receives the large amount of energy released by the

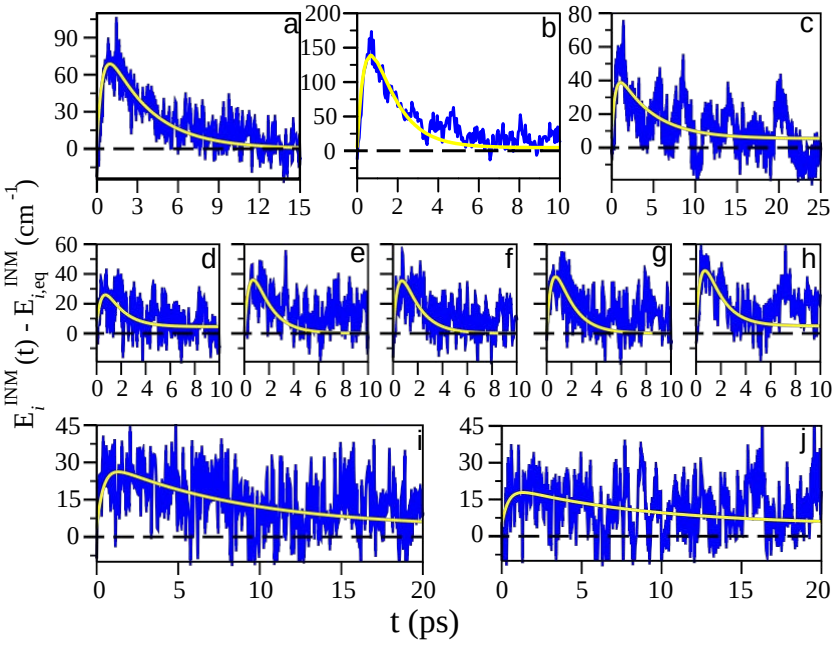

Figure 3.57: Time evolution of the vibrational energy (in cm^{-1}) of the (a) 25th, (b) 31s, (c) 33rd, (d) 14th, (e) 15th, (f) 16th, (g) 17th, (h) 18th, (i) 44th and (j) 45th INMs (blue lines) and the fits to Eq. (3.14) (yellow lines) following the initial excitation of the acend amide I mode.

amend amide I mode. This is due to the large atomic contribution of the carbon atom of the amend carbonyl group to the definition of the 22nd INM shown in Figure 3.56 which enhances the coupling between that INM and the amend amide I mode. The excitation of the 44th and 45th is facilitated by the small frequency gap between them and the initially excited mode.

After the second stage the analysis of the energy flows becomes more complicated because the energy is distributed among a higher number of INMs due to the appearance of secondary IVR process, that is, energy transfer between INMs different from the initially excited mode, and also the intermolecular energy transfer into the solvent.

The third relaxation channel of the acend amide I mode has a relaxation time of 0.919 ps and accounts for 26.9% of the energy released. As seen in Table 3.34 half of the energy goes to the solvent while the other half is transferred through IVR process. In Figure 3.59 we show the time evolution of the vibrational energy of the 24th, 26th, 28th, 29th and 30th INMs which are the modes that receive more energy during this stage with a 0.919 ps excitation time as shown in Table 3.35. The simultaneous excitation of these INMs and the energy flow into the bath suggest that the frequency resonance condition is obtained as a combination of one the INMs and the librations of the solvent although these process could be mediated by some low frequency modes of the solute molecule.

We note that some additional small contribution (see Table 3.35) come from the 34th and 35th INMs and the acend CH bending modes which correspond to the 36th, 38th and

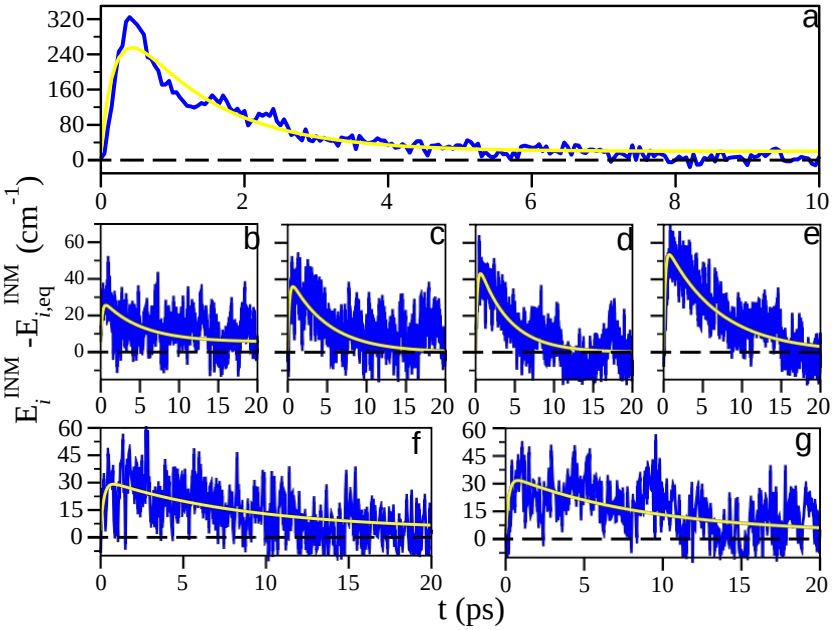

Figure 3.58: Time evolution of the vibrational energy (in cm^{-1}) of the (a)22nd, (b) 19th, (c) 20th, (d) 21st, (e) 23rd, (f) 44th and (g) 45th INMs (blue lines) and the fits to Eq. (3.14) (yellow lines) following the initial excitation of the amend amide I mode.

40th INMs.

The fourth and slower relaxation channel of the acend amide I mode has a relaxation time of 1.737 ps and accounts for 14.8% of the energy released. According to our simulation the main receptors are the amend CH bending modes (39th and 41st INMs) and $C_\beta H$ bending modes (37th, 42nd and 43rd INMs). The corresponding energy curves are shown in Figure 3.60 and the fit parameter are given in Table 3.35.

Concerning the third relaxation stage of the relaxation of the amend amide I mode we conclude from the data included in Table 3.34 that it only involves the intermolecular energy transfer into the solvent with a 0.744 ps life time. The fourth relaxation stage proceeds with a 1.687 ps lifetime being excited the 34th and 35th INMs as well as the acend CH bending (36th, 38th and 40th INMs), the amend CH bending (39th and 41st INMs) and the $C_\beta H$ bending (37th, 42nd and 43rd INMs) modes. The vibrational energy curves for these modes are shown in Figure 3.61 and the corresponding fit parameters are included in Table 3.36. Taking into account the frequencies of these INMs the participation of some low frequency modes is probably invoked.

Let us now discuss the secondary IVR process originated from the relaxation of the modes that receive their energy from the initially excited amide I mode. Among these processes the most important ones are those following the resonance energy transfer between the two amide I modes. As we can see in Table 3.35, in the case of the initial excitation of the acend amide I mode, the amend amide I mode relaxes through three different pathways with lifetimes and weights similar to those obtained when the amend amide I mode was

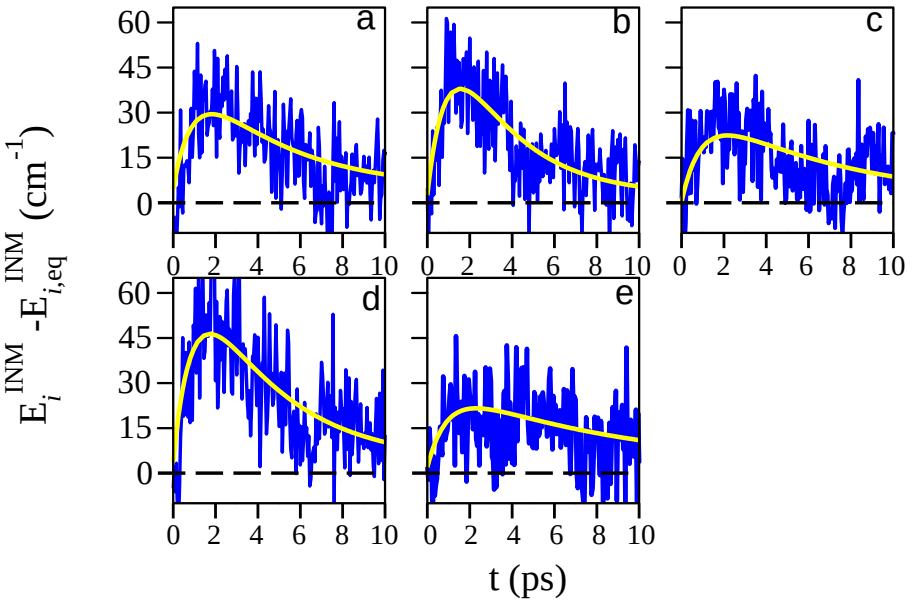

Figure 3.59: Time evolution of the vibrational energy (in cm^{-1}) of the (a) 24th, (b) 26th, (c) 28th, (d) 29th and (e) 30th INMs (blue lines) and the fits to Eq. (3.14) (yellow lines) following the initial excitation of the acend amide I mode.

directly excited (see Table 3.34). Moreover, we also find energy flows to the same INMs. For instance we see that the 19th-22nd INMs are excited with a lifetime of 0.201 ps (see Figure 3.58 and Figure 3.62 and Table 3.35 and Table 3.36) in both cases. We also find similar excitation of the amend CH and $C_\beta H$ bending modes (see Figure 3.60 and Figure 3.61 and Table 3.35 and Table 3.36), although we note that these modes could be also partially excited directly from the acend amide I mode.

A similar behavior is found when we study the relaxation of the acend amide I mode following the initial excitation of the amend amide I mode (see Table 3.36). This mode relaxes with similar lifetimes and weights than those found when it was initially excited. However, the identification of the INMs that receive energy from the acend amide I mode is complicated by the previous vibrational excitation of many INMs following the second relaxation channel of the amend amide I mode. Nevertheless we find that the 24th-33rd INMs show excitation lifetimes in the 0.4-1.7 ps range (see Figure 3.63 and Table 3.36), in general agreement with the tendencies observed when the acend amide I was initially excited (see Table 3.35).

Apart from the energy flows following the resonance energy transfer between the two amide I modes, the most important secondary IVR process that we have found corresponds to the excitation of the 27th and 32nd INMs when the acend amide I mode was initially excited as shown in Figure 3.62. Although the 1.613 ps excitation lifetime of these modes (see Table 3.35) is similar to the fourth relaxation time of the acend amide I mode we consider more reasonable that these modes are excited from the 31st INM which has a

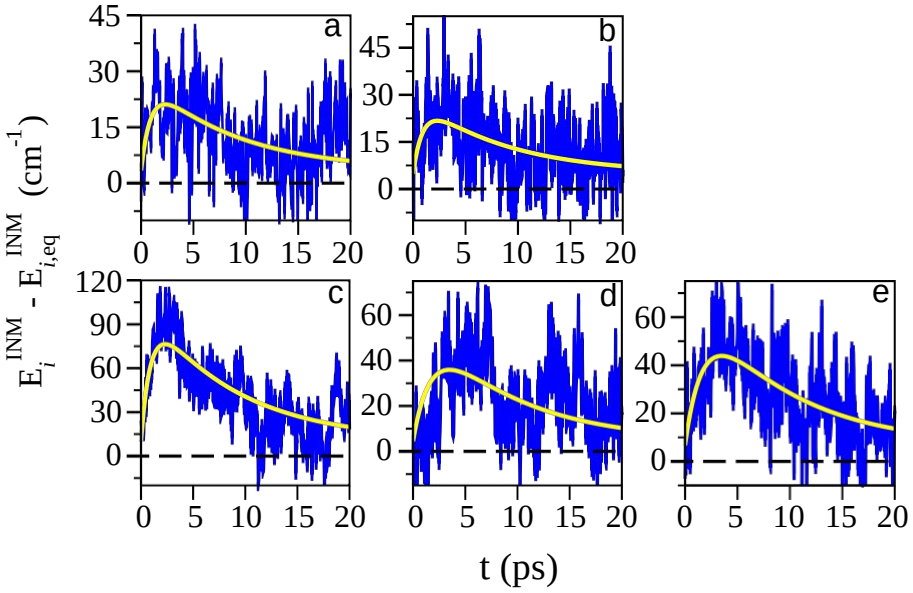

Figure 3.60: Time evolution of the vibrational energy (in cm^{-1}) of the (a) 34th, (b) 35th INMs (c) acend CH bending (36th, 38th and 40th INMs), (d) amend CH bending (39th and 41st INMs) and (e) $C_\beta H$ bending (37th, 42nd and 43rd INMs) (blue lines) and the fits to Eq. (3.14) (yellow lines) following the initial excitation of the acend amide I mode.

small frequency gap and receives a great energy flow from the acend amide I mode. We note that the sum of the excitation and relaxation times of the 31st INM (0.415+1.20 ps) is almost identical to the excitation time of the 27th and 32nd INMs.

As a final remark we note that we have found energy flows to the 49th-60th INMs which frequencies are higher than that of the amide I modes as we can see in Figure 3.64. The unphysical energy transfer from low to high frequency modes is a well known drawback of the classical calculations [Ohmine 90, Moritsugu 00, Moritsugu 03, Fujisaki 09, Bastida 10a, Bastida 10b, Soler 11]. The excitation time of these high frequency mode is in the 4-6 ps range (see Table 3.35 and Table 3.36) so that they are excited through secondary IVR process, that we were unable to identify. Anyway the amount of energy stored in these high frequency modes is just ~12% of the amide I vibrational quantum so that its effect in the whole IVR mechanism is small. It is interesting to realize that the percentage is smaller than that found during the relaxation of the amide I mode of the NMAD molecule in D_2O solution [Soler 11] where 18% of the energy flowed to high frequency INMs. We think that the transfer to low frequency modes is favored in the AlaD-d_2 molecule due to the increase of the vibrational density of states.

3.3.6.4 Energy transfer into the solvent

In Figure 3.65 we show the time evolution of the normalized vibrational energy of the AlaD-d_2 molecule in liquid D_2O following the excitation of the acend and amend amide I

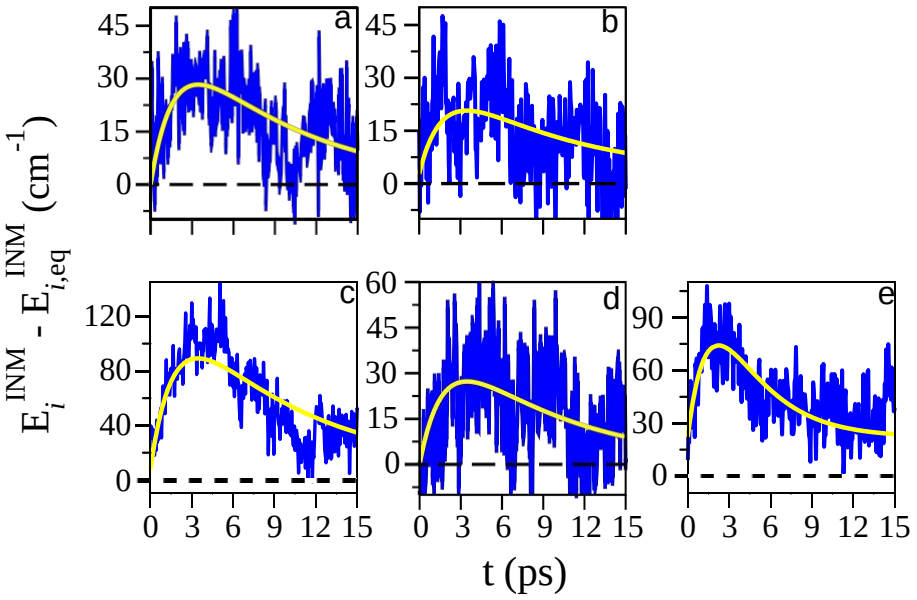

Figure 3.61: Time evolution of the vibrational energy (in cm^{-1}) of the (a) 34th, (b) 35th INMs, (c) CH-acend bending (36th, 38th and 40th INMs), (d) CH-amend bending (39th and 41st INM) and (e) C$_\beta$H bending (37th, 42nd and 43rd INMs) (blue lines) and the fits to Eq. (3.14) (yellow lines) following the initial excitation of the amend amide I mode.

modes. Both curves are well reproduced using a biexponential function as follows

$$\frac{E^{vib}_{AlaD-d_2}(t) - E^{vib,eq}_{AlaD-d_2}}{E^{vib}_{AlaD-d_2}(0) - E^{vib,eq}_{AlaD-d_2}} = c_{rel,1}\, e^{-t/\tau_{rel,1}} + c_{rel,2}\, e^{-t/\tau_{rel,2}} \qquad (3.15)$$

where the weights satisfy $c_{rel,1} + c_{rel,2} = 1$ and $\tau_{rel,i}$ are the relaxation times. For the curve corresponding to the relaxation of the acend amide I mode we obtain $\tau^{acend}_{rel,1}$=0.919 ps (13%) and $\tau^{acend}_{rel,2}$=8.66 ps (87%) and for the amend amide I curve $\tau^{amend}_{rel,1}$=0.744 ps (13%) and $\tau^{amend}_{rel,2}$=10.1 ps (87%). In both curves the shortest relaxation times and their corresponding weights are associated to the energy flow from amide I modes to the solvent (see Table 3.34) while the larger ones are average values which accounts for the transfers from the remaining INMs. In order to compare both curves we have calculated the time at which the initial vibrational energy decays by a factor $1/e$. So we obtain the relaxation times 7.5 ps and 8.7 ps for the acend and amend amide I modes respectively. Thus the energy transfer into the solvent is faster when the acend amide I mode is initially excited than following the amend amide I excitation.

Anyway both times are shorter than those obtained in our previous study about the vibrational relaxation of the amide I (9.6 ps) and CH stretching (11.7 ps) modes of the NMAD molecule in liquid D_2O [Bastida 10a, Bastida 10b]. The acceleration of the relaxation process in the AlaD-d_2 molecule with respect to the NMAD molecule is probably due to the higher density of vibrational states what increase the probability of resonance facilitating the energy flows.

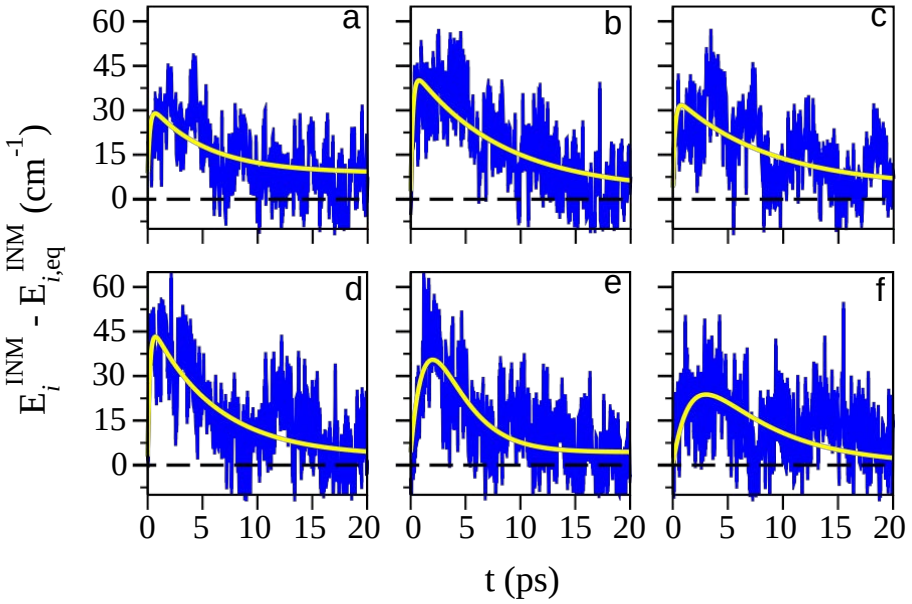

Figure 3.62: Time evolution of the vibrational energy (in cm^{-1}) of the (a) 19th, (b) 20th, (c) 21st, (d) 22nd, (e) 27th and (f) 32nd INMs (blue lines) and the fits to Eq. (3.14) (yellow lines) following the initial excitation of the acend amide I mode.

In order to analyze which INMs transfer large energy into the solvent apart from the amide I modes we have applied the SMF method and the results are plotted in Figure 3.66. We note that in these plots the energy transfered from the initially excited amide I mode (~ 220 cm^{-1}) is out of the scale. We see that the energy transferred into the solvent tends to be bigger as the frequency of the INM is smaller. As a guide we have included a dashed line which corresponds to the average energy transferred by every mode into the solvent obtained as 1680/60=28 cm^{-1}. As seen the contribution of the lower 1st-9th INMs are all over the average value while the contributions of the higher frequency modes are always under the average. This is the same behavior that we have obtained in our previous study of the relaxation of the amide I mode of the NMAD molecule [Soler 11] where we obtained that the low frequency modes act as doorways for the intramolecular energy flow into the solvent. Apart from the general trend we observe some mid frequency modes which significant energy flows into the solvent as the 31st INM in the acend amide I relaxation and the 22nd INM in the amend curve. We note that these INMs are highly excited during the relaxation process as previously discussed. For the case of the 25th and 29th INMs for the relaxation of the acend amide I mode their relative important contribution to the intermolecular energy transfer is probably due to a casual resonance with the vibrational motions of the solvent.

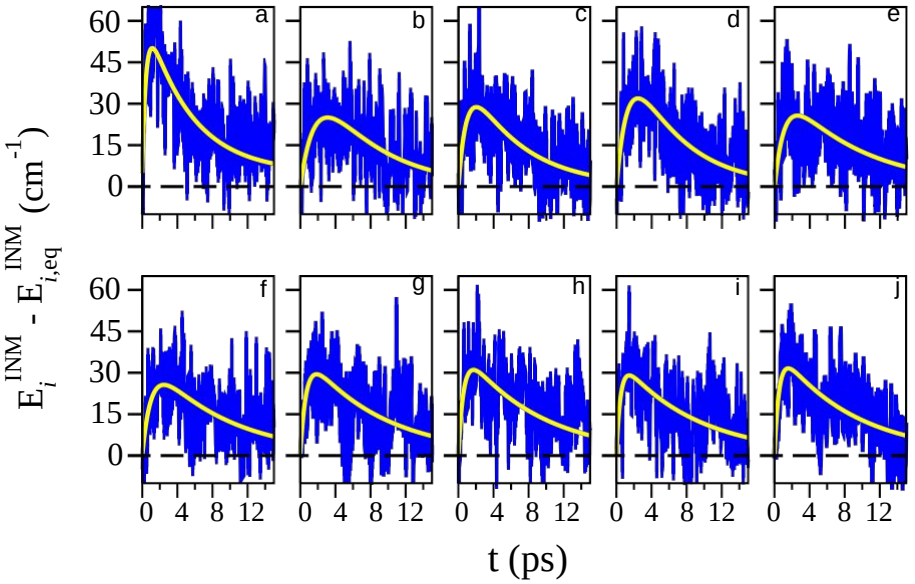

Figure 3.63: Time evolution of the vibrational energy (in cm^{-1}) of the (a) 24th, (b) 25th, (c) 26th, (d) 27th, (e) 28th, (f) 29th, (g) 30th, (h) 31st, (i) 32nd, and (j) 33rd INMs (blue lines) and the fits to Eq. (3.14) (yellow lines) following the initial excitation of the amend amide I mode.

3.3.7 The ^{13}C-AlaD-d_2 molecule

From an experimental point of view the study of the vibrational relaxation of the acend and amend amide I modes of the AlaD-d_2 molecule is complicated because of the overlap between both bands [Kim 05a] with maxima placed at 1629 cm^{-1} and 1642 cm^{-1} respectively.

In order to obtain a selective excitation of each amide I mode, Hochstrasser *et al.* [Kim 05a] used the ^{13}C isotopic substitution of the carbon atom of the carbonyl group in the acetyl end of the AlaD-d_2 molecule. The resulting molecule that we represent as ^{13}C-AlaD-d_2 shows a 40 cm^{-1} red shift of the acend band up to 1589 cm^{-1} while the amend band is blue shifted by only 1 cm^{-1} up to 1643 cm^{-1}. The 54 cm^{-1} frequency gap of the two amide I modes of the ^{13}C-AlaD-d_2 molecule allow then a selective excitation.

We have carried out MD simulations and the INM analysis of the ^{13}C-AlaD-d_2 molecule. The time averaged frequencies obtained are included in Table 3.38. If we compare the frequencies of the two amide I modes with those obtained for the AlaD-d_2 molecule (see Table 3.37) we observe that the frequency of the acend amide I mode is red shifted by 45.6 cm^{-1} up to 1638.2 cm^{-1} while the amend band is largely unaffected with a 0.2 cm^{-1} red shifted up to 1685.3 cm^{-1}. Therefore the theoretical value of the frequency gap between both amide I modes is 47.1 cm^{-1}.

Although both amide I mode frequencies are overestimated by 40 cm^{-1} and the frequency gap is underestimated by 7 cm^{-1} in our simulations with respect to the measured data we think that the relative deviations (2.4% and 13%) are small enough to consider

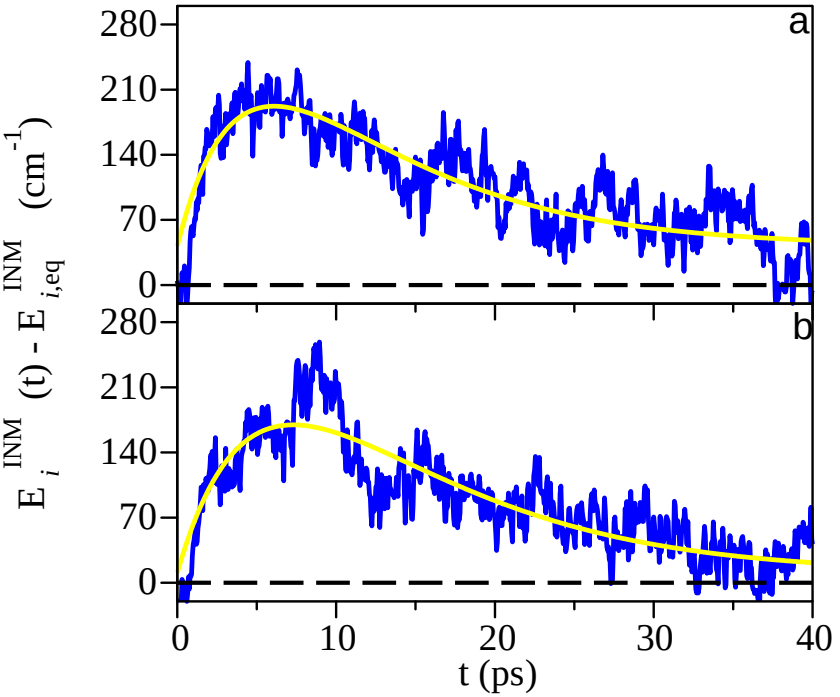

Figure 3.64: Time evolution of the sum of the vibrational energy of the 49th-60th INMs after the initial excitation of the (a) acend and (b) amend amide I modes (blue lines). The fits to Eq. (3.14) are also shown (yellow lines).

our results as realistic.

3.3.7.1 Amide I modes relaxation lifetimes

In Figure 3.67 (a) and Figure 3.68 (a) we show the time evolution of the vibrational energy of the acend and amend amide I modes following their initial excitation respectively. The acend amide I mode curve can be well reproduced using a biexponential functions (see Eq. (3.10) with N =2) while the amend one require a three exponential function (see Eq. (3.10) with N = 3). The resulting fit parameters are given in Table 3.39. In order to analyze the origin of the different exponential terms we have applied the SMF method [Soler 11] to distinguish which percentages of the energy released by the amide I modes flow through intramolecular transfers (IVR processes) and through intermolecular exchange into the solvent (bath). We show in Figure 3.67 (b) and Figure 3.68 (b) the time evolution of the accumulated energy flows from the acend and amend amide I modes to the bath and the rest of the INMs of the molecule. These energy flow curves are well reproduced using Eq. (3.11) and Eq. (3.12). The corresponding fit parameters are included in Table 3.39. As seen the lifetimes and weights derived from the kinetic analysis and the SMF method match nicely. Then we can conclude that the shorter relaxation time of the acend amide I corresponds to an IVR process which account for 84.1% of the energy released while the

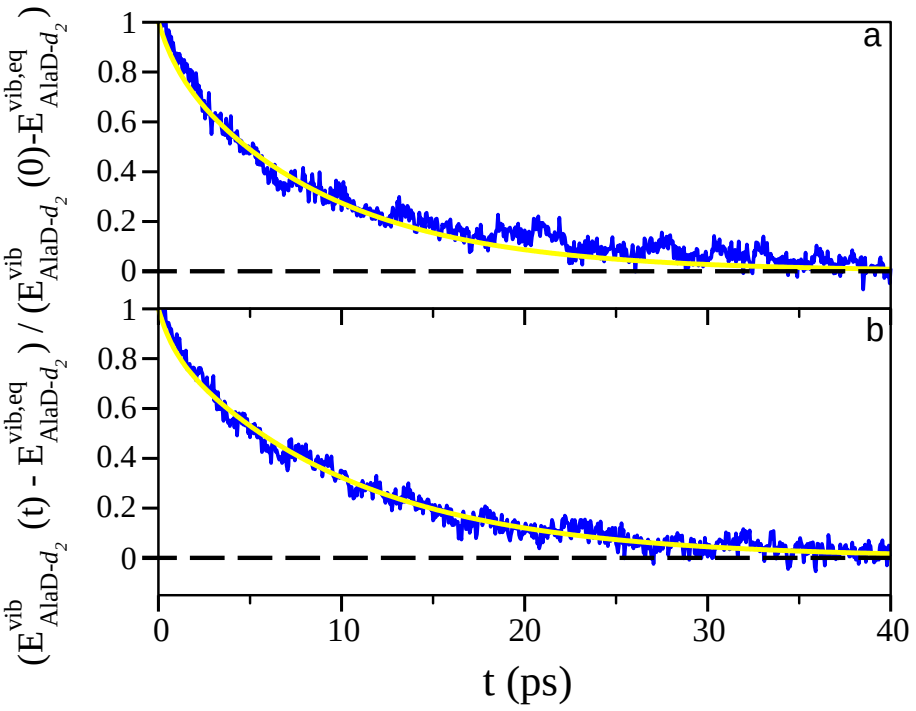

Figure 3.65: Time evolution of the normalized vibrational energy of the AlaD-d_2 molecule in liquid D_2O following the initial excitation of the (a) acend and (b) amend amide I modes (blue lines) and the fits to Eq. (3.15) (yellow lines).

longer one characterizes the comparatively less important (15.9%) energy transfer into the bath. For the amend amide I mode we observe two time scales for the IVR process with 0.26 ps and 1.86 ps lifetimes and 64.2% and 24.0% weights respectively. The energy flows into the solvent has an 0.90 ps intermediate lifetime and account for 11.8% of the energy released.

In order to compare the MD-INM results with the experimental findings we have also plotted in Figure 3.67 (a) and Figure 3.68 (a) the fits to the measured data [Kim 05a]. In general the agreement between both sets of results is reasonable specially if we take into account that our result are based on standard MM force fields and MD without additional adjustable parameters or corrections. However some discrepancies are relevant. We observe that during the first 2 ps the decay of the acend and amend amide I relaxation curves is slower and faster respectively than the experimental results. That is why when we calculate the overall relaxation time as the time when the energy decrease in a factor $1/e$ (see Table 3.39) the theoretical and experimental results are in opposite order.

3.3.7.2 IVR pathways

The next issue that we address is the IVR relaxation pathways of the amide I modes. As it was discussed in the previous section the acend amide I decay curve can be reproduced

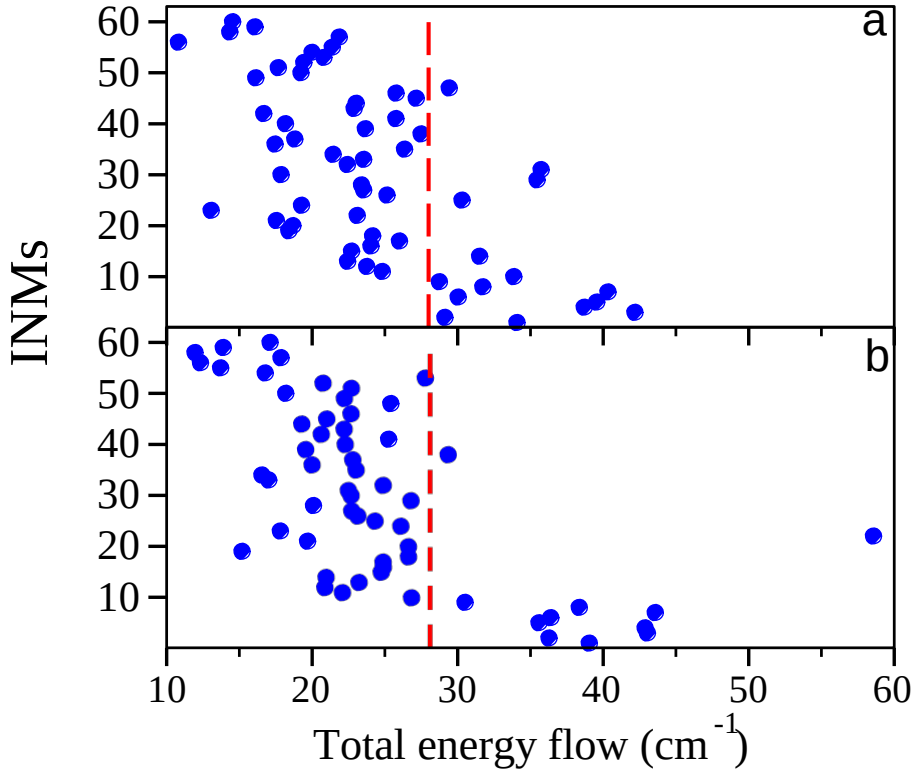

Figure 3.66: Vibrational energy (in cm^{-1}) transferred from the INMs of the AlaD-d_2 molecule into the solvent calculated using the SMF method following the initial excitation of the (a) acend and (b) amend amide I modes. Dashed red lines indicate the average energy transfer.

considering a single 0.74 ps IVR lifetime and the IVR process accounts for 84% of the energy released by the acend amide I mode. We have found up to 25 different INMs which are excited in that time scale. These INMs are listed in Table 3.40 where we give the fitting parameters obtained when their vibrational energy curve (see Figure 3.69 and Figure 3.70) were fitted using Eq. (3.14). The high number of INMs that participate in the relaxation is a consequence of the multiple combinations of INM frequencies that satisfy the resonance condition. So different sums of the frequencies of the 14th-20th INMs with the 24th-33rd INMs reproduce quite well the acend amide I mode frequency. Interestingly, one of the best coincidence corresponds to the sum of frequencies of 16th and 30th INMs which are two of the INMs that are more excited during the relaxation process as we can see in Figure 3.69. For the 34th-46th INMs the resonance condition implies the participation of low frequency modes in the 100-300 cm^{-1} range. These values overlap quite well with libration bands of the D_2O solvent and therefore the energy stored in the low frequency modes is always small so that we can not quantify it in our analysis.

Concerning the relaxation of the amend amide I mode, the kinetic and SMF analysis state the presence of two different sets of IVR processes. The faster IVR channel has a lifetime of 0.26 ps and accounts for 64.2% of the energy transferred. We have found 15 INMs

Table 3.38: Time averaged frequencies (in cm^{-1}) of the INMs of the ^{13}C-AlaD-d_2 molecule together with the standard deviations as obtained from our MD simulations and applying the EAMC method with a frequency window of width $\Delta\omega = 400$ cm^{-1}.

INM	Frequency	INM	Frequency
1	40.71 ± 109.5	31	1057.96 ± 67.8
2	-145.11 ± 238.5	32	1097.53 ± 68.6
3	67.85 ± 134.8	33	1172.22 ± 40.8
4	-15.55 ± 253.0	34	1301.50 ± 47.5
5	158.42 ± 111.6	35	1381.52 ± 49.2
6	218.46 ± 95.5	36	1407.21 ± 80.7
7	183.44 ± 109.2	37	1419.79 ± 76.7
8	223.88 ± 83.9	38	1417.23 ± 63.9
9	293.36 ± 102.4	39	1416.73 ± 67.3
10	168.05 ± 284.6	40	1417.08 ± 60.3
11	307.00 ± 86.3	41	1429.36 ± 52.0
12	355.93 ± 75.5	42	1432.62 ± 67.6
13	417.81 ± 73.1	43	1458.61 ± 53.9
14	532.81 ± 60.5	44	1449.30 ± 62.1
15	576.45 ± 126.8	45	1558.23 ± 72.5
16	563.11 ± 86.6	46	1560.58 ± 70.2
17	539.29 ± 75.7	47	1638.19 ± 3.9
18	617.37 ± 48.7	48	1685.29 ± 10.5
19	746.20 ± 57.1	49	2444.73 ± 3.7
20	767.97 ± 49.1	50	2442.75 ± 3.9
21	785.06 ± 56.3	51	2858.26 ± 6.7
22	843.82 ± 40.6	52	2909.34 ± 10.7
23	854.77 ± 68.6	53	2910.85 ± 11.0
24	921.64 ± 75.6	54	2925.03 ± 11.0
25	983.15 ± 72.4	55	2915.08 ± 15.8
26	997.82 ± 73.3	56	2923.11 ± 8.4
27	1006.12 ± 81.7	57	2965.38 ± 18.5
28	1070.50 ± 55.6	58	2965.89 ± 12.8
29	1029.20 ± 64.5	59	2976.29 ± 16.0
30	1051.15 ± 97.7	60	2986.97 ± 29.7

which energy curves can be well fitted using that excitation time in Eq. (3.14) and they are listed in Table 3.41. The corresponding energy curves are plotted in Figure 3.71 and Figure 3.72. We find that these energy flows can be justified by taking into account the frequency resonant conditions. The sum of one frequency the 15th-16th INMs with another of the 27th-29th INMs or the sum of two frequencies of the 20th-24th INMs provide values quite close to the amend amide I frequency. For the 34th, 35th, 43rd, 45th and 46th we invoke the participation of low frequency modes that fill the frequency gap. We note the special

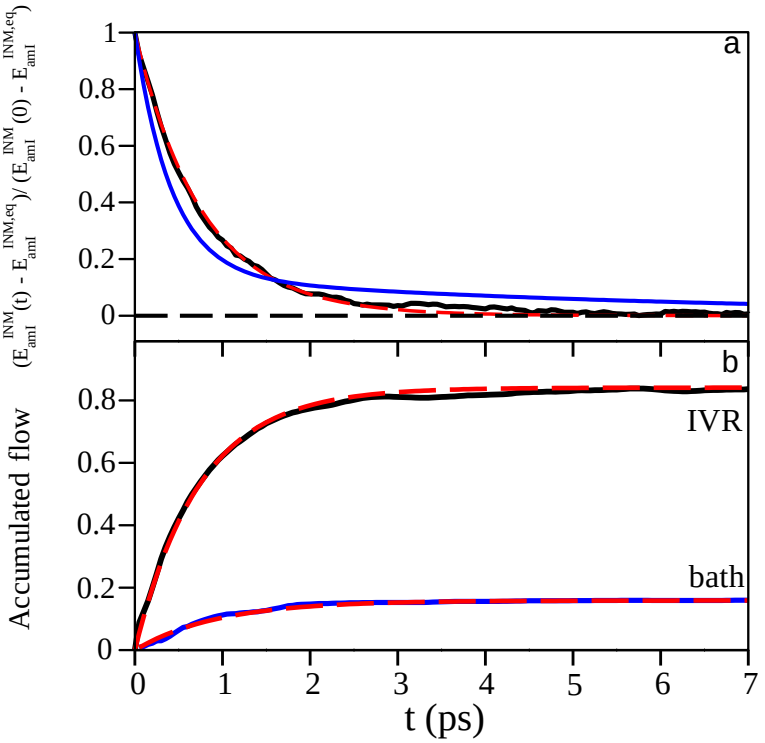

Figure 3.67: (a) Time evolution of the normalized vibrational energy of the acend amide I mode with respect to its equilibrium value at 300 K (black line) and the fit to Eq. (3.10) (red dashed line) together with the experimental results (blue line) and (b) time evolution of the normalized accumulated energy that flows from the acend amide I into the remaining INMs of the ^{13}C-AlaD-d_2 molecule through IVR process (black line) and into the bath (blue line) and their fits (red dashed line) to Eq. (3.11) and Eq. (3.12) respectively.

Table 3.39: Vibrational relaxation times of the amide I mode (in ps) and amplitudes for the ^{13}C-AlaD-d_2 molecule as obtained from the fitting.

		$\tau_{rel,1}$ ($c_{rel,1}$)	$\tau_{rel,2}$ ($c_{rel,2}$)	$\tau_{rel,3}$ ($c_{rel,3}$)	T_1
Kinetic[a]	acend	0.740(0.841)	0.943(0.159)		0.73
	amend	0.260(0.642)	0.900(0.118)	1.860(0.240)	0.44
Exp.[b]	acend	0.415(0.858)	5.700(0.142)		0.51
	amend	0.576(0.735)	1.860(0.265)		0.78
		τ_1^{IVR} (c_1^{IVR})	τ_2^{IVR} (c_2^{IVR})	τ^{bath} (c^{bath})	
SMF [c]	acend	0.74(0.841)		0.943(0.159)	
	amend	0.260(0.642)	1.86(0.240)	0.900(0.118)	

a.- See Eq. (3.10)
b.- Ref. [Kim 05a]
c.- See Eq. (3.11) and Eq. (3.12)

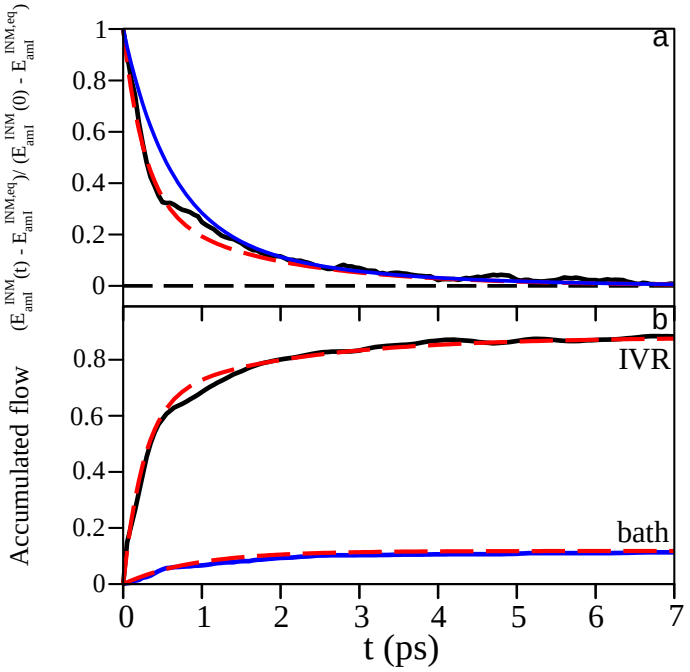

Figure 3.68: (a) Time evolution of the normalized vibrational energy of the amend amide I mode with respect to its equilibrium value at 300 K (black line) and the fit to Eq. (3.10) (red dashed line) together with the experimental results (blue line) and (b) time evolution of the normalized accumulated energy that flows from the amend amide I into the remaining INMs of the ^{13}C-AlaD-d_2 molecule through IVR process (black line) and into the bath (blue line) and their fits (red dashed line) to Eq. (3.11) and Eq. (3.12) respectively.

case of the 22nd INM which is in an excellent 2:1 Fermi resonance (2×843.8=1687.6 cm^{-1}) with the initially excited mode what justifies that this INM receives the larger amount of energy as shown in Figure 3.71. The second IVR channel is much slower ($\tau_{rel,2}$ = 1.86 ps) and quantitatively less important (24%). We find that the energy is more equally distributed than in the previous channel among the 30th-33rd INMs and the acend CH, amend CH and C$_\beta$H bending modes. The energy curves are plotted in Figure 3.73 and the fitting parameters to Eq. (3.14) are included in Table 3.41.

Now, we focus our attention on the secondary IVR processes. In the case of the relaxation of the acend amide I mode the 27th INM is the one that receives more energy (see Figure 3.74). The fit parameters corresponding to Eq. (3.14) are included in Table 3.40 and reveals that this mode is excited in 1.80 ps (see Table 3.40). Although multiple of INMs previously excited from the amend amide I mode could justify the excitation of the 27th INM mode (see Table 3.40), we think that the most probable candidate is the 30th INM. The arguments that support our guess are that the 30th INM receive a significant amount of energy from the initially excited mode (see Figure 3.69), its frequency is quite similar to the frequency of the 27th mode and its relaxation time is much shorter than that found for other INMs with similar frequencies (see Table 3.40).

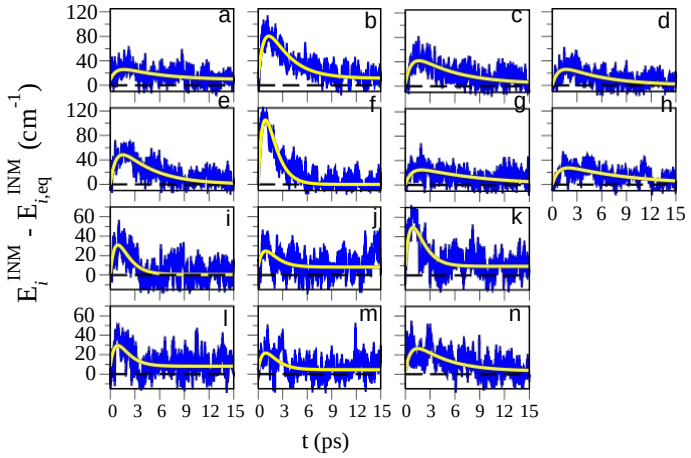

Figure 3.69: Time evolution of the vibrational energy (in cm^{-1}) of the (a) 24th (b) 25th (c) 26th (d) 28th (e) 29th (f) 30th (g) 31st (h) 33rd (i) 14th (j) 15th (k) 16th (l) 17th (m) 18th and (n) 20th INMs (blue lines) and fits to Eq. (3.14) (yellow lines) following the initial excitation of the acend amide I mode.

Similar arguments can be used to explain why we consider that the excitation of the 25th and 26th INMs (see Figure 3.75) which are the most important secondary IVR process following the relaxation of the amend amide I mode is probably due to an energy flow from the 22nd INM.

We finally remark that we have found energy flows to the 49th-60th INMs which frequencies are higher than that of the amide I modes as we can see in Figure 3.76. In the acend amide I mode, these modes are excited in 1.64 ps so that they probably receive

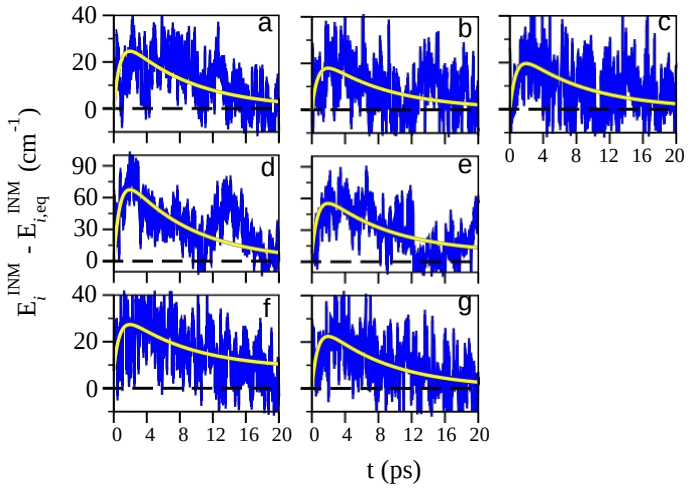

Figure 3.70: Time evolution of the vibrational energy (in cm^{-1}) of the (a) 34th (b) 35th (c) 43rd (d) acend CH bending (e) $C_\beta H$ bending (f) 45th and (g) 46th INMs (blue lines) and the fits to Eq. (3.14) (yellow lines) following the initial excitation of the acend amide I mode.

Table 3.40: Fit parameters for the vibrational energy curves of different INMs of the ^{13}C-AlaD-d_2 molecule after the initial excitation of the acend amide I mode. The relaxation and excitation times are in ps and the parameters A and B in cm^{-1}. The INMs were fitted using Eq. (3.14).

INM	τ_{exc}	τ_{rel}	A	B
14th	0.74	1.18	178.7	0.5
15th	0.74	1.18	96.8	8.2
16th	0.74	1.18	236.0	9.4
17th	0.74	1.18	125.1	8.2
18th	0.74	1.18	101.1	4.6
20th	0.74	3.82	43.0	3.1
24th	0.74	4.97	27.7	8.8
25th	0.74	2.57	132.9	11.3
26th	0.74	4.90	62.8	3.7
28th	0.74	5.12	42.3	0.0
29th	0.74	3.95	87.5	0.0
30th	0.74	1.09	743.3	0.0
31st	0.74	8.16	34.5	0.0
33rd	0.74	8.16	38.0	0.0
34th	0.74	8.16	34.4	0.0
35th	0.74	8.16	25.0	0.0
acend CH bending[a]	0.74	8.16	94.2	0.0
C_βH bending[b]	0.74	8.16	66.5	7.6
43rd	0.74	8.16	27.4	0.0
45th	0.74	8.16	26.8	8.1
46th	0.74	8.16	31.3	0.0
27th	1.80	3.16	137.8	5.4
49th-60th	1.64	7.81	424.4	5.0

a.- 36th, 39th and 40th INMs
b.- 37th, 42nd and 44th INMs

the energy from some of the modes previously excited from the amide I mode showing the shorter relaxation times as the 14th-18th and the 30th INMs. In the amend case the excitation time is 1.86 ps so that the energy could come directly from the initially excited mode or more probably through an efficient 2:1 Fermi resonance from some bending modes as we found for the NMAD molecule [Bastida 10a, Bastida 10b, Soler 11]

3.3.7.3 Energy transfer into the solvent

In Figure 3.77 we plot the time evolution of the normalized vibrational energy of the ^{13}C-AlaD-d_2 molecule in liquid D_2O following the excitation of the acend and amend amide I modes. Both curves are well fitted using the biexponential function given in Eq. (3.15). For the curve corresponding to the relaxation of the acend amide I mode we obtain $\tau_{rel,1}^{acend}$=0.943 ps (15.9%) and $\tau_{rel,2}^{acend}$=8.16 ps (84.1%) and for the amend amide I curve $\tau_{rel,1}^{amend}$=0.90 ps

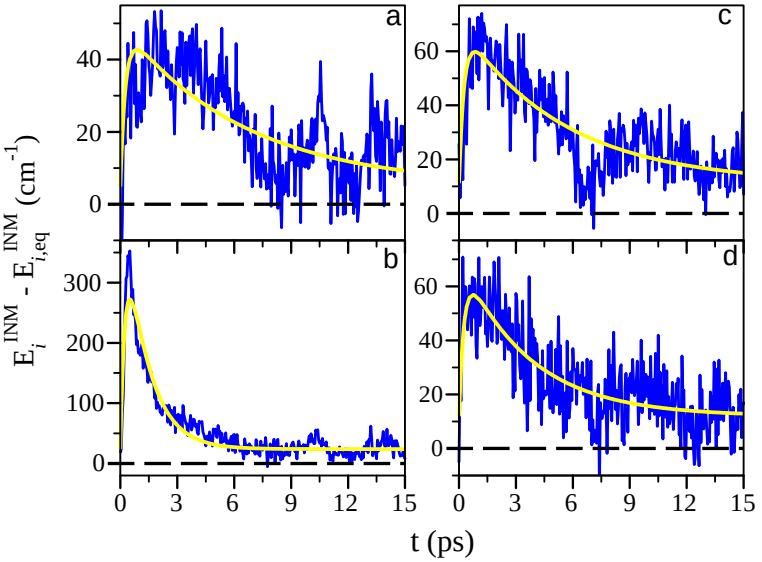

Figure 3.71: Time evolution of the vibrational energy (in cm^{-1}) of the (a) 21st (b) 22nd (c) 23rd and (d) 24th INMs (blue lines) and the fits to Eq. (3.14) (yellow lines) following the initial excitation of the amend amide I mode.

(11.8%) and $\tau_{rel,2}^{amend}$=9.36 ps (88.2%). In both cases the shorter relaxation times and their corresponding weights are associated to the energy flow from the initially excited amide I modes into the solvent (see Table 3.39) while the longer ones are average values which accounts for the transfers from the remaining INMs. In order to compare both curves we

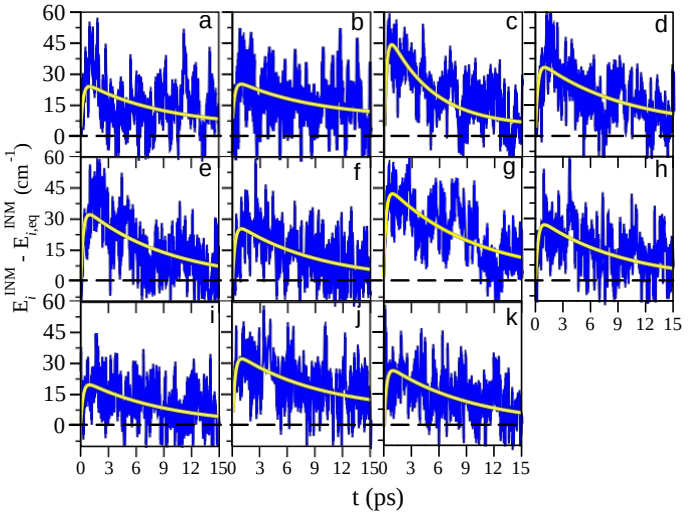

Figure 3.72: Time evolution of the vibrational energy (in cm^{-1}) of the (a) 15th (b) 16th (c) 20th (d) 27th (e) 28th (f) 29th (g) 34th (h) 35th (i) 43rd (j) 45th and (k) 46th INMs (blue lines) and the fits to Eq. (3.14) (yellow lines) following the initial excitation of the amend amide I mode.

Table 3.41: Fit parameters for the vibrational energy curves of different INMs of the ^{13}C-AlaD-d_2 molecule after the initial excitation of the amend amide I mode. The relaxation and excitation times are in ps and the parameters A and B in cm^{-1}. The INMs were fitted using Eq. (3.14).

INM	τ_{exc}	τ_{rel}	A	B
15th	0.26	9.36	22.6	4.4
16th	0.26	9.36	19.1	8.6
20th	0.26	4.83	39.1	4.8
21st	0.26	6.46	45.3	4.8
22nd	0.26	1.20	485.0	23.7
23rd	0.26	5.44	51.2	11.2
24th	0.26	3.62	59.3	11.9
27th	0.26	9.36	33.1	4.4
28th	0.26	9.36	36.6	0.0
29th	0.26	9.36	28.9	0.0
34th	0.26	9.36	45.4	2.1
35th	0.26	9.36	31.1	0.0
43rd	0.26	9.36	22.5	0.0
45th	0.26	9.36	29.2	6.6
46th	0.26	9.36	30.1	0.0
30th	1.86	6.75	44.7	0.0
31st	1.86	5.18	52.9	8.0
32nd	1.86	4.69	63.2	5.6
33rd	1.86	6.86	58.5	0.0
acend CH bending[a]	1.86	9.36	83.2	8.1
amend CH bending[b]	1.86	9.36	80.3	−11.7
C_βH bending[c]	1.86	9.36	100.0	6.1
25th	1.46	7.78	33.6	10.5
26th	1.46	7.26	34.8	11.0
49th-60th	1.86	8.71	338.0	37.8

a.- 36th, 39th and 40th INMs
b.- 38th and 41st INMs
c.- 37th, 42nd and 44th INMs

have calculated the time at which the initial vibrational energy decays by a factor $1/e$. In this way we obtain the overall relaxation times 6.75 ps and 8.20 ps for the acend and amend amide I modes respectively. Thus the energy transfer into the solvent is faster when the acend amide I mode is initially excited than following the amend amide I excitation.

In order to analyze which INMs transfer more energy into the solvent apart from the amide I mode we have applied the SMF method and the results are plotted in Figure 3.78. We note that the energy transferred from the initial excited acend and amend amide I modes (260.5 cm^{-1} and 198.9 cm^{-1} respectively) is out of the scale in these plots. We see that the energy transferred into the solvent tends to be bigger as the frequency of

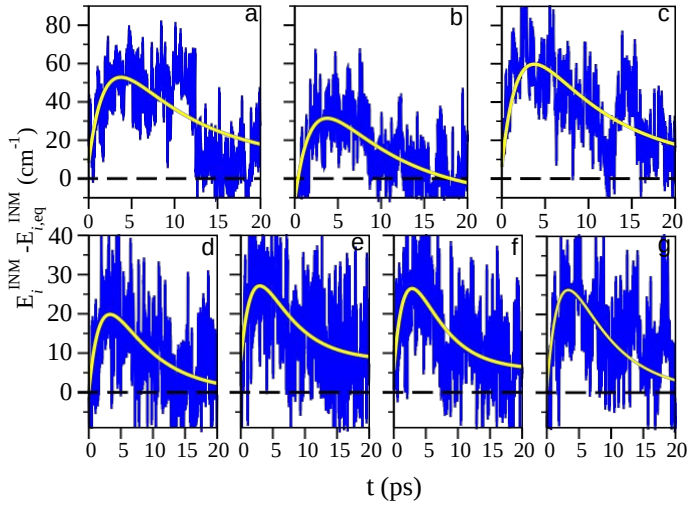

Figure 3.73: Time evolution of the vibrational energy (in cm^{-1}) of the (a) acend CH bending, (b) amend CH bending, (c) $C_\beta H$ bending, (d) 30th, (e) 31st, (f) 32nd and the (g) 33rd INMs (blue lines) and the fits to Eq. (3.14) (yellow lines) following the initial excitation of the amend amide I mode.

the INM is smaller. As a guide we have included dashed line which correspond to the average energies transferred by every mode into the solvent obtained as (1638.2/60≈27.3 cm^{-1}) for the acend and (1685.3/60≈28.1 cm^{-1}) for the amend amide I modes. As seen the contribution of the lower frequency INMs are all over the average value while the contributions of the higher frequency modes are always under it. This is the same behavior that we have observed in our previous study of the relaxation of the amide I mode of the

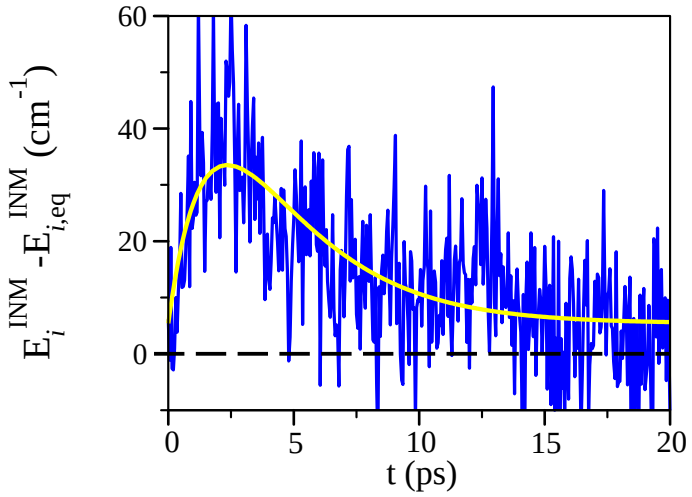

Figure 3.74: Time evolution of the vibrational energy (in cm^{-1}) of the 27th INM (blue line) and the fit to Eq. (3.14) (yellow line) following the initial excitation of the acend amide I mode.

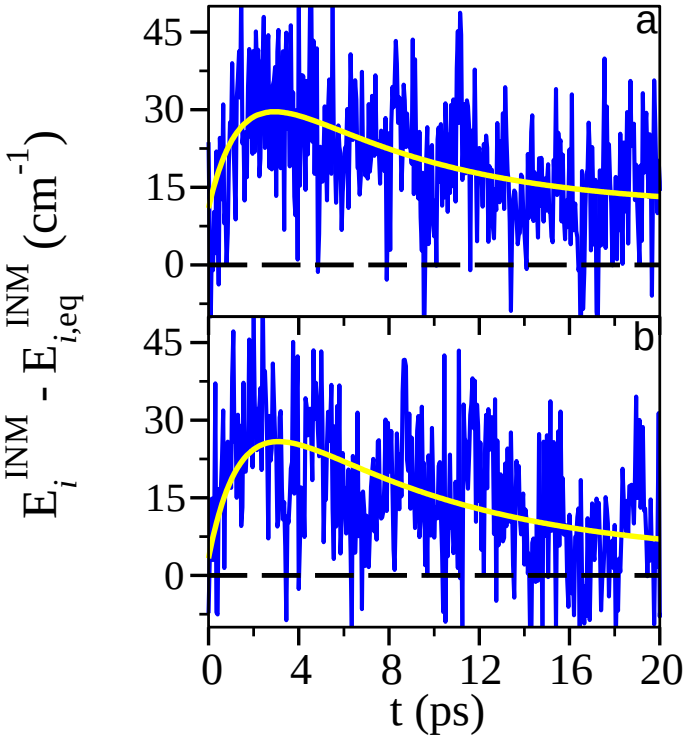

Figure 3.75: Time evolution of the vibrational energy (in cm^{-1}) of the (a) 25th and (b) 26th INMs (blue lines) and the fits to Eq. (3.14) (yellow lines) following the initial excitation of the amend amide I mode.

NMAD molecule citeMiguel:11 where we obtained that the low frequency modes act as doorways for the intermolecular energy flow into the solvent. Apart from the general trends we observe few mid-frequency modes which significant energy flows into the solvent as the 25th and 30th INMs in the acend amide I relaxation and the 22nd INM in the amend case. We note that these INMs are highly excited during the relaxation process as previously discussed.

3.3.8 Comparison of the relaxation pathways

We consider now the comparison between the relaxation pathways obtained for the AlaD-d_2 and the ^{13}C-AlaD-d_2 molecules. The overall relaxation times of both amide I modes are larger for the ^{13}C-AlaD-d_2 molecule as we can see in Table 3.34 and Table 3.39. This is a direct consequence of the isotopic substitution that shifts ~45 cm^{-1} the frequency of the acend amide I mode. In the ^{13}C-AlaD-d_2 the two amide I modes are off resonance and therefore the ultrafast resonant relaxation channel that we find in the AlaD-d_2 molecule is absent in the ^{13}C-AlaD-d_2 one. Moreover, the overlap of the two amide I modes is smaller in the ^{13}C-AlaD-d_2 molecule as we can see in Table 3.42 where we include the atomic contribution of the carbon and oxygen atoms of the carbonyl groups to both amide

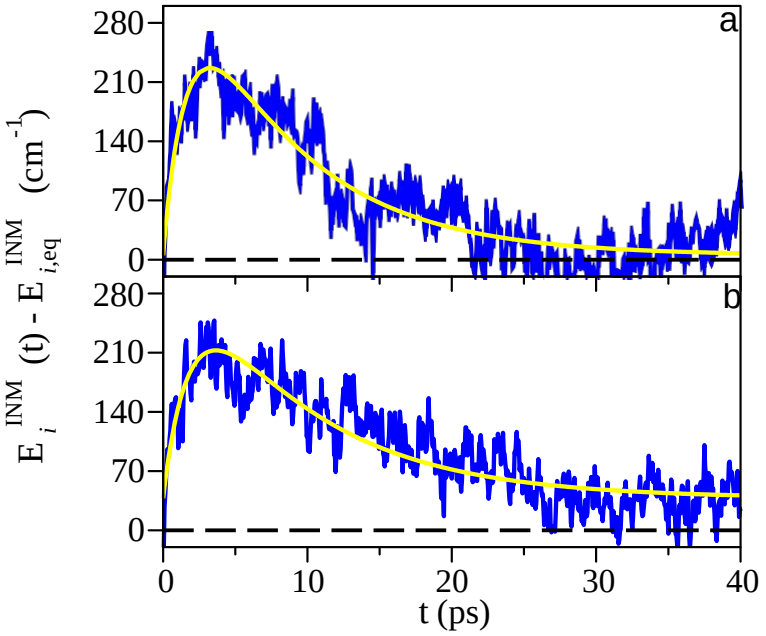

Figure 3.76: Time evolution of the sum of the vibrational energy of the 49th-60th INMs after the initial excitation of the (a) acend and (b) amend amide I modes (blue lines). The fits to Eq. (3.14) are also shown (yellow lines).

Table 3.42: Atomic displacement contributions (in %) of the carbonyl groups to the definition of the amide I INMs of the AlaD-d_2 /^{13}C-AlaD-d_2 molecules in solution.

	amide I mode	
carbonyl group	acend	amend
acend	81.2/88.7	10.4/0.4
amend	9.6/0.6	74.1/83.5

I modes. As seen the two amide I modes are more localized in the ^{13}C-AlaD-d_2 molecule and the cross contributions are significantly smaller. The disappearance of the ultrafast resonant channel is the main reason for the increase of the overall relaxation lifetime that we observe in the ^{13}C-AlaD-d_2 molecule with respect to the AlaD-d_2 molecule.

The frequency shift also modifies the resonance condition of the acend amide I mode with the remaining INMs. We find an excellent example in the important role played by the 31st INM in the relaxation of the AlaD-d_2 molecule that moves into the 30th in the ^{13}C-AlaD-d_2 molecule. As expected these decays also modify the acend amide I relaxation lifetime what explains why these quantities are quite different in both molecules. On the contrary the isotopic substitution has a comparatively small effect on the relaxation pathways of the amend amide I mode, apart from the lack or energy flow with the other amide I mode. The relaxation lifetimes are slightly increased after the isotopic substitution

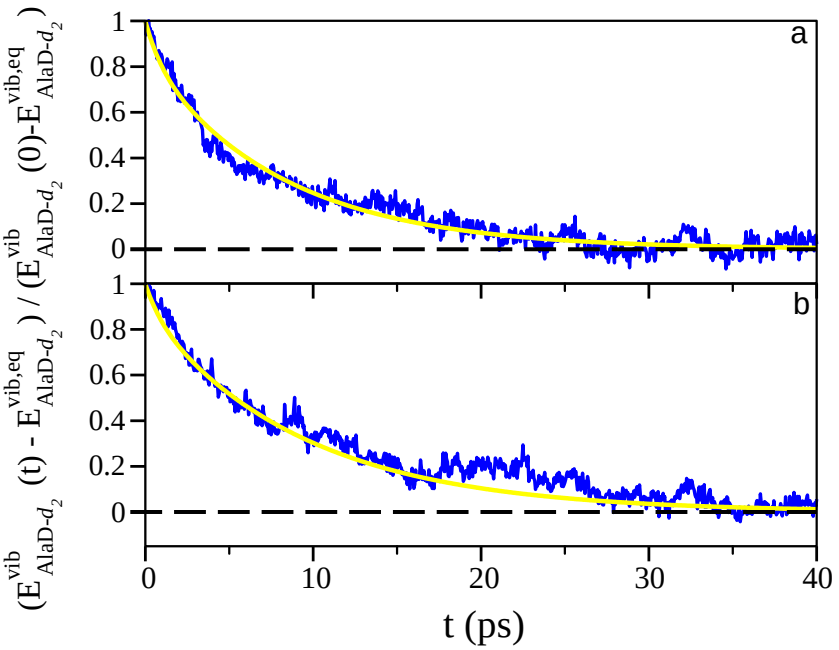

Figure 3.77: Time evolution of the normalized vibrational energy of the ^{13}C-AlaD-d_2 molecule in liquid D_2O following the initial excitation of the (a) acend and (b) amend amide I modes (blue lines) and the fits to Eq. (3.15) (yellow lines).

(see Table 3.34 and Table 3.39) probably because of small frequency shifts of some INMs participating in the IVR mechanism. Anyway, the most significant patterns remain as the strong 2:1 Fermi resonance with the 22nd INM.

3.3.9 Dihedral angle distributions

It is known that the conformational equilibrium of the peptides is sensitive to the environmental conditions [Daggett 92, Takekiyo 04]. Therefore it is interesting to analyze if the conformational distribution of the AlaD-d_2 molecule is modified during the amide I relaxation process. In particular we have considered the case of the relaxation of the acend amide I mode of the AlaD-d_2 molecule. As discussed in Section 3.3.4 the AlaD-d_2 molecule has equilibrium populations of 58.5% and 41.5% in the alpha R and beta regions respectively (see Table 3.29).

In order to have a significant statistics we have considered 2660 relaxation trajectories where the conformations were averaged at 0.25 ps intervals. The results are shown in Figure 3.79 where we can see that the population of the alpha R region conformers decreases and consequently the population of the beta region conformers increases smoothly during the first 40 ps. The initial populations change during that time interval from the initial 58.5%/41.5% ratio to the 55%/45% one. Interestingly the minimum values are reached approximately in the same time that the AlaD-d_2 molecule requires to transfer all its excess energy into the solvent (see Figure 3.65). For longer times the population of the alpha R

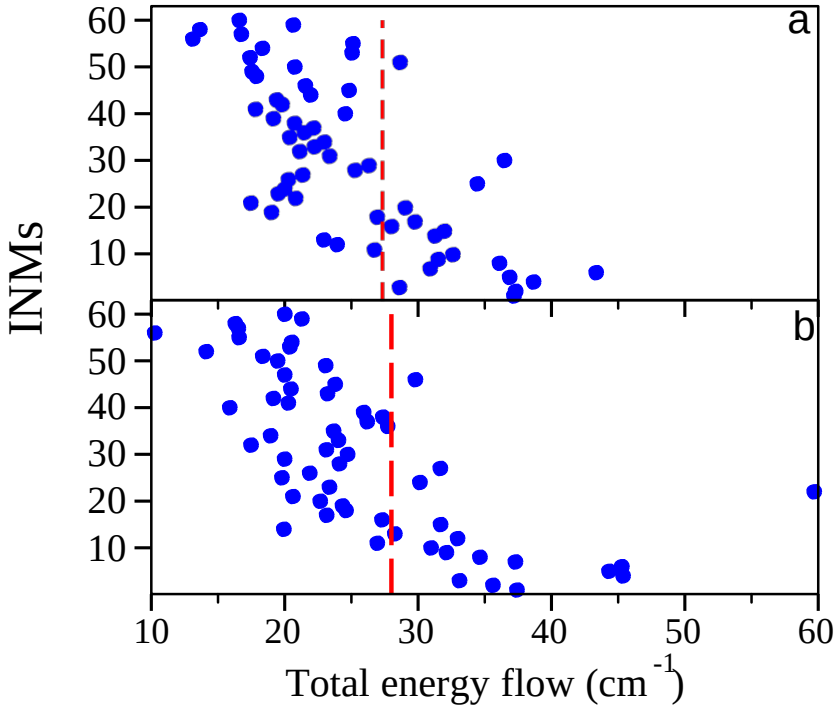

Figure 3.78: Vibrational energy (in cm^{-1}) transferred from the INMs of the ^{13}C-AlaD-d_2 molecule into the solvent calculated using the SMF method following the initial excitation of the (a) acend and (b) amend amide I modes. Dashed lines indicate the average energy transfer.

region conformers increase and the molecule returns to the conformational equilibrium populations at 60 ps.

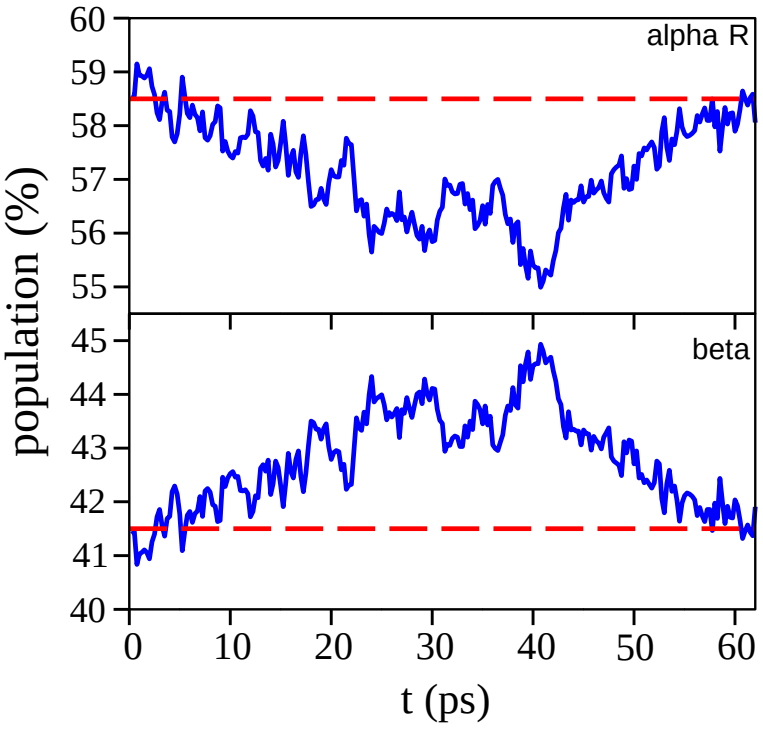

Figure 3.79: The conformational distribution (in %) as a function of time (averaged over 0.25 ps intervals) of the AlaD-d_2 molecule as extracted from the nonequilibrium MD simulations when the acend amide I was initially excited (blue lines) and the conformational equilibrium values (dash red lines).

CHAPTER 4

Conclusions

In the present thesis we have investigated the infrared spectra of solvated NMA using molecular dynamics simulations in which the electronic Hamiltonian of the whole solute-solvent system is described by a semiempirical quantum mechanical method. Further analysis has been performed for describing in details to what extent the electrostatic interaction, polarization, charge transfer affect the position of the amide I band. We have also performed nonequilibrium MD simulations of the vibrational relaxation dynamics of two different peptide model the *N*-methylacetamide (NMA) molecule (monopeptide model) and the alanine dipeptide (AlaD) molecule (dipeptide model) in water solution and used the INMs to analyze the energy flows created by the relaxation of the amide I mode through the rest of the molecule modes. The main conclusions derived from our study are:

First: We have carried out a study of the infrared spectrum of *N*-methylacetamide (NMA) using a recently developed method in the group of Nancy, based on the Born-Oppenheimer approximation at a semiempirical level of quantum chemistry (SEBOMD). We focused on the solvent effect on the infrared spectrum of the solute, its geometry, and its electrostatic properties. We have identified the infrared bands that are more significant as signatures of the peptide bond (amide I, II and III and the N-H stretch) and we have also evaluated their corresponding solvent shifts. We have found a satisfying agreement between our model and experimental measurements, not only for the solvent shift but also for the structure and electrostatic properties of the solute. On the other hand, when a molecular mechanics, nonpolarizable force field is used to run MD, very little or nil solvent effect is observed. This finding stresses the importance of a correct description of electronic properties (polarization, charge transfer, etc) for an adequate molecular modeling of absorption spectra in solution.

Second: We have proposed a method to relate the solvent-induced shift of the amide I band of a model peptide to the different terms arising from the solute-solvent interaction energy decomposition. We have performed our analysis for different NMA-water complexes. We always found that the largest contribution to the total shift comes from the deformation term with a little contributions from the electrostatic and charge transfer terms. However

the polarization term has only a minor contribution. Furthermore, we have observed that due to the charge flux from NMA to water, the sign of the charge transfer force constant changes.

Third: We have adapted the Min-Cost algorithm to used to identify the INMs using the ENMs as templates to study flexible biomolecules. We have proposed the definition of an overlap matrix between both sets of normal modes based on their certain components. The resulting Effective Atomic Min-Cost algorithm was shown to provide robust identifications of the INMs which do not depend on the set of ENMs used as templates.

Fourth: We have developed the so-called Statistical Minimum Flow (SMF) method to analyze the vibrational energy flow in relaxation process of molecules in solution. The SMF method relies in the study of the knowledge of the time evolution of the energy stored in the vibrational modes, thereby requiring the performance of an INM analysis to express the total internal energy of the molecule as the sum of the individual INM contributions. Its application thus provides the amount of energy that flow between the vibrational modes of the molecule and also to the solvent, under the basic assumptions that the total energy exchanged between the modes is minimum and the distribution of the energy is essentially statistical. It has been shown that the accumulated energy that flows between any pair of INM modes is well reproduced by first order exponential functions containing two parameters that provide the total energy transferred and the lifetime of the process. This supports the interpretation of the relaxation process provided by the master equation. The SMF methods is well suited to the use of the input data provided by standard MD packages and can be applied as well to the analysis of experimentally measured time dependent populations of the vibrational modes.

Fifth: We have tested the SMF method by considering the relaxation of the amide I mode of NMAD in D_2O solution previously studied by our group in Murcia using the INM methodology. We have shown that the SMF method is able to quantify the relative magnitude of the IVR and intermolecular relaxation channels taking place after relaxation of the amide I mode, and the cooling of the solute by energy transfer to the solvent. The SMF method confirms the vibrational decay of the amide I mode is mainly IVR with a little energy transfer into the solvent. In addition it provides further insights into the time scale and the magnitudes of the pathways involved in the relaxation process.

Sixth: We have studied the vibrational relaxation dynamics of the NMAD amide I mode in liquid D_2O using the INMs of the NMAD molecule to analyze the energy flows through the rest of the NMAD modes, and thus elucidate the relaxation mechanism that control the whole process. This study has been performed using nonequilibrium MD simulations in which the electronic Hamiltonian of the whole solute-solvent system is described by a semiempirical quantum mechanical method, SEBOMD. The main scope of this study was to show to what extent the relaxation process could be affected by incorporating explicity the polarization and the charge transfer effects into the potential surface. The results obtained show that the inclusion of the quantum electronic Hamiltonian modifies notably the dynamics of the vibrational relaxation of the amide I mode, which turns out to be faster than that obtained using MM and QM/MM force fields in better agreement

with experiments. We have also identified and described the IVR relaxation pathways that follow the relaxation of the amide I mode. As a general remark our analysis showed that although introducing the electronic Hamiltonian for the whole system allows a better agreement with experiment, the relaxation pathways are not significantly modified from those derived using the MM and QM/MM force fields.

Seventh: We have performed nonequilibrium MD simulations of the vibrational relaxation dynamics of the AlaD-d_2 amide I modes. The AlaD-d_2 molecule provides a different situation from the NMAD due to its flexibility and the presence of two amide I groups one in the acetyl end (acend) and the other in the amino end (amend). The vibrational decay of the amide I modes shows that the relaxation of the amend amide I mode is faster than the acend amide I mode. Moreover, we confirmed that the relaxation of the amide I modes is essentially an intramolecular vibrational redistribution process. We have identified and described the relaxation pathways that follows the relaxation of the amide I modes. Interestingly, both amide I modes provide different pathways. The fastest relaxation channel is associated with a rapid exchange of vibrational excitation between the acend amide I mode initially excited and amend amide I mode and vice versa. The slower mechanisms are funneled through specific mid-range and high frequency modes.

Eighth: We have analyzed the vibrational energy relaxation of the two amide I modes using the isotopic substitution of the acend carbonyl group $^{12}C{=}O$ with $^{13}C{=}O$ following the experimental work in the literature. We showed that the amide I modes relaxation lifetimes are in a reasonable agreement with the experiment. In addition we detected that the relaxation process does not change significantly compared to the AlaD-d_2 molecule. However, we found no energy exchange between the amide I modes as has been observed in the AlaD-d_2 molecule.

Ninth: We have analyzed the conformational distribution of the AlaD-d_2 molecule as obtained from equilibrium and during the amide I relaxation process. We observed that the relative population of alpha R and beta region is modified in the nonequilibrium condition. We also note that although the AlaD-d_2 molecule lost all the excess energy in less than 40 ps, the AlaD-d_2 molecule require 60 ps to reach the conformational equilibrium populations.

CHAPTER 5

Resumen

Cuando se excita una proteína mediante la formación de enlace con un ligando, la complejación con ATP o un pulso láser, tiene lugar a continuación un proceso de relajación de energía vibracional (VER) [Leitner 10b]. La energía depositada inicialmente en una región localizada de la proteína fluye hacia el resto de la misma y hacia al disolvente que la rodea [Kong 09b]. Los procesos VER en péptidos ocupan por tanto un papel central en la comprensión de los mecanismos biológicos de transferencia de energía vibracional y en las reacciones químicas de las proteínas. La dinámica vibracional inducida por las fluctuaciones estructurales de los átomos del entorno afecta de forma fundamental a las velocidades, los mecanismos y las eficiencias de las reacciones en disolución [Gruebele 04]. El desarrollo de un marco teórico preciso de la relajación de energía vibracional de proteínas en disolución es esencial para la comprensión general de la dinámica de las proteínas [Dian 02] y en particular para la simulación de los procesos de plegamiento que están íntimamente relacionados con su funcionalidad [Mohammed 09, Peng 10].

El reciente desarrollo experimental de las espectroscopías ultrarápidas de infrarrojo (IR) y Raman de proteínas en disolución ha puesto de manifiesto las tremendas posibilidades que estos métodos ofrecen en la determinación de las estructuras y la dinámica conformacional de moléculas de interés biológico [Fayer 09]. Las proteínas tienen espectros vibracionales que contienen información importante sobre su estructura. Las estructuras secundarias de las proteínas, en particular, son elementos primordiales que determinan los campos de fuerzas y por tanto los espectros de las bandas amida, que tienen su origen en los movimientos de los átomos peptídicos. Por esta razón el espectro vibracional de la banda amida I, que proviene fundamentalmente de los desplazamientos de tensión de los enlaces C=O de la estructura peptídica con contribuciones de los movimientos de los enlaces CN y NH, ha sido ampliamente utilizado como indicador de la estructura secundaria de las proteínas [Hamm 98]. Las proteínas que contienen mayoritariamente láminas beta dan, por ejemplo, bandas de la amida I a frecuencias menores que las de las proteínas en las que dominan las hélices alfa.

Las transiciones de la amida I son ideales en espectroscopía infrarroja ya que el mo-

mento dipolar varía fuertemente en ellas y son claramente distinguibles de las transiciones vibracionales asociadas a la cadena de aminoácidos. De hecho, se asume habitualmente que el subespacio vibracional de la amida I está desacoplado de los restantes modos vibracionales de la proteína. Su intensidad Raman visible es moderada mientras que su resonancia Raman-UV es, en general, débil. Dependiendo del disolvente y del entorno del péptido, la banda aparece en la región comprendida entre 1610 y 1700 cm-1, lo que refleja una fuerte dependencia con los enlaces por puente de hidrógeno aceptores y dadores hacia los grupos carbonilo y NH, respectivamente. Si se utiliza agua como disolvente, la banda de la amida I se mezcla con los modos angulares de las moléculas de agua que constituyen la correspondiente esfera de hidratación del péptido. Sin embargo este efecto y la contaminación con el enlace NH queda eliminados si se utiliza agua deuterada D_2O en lugar de H_2O como disolvente.

Aunque los espectros infrarrojos de la amida I de proteínas con diferentes estructuras difieren, estos espectros no muestran picos diferenciados para los diversos modos amida I que constituyen conjuntamente la banda amida I. Los mecanismos de ensanchamientos homogéneo e inhomogéneo difuminan el espectro, dando lugar a una banda relativamente ancha con una débil subestructura en forma de picos poco pronunciados. Las técnicas de aumento de resolución como la consideración de la segunda derivada o la deconvolución del espectro no resuelven este problema. Debido a ello se han desarrollado espectroscopías infrarrojas no lineales para obtener información adicional relativa a la composición de las vibraciones amida I en péptidos [DeCamp 05, Hamm 98, Fang 09, Fayer 09, Schade 09b, Bagchi 09]. Estos estudios han proporcionado información directa sobre aspectos como la escala temporal del proceso de relajación [DeCamp 05, Hamm 98], la eficiencia del transporte de energía vibracional [Schade 09b] y, más recientemente, sobre los mecanismos de relajación [Shigeto 07, Fang 09]. Estos trabajos experimentales son impresionantes, si bien sigue siendo difícil extraer información detallada sobre la relajación vibracional únicamente a partir de dichas medidas experimentales.

Las aproximaciones teóricas, incluyendo las simulaciones a escala atómica, pueden proporcionar una información más detallada. A su vez, los datos experimentales pueden utilizarse para refinar los métodos de simulación y los campos de fuerza empíricos. Esta combinación de estudios experimentales y teóricos sobre la estructura y las dinámica de proteínas esta actualmente empezando a alcanzar su plenitud. Conforme se desarrollen nuevos estudios experimentales y aumente la precisión de los cálculos teóricos, cabe esperar que esta relación sea todavía más fructífera. Desde un punto de vista teórico, la aplicación de métodos sistemáticos para el estudio de grandes moléculas, como las biológicas, se ha transformado en un todo un reto ya que no solo hace falta una mayor potencia de cálculo, sino que también, y mucho más importante, hay que desarrollar los conceptos y técnicas necesarios para extraer la información física de dichos cálculos.

Algunos aspectos de la relajación de energía vibracional en proteínas y péptidos pueden explicarse mediante fórmulas perturbativas basadas en la condición de equilibrio [Fujisaki 05, Fujisaki 08], pero la aplicabilidad de estos tratamientos perturbativos es demasiado restrictiva como para describir de forma general la dinámica de proteínas en disolución

a temperatura ambiente, especialmente cuando el proceso de relajación transcurre mediante sucesivas etapas elementales. Las simulaciones fuera del equilibrio aparecen entonces como la herramienta adecuada para elucidar la dinámica de los procesos de relajación vibracional. En este caso la descripción cuántica de todos los grados de libertad vibracionales resulta computacionalmente prohibitiva, incluso para los péptidos más sencillos. El uso de diversas aproximaciones puede aliviar este problema, pero es difícil garantizar la calidad de las mismas a partir de los resultados que proporcionan [Fujisaki 05]. En contrapartida, las simulaciones de Dinámica Molecular clásica permiten abordar sistemas formados por miles de átomos como los formados por proteínas y péptidos en disolución.

Aunque la utilización de la dinámica clásica para la descripción de las vibraciones cuya frecuencia es mucho mayor que la energía térmica a temperatura ambiente puede ser cuestionable debido a la naturaleza cuántica de dichas vibraciones, las simulaciones realizadas hasta ahora han sido capaces de proporcionar tiempos de relajación realistas [Nguyen 03, Bu 03b]. Sorprendentemente, el principal problema de las simulaciones de Dinámica Molecular clásicas es el análisis de los flujos energéticos que tiene lugar fundamentalmente en el interior de la molécula peptídica inicialmente excitada, en lo que se denomina proceso de redistribución de energía vibracional intramolecular (IVR). Los acoplamientos entre los diferentes modos vibracionales se intensifican durante la relajación debido a que la molécula explora regiones del espacio de fases muy alejadas de su geometría de equilibrio y a que tienen lugar, además, fuertes interacciones intermoleculares con las moléculas de disolvente. La aproximación tradicional de los modos normales de equilibrio (ENM) falla entonces, lo que impide la determinación de la cantidad de energía que se deposita en cada modo vibracional. Aunque se han desarrollado algunas aproximaciones teóricas para resolver este problema [Stratt 01, Nguyen 03, Moritsugu 04], no existe todavía ningún método teórico sistemático que permita determinar los flujos de energía vibracional en función del tiempo. Dicho método debería ser capaz de establecer los mecanismos de relajación vibracional, el papel que desempeñan las moléculas del disolvente y las escalas temporales de las diferentes transferencias de energía intra e intermoleculares que ocurran, situando de este modo a las simulaciones teóricas al mismo nivel de los métodos experimentales más recientes [Shigeto 07, Fang 09].

En la presente tesis hemos investigado el espectro de infrarrojo de la molécula *N*-metilacetamida (NMA) solvatada con agua utilizando simulaciones de Dinámica Molecular en las que el Hamiltoniano electrónico del sistema completo soluto-disolvente se describe mediante un método mecanocuántico semiempírico. Mediante un novedoso procedimiento hemos analizado en detalle en que medida las interacciones electrostáticas, la polarización y lo efectos de transferencia de carga afectan a la posición de la banda amida I. Así mismo hemos realizado simulaciones de Dinámica Molecular de no equilibrio de la dinámica de relajación de dos moléculas peptídicas modelo: la *N*-metilacetamida (modelo monopeptídico) y el dipéptido alanina (modelo dipeptídico) en solución acuosa utilizando los Modos Normales Instantáneos (INM) para analizar los flujos de energía creados por la relajación del modo amida I hacia el resto de los modos de la molécula y el disolvente. Las principales conclusiones presentadas en este trabajo de tesis son:

Primera. Hemos realizado un estudio del espectro de infrarrojo de la molécula NMA utilizando el método SEBOMD recientemente desarrollado por el grupo de Nancy basado en una aproximación de tipo semiempírico del Hamiltoniano del sistema. Hemos analizado en detalle el efecto del disolvente sobre el espectro de infrarrojo del soluto, su geometría y sus propiedades electrostáticas. Hemos identificado las bandas de infrarrojo que están más directamente relacionadas con el enlace peptídico (amida I, II y III y la tensión N-H) y evaluado los correspondientes desplazamientos de las frecuencias inducidos por la presencia del disolvente. Hemos encontrado un acuerdo satisfactorio entre los resultados derivados de nuestro modelo y las medidas experimentales tanto para los desplazamientos de las frecuencias como para la estructura y las propiedades electrostáticas de la molécula de soluto. Por el contrario, hemos demostrado que cuando se utiliza un campo de fuerzas de Mecánica Molecular no polarizable se observa un efecto del disolvente casi o totalmente despreciable. Esta conclusión refuerza la importancia de la realización de una descripción correcta de las propiedades electrostáticas (polarización, transferencia de carga, etc) para obtener un modelado adecuado del espectro de absorción de péptidos en disolución.

Segunda. Hemos propuesto un método para relacionar los desplazamientos de frecuencia inducidos por el disolvente en el modo amida I de una molécula peptídica con los diferentes términos provenientes de la descomposición de la interacción soluto-disolvente. Hemos aplicado nuestro análisis a diferentes complejos NMA-agua y siempre hemos encontrado que la máxima contribución al desplazamiento proviene del término de deformación con pequeñas contribuciones de los términos electrostáticos y de transferencia de carga mientras que el término de polarización solo tiene una contribución menor. También hemos observado que el signo de la contribución de la transferencia de carga a la constante de fuerza es negativa debido al flujo de carga desde la molécula de NMA hacia las de agua.

Tercera. Hemos adaptado el algoritmo Min-Cost utilizado para identificar los INM utilizando los Modos Normales de Equilibrio (ENM) como patrón al estudio de biomoléculas flexibles. Hemos propuesto la definición de una matriz de solapamiento entre ambos conjuntos de modos normales basada en sus componentes cartesianas. Hemos mostrado que el método resultante denominado algoritmo Min-Cost Atómico Efectivo proporciona una identificación fiable de los INM y no depende fundamentalmente del conjunto de ENM utilizados como patrón.

Cuarta. Hemos desarrollado el denominado método del Mínimo Flujo Estadístico (SMF) para analizar los flujos de energía vibracional en procesos de relajación de moléculas en disolución. El método SMF necesita disponer de la evolución temporal de la energía almacenada en cada modo vibracional y por tanto requiere la realización precia del análisis INM para expresar la energía interna total de la molécula como suma de contribuciones individuales de cada INM. Su aplicación proporciona entonces la cantidad de energía que fluye entre los modos vibracionales de la molécula de soluto y también hacia el disolvente bajo las hipótesis de que la energía total intercambiada entre los modos es mínima y que la distribución de la energía es básicamente estadística. Hemos demostrado que la energía acumulada que fluye entre cualquier par de modos INM puede ajustarse correctamente a una función exponencial de primer orden dependiente de dos parámetros que proporcio-

nan la energía total transferida y el tiempo de vida media del proceso. El método SMF puede aplicarse fácilmente utilizando los datos proporcionados por los paquetes estándar de Dinámica Molecular y también puede utilizarse para analizar las medidas experimentales de las poblaciones vibracionales dependientes del tiempo.

Quinta. Hemos comprobado la fiabilidad del método SMF mediante su aplicación a la relajación del modo amida I de la molécula NMAD disuelta en D_2O que fue previamente estudiado por nuestro grupo utilizando la metodología INM. Hemos demostrado que el método SMF es capaz de cuantificar la magnitud relativa de los canales de relajación intra e intermolecular tras la excitación del modo amida I y el subsiguiente proceso de enfriamiento de la molécula de soluto mediante la transferencia de energía hacia el disolvente. El método SMF confirma que la relajación del modo amida I es fundamentalmente un proceso intramolecular mientras que la transferencia de energía directamente hacia el disolvente juega un papel menor en este caso. Además hemos demostrado como el método SMF proporciona información detallada sobre la magnitud de los diversos mecanismos de relajación así como de la escala temporal en que se desarrollan.

Sexta. Hemos estudiado la dinámica de relajación vibracional del modo amida I de la molécula NMAD disuelta en D_2O utilizando los INM de la molécula de soluto para analizar los flujos de energía hacia los restantes modos de la molécula y así resolver el mecanismo de relajación que controlo el proceso. Este estudio ha sido realizado mediante simulaciones de Dinámica Molecular de no equilibrio en las que el Hamiltoniano electrónico del sistema completo soluto-disolvente se describió utilizando un método mecanocuántico semiempírico (SEBOMD) desarrollado por el grupo de Nancy. El principal objetivo de dicho estudio era comprobar hasta que punto la incorporación explicita de los efectos de polarización y de transferencia de carga en la superficie de energía potencial afectaba al proceso de relajación del modo amida I. Los resultados obtenidos demuestran que la utilización del Hamiltoniano electrónico cuántico modifica notablemente la dinámica del proceso que resulta ser más rápida que cuando se utilizan campos de fuerza de Mecánica Molecular (MM) o QM/MM en los que la descripción cuántica se reserva exclusivamente para el disolvente. Así mismo los resultados presentados muestran una mejor concordancia con las medidas experimentales. También hemos identificado y descrito los canales de transferencia intramolecular si bien resulta interesante destacar que la utilización de un Hamiltoniano electrónico cuántico para el sistema completo no modifica sustancialmente los caminos de relajación respecto a los obtenidos mediante el uso de campos de fuerza MM o QM/MM.

Séptima. Hemos realizado simulaciones de no equilibrio de la relajación vibracional del modo amida I de la molécula alanina dipéptido deuterada (AlaD-d_2). Esta molécula constituye un modelo bien diferenciado de la molécula NMA debido a su flexibilidad y a la presencia de dos modos amida I en los extremos acetílico y amídico. Los resultados de nuestras simulaciones establecen que el proceso de relajación de estos dos modos es esencialmente intramolecular y que el canal más rápido corresponde a la transferencia resonante de energía entre ambos modos amida I mientras que la transferencia a combinaciones de modos de media y baja frecuencia resulta ser sustancialmente más lenta.

Octava. Hemos analizado la relajación de los modos amida I en la molécula AlaD en la que se sustituyó el grupo $^{12}C{=}O$ del extremo acetilo por un grupo $^{13}C{=}O$ siguiendo los trabajos experimentales previos. La sustitución isotópica modifica la frecuencia de uno de los modos amida I de modo que el proceso de transferencia resonante desaparece. Hemos obtenido tiempos de relajación para ambos modos en razonable acuerdo con las medidas experimentales y también hemos identificado los canales de relajación a través de combinaciones de modos de media y baja frecuencia que resultan ser similares a los derivados previamente para la molécula $^{12}C{=}O$-AlaD.

Novena. Hemos analizado la distribución conformacional de la molécula AlaD obtenida en simulaciones de equilibrio y durante el proceso de relajación del modo amida I. Hemos observado que las poblaciones relativas de los confórmeros de las regiones alfa R y beta cambian durante el proceso de relajación respecto a sus valores de equilibrio. Resulta interesante destacar que la distribución conformacional retorna al equilibrio más lentamente que el proceso de transferencia intramolecular de energía hacía el disolvente.

References

[Ackels 09] L. Ackels, P. Stawski, K. E. Amunson and J. Kubelka. *On the temperature dependence of amide I intensities of peptides in solution*. Vib. Spectrosc., vol. 50, page 2, 2009.

[Ahlborn 99] H. Ahlborn, X.D. Ji, B. Space and P.B. Moore. *A combined instantaneous normal mode and time correlation function description of the infrarred vibrational spectrum of ambient water*. J. Chem. Phys., vol. 111, pages 10622–10632, 1999.

[Alexander 04] D. Alexander, Alan Grossfield and Rohit V. Pappu. *Role of Solvent in Determining Conformational Preferences of Alanine Dipeptide in Water*. Journal of the American Chemical Society, vol. 126, no. 8, pages 2574–2581, 2004.

[Allen 87] M. P. Allen and D. J. Tildesley. Computer simulation of liquids. Oxford Science Publications. Oxford, 1987.

[Andersen 80] H. C. Andersen. *Molecular dynamics simulations at constant pressure and/or temperature*. J. Chem. Phys., vol. 72, page 2384, 1980.

[Anderson 54] P. W. Anderson. *A mathematical model for the narrowing of the spectral lines by exchange or motion*. J. Phys. Soc. Jpn, vol. 9, page 316, 1954.

[Andrushchenko 09] V. Andrushchenko, P. Matějka, D. T. Anderson, J. Kaminský, J. Horník, L. O. Paulson and P. Bouř. *Solvent Dependence of the N-Methylacetamide Structure and Force Field*. J. Phys. Chem. A, vol. 113, page 9727, 2009.

[Ataka 84] S. Ataka, H. Takeuchi and M. Tasumi. *Infrared studies of the less stable cis form of n-methylformamide and n-methylacetamide in low-temperature nitrogen matrices and vibrational analyses of the trans and cis forms of these molecules*. J. Mol. Struct., vol. 113, pages 147–160, 1984.

[Bagchi 09] S. Bagchi, A.K. Charnley, A.B. Smith and R.M. Hochstrasser. *Equilibrium Exchange Processes of the Aqueous Tryptophan Dipeptide*. J. Phys. Chem. B, vol. 113, pages 8412–8417, 2009.

[Balázs 90] A. Balázs. *Ab initio study of the force field and vibratioanl assignemnt of the N-acetyl-N-methylalaninamide*. J. Phys. Chem., vol. 94, page 2754, 1990.

[Bastida 10a] Adolfo Bastida, Miguel A. Soler, Jose Zuñiga, Alberto Requena, Adrian Kalstein and Sebastian Fernandez-Alberti. *Instantaneous normal modes, resonances, and decay channels in the vibrational relaxation of the amide I mode of N-methylacetamide-D in liquid deutrated water*. J. Chem. Phys., vol. 132, page 224501, 2010.

[Bastida 10b] Adolfo Bastida, Miguel A. Soler, Jose Zuñiga, Alberto Requena, Adrian Kalstein and Sebastian Fernandez-Alberti. *Molecular dynamics Simulations and Instantaneous normal mode analysis of the vibrational relaxation of the C-H stretching modes of N-methyl acetamide-d in liquid deutrated water*. J. Phys. Chem. A, vol. 114, pages 11450–11461, 2010.

[Bastida 12] Adolfo Bastida, Miguel A. Soler, Jose Zuñiga, Alberto Requena, Adrian Kalstein and Sebastian Fernandez-Alberti. *Hybrid Quantum/Classical Simulations of the Vibrational Relaxation of the Amide I Mode of N-methylacetamide in D2O solution*. J. Phys. Chem. B, vol. 116, page 2969, 2012.

[Bekker 96] H. Bekker. *Molecular Dynamics Simulation Methods Revised*. PhD thesis, Rijksuniversiteit Groningen, 1996.

[Berenal-Uruchurtu 00] M. I. Berenal-Uruchurtu, M. T. C. Martins-Costa, C. Millot and M.F. Ruiz-López. *Improving Description of Hydrogen bonds at the semiempirical level: Water-Water interaction as Test case*. J. Comput. Chem., vol. 21, pages 572–581, 2000.

[Berendsen 84] H. J. C. Berendsen, J. P. M. Postma, W. F. van Gunsteren, A. DiNola and J. R. Haak. *Molecular dynamics with coupling to an external path*. J. Chem. Phys., vol. 81, page 3684, 1984.

[Berendsen 87] H. J. C. Berendsen, J. R. Grigera and T. P. Straatsma. *The missing term in effective pair potentials*. J. Phys. Chem., vol. 91, page 6269, 1987.

[Berens 81] P. H. Berens and K. R. Wilson. *Molecular Dynamics and spectra . I. Diatomic rotation and vibration.* J. Chem. Phys., vol. 74, page 4872, 1981.

[Besley 04] N. A. Besley. *Ab Initio Modeling of Amide Vibrational Bands in Solution*. J. Phys. Chem. A, vol. 108, page 10794, 2004.

[Bloem 08] R. Bloem, R. G. Dijkstra, T. C. Jansen and J. Knoester. *Simulation of vibrational energy transfer in two-dimensional infrared spectroscopy of amide I and amide II modes in solution*. J. Chem. Phys., vol. 129, page 055101, 2008.

[Boehm 91] H. J. Boehm and S. Brode. *Ab initio SCF calculations on low-energy conformers of N-acetyl-N'-methylalaninamide and N-acetyl-N'-methylglycinamide*. J. Am. Chem. Soc., vol. 113, no. 19, pages 7129–7135, 1991.

[Bouř 03] P. Bouř and T. A. Keiderling. *Emperical modeling of the peptide amide I band IR intensity in water solution*. J. Chem. Phys., vol. 119, page 11253, 2003.

[Bu 03a] L. Bu and J. E. Straub. *Vibrational Frequency Shifts and Relaxation Rates for a Selected Vibrational Mode in Cytochrome c*. Biophys. J., vol. 85, pages 1429–1439, 2003.

[Bu 03b] L.T. Bu and J. E. Straub. *Simulating vibrational energy flow in proteins: Relaxation rate and mechanism for heme cooling in cytochrome c*. J. Phys. Chem. B, vol. 107, pages 12339–12345, 2003.

[Buchner 92] M. Buchner, B. Ladanyi and R. M. Stratt. *The short-time dynamics of molecular liquids. Instantaneous normal mode theory*. J. Chem. Phys., vol. 97, pages 8522–8535, 1992.

[Cances 98a] E. Cances and B. Mennucci. *Analytical derivatives for geometry optimization in solvation continuum models. I. Theory*. J. Chem. Phys., vol. 109, page 249, 1998.

[Cances 98b] E. Cances and B. Mennucci. *New applications of integral equations methods for solvation continuum models: ionic solutions and liquid crystals*. J. Math. Chem., vol. 23, page 309, 1998.

[Car 85] R. Car and M. Parrinello. *Unified Approach for Molecular Dynamics and Density-Functional Theory*. Chem. Phys. Lett., vol. 55, page 2471, 1985.

[Carloni 02] P. Carloni, U. Rothlisberger and M. Parrinello. *The Role and Perspective of Ab initio Molecular Dynamics in the Study of Biological Systems*. Acc. Chem. Res., vol. 35, page 455, 2002.

[Carpaneto 88] G. Carpaneto, S. Martello and P. Toth. *Algorithms and codes for the assigment problem*. Annals of Operations Research, vol. 13, pages 193–223, 1988.

[Case 06] D. A. Case, T. A. Darden, T. E. Cheatham, C. L. Simmerling, j. Wang, R. E. Duke, R. Luo, J. M. K. Merz, D. A. Pearlman, M. Crowley, R. C. Walker, W. Zhang, B. Wang, S. Hayik, A. Roitberg, G. Seabra, K. F. Wong, F. Paesani, X. Wu, S. Brozell, V. Tsui, H. Gohlke, L. Yang, C. Tan, J. Mongan, V. Hornak, G. Cui, P. Beroza, D. H. Mathews, c. Schafmeister, W. S. Ross and P. A. Kollman. *AMBER9*. University of California:San Francisco, 2006.

[Chen 94] X. G. Chen, R. Schweitzer-Stenner, S. Krimm, N. G. Mirkin and S. A. Asher. *N-Methylacetamide and Its Hydrogen-Bonded Water Molecules Are Vibrationally Coupled*. J. Am. Chem. Soc., vol. 116, no. 24, pages 11141–11142, 1994.

[Chen 95] X.G. Chen, R. Schweitzer-Stenner, S.A. Asher, N.G. Mirkin and S. Krimm. *Vibrational Assignments of trans-N-Methylacetamide and Some of Its Deuterated Isotopomers from Band Decomposition of IR, Visible, and Resonance Raman Spectra*. J. Phys. Chem., vol. 99, page 3074, 1995.

[Chennubhotla 05] C. Chennubhotla and I. Bahar. *Signal propagation in proteins and relation to equilibrium fluctuations*. PLOS Comput. Biol., vol. 3, pages 1716–1726, 2005.

[Chipot 98] C. Chipot and A. Pohorille. *Conformational Equilibria of Terminally Blocked Single Amino Acids at the Water Hexane Interface. A Molecular Dynamics Study*. J. Phys. Chem. B, vol. 102, no. 1, pages 281–290, 1998.

[Cho 94] M. Cho, G. R. Fleming, S. Saito, I. Ohmine and R. M. Stratt. *Instantaneous normal mode analysis of liquid water*. J. Chem. Phys., vol. 100, pages 6672–6683, 1994.

[Ciccotti 86] G. Ciccotti and J. P. Ryckaert. *Molecular-Dynamics Simulation of rigid molecules*. Comp. Phys. Rep., vol. 4, page 345, 1986.

[Cornell 95] W. D. Cornell, P. Cieplak, C. I. Bayly, I. R. Gould, K. M. Merz Jr., D. M. Ferguson, D. C. Spellmeyer, T. Fox, J. W. Caldwell and P. A. Kollman. *A second generation force field for the simulation of proteins, nucleic acids, and organic molecules*. J. Am. Chem. Soc., vol. 117, pages 5179–5197, 1995.

[Cramer 94] C .J. Cramer and D. G. Truhlar. *Quantum chemical conformational analysis of 1,2-ethanediol: Correlation and solvation effects on the tendency to form internal hydrogen bonds in gas phase and in aqueous solution.* J Am. Chem. Soc, vol. 116, page 3892, 1994.

[Cramer 04] C. J. Cramer. Essentials of computational chemistry (theories and models). John Wiely & Sons, Ltd, 2004.

[Cremeens 06] M.E. Cremeens, H. Fujisaki, Y. Zhang, J. Zimmermann, L.B. Sagle, S. MAtsuda, P.E. Dawson, J.E. Straub and F.E. Romesberg. *Efforts toward developing direct probes of protein dynamics*. J. Am. Chem. Soc., vol. 128, pages 6028–6029, 2006.

[Csonka 93] G.I. Csonka. *Analysis of the core-repulsion functions used in AM1 and PM3 semiempirical calculations: Conformational analysis of ring systems*. J. comput. Chem, vol. 14, pages 895–898, 1993.

[Csonka 97] G.I. Csonka and János G. Ángyán. *The orgin of the problems with the PM3 core repulsion function*. J. Mol. Struct (Theochem), vol. 393, pages 31–38, 1997.

[Cuevas 02] G. Cuevas, V. Renugopalakrishnan, G. Madrid and A. T. Hagler. *Density function studies of peptides - Part I. Vibrational frequencies including isotopic effects and NMR chemical shifts of N-methylacetamide, a peptide model, from density function and MP2 calculations*. Phys. Chem. Chem. Phys., vol. 4, page 1490, 2002.

[Cui 06] Qiang Cui and Ivet Bahar. Normal mode analysis theory and applications to biological and chemical system. Chapman & Hall/CRC, 2006.

[Daggett 92] Valerie Daggett and Michael Levitt. *Molecular dynamics simulations of helix denaturation*. Journal of Molecular Biology, vol. 223, no. 4, pages 1121–1138, 1992.

[David 98] E. F. David and R. M. Stratt. *The anharmonic features of the short-time dynamics of fluids: The time evolution and mixing of instantaneous normal modes*. J. Chem. Phys., vol. 109, pages 1375–1390, 1998.

[DeCamp 05] M. F. DeCamp, L. DeFlores, J. M. McCracken, A. Tokmakoff, K. Kwac and M. Cho. *Amide I vibrational dynamics of N-methylacetamide in polar solvents: The role of electrostatic interactions*. J. Phys. Chem. B, vol. 109, no. 21, pages 11016–11026, 2005.

[DeFlores 06] L. P. DeFlores, Z. Ganim, S. F. Ackley, H. S. Chung and A. Tokmakoff. *The Anharmonic Vibrational Potential and Relaxation Pathways of the Amide I and II Modes of N-Methylacetamide*. J. Phys. Chem. B, vol. 110, no. 38, pages 18973–18980, 2006.

[Deng 02] Y.Q. Deng, B.M. Ladanyi and R.M. Stratt. *High-frequency vibrational energy relaxation in liquids: The foundations of instantaneous-pair theory and some generalizations*. J. Chem. Phys., vol. 117, pages 10752–10767, 2002.

[der Vaart 99] A. Van der Vaart and Merz K. M.Jr. *Divide and conquer interaction energy decomposition*. J. Phys. Chem. A, vol. 103, pages 3321–3329, 1999.

[Dewar 77] Michael J. S. Dewar and Walter Thiel. *Ground states of molecules. 39. MNDO results for molecules containing hydrogen, carbon, nitrogen, and oxygen*. J. Am. Chem. Soc., vol. 99, no. 15, pages 4907–4917, 1977.

[Dewar 85] Michael J. S. Dewar, Eve G. Zoebisch, Eamonn F. Healy and James J. P. Stewart. *Development and use of quantum mechanical molecular models. 76. AM1: a new general purpose quantum mechanical molecular model*. Journal of the American Chemical Society, vol. 107, no. 13, pages 3902–3909, 1985.

[Dian 02] B.C. Dian, A. Longarte and T.S. Zwier. *Conformational dynamics in a dipeptide after single-mode vibrational excitation*. Science, vol. 296, pages 2369–2373, 2002.

[Dijkstra 07] R. G. Dijkstra, T. C. Jansen, R. Bloem and J. Knoester. *Vibrational relaxation in simulated two-dimensional infrared spectra of two amide modes in solution*. J. Chem. Phys., vol. 127, page 194505, 2007.

[Dijkstra 11] A. G. Dijkstra, T. la Cour Jansen and J. Knoester. *Modeling the vibrational dynamics and nonlinear infrared spectra of coupled amide I and II modes in peptide*. J. Phys. Chem. B, vol. 115, pages 5392–5401, 2011.

[Dixon 96] S. L. Dixon and K.M. Merz. *Semiempirical Molecular orbital calculations with linear system size scaling*. J. Chem. Phys., vol. 104, pages 6643–6649, 1996.

[Dlott 01] Dana D. Dlott. *Vibrational energy redistribution in polyatomic liquids: 3D infrared Raman spectroscopy*. Chem. Phys., vol. 266, pages 149–166, 2001.

[Dmitriy 04] C. Dmitriy, Tateki Ishida and Ronald M. Levy. *Long-Time Conformational Transitions of Alanine Dipeptide in Aqueous Solution: Continuous and Discrete-State Kinetic Models*. The Journal of Physical Chemistry B, vol. 108, no. 50, pages 19487–19495, 2004.

[Drankenberg 71] T. Drankenberg and S. Forsen. J. Chem. Soc. Chem. Commun., page 1404, 1971.

[Du 03] Q. Du and D. Wei. *Solvation and Polarization of the N-Methyl Amine Molecule in Aqueous Solution: A Combined Study of Quantum Mechanics and Integral Equation Theory in Three Dimensions*. J. Phys. Chem. B, vol. 107, page 13463, 2003.

[Duan 03] Y. Duan, C. WU, S. Chowdhury, M. C. Lee, G. Xiong, W. Zhang, R. Yang, P. Cieplak, R. Luo, T. Lee, J. Caldwell, J. Wang and P. Kollman. *A point charge force fiel for molecular mechanics simulations of proteins based on condensed phase quantum mechanical calculations.* J. Comput. Chem., vol. 24, pages 1999–2012, 2003.

[Edsall 66] J. T. Edsall, P. J. Flory, J. C. Kenndrew and A. M. Liquori. *A Proposal of Standard Conventions and Nomenclature for Description of Polypeptide Conformations*. Biopolymers, vol. 4, page 121, 1966.

[Edsall 85] John T. Edsall. *Proteins, Thomas E. Creighton, W. H. Freeman, New York, 1984, 515 pp.* Journal of Polymer Science: Polymer Letters Edition, vol. 23, no. 2, pages 119–120, 1985.

[Egorov 97] S. A. Egorov, M. D. Stephens and J. L. Skinner. *Absorption line shapes and solvation dynamics of CH3I in supercritical Ar*. J. Chem. Phys., vol. 107, pages 10485–10491, 1997.

[Egorov 99] S. A. Egorov, K. F. Everitt and J. L. Skinner. *Quantum dynamics and vibrational relaxation*. J. Phys. Chem. A, vol. 103, page 9494, 1999.

[Elber 87] R. Elber and M. Karplus. *Multiple Conformational States of Proteins: A Molecular Dynamics Analysis of Myoglobin*. Science, vol. 235, page 318, 1987.

[Fang 09] Y. Fang, S. Shigeto, N. Seong and D. Dlott. *Vibrational Energy Dynamics of Glycine, N-Methylacetamide, and Benzoate Anion in Aqueous (D2O) Solution*. J. Phys. Chem. A, vol. 113, no. 1, pages 75–84, 2009.

[Fayer 01a] M. D. Fayer. *Fast protein dynamics probed with infrared vibrational echo experiments*. Annu. Rev. Phys. Chem., vol. 52, page 315, 2001.

[Fayer 01b] M. D. Fayer. Ultrafast infrared and raman spectroscopy. Marcel Dekker Inc., 2001.

[Fayer 09] M. D. Fayer. *Dynamics of Liquids, Molecules, and Proteins Measured with Ultrafast 2D IR Vibrational Echo Chemical Exchange Spectroscopy*. Annu. Rev. Phys. Chem., vol. 60, pages 21–38, 2009.

[Feig 07] M. Feig. *Kinetics from Implicit Solvent Simulations of Biomolecules as a Function of Viscosity*. Journal of Chemical Theory and Computation, vol. 3, no. 5, pages 1734–1748, 2007.

[Feig 08] M. Feig. *Is Alanine dipeptide a good model for representing the torsional preferences of protein backbones?* J. Chem. Theory Comput., vol. 4, pages 1555–1564, 2008.

[Frauenfelder 91] H. Frauenfelder, sligar S.G. and Wolynes P. G. *The energy landscapes and motions of proteins*. Science, vol. 254, pages 1598–1603, 1991.

[Frauenfelder 97] H. Frauenfelder, Bishop A. R., Garcia A., Schuster P., Sherrington D. and Swart P. J. Landscape paradigms in physics and biology:concepts, structures, and dynamics. North-Holand:Amsterdam, 1997.

[Frauenfelder 01] H. Frauenfelder, B. H. McMahon, R. H. Austin, K. Chu and J. T. Groves. *The role of structure, energy landscape, dynamics, and allostery in the enzymatic function of myoglobin*. Proc. Natl. Acad. Sci. U.S.A., vol. 98, pages 2370–2374, 2001.

[Frauenfelder 03] H. Frauenfelder, B. H. McMahon and P. W. Fenimore. *Myoglobin: The hydrogen atom of biology and a paradigm of complexity*. Proc. Natl. Acad. Sci, vol. 100, pages 8615–8617, 2003.

[Frenkel 96] D. Frenkel and B. Smit. Understanding molecular simulations. from algorithms to applications. Academic Press, 1996.

[Frisch 03] M. J. Frisch, G. W. Trucks, H. B. Schlegel, G. E. Scuseria, M. A. Robb, J. R. Cheeseman, J. A. Montgomery Jr., T. Vreven, K. N. Kudin, J. C. Burant, J. M. Millam, S. S. Iyengar, J. Tomasi, V. Barone, B. Mennucci, M. Cossi, G. Scalmani, N. Rega, G. A. Petersson, H. Nakatsuji, M. Hada, M. Ehara, K. Toyota, R. Fukuda, J. Hasegawa, M. Ishida, T. Nakajima,

Y. Honda, O. Kitao, H. Nakai, M. Klene, X. Li, J. E. Kno, H. P. Hratchian, J. B. Cross, C. Adamo, J. Jaramillo, R. Gomperts, R. E. Stratmann, O. Yazyev, A. J. Austin, R. Cammi, C. Pomelli, J. W. Ochterski, P. Y. Ayala, K. Morokuma, G. A. Voth, P. Salvador, J. J. Dannenberg, V. G. Zakrzewski, S. Dapprich, A. D. Daniels, M. C. Strain, O. Farkas, D. K. Malick, A. D. Rabuck, K. Raghavachari, J. B. Foresman, J. V. Ortiz, Q. Cui, A. G. Baboul, S. Clifford, J. Cioslowski, B. B. Stefanov, G. Liu, A. Liashenko, P. Piskorz, I. Komaromi, R. L. Martin, D. J. Fox, T. Keith, M. A. Al-Laham, C. Y. Peng, A. Nanayakkara, M. Challacombe, P. M. W. Gill, B. Johnson, W. Chen, M. W. Wong, C. Gonzalez and J. A. Pople. Gaussian 2003, revision b.03. Gaussian, Inc., Pittsburgh PA, 2003.

[Fujisaki 05] H. Fujisaki and J. E. Straub. *Vibrational energy relaxation in proteins*. Proc. Natl. Acad. Sci. U.S.A., vol. 102, pages 6726–6731, 2005.

[Fujisaki 06] H. Fujisaki, Y. Zhang and J. E. Straub. *Time-dependent perturbation theory for vibrational energy relaxation and dephasing in peptides and proteins*. J. Chem. Phys., vol. 124, page 144910, 2006.

[Fujisaki 07a] H. Fujisaki and J. E. Straub. *Vibrational Energy Relaxation of Isotopically Labeled Amide I Modes in Cytochrome c: Theoretical Investigation of Vibrational Energy Relaxation Rates and Pathways*. J. Phys. Chem. B, vol. 111, pages 12017–12023, 2007.

[Fujisaki 07b] H. Fujisaki, K. Yagi, K. Hirao and J. E. Straub. *Quantum dynamics of N-methylacetamide studied by the vibrational configuration interaction method*. Chem. Phys. Lett., vol. 443, pages 6–11, 2007.

[Fujisaki 08] H. Fujisaki and G. Stock. *Dynamic treatment of vibrational energy relaxation in a heterogeneous and fluctuating environment*. J. Chem. Phys., vol. 129, page 134110, 2008.

[Fujisaki 09] H. Fujisaki, K. Yagi, J. E. Straub and G. Stock. *Quantum and classical vibrational relaxation dynamics of N-methylacetamide on ab-initio potential energy surfaces*. Int. J. Quant. Chem., vol. 109, pages 2047–2057, 2009.

[Gaigeot 03] Marie-Pierre Gaigeot and Michiel Sprik. *Ab Initio Molecular Dynamics Computation of Infrared Spectrum of Aqueous Uracil*. J. Phys. Chem. B, vol. 107, pages 10344–10358, 2003.

[Gaigeot 05] M. P. Gaigeot, R.Vuilleumier, M.Sprik and D.Borgis. *Infrared Spectroscopy of N-Methylacetamide Revisted by ab Initio Molecular Dynamics Simulation*. J. Chem. Theory Comput., vol. 1, pages 772–789, 2005.

[Gaigeot 09] M. P. Gaigeot. *Unravelling the Conformational Dynamics of the Aqueous Alanine Dipeptide with First-Principle Molecular Dynamics*. J. Phys. Chem. B, vol. 113, page 10059, 2009.

[Gaigeot 10] M. P. Gaigeot. *Infrared spectroscopy of the alanine dipeptide analog in liquid water with DFT-MD. Direct evidence for PII/B conformations*. Phys. Chem. Chem. Phys., vol. 12, page 10198, 2010.

[Gao 97] J. Gao and M. Freindorf. *Hybrid ab Initio QM/MM Simulation of N-Methylacetamide in Aqueous Solution*. J. Phys. Chem. A, vol. 101, page 3182, 1997.

[Garberoglio 02] G. Garberoglio and R. Vallauri. *Instantaneous normal mode analysis of short-time dynamics in hydrogen-bonded liquids*. Physica A, vol. 314, pages 492–500, 2002.

[Garcia-Martinez 02] A. Garcia-Martinez, E. Teso-Vilar, A. Garcia-Fraile and P. Martinez-Ruiz. *A computational and experimental study on the relative stabilities of cis and trans isomers of N-alkylamides in gas phase and in solution*. J. Phys. Chem. A, vol. 106, page 4942, 2002.

[Garcia-Viloca 04] M. Garcia-Viloca, K. Nam, C. Alhambra and J. L. Gao. *Solvent and protein effects on the vibrational frequency shift and energy relaxation of the azide ligand in carbonic anhydrase*. J. Phys. Chem. B, vol. 108, page 13501, 2004.

[Gilmanshin 97] R. Gilmanshin, S. Williams, R. H. Callender, W. H. Woodruff and R. B. Dyer. *Fast events in protein folding: Relaxation dynamics and structure of the I form of apomyoglobin*. Biochemistry, vol. 36, page 15006, 1997.

[Gnanakaran 01] S. Gnanakaran and R. M. Hochstrasser. *Conformational preference and vibrational frequency distributions of short peptides in relation to multidimensional infrared spectroscopy*. J. Am. Chem. Soc., vol. 123, pages 12886–12898, 2001.

[Go 83] N. Go, T. Noguti and T. Nishikawa. *Dynamics of a small globular protein in terms of low-frequency vibrational-modes*. Proc. Natl. Acad. Sci. U.S.A., vol. 80, page 3696, 1983.

[Goldstein 02] Herbert Goldstein, Charles Poole and John Safko. Classical mechanics. Pearson Education International, 2002.

[Goodyear 96] G. Goodyear and R. M. Stratt. *The short time intramolecular dynamics of solutes in liquids. I. An instantaneous normal mode theory for friction.* J. Chem. Phys., vol. 105, pages 10050–10071, 1996.

[Goodyear 97] G. Goodyear and R. M. Stratt. *The short-time intramolecular dynamics of solutes in liquid. II. Vibrational population relaxation*. J. Chem. Phys., vol. 107, pages 3098–3120, 1997.

[Gordon 65] R. G. Gordon. *Molecular motion in Infrared and Raman spectra*. J. Chem. Phys., vol. 43, page 1307, 1965.

[Gordon 68] R. G. Gordon. *Correlation functions for molecular motion.* Adv. Mag. Reson., vol. 3, page 1, 1968.

[Gould 92] R. I. Gould and P. A. Kollman. *Ab initio SCF and MP2 calculations on four low-energy conformers of N-acetyl-N'-methylalaninamide*. J. Phys. Chem., vol. 96, pages 9255–9258, 1992.

[Gould 94] I. R. Gould, W. D. Cornell and I. H. Hillier. *A quantum Mechanical Investigation of the Conformational Energetics of the Alanine and Glycine Dipeptides in the Gas Phase and in Aqueous Solution*. J. Am. Chem. Soc., vol. 116, pages 9250–9259, 1994.

[Grdadolnik 08] J. Grdadolnik, S. G. Grdadolnik and F. Avbelj. *Determination of conformational preferences of dipeptides using vibrational spectroscopy*. J. Phys. Chem. B, vol. 112, page 2712, 2008.

[Gregurick 02] S. K. Gregurick, G. M. Chaban and R. B. Gerber. *Ab initio and improved empirical potentials for the calculation of the anharmonic vibrational states and intramolecular mode coupling of N-methylacetamide*. J. Phys. Chem. A, vol. 106, no. 37, pages 8696–8707, 2002.

[Grenie 75] Y. Grenie, M. Avignon and C. Garrigou-Lagrange. *Molecular structure study of dipeptides isolated in an argon matrix by infrared spectroscopy*. Journal of Molecular Structure, vol. 24, no. 2, pages 293 – 307, 1975.

[Gruebele 04] M. Gruebele and P. G. Wolynes. *Vibrational Energy Flow and Chemical Reactions*. Acc. Chem. Res., vol. 37, pages 261–267, 2004.

[Guo 92] H. Guo and M. Karplus. *Ab initio studies of hydrogen-bonding of N-methylacetamide: structure, cooperativity, and internal rotational barriers*. J. Phys. Chem., vol. 96, pages 7273–7287, 1992.

[Haile 97] J.M. Haile. Molecular dynamics simulation. elementary methods. John Wiley & Sons, Inc, 1997.

[Ham 02] Sihyun Ham, Joo-Hee Kim, Hochan Lee and Minhaeng Cho. *Correlation between electronic and molecular structure distorions and vibrational properties.II.Amide I modes of NMA-nD2O complexes*. J. Chem. Phys., vol. 118, page 3491, 2002.

[Ham 03] Sihyun Ham and Minhaeng Cho. *Amide I modes in the N-methylacetamide dimer and glycine dipeptide analog: Diagonal force constants*. J. Chem. Phys., vol. 118, page 6915, 2003.

[Hamm 98] P. Hamm, M. H. Lim and R. M. Hochstrasser. *Structure of the amide I band of peptides measured by femtosecond nonlinear-infrared spectroscopy*. J. Phys. Chem. B, vol. 102, no. 31, pages 6123–6138, 1998.

[Han 96] W. G. Han and S. Suhai. *Density functional studies on N-methylacetamide water complexes*. J. Phys. Chem., vol. 100, page 3942, 1996.

[Han 98] W. G. Han, K. J. Jalkanen, M. Elstner and S. Suhai. *Theoretical study of aqueous N-acetyl-L-alanine N'-methylamide: Structures and Raman, VCD, and ROA spectra*. J. Phys. Chem. B, vol. 102, page 2587, 1998.

[Harb 04] W. Harb, M. I. Berenal-Uruchurtu and M.F. Ruiz-López. *An improved PM3 method for hydrated systems*. Theor. Chem. Acc., vol. 112, page 204, 2004.

[Hayashi 05] T. Hayashi, W. Zhuang and S. Mukamel. *Electrostatic DFT Map for complete vibrational amide band of NMA*. J. Phys. Chem. A, vol. 109, page 9747, 2005.

[Hayward 94] S. Hayward, A. Kitao and N. Go. *Harmonic and anharmonic aspects in the dynamics of BPTI: a normal mode analysis and principal component analysis*. Protein Sci., vol. 3, pages 936–943, 1994.

[Hayward 95] S. Hayward, A. Kitao and N. Go. *Harmonicity and anharmonicity in protein dynamics: a normal mode analysis and principal component analysis.* Proteins, vol. 23, pages 177–186, 1995.

[Head-Gordon 91] T. Head-Gordon, M. Head-Gordon, M. J. Frisch, C. L. Brooks and J. A. pople. *Theoretical study of blocked glycine and alanine peptide analogs*. J. Am. Chem. Soc., vol. 113, pages 5989–5997, 1991.

[Herbert 05] J. M. Herbert and M. Head-Gordon. *Accelerated, energy-conserving Born-Oppenheimer molecular dynamics via Fock matrix extrapolation*. Phys. Chem. Chem. Phys., vol. 7, page 3269, 2005.

[Herrebout 01] W. A. Herrebout, K. Clou and H. O. Desseyn. *Vibrational Spectroscopy of N-Methylacetamide Revisited*. J. Phys. Chem. A, vol. 105, page 4865, 2001.

[Hill 96] Jeffrey R. Hill, Christopher J. Ziegler, Kenneth S. Suslick, Dana D. Dlott, C. W. Rella and M. D. Fayer. *Tuning the Vibrational Relaxation of CO Bound to Heme and Metalloporphyrin Complexes*. J. Phys. Chem., vol. 100, pages 18023–18032, 1996.

[Hu 03] H. Hu, M. Elstner and J. Hermans. *Comparison of a QM/MM force field and Molecular Mechanics force field in simulations of Alanine and Glaycine (Dipeptides) (Ace-Ala-Nme and Ace-Gly-Nme) in water in relation to the problem of Modeling the unfolded peptide backbone in solution*. Protein, vol. 50, pages 451–463, 2003.

[Iftimie 05] R. Iftimie, P. Minary and M. E. Tuckerman. *Ab initio molecular dynamics: Concepts, recent developments, and future trends*. Proc. Natl. Acad. Sci. USA, vol. 102, page 6654, 2005.

[Ingrosso 11] F. Ingrosso, G. Monard, M. Hamdi Farag, A. Bastida and M. F. Ruiz-Lopez. *Importance of polarization and charge transfer effect to model the infrared spectra of peptides in solution.* J. Chem. Theory Comput., vol. 7, pages 1840–1849, 2011.

[Ishikura 06] T. Ishikura and T. Yamato. *Energy transfer pathways relevant for long-range intramolecular signaling of photosensory protein revealed by microscopic energy conductivity analysis*. Chem. Phys. Lett., vol. 432, pages 533–537, 2006.

[Iuchi 02] Satoru Iuchi, Akihiro Morita and Shigeki Kato. *Molecular Dynamics Simulation with the Charge Response Kernel: Vibrational Spectra of Liquid Water and N-Methylacetamide in Aqueous Solution*. J. Phys. Chem. B, vol. 106, no. 13, pages 3466–3476, 2002.

[Iwaki 01] L. Iwaki and D. D. Dlott. *Vibrational energy transfer in condensed phases*. En J. H. Moore and N. D. Spencer, editores, Encyclope-

dia of Chemical Physics and Physical Chemistry, page 2717. IOP Publishing Ltd., 2001.

[Jacob 09] C.R. Jacob and M. Reiher. *Localizing normal modes in large molecules*. J. Chem. Phys., vol. 130, page 084106, 2009.

[Jensen 07] F. Jensen. Introduction to computational chemistry. John Wiely & Sons, Ltd, second edition, 2007.

[Jeon 10] J. Jeon and M. Cho. *Direct quantum mechanical/molecular mechanical simulations of two-dimensional vibrational responses: N-methylacetamide in water*. New. J. Phys., vol. 12, page 065001, 2010.

[Jeon 11] J. Jeon and M. Cho. *Redistribution of carbonyl stretch mode energy in isolated and solvated N-methylacetamide: Kinetic energy spectral density analyses*. J. Chem. Phys., vol. 135, page 214504, 2011.

[Ji 00] X.D. Ji, H. Alhborn, B. Space, P.B. Moore, Y. Zhou, S. Constantine and L.D. Ziegler. *A combined instantaneous normal mode and time correlation function description of the optical Kerr effect and Raman spectroscopy of liquid CS_2*. J. Chem. Phys., vol. 112, pages 4186–4192, 2000.

[Jorgensen 88] W. L. Jorgensen and J. Gao. *Cis-trans energy difference for the peptide bond in the gas phase and in aqueous solution*. J. Am. Chem. Soc., vol. 110, page 4212, 1988.

[Jorgensen 96] W. L. Jorgensen, Maxwell D. S. and Tirado-Rives J. *Development and Testing of the OPLS All-Atom force field on conformational energetics and properties of organic liquids*. J. Am. Chem. Soc., vol. 118, pages 11225–11236, 1996.

[Kabadi 04] V. N. Kabadi and B. M. Rice. *Molecular dynamics simualtions of normal mode vibrational energy transfer in liquid nitromethane*. J. Phys. Chem. A, vol. 108, pages 532–540, 2004.

[Kalbfleisch 96] T. S. Kalbfleisch, L. D. Ziegler and T. Keyes. *An instantaneous normal mode analysis of solvation: Methyl iodide in high pressure gases*. J. Chem. Phys., vol. 105, pages 7034–7046, 1996.

[Kalstein 11] Adrián Kalstein, Sebastian Fernández-Alberti, Adolfo Bastida, Miguel A. Soler, , Marwa H. Farag, Jose Zuñiga and Alberto Requena. *Vibrational dynamics of polyatomic molecules in solution: assignment, time evolution and mixing of instantaneous normal modes*. Theor. Chem. Acc., vol. 128, pages 769–782, 2011.

[Kaminski 01] G. A. Kaminski, R. A. Friesner, Tirado-Rives J. and Jorgensen W. L. *Evaluation and reparametrization of the OPLS-AA force field for poretins via comparison with accurate quantum chemical calculations on peptides*. J. Phys. Chem. B, vol. 105, pages 6474–6487, 2001.

[Kandratsenka 09] A. Kandratsenka, J. Schroeder, D. Schwarzer and V. S. Vikhrenko. *Nonequilibrium molecular dynamics simulations of vibrational energy relaxation of HOD in D_2O*. J. Chem. Phys., vol. 130, page 174507, 2009.

[Karplus 81] M. Karplus and J. Kushick. *Method for estimating the configurational entropy of macromolecules*. Macromolecules, vol. 14, pages 325–332, 1981.

[Keyes 97] T. Keyes. *Instantaneous normal mode approach to liquid state dynamics*. J. Phys. Chem. A, vol. 101, pages 2921–2930, 1997.

[Kim 05a] Y. S. Kim and R. M. Hochstrasser. *Dynamics of amide I modes of the alanine dipeptide in D2O*. J. Phys. Chem. B, vol. 109, pages 6884–6891, 2005.

[Kim 05b] Y. S. Kim, J. Wang and R. M. Hochstrasser. *Two-Dimensional infrared spectroscopy of the alanine dipeptide in aqueous solution*. J. Phys. Chem. B, vol. 109, pages 7511–7521, 2005.

[Kinnaman 06] C. S. Kinnaman, M. E. Cremeens, F. E. Romesberg and S. A. Corcelli. *Infrared Line Shape of an α-Carbon Deuterium-Labeled Amino Acid*. J. Am. Chem. Soc., vol. 128, page 13334, 2006.

[Kitaura 76] K. Kitaura and K. Morokuma. *New energy decomposition scheme for molecular-interactions within Hartree-Fock approximation*. Int. J. Quantum Chem., vol. 10, pages 325–340, 1976.

[Kobus 11] M. Kobus, P.H. Nguyen and G. Stock. *Coherent vibrational energy transfer along a peptide helix*. J. Chem. Phys., vol. 134, page 124518, 2011.

[Kong 07] Y. Kong and M. Karplus. *The Signaling Pathway of Rhodopsin*. Structure, vol. 15, pages 611–623, 2007.

[Kong 09a] Y. Kong and M. Karplus. *Signaling pathways of PDZ2 domain: A molecular dynamics interaction correlation analysis*. Proteins, vol. 74, pages 145–154, 2009.

[Kong 09b] Y. Kong and M. Karplus. *Signaling pathways of PDZ2 domain: A molecular dynamics interaction correlation analysis*. Proteins, vol. 74, pages 145–154, 2009.

[Kramer 98] N. Kramer, M. Buchner and T. Dorfmuller. *Normal mode dynamics in simple liquids*. J. Chem. Phys., vol. 109, pages 1912–1919, 1998.

[Kubelka 01] J. Kubelka and T. A. Keideling. *Ab Initio Calculation of Amide Carbonyl Stretch Vibrational Frequencies in Solution with Modified Basis Sets. 1. N-Methyl Acetamide*. J. Phys. Chem. A, vol. 105, page 10922, 2001.

[Kubo 54] R. Kubo. *Note on the stochastic theory of resonance absorption*. J. Phys. Soc. Jpn, vol. 9, page 935, 1954.

[Kwac 03] Kijeong Kwac and Minhaeng Cho. *Molecular dynamics simulation study of N-methylacetamide in water. I. Amide I mode frequency fluctuation*. J. Chem. Phys., vol. 119, no. 4, pages 2247–2255, 2003.

[Kwac 08] K. Kwac, K.-Koo Lee, J. B. Han, K.-Im Oh and M. Cho. *Classical and quantum mechanical/molecular mechanical molecular dynamics simulations of alanine dipeptide in water: comparisons with IR and vibrational circular dichroism spectra*. J. Chem. Phys., vol. 128, page 105106, 2008.

[la Cour Jansen 06] T. la Cour Jansen and J. Knoester. *A transferable electrostatic map for solvation effects on amide I vibrations and its application to linear and two-dimensional spectroscopy*. J. Chem. Phys., vol. 124, page 044502, 2006.

[Laasonen 93] K. Laasonen, M. Sprik, M. Parrinello and R. Car. *"Ab initio" liquid water*. J. Chem. Phys, vol. 99, page 9080, 1993.

[Ladanyi 96] B. M. Ladanyi and S. Klein. *Contributions of rotation and translation to polarizability anisotropy and solvation dynamics in acetonitrile*. J. Chem. Phys., vol. 105, pages 1552–1561, 1996.

[Ladanyi 98] B. M. Ladanyi and R. M. Stratt. *The short-time dynamics of vibrational relaxation in molecular liquids*. J. Phys. Chem. A., vol. 102, pages 1068–1082, 1998.

[Lagant 04] P. Lagant, D. Nolde, R. Stote, G. Vergoten and M. Karplus. *Increasing Normal Modes Analysis Accuracy: The SPASIBA Spectroscopic Force Field Introduced into the CHARMM Program*. J. Phys. Chem. A, vol. 108, page 4019, 2004.

[Lawrence 05] C. P. Lawrence and J. L. Skinner. *Quantum correlations in vibrational and electronic condensed phase spectroscopy: line shapes and echoes*. Natl. Acad. Sci U.S.A, vol. 102, page 6720, 2005.

[Lee 07] Kyung-Koo Lee, Kwang-Im Oh, Hochan Lee, Cheonik Joo, Hogyu Han and Minhaeng Cho. *Dipeptide Structure Determination by Vibrational Circular Dichroism Combined with Quantum Chemistry Calculations*. ChemPhysChem, vol. 8, pages 2218–2226, 2007.

[Lee 09] M.-Eun Lee, S. Y. Lee, S.-Woo Joo and K.-Hwi Cho. *Amide I bands of terminally blocked alanine in Solution Investigated by infrared spectroscopy and density function theory calculation: Hydrogen bonging interactions and solvent effects*. J. Phys. Chem. B, vol. 113, pages 6894–6897, 2009.

[Leitner 05] D. M. Leitner. Adv. Chem. Phys., vol. 130(B), pages 205–206, 2005.

[Leitner 08] David M. Leitner. *Energy flow in protein*. Ann. Rev. Phys. Chem., vol. 59, page 233, 2008.

[Leitner 09] D. M. Leitner. *Frequency-resolved communication maps for proteins and other nanoscale materials*. J. Chem. Phys., vol. 130, page 195101, 2009.

[Leitner 10a] D. M. Leitner. *Quantum localization and protein-assisted vibrational energy flow in cofactors*. New J. Phys., vol. 12, page 085004, 2010.

[Leitner 10b] D. M. Leitner and J. E. Straub. Proteins: Energy, heat and signal flow (computation in chemistry). Taylor and Francis Group, Boca Raton, 2010.

[Lemmom 11] E. Lemmom, M. McLinden and D. Friend. Thermophysical properities of fluid systems in nist chemistry webboob, nist standard reference database number 69. Eds. Linstrom and P. J. and Mallard W. G. National Institute of Standards and Technology, Gaithersburg MD, 20899, http://webbook.nist.gov, 2011.

[Levine 75] IRA N. Levine. Molecular spectroscopy. John Wiley and Sons, 1975.

[Levy 82] R. M. Levy, D. Perahia and M. Karplus. *Molecular-Dynamics of an Alpha-helical polypeptide - temperature-dependence and deviation from harmonic behavior*. Proc. Natl. Acad. Sci. U.S.A., vol. 79, pages 1346–1350, 1982.

[Levy 84] R. M. Levy, M. Karplus, J. Kushick and D. Perahia. *Evaluation of the configurational entropy for proteins - Application to Molecular-Dynamics simulations of an Alpha-Helix*. Macromolecules, vol. 17, pages 1370–1374, 1984.

[Li 98] J. Li, T. Zhu, C. J. Cramer and D. G. Truhlar. *New class IV charge model for extracting accurate partial charges from wave functions*. J. Phys. Chem. A, vol. 102, page 1820, 1998.

[Li 06] S. Li, J. R. Schmidt, S. A. Corcelli, C. P. Lawrence and J. L. Skinner. *Approaches for the calculation of vibrational frequencies in liquids: Comparison to benchmarks for azide/water clusters*. J. Chem. Phys., vol. 124, page 2041, 2006.

[Lubchenko 05] V. Lubchenko, P. G. Wolynes, and H. Frauenfelder. *Mosaic energy landscapes of liquids and the control of protein conformational dynamics by glass-forming solvents*. J. Phys. Chem. B, vol. 109, pages 7488–7499, 2005.

[Luque 93] F. J. Luque and M. Orozco. *Theoretical-study of N-methylacetamide in vacuum and aqueous-solution - implications for the peptide-bond isomerization*. J. Org. Chem., vol. 58, page 6397, 1993.

[MacKerell 98] A. D. Jr. MacKerell, D. Bashford, M. Bellott, R. L. Dunbrack Jr., J. D. Evanseck, M. J. Field, S. Fischer, J. Gao, H. Guo, S. Ha, D. Joseph-McCarthy, L. Kuchnir, K. Kuczera, F. T. K. Lau, C. Mattos, S. Michnick, T. Ngo, D. T. Nguyen, B. Prodhom, W. E. Reiher III, B. Roux, M. Schlenkrich, J. C. Smith, R. Stote, J. Straub, M. Watanabe, J. Wiórkiewicz-Kuczera, D. Yin and M. Karplus. *All-Atom Empirical Potential for Molecular Modeling and Dynamics Studies of Proteins*. J. Phys. Chem. B, vol. 102, no. 18, pages 3586–3616, 1998.

[Mannfors 03] B. E. Mannfors, N. M. Mirkin, K. Palmo and S. Krimm. *Analysis of the Pyramidalization of the Peptide Group Nitrogen: Implications for Molecular Mechanics Energy Functions*. J. Phys. Chem. A, vol. 107, page 1825, 2003.

[Mantz 04] Yves A. Mantz, Helene Gerard, Radu Iftimie and Glenn J.Martyna. *Isomerization of a Peptidic Fragment Studied Theoretically in Vacuum and in Explicit Water Solvent at Finite Temperature*. J. Am. Chem. Soc., vol. 126, page 4080, 2004.

[Mantz 06] Y. A. Mantz, H. Gerard, R. Iftimie and G. J.Martyna. *Ab initio and empirical model MD simulation studies of solvent effects on the*

properties of N-methylacetamide along a cis-trans isomerization pathway. J. Phys. Chem. B, vol. 110, page 13523, 2006.

[Mantz 09] Y. A. Mantz, D. Branduardi, G. Bussi and M. Parrinello. *Ensemble of Transition State Structures for the Cis-Trans Isomerization of N-Methylacetamide*. J. Phys. Chem. B, vol. 113, page 12521, 2009.

[Marx 00] D. Marx and J. Hutter. *Ab initio Molecular Dynamics: Theory and Implementation*. En J. Grotendorst, editor, Modern Methods and Algorithms of Quantum Chemistry, page 239. John von Neumann Institute for Computing, Jülich, Germany, 2nd edn, 2000.

[Mayne 91] L.C. Mayne and B. Hudson. *Resonance raman-spectroscopy of N-methylacetamide - overtones and combinations of the C-N stretch (Amide-II') and effect of solvation on the C=O stretch (Amide-I) intensity*. J. Phys.Chem., vol. 95, page 2962, 1991.

[McQuarrie 00] D. A. McQuarrie. Statistical mechanics. University Science Books. Sausalito, California, 2000.

[Mehta 04] M. A. Mehta, E. A. Fry, M. T. Eddy, M. T. Dedeo, A. E. Anagnost and J. R. Long. *Structure of the alanine dipeptide in condensed phases determined by C-13 NMR*. J. Phys. Chem. B, vol. 108, page 2777, 2004.

[Meighan 64] R. M. Meighan and R. H. Cole. *Dielectric Properties of Alkyl Amides. I. Vapor Phase Dipole Moments and Polarization in Benzene Solution*. J. Phys. Chem., vol. 68, page 503, 1964.

[Mennucci 05] B. Mennucci and José M. Martínez. *How to model solvation of peptides? Insights from a quantum mechanical and molecular dynamics study of N-methylacetamide.1. Geometries, infrared and ultraviolet spectra in water*. J. Phys. Chem. B, vol. 109, page 9818, 2005.

[Miller 80] W. H. Miller, N. C. Handy and J. E. Adams. *Reaction path hamiltonian for polyatomic molecules*. J. Chem. Phys., vol. 72, pages 99–112, 1980.

[Mirkin 96] N. G. Mirkin and S. Krimm. *Ab initio vibrational analysis of isotopic derivatives of aqueous hydrogen-bonded trans-N-methylacetamide*. J. Mol. Struct., vol. 377, page 219, 1996.

[Mirkin 04] N. G. Mirkin and S. Krimm. *Structural Dependence of NH Stretch Mode Frequency Shifts in Amide and Peptide Systems*. J. Phys. Chem. A, vol. 108, page 5438, 2004.

[Miyazawa 58] Tatsuo Miyazawa, Takehiko Shimanouchi and San ichiro Mizushima. *Normal Vibrations of N-Methylacetamide*. The Journal of Chemical Physics, vol. 29, no. 3, pages 611–616, 1958.

[Mohammed 09] O.F. Mohammed, G.S. Jas, M.M. Lin and A.H. Zewail. *Primary Peptide Folding Dynamics Observed with Ultrafast Temperature Jump*. Angew. Chem. Int. Ed., vol. 48, pages 5628–5632, 2009.

[Mokrane 97] A. Mokrane, P. Friant-Michel, A. Cartier and J.-L. Rivail. *Scaled semiempirical method for the calculation of vibrational spectra - Molecular vibrational frequencies of monosaccharides and disaccharides by PM3 method*. J. Mol. Structure: THEOCHEM, vol. 395, page 71, 1997.

[Monard 05] G. Monard, M. Bernal-Uruchurtu, A. Van des Vaart K. M. Jr Merz and M. F. Ruiz-Lopez. *Simulation of liquid water using semiempirical Hamiltonians and the divide and conquer approach*. J. Phys.Chem. A, vol. 109, page 3425, 2005.

[Montalvo 10] G. Montalvo, M. M. Waegele, S. Shandler, F. Gai and W. F. De Grado. *Infrared Signature and Folding Dynamics of a Helical β-Peptide*. J. Am. Chem. Soc., vol. 132, page 5616, 2010.

[Moore 98] P.B. Moore, X.D. Ji, H. Ahlborn and B. Space. *An instantaneous normal mode theory of condensed phase absortion: the vibrational spectrum of condensed CS_2 from bpiling to freezing*. Chem. Phys. Lett., vol. 296, pages 259–265, 1998.

[Moritsugu 00] K. Moritsugu, O. Miyashita and A. Kidera. *Vibrational energy transfer in a protein molecule*. Phys. Rev. Lett., vol. 85, page 3970, 2000.

[Moritsugu 03] K. Moritsugu, O. Miyashita and A. Kidera. *Temperature dependence of vibrational energy transfer in a protein molecule*. J. Phys. Chem. B, vol. 107, page 3309, 2003.

[Moritsugu 04] K. Moritsugu and A. Kidera. *Protein motions represented in moving normal mode coordinates*. J. Phys. Chem. B, vol. 108, pages 3890–3898, 2004.

[Nakamura 95] M. Nakamura, K. Tamura and S. Murakami. *Isotope effects on thermodynamic properties: mixtures of $x(D_2O$ or $H_2O) + (1-x)CH_3CN$ at 298.15 K*. Thermochim. Acta, vol. 253, pages 127–136, 1995.

[Nam 05] K. Nam, J. Gao and D. M. York. *An efficient linear-scaling Ewald method for long-range electrostatic interactions in combined QM/MM calculations*. J. Chem. Theory Comput., vol. 1, page 2, 2005.

[Nguyen 03] P. H. Nguyen and stock G. *Nonequilibrium Molecular Dynamics study of the vibrational energy relaxation of peptides in water*. J. Chem. Phys., vol. 119, pages 11350–11358, 2003.

[Nguyen 06a] P. H. Nguyen, R. D. Gorbunov and G. Stock. *Photoinduced Conformational Dynamics of a Photoswitchable Peptide: A Nonequilibrium Molecular Dynamics Simulation Study*. Biophys. J., vol. 91, pages 1224–1234, 2006.

[Nguyen 06b] P. H. Nguyen and G. Stock. *Nonequilibrium molecular-dynamics simulation of a photoswitchable peptide*. Chem. Phys., vol. 323, pages 36–44, 2006.

[Nguyen 10] P. H. Nguyen, S. Park and G. Stock. *Nonequilibrium molecular dynamics simulation of the energy transport through a peptide helix*. J. Chem. Phys., vol. 132, page 025102, 2010.

[Niklasson 06] A. M. N. Niklasson, C. J. Tymczak and M. Challacombe. *Time-Reversible Born-Oppenheimer Molecular Dynamics*. Phys. Rev. Lett., vol. 97, page 123000, 2006.

[Ohmine 90] Iwao Ohmine and Hideki Tanaka. *Potential energy surfaces for water dynamics. II. Vibrational mode excitations, mixing, and relaxations*. J. Chem. Phys., vol. 93, no. 11, pages 8138–8147, 1990.

[Ohmine 93] I. Ohmine and H. Tanaka. *Fluctuation, Relaxations, and Hydration in Liquid Water. Hydrogen-Bond Rearrangement Dynamics*. Chem. Rev., vol. 93, pages 2545–2566, 1993.

[Ota 05] N. Ota and D. A. Agard. *Intramolecular Signaling Pathways Revealed by Modeling Anisotropic Thermal Diffusion*. J. Mol. Biol., vol. 351, pages 345–354, 2005.

[Palmo 03] K. Palmo, N. M. Mirkin and S. Krimm. *Potential energy functions: From consistent force fields to spectroscopically determined polarizable force fields*. Biopolymers., vol. 68, page 383, 2003.

[Palmo 07] K. Palmo and S. Krimm. *Group Polarizability Model for Molecular Mechanics Energy Functions*. J. Chem. Theory Comput., vol. 3, page 2120, 2007.

[Peng 10] C. Peng, L. Zhang and T. Head-Gordon. *Instantaneous Normal Modes as an Unforced Reaction Coordinate for Protein Conformational Transitions*. Biophys. J., vol. 98, pages 2356–2364, 2010.

[Perry 03] A. Perry, H. Ahlborn, B. Space and P.B. Moore. *A combined time correlation function and instantaneous normal mode study of the sum frequency generation spectroscopy of the water/vapor interface*. J. Chem. Phys., vol. 118, pages 8411–8419, 2003.

[Peterson 99] K. A. Peterson, C. W. Rella, J. R. Engholm and H. A. Schwettman. *Ultrafast Vibrational Dynamics of the Myoglobin Amide I Band*. The Journal of Physical Chemistry B, vol. 103, pages 557–561, 1999.

[Philipp 99] D. M. Philipp and R. A. Friesner. *Mixed ab initio QM/MM modeling using frozen orbitals and tests with alanine dipeptide and tetrapeptide*. J. Comput. Chem., vol. 20, page 1468, 1999.

[Piatkowski 10] L. Piatkowski and H. J. Bakker. *Vibrational relaxation pathways of AI and AII Modes in N-methylacetamide clusters*. J. Phys. Chem. A, vol. 114, page 11462, 2010.

[Piatkowski 12] L. Piatkowski and H. J. Bakker. *Vibrational relaxation pathways of amide I and amide II modes in N-methylacetamide*. J. Chem. Phys,, vol. 136, page 164504, 2012.

[Piazza 09] F. Piazza and Y-H. Sanejouand. *Long-range energy transfer in proteins*. Phys. Biol., vol. 6, page 046014, 2009.

[Pinilla 12] Carlos Pinilla, Amir H. Irani, Nicola Seriani and Sandro Scandolo. *Ab initio parameterization of an all-atom polarizable and dissociable force field for water*. J. Chem. Phys., vol. 136, no. 11, page 114511, 2012.

[Piquemal 12] Jean-Philip Piquemal and Kenneth Jordan. *From quantum mechanics to force fields: new methodologies for the classical simulation of complex systems*. Theoretical Chemistry Accounts: Theory, Computation, and Modeling (Theoretica Chimica Acta), vol. 131, pages 1–2, 2012.

[Pivcova 65] H. Pivcova, B. Schneider, J. Stokr and Collec. Czech. *On structure and properties of polyamides .20. fermi resonance effects in vibrational spectra of N-methylacetamide*. Chem. Comm., vol. 30, page 2215, 1965.

[Pohl 07] G. Pohl, A. Perczel, E. Vass, G. Magyarfalvi and G. Tarczay. *A matrix isolation study on Ac-Gly-NHMe and Ac-L-Ala-NHMe that simplest chiral and achiral building blocks of peptides and proteins*. Phys. Chem. Chem. Phys., vol. 9, pages 4698–4708, 2007.

[Poon 00] Chi-Duen Poon, Edward T. Samulski, Christoph F. Weise and James C. Weisshaar. *Do Bridging Water Molecules Dictate the Structure of a Model Dipeptide in Aqueous Solution?* J. Am. Chem. Soc., vol. 122, no. 23, pages 5642–5643, 2000.

[Press 92] H.W. Press, S. A. Teukolosky, W. R. Vetterling and B. P. Flannery. Numerical recipes in fortran 77 (the art of scientific computing). Cambridge university press: Cambridge, UK (second edition), 1992.

[Raff 88] L. M. Raff. *Projection methods for obtaining intramolecular energy-transfer rates from classical trajectory results - application to 1,2-difluoroethane*. J. Chem. Phys., vol. 89, no. 9, pages 5680–5691, 1988.

[Rainey 03] J. K. Rainey. *Collagen structure and preferential assembly explored by parallel microscopy and bioinformatic*. PhD thesis, University of Tronto, 2003.

[Ramachandran 63] G. N. Ramachandran, C. Ramakrishnan and V. Sasisekharan. *Stereochemistry of polypeptide chain configuration*. J. Mol. Bio., vol. 7, pages 95–99, 1963.

[Ramachandran 68] G. N. Ramachandran and V. Sasisekharan. *Conformation of polypeptides and proteins*. Adv. Protein Chem., vol. 23, pages 283–438, 1968.

[Ramírez 04] R. Ramírez, T. López-Ciudad, P. Kumar and D. Marx. *Quantum corrections to classical time-correlation functions: Hydrogen bonding and anharmonic floppy modes*. J. Chem. Phys., vol. 121, page 3973, 2004.

[Rao 10] F. Rao and M. Karplus. *Protein dynamics investigated by inherent structure analysis*. Proc. Natl. Acad. Sci. U.S.A., vol. 107, pages 9152–9157, 2010.

[Reddy 89] M. Rami Reddy and M. Berkowitz. *The dielectric constant of SPC/E water*. Chem. Phys. Lett., vol. 155, page 173, 1989.

[Ren 02] P. Ren and J.W. ponder. *A consistent treatment of inter- and intramolecular polarization in Molecular Mechanics calculations*. J. comput. chem., vol. 23, pages 1497–1506, 2002.

[Ren 03] P. Ren and J.W. ponder. *Polarizable atomic multipole water model for Molecular Mechanics simulation*. J. Phys. chem. B, vol. 107, pages 5933–5947, 2003.

[Requena 04] Alberto Requena and J. Zúñiga. Espectroscopía. Pearson Education, Madrid, 2004.

[Rey-Lafon 73] M. Rey-Lafon, M. T. Forel and C. Garrigou-Lagrange. *Discussion des modes normaux des groupements amides cis et trans á partir des champs de force du δ-valérolactame et du N-methylacetamide*. Spectr. Acta, vol. 29A, pages 471–486, 1973.

[Richardi 05] J. Richardi, P. Fries and C. Millot. *Fast hybride methods for the simulations of dielectric constants*. J. Mol. Liq., vol. 117, page 3, 2005.

[Rodrigo 86] M. M. Rodrigo, M. P. Tarazona and E. Saiz. *Experimental determination and analysis of the direction of the dipole moments of some substituted amides*. J. Phys. Chem., vol. 90, page 2236, 1986.

[Roitberg 97] A. Roitberg, B. B. Gerber and M. A. Ratner. *A Vibrational Eigenfunction of a Protein: Anharmonic Coupled-Mode Ground and Fundamental Excited States of BPTI*. J. Phys. Chem. B, vol. 101, pages 1700–1706, 1997.

[Rubtsov 03a] I. V. Rubtsov, J. Wang and R. M. Hochstrasser. *Dual-frequency 2D-IR spectroscopy heterodyned photo echo of the peptide bond*. Proc. Natl. acad. Sci, vol. 100, page 5601, 2003.

[Rubtsov 03b] I. V. Rubtsov, J. Wang and R. M. Hochstrasser. *vibrational coupling between amide I and amide A modes Revealed by Femtosecond Two color Infrared Spectroscopy*. J. Phys. Chem. A, vol. 107, pages 3384–3396, 2003.

[Ryckaert 77] J. P. Ryckaert, G. Ciccotti and H. J. C. Berendsen. *Numerical-Integration of cartesian equations of motion of a system with constants - Molecular-Dynamics of N-ALkanes*. J. Comput. Phys., vol. 23, page 327, 1977.

[Sagnella 99] D. E. Sagnella and J. E. Straub. *A study of vibrational relaxation of B-state carbon monoxide in the heme pocket of photolyzed carboxymyoglobin*. Biophys. J., vol. 77, pages 70–84, 1999.

[Schade 09a] M. Schade and P. Hamm. *Vibrational energy transport in the presence of intransite vibrational energy redistribution*. J. Chem. Phys., vol. 131, page 044511, 2009.

[Schade 09b] M. Schade, A. Moretto, M. Crisma, C. Toniolo and P. Hamm. *Vibrational energy trasnport in pepetide helices after excitation of C-D modes in Leu-d_{10}*. J. Phys. Chem. A, vol. 113, pages 13393–13397, 2009.

[Schafer 95] L. Schafer, I. S. Bindrees, R. F. Frey, C. Vanalsenoy and C. Ewbank. *molecular-orbital constrained gas electron-diffraction study of N-acetyl N'-methyl alanine amide*. J. Mol. Struct (THEOCHEM), vol. 338, pages 71–82, 1995.

[Schmidt 04] J. R. Schmidt, S. A. Corcelli and J. L. Skinner. *Ultrafast vibrational spectroscopy of water and aqueous N-methylacetamide: Comparison of different electronic structure/molecular dynamics approaches*. J. Chem. Phys., vol. 121, no. 18, pages 8887–8896, 2004.

[Schmidt 08] J. R. Schmidt and S. A. Corcelli. *Infrared absorption line shapes in the classical limit: A comparison of the classical dipole and fluctuating frequency approximation*. J. Chem. Phys., vol. 128, page 184504, 2008.

[Schneider 65] B. Schneider, A. Horeni, H. Pivcova, J. Honzl and Collec. Czech. *On structure and properties of polyamides .19. vibrational spectra of N-methylacetamide*. Chem. Comm., vol. 30, page 2196, 1965.

[Schröder 09] C. Schröder, V. Vikhrenko and D. Schwarzer. *Molecular Dynamics Simulation of Heat Conduction through a Molecular Chain*. J. Phys. Chem. A, vol. 113, pages 14039–14051, 2009.

[Schultheis 08] V. Schultheis, R. Reichold, B. Schropp and P. Tavan. *A polarizable force field for computing the infrared spectra of the polypeptide backbone*. J. Phys. Chem. B, vol. 112, page 12217, 2008.

[Schulz 09] R. Schulz, M. Krishnana, I. Daidone and J. C. Smith. *Instantaneous Normal Modes and the Protein Glass Transition*. Biophys. J., vol. 96, pages 476–484, 2009.

[Seabra 07] Gustavo de M. Seabra, Ross C. Walker, Elstner Marcus Elstner, David A.Case and Adrian E. Roitberg. *Implementation of the SCC-DFTB Method for Hybrid QM/MM Simulations within the Amber Molecular Dynamics Package*. J. Phys. Chem. A, vol. 111, no. 26, pages 5655–5664, 2007.

[Segal 03] D. Segal, A. Nitzan and P. Hänggi. *Thermal conductance through molecular wires*. J. Chem. Phys., vol. 119, page 6840, 2003.

[Sharp 06] K. Sharp and J. J. Skinner. *Pump-Probe Molecular Dynamics as a Tool for Studying Protein Motion and Long Range Coupling*. Proteins, vol. 65, pages 347–361, 2006.

[Shigeto 07] S. Shigeto and D.D. Dlott. *Vibrational relaxation of an amino acid in aqueous solution*. Chem. Phys. Lett., vol. 447, pages 134–139, 2007.

[Shigeto 08] S. Shigeto, Y. Pang, Y. Fang and D. D. Dlott. *Vibrational Relaxation of Normal and Deuterated Liquid Nitromethane*. J. Phys. Chem. B, vol. 112, no. 2, pages 232–241, 2008.

[Silvestrelli 97] P. L. Silvestrelli, M. Bernasconi and M. Parrinello. *Ab initio infrared spectrum of liquid water*. Chem. Phys. Lett., vol. 277, page 478, 1997.

[Silvestrelli 98] P. L. Silvestrelli and M. Parrinello. *Ab Initio Infrared Absorption Study of the Hydrogen-Bond Symmetrization in Ice*. Phys. Rev. Lett., vol. 81, page 1235, 1998.

[Smith 99] P. E. Smith. *The alanine dipeptide free energy surface in solution*. J. Chem. Phys., vol. 111, pages 5568–5578, 1999.

[Soler 10] Miguel Ángel Soler. *Estodio de la relajación vibracional de N-metilacetamida en disolución acuosa*. PhD thesis, Universidad de Maurcia, 2010.

[Soler 11] Miguel A. Soler, A. Bastida, Marwa H. Farag, J. Zuñiga and Alberto Requena. *A method for analyzing the vibrational energy flow in biomolecules*. J. Chem. Phys., vol. 135, page 204106, 2011.

[Stewart 89] J. J. Stewart. *Optimization of parameters for semiempirical methods. I. Method*. J. Comput. Chem., vol. 10, page 209, 1989.

[Storer 95] J. W. Storer, D. J. Giesen, C. J. Cramer and D. G. Truhlar. *Class-IV charge models - A new semiempirical approach in quantum-chemistry*. J. Comput. Aided Mol. Des., vol. 9, page 87, 1995.

[Stratt 94] R. M. Stratt and M. Cho. *The short-time dynamics of solvation*. J. Chem. Phys., vol. 100, pages 6700–6708, 1994.

[Stratt 95] Richard M. Stratt. *The instantaneous normal modes of liquids*. Acc. Chem. Res., vol. 28, pages 201–207, 1995.

[Stratt 01] R. M. Stratt. *The molecular mechanism behind the vibrational population relaxation of small molecules in liquids*. En M. D. Fayer, editor, Ultrafast infrared and Raman spectroscopy, pages 149–190. Marcel Dekker Inc., 2001.

[Sugawara 84] Y. Sugawara, A. Y. Hirakawa and M. Tsuboi. *In-plane force constants of the peptide group: Least-squares adjustment starting from ab initio values of N-methylacetamide*. J. Mol. Spectrosc, vol. 108, page 206, 1984.

[Szabo 96] A. Szabo and N. S. Ostlund. Modern quantum chemistry: Introduction to advanced electronic structure theory. Dover Publications, INC, Mineola, New York, 1996.

[Takekiyo 04] T. Takekiyo, T. Imai, M. Kato and Y. Taniguchi. *Temperature and pressure effects on conformational equilibria of alanine dipeptide in aqueous solution*. Biopolymers, vol. 173, page 283, 2004.

[Torii 98] Hajime Torii, Tomoaki Tatsumi and Mitsuo Tasumi. *Effects of hydration on the structure, vibrational wavenumbers, vibrational force field and resonance raman intensities of the N-methylacetamide*. J. Raman Spectrosc., vol. 29, page 537, 1998.

[Torii 04] Hajime Torii. *Vibrational interactions in the amide I subspace of the oligomers and Hydration clusters of N-methylacetamide*. J. Phys. Chem. A, vol. 108, page 7272, 2004.

[Van-Kampen 07] N. G. Van-Kampen. Stochastic processes in physics and chemistry. 3rd ed. (North-Holland, Amsterdam), 2007.

[Vargas 02] R. Vargas, J. Garza, B. P. Hay and D. A. Dixon. *Conformational study of the alanine dipeptide at MP2 and DFT levels*. J. Phys. Chem. A, vol. 106, page 3213, 2002.

[Vikhrenko 99] V.S. Vikhrenko, C. Heidelbach, D. Schwarzer, V.B. Nemtsov and J. Schroeder. *Molecular dynamics simulation of vibrational energy relaxation of highly excited molecules in fluids. I. General considerations*. J. Chem. Phys., vol. 110, pages 5273–5285, 1999.

[Villani 99] V. Villani, G. Alagona and C. Ghio. *Ab Initio Studies on N-Methyl-Acetamide: Stationary Point Search and Intrinsic Reaction Coordinate*. Mol. Eng., vol. 8, page 135, 1999.

[Wang 04] Zhi-Xiang Wang and Y. Duan. *Solvation effects on alanine dipeptide: A MP2/cc-pVTZ//MP2/6-31G** study of ($\hat{I}$, $\hat{I}$¨) energy maps and conformers in the gas phase, ether, and water*. J. Comput. Chemist, vol. 25, pages 1699–1716, 2004.

[Wang 07] Z. H. Wang, J. A. Carter, A. Lagutchev, Y. K. Koh, N.-H. Seong, D. G. Cahill and D. D. Dlott. *Ultrafast flash thermal conductance of molecular chains*. Science, vol. 317, page 787, 2007.

[Warshel 07] Arieh Warshel, Mitsunori Kato and Andrei V. Pisliakov. *Polarizable Force Fields: History, Test Cases, and Prospects*. Journal of Chemical Theory and Computation, vol. 3, no. 6, pages 2034–2045, 2007.

[Weise 03] C. F. Weise and J. C. Weisshaar. *Conformational Analysis of Alanine Dipeptide from Dipolar Couplings in a Water-Based Liquid Crystal*. J. phys. Chem. B, vol. 107, page 3265, 2003.

[Yang 95] W. Yang and T. S. Lee. *A density matrix form of the divide and conquer approach for electronic structure calculations of large molecules*. J. chem. Phys., vol. 103, pages 5674–5678, 1995.

[Yang 05] S. Yang and M. Cho. *IR spectra of N-methylacetamide in water predicted by combined quantum mechanical/molecular mechanical molecular dynamics simulations*. J. Chem. Phys, vol. 123, page 134503, 2005.

[Yang 09] S. Yang and M. Cho. *Direct calculations of vibrational absorption and circular dichroism spectra of alanine dipeptide analog in water:Quantum mechanical/molecular mechanical molecular dynamics simulations.* J. Chem. Phys., vol. 131, page 135102, 2009.

[Yu 03] X. Yu and D. M. Leitner. *Vibrational Energy Transfer and Heat Conduction in a Protein*. J. Phys. Chem. B, vol. 107, pages 1698–1707, 2003.

[Yu 05] X. Yu and D. M. Leitner. *Heat flow in proteins: Computation of thermal transport coefficients*. J. Chem. Phys., vol. 122, page 054902, 2005.

[Zanni 01] M. T. Zanni, M. C. Asplund and R. M. Hochstrasser. *Two-dimensional heterodyned and stimulated infrared photon echoes of N-methylacetamide-D*. J. Chem. Phys., vol. 114, no. 10, pages 4579–4590, 2001.

[Zelsmann 95] H. R. Zelsmann. *Temperature dependence of the optical constants for liquid H2O and D2O in the far IR region*. J. Mol. Struct., vol. 350, page 95, 1995.

[Zhang 09] Y. Zhang, H. Fujisaki and J. E. Straub. *Mode-specific vibrational energy relaxation of the amide I' and II' modes in N-methilacetamide/water clusters: Intra- and intermolecular energy transfer mechanism*. J. Phys. Chem. A, vol. 113, pages 3051–3060, 2009.